Institute of Cancer and Genetics
School of Medicine
Cardiff University

An Investigation into the Chromatin Structure of Human Telomeres

A thesis submitted to the School of Medicine, Cardiff University in partial fulfilment for the degree of Doctor of Philosophy

Kevin Norris

2013

NOTICE OF SUBMISSION OF THESIS FORM:
POSTGRADUATE RESEARCH

APPENDIX 1:
Specimen layout for Thesis Summary and Declaration/Statements page to be included in a Thesis

DECLARATION

This work has not previously been accepted in substance for any degree and is not concurrently submitted in candidature for any degree.

Signed …… (candidate) Date ……

STATEMENT 1

This thesis is being submitted in partial fulfillment of the requirements for the degree of ……(insert MCh, MD, MPhil, PhD etc, as appropriate)

Signed …… (candidate) Date ……

STATEMENT 2

This thesis is the result of my own independent work/investigation, except where otherwise stated. Other sources are acknowledged by explicit references.

Signed …… (candidate) Date ……

STATEMENT 3

I hereby give consent for my thesis, if accepted, to be available for photocopying and for inter-library loan, and for the title and summary to be made available to outside organisations.

Signed …… (candidate) Date ……

STATEMENT 4: PREVIOUSLY APPROVED BAR ON ACCESS

I hereby give consent for my thesis, if accepted, to be available for photocopying and for inter-library loans **after expiry of a bar on access previously approved by the Graduate Development Committee.**

Signed …… (candidate) Date ……

Acknowledgments

Firstly I would like to thank my supervisor Dr Duncan Baird for giving me the opportunity to undertake this PhD and his continued support and supervision during the course of the project.

I would like to thank all the members of the STELA group: Dr Maira Tankimanova, Dr Rhiannon Robinson, Julia Grimstead, Dr Kate Simpson, Dr Thet Thet Lin, Dr Ceri Jones, Dr Kate Liddiard, Dr Bethan Britt-Compton, Dr Laureline Roger, Dr Nicole Heppel and Raniah Alitobi for their guidance and friendship during the last three years. I especially want to thank Maira and Julia who helped me considerably with tissue culture.

A huge thank you goes to my wife Amanda who has been a constant source of support and positivity throughout, especially during writing my thesis when I took on a sub-human form. Without your support this PhD would not have been possible. I would like to thank baby Norris who gave me a much appreciated kick up the backside to get the thesis written. I very much look forward to meeting you. I would also like to thank Paul for keeping me entertained during the thesis writing months.

Finally I would like to thank my family for their support, particularly my Grandmother who passed on when I commenced this PhD - you did a lot for me when you were here and you are greatly missed.

Summary

Telomeres cap the end of eukaryotic chromosomes and prevent the natural end of a chromosome from being recognised as a double-stranded DNA break. Dysfunctional telomeres may trigger replicative senescence, or fuse with other telomeres or with non-telomeric DNA breaks. The length of a telomere plays a key role in telomere function. Relatively little is known about how telomeric chromatin influences telomere length and function. A number of studies in mammalian cells have identified a handful of chromatin remodelling proteins and the chromatin marks they deposit in telomere length regulation. However such examples at human telomeres are scarce.

The primary aim of this thesis was to investigate whether the chromatin structure of a telomere is a determinant of its length in human cells. Two approaches were taken to address this issue: Firstly, the chromatin structure of telomeres of differing lengths were directly analysed by measuring enrichment of histone modifications known to be prominent at telomeres in other model organisms. Secondly, selected chromatin remodelling proteins were studied to determine whether they play a role in telomeric chromatin structure and telomere length.

Single Telomere Length Analysis (STELA) provides a high resolution method to measure telomere length distributions at individual chromosome ends. STELA assays were previously designed for the 2p, 9p, 11q, 12q, 16p, 17p and 18q telomeres. An allele-specific STELA assay has also been designed for the XpYp chromosome end. In this study novel telomere and telomeric allele-specific qPCR assays were developed for the same chromosome ends. These qPCR assays, when used in conjunction with ChIP provide a tool for analysing telomeric chromatin structure at individual chromosome ends. Applying this ChIP-qPCR approach alongside STELA allows any correlations between telomeric chromatin structure and telomere length to be identified. This approach suggested differences in telomeric chromatin structure between telomeres of different lengths in telomerase-positive HT1080 fibrosarcoma cells. Shorter HT1080 telomeres were less abundant in H3 and TRF1 and also had lower levels of H4K20me3 and, to a lesser extent, H3K4me3 compared to longer telomeres. Differences in chromatin structure were not observed between telomeres of different lengths in telomerase negative MRC5 fibroblasts. Changes in chromatin structure were observed at individual telomeres/telomere alleles were observed between actively proliferating cells and in cells undergoing senescence. Telomeric enrichment of H3 and TRF1 as well as the histone methylation marks H3K4me3, H3K9me3 and H4K20me3 were reduced in senescent cells. The degree of chromatin structural change as the cells entered senescence differed between chromosome ends. This highlights the benefits of using the telomere-specific ChIP-qPCR approach over the more traditional ChIP-dot blot assays which would not be able to differentiate between the chromatin structure of different chromosome ends.

To identify roles for chromatin remodelling proteins in telomere length maintenance siRNA mediated knockdown of selected chromatin remodelers was performed in a clonal population of HT1080 cells followed by STELA analysis. RNAi-depletion of the histone methyltransferase (HMTase)

EHMT2 resulted in an increase in very short 17p telomeres whereas loss of another HMTase, DOT1L caused a divergence in the 17p telomere length distribution suggesting the presence of two subpopulations of cells each with differing telomere length distributions. Subtle changes in mean telomere length was observed after siRNA mediated knockdown of the HMTases MLL and EZH2, the histone deacetylases (HDACs) HDAC1 and SIRT6, the ATP dependent chromatin remodelling complex subunit BAF155 and the H3.3 histone chaperone DAXX. However due to certain limitations of the RNAi screen the validity of these observations is questionable and more work would have to be performed to confirm whether these chromatin remodelers have an effect on telomere length. Finally, dramatic telomere shortening was observed in a keratinocyte holoclone population after siRNA mediated knockdown of DAXX at number of chromosome ends. Prolonged depletion of DAXX also caused an increase in telomere-to-telomere fusions. A similarly dramatic loss in telomere length was seen in these cells after knockdown of EHMT2.

Table of Contents

Abbreviations

ALT	Alternative Lengthening of Telomeres
A-NHEJ	Alternative Non-homologous End Joining
ANOVA	Analysis of Variance
APB	ALT-associated PML body
ATM	Ataxia Telangiesctasia Mutated
ATR	Ataxia Telangiesctasia and Rad3 Related
ATRX	alpha thalassemia/mental retardation syndrome X-linked
AT	Ataxia Telangiesctasia
ATP	Adenosine Triphosphate
BFB	Breakage-Fusion-Bridge
bp	Base pairs
Caf1	Chromatin Assembly Factor 1
Cbx1, 3 & 5	Chromobox homolog 1, 3 & 5
Cdc25	Cell Division Cycle 25
CDK	Cell Division Kinase
CenH3/CENPA	Centromeric H3 histone variant
ChIP	Chromatin Immunoprecipitation
Chk1 & 2	Checkpoint kinase 1 & 2
DAXX	Death Domain-Associated Protein
DDR	DNA Damage Response
DKC	Dyskeratosis Congenita
DKC1	Dyskerin
D-loop	Displacement loop
DMEM	Dulbecco's Modified Eagle's Medium
DMSO	Dimethyl sulphoxide
DNA	Deoxyribonucleic acid
DNMT	DNA methyltransferase
dNTP	Deoxyribonucleotide

DSB	Double Strand Break
EHMT2	Euchromatic Histone-lysine-N-Methyltransferase
EMEM	Eagle's Minimum Essential Medium
ES	Embryonic Stem cell
EZH2	Enhancer of Zeste Homolog 2
FA	Fanconi Anemia
FISH	Fluorescent in-situ hybridization
GAPDH	Glyceraldehyde-3-Phosphate dehydrogenase
GBM	Glioblastoma Multiforme
HAT	Histone Acetyltransferase
HDAC	Histone Deacetylase
HDACi	Histone Deacetylase Inhibitor
HipHop	HP1-HOAP-interacting protein
HMTase	Histone Methyltransferase
HOAP	HP1/ORC-associated protein
HP1	Heterochromatin protein 1
HR	Homologous Recombination
iPSC	Induced Pluripotent Stem Cell
IP	Immunoprecipitation
IPF	Idiopathic Pulmonary Fibrosis
JARID	Jumonji/ARID domain-containing histone demthylase
K	Lysine
kb	kilobases
kC1B	Keratinocyte holoclone C1B
MBD	Methyl-binding Domain
MDC1	Mediator of DNA damage Checkpoint 1
MEF	Mouse embryonic fibroblast
MLL	Myeloid/Lymphoid, or Mixed-Lineage, Leukemia
MRE11	Meiotic Recombination 11 Protein
ncRNA	non-coding RNA

NHEJ	Non-Homologous End Joining
nt	nucleotides
O-GlcNAc	β-N-acetylglucosamine
ORC	Origin of Recognition Complex
P	Phosphate
PanNET	Pancreatic Neuroendocrine Tumours
PCR	Polymerase Chain Reaction
PD	Population Doubling
POT1	Protection Of Telomeres 1
pRB	Retinoblastoma protein
PRC	Polycomb Repressive Complex
qPCR	Quantitative PCR
R	Arginine
RAP1	Repressor Activator Protein 1
RNA	Ribonucleic Acid
RPA	Replication Protein A
RNAi	RNA interference
RT	Reverse Transcription
RT-PCR	Real-time PCR
ssDNA	single stranded DNA
Sir	Silent Information Regulator
siRNA	Small interfering RNA
SNP	Single Nucleotide Polymorphism
STELA	Single Telomere Length Analysis
Suv39h1 & h2	suppressor of variegation 3-9 homolog 1 & 2
Suv4-h20 1 & 2	suppressor of variegation 4-20 homolog 1 & 2
Taz1	Telomere Assocaited in *Schizosaccharomyces pombe*
TERRA	Telomere Repeat containing RNA
TIN2	TRF1-Interating Factor
TERC	Telomerase RNA component

TERT	Telomerase Reverse Transcriptase
TIF	Telomere dysfunction-induced foci
T-loop	Telomere-loop
Tm	Melting Temperature
TPE	Telomere Position Effect
TPP1	Tripeptidyl Peptidase 1
TRF1	Telomeric repeat Binding Factor 1
TRF2	Telomeric repeat Binding Factor 2
TSA	Trichostatin A
T-SCE	Telomere Sister Chromatid Exchange
TVR	Telomere Variant Repeat
U	Ubiquitin
WRN	RecQ helicase
WS	Werners Syndrome
ZNF554	Zinc Finger Protein 554

Chapter 1

Introduction

1.1 The history of the telomere

The ends of linear eukaryotic chromosomes or telomeres were first described over 70 years ago in two independent pioneering studies by the geneticists Hermann Joseph Muller and Barbara McClintock. Whist studying X ray-induced DNA breaks in *Drosophila melanogaster* Muller observed that chromosomal aberrations resulting from ionizing radiation such as inversions, deletions and translocations never involved the natural ends of chromosomes (Muller 1938). This led Muller to speculate about the presence of a terminal gene with a specialised function of sealing the chromosome end. Muller coined the term telomere for this terminal gene from the Greek, *telo* = end, and mere = part.

Similar observations were made by Barbara McClintock in maize (*Zea mays*) where X-ray induced chromosomal aberrations resulted in fusion events between sister chromatids. These dicentric chromosomes formed a bridge which breaks during the anaphase stage of mitosis when the two centromeres are pulled to opposite poles. Following DNA replication in the cell cycle of the daughter cells, sister chromatids fuse again and the breakage-fusions-bridge cycle (BFB) cycle continues (McClintock 1941). These BFB cycles can lead to unequal exchange of genetic information causing gene amplifications and deletions. McClintock also found that propagation of the BFB cycles only occured within somatic cells, in embryonic sporophytes the broken chromosome ends were permanently healed (McClintock 1941).

Prior to the discovery of telomeres Alexis Carrel postulated that vertebrate cells can divide indefinitely in culture and are therefore “immortal” based on the continuous culture of chick heart fibroblasts for 34 years (Carrel and Ebeling 1921). This concept of cell immortality was

definitively disproved by the work of Paul Moorhead and Leonard Hayflick who demonstrated that normal human fibroblasts have a finite proliferative capacity (Hayflick and Moorhead 1961, Hayflick 1965). They observed that fibroblast cultures derived from human skin stop dividing after 40-50 cell divisions at which point they senesce. These cells appeared to have a cellular division counting mechanism.

In the 1970s James Watson and Alexey Olovnikov noted that DNA replication was unable to produce a complete copy of a linear chromosome (Olovnikov 1971, Watson 1972). This was referred to as "the end replication problem" and would in theory result in a shortening of a chromosome after each round of cell division. A link between the end replication problem and cellular senescence described by Hayflick was proposed by Olovnikov: he reasoned that the continual shortening of the terminal gene or the 'telogene' at each round of replication may act as a molecular clock and might explain why normal cells can only divide a specific number of times (Olovnikov 1973).

The presence of the hexameric telomeric repeat TTGGGG in *Tetrahymena thermophila* was discovered in 1978 by Elizabeth Blackburn (Blackburn and Gall 1978). The discovery a few years later that yeast could recognise and maintain *Tetrahymena* telomeric DNA suggested that a fundamental cellular mechanism was involved and that the presence of telomeric repeats was conserved throughout eukaryotic evolution (Szostak and Blackburn 1982).

1.2 Telomere Structure

Telomeric DNA has since been shown to be highly conserved amongst eukaryotes. Despite variation in sequence composition and length, telomeric DNA, for most eukaryotes, is composed of double stranded short tandem repeats. Bound to these telomeric repeats are a multitude of proteins including the shelterin complex and other transiently-binding proteins

which has led to the telomere being described as a nucleoprotein complex. At the telomere terminus is a single stranded 3' protrusion of the G strand referred to as the 3' overhang which is maintained throughout the replicative lifespan of the cell (Chai, Shay et al. 2005). Like the length of telomeres themselves, the length of the G-strand overhang varies between species: in protozoa the average length is between 10-20bp whereas in mammalian cells it is considerably longer. Human 3' overhang length is generally considered to be 50-200bp long (Makarov, Hirose et al. 1997, McElligott and Wellinger 1997). 3' overhangs were originally thought to result from incomplete synthesis of the lagging strand during DNA replication however the fact that 3' overhangs are also found on leading strands shows the requirement of telomerase-mediated expansion of the G-rich strand or nucleolytic degradation of the C-rich strand at these chromosome ends (Dionne and Wellinger 1996, Parenteau and Wellinger 2002). The 3' overhang is thought to strand invade the duplex telomeric repeats to form a higher order 't-loop' structure (Griffith, Comeau et al. 1999). The overhang then base pairs with the C-rich strand, displacing the G-rich strand at this site into a displacement loop (D loop). T-loops have been observed in a number of eukaryotes including protozoa (Munoz-Jordan, Cross et al. 2001) plants (Cesare, Quinney et al. 2003), yeast (Tomaska, Willcox et al. 2004) and humans (Griffith, Comeau et al. 1999) however little is known about their dynamics, how they are regulated by telomeric proteins or whether they are present throughout the cell cycle or displaced during DNA replication (Palm and de Lange 2008). In vitro, telomeric ssDNA readily forms higher order G-quadruplex structures (Neidle and Parkinson 2003) although these structures have only thus far been reported in vivo at ciliate telomeres (Lipps and Rhodes 2009). These G-quadruplex structures have been shown to be implicated in telomere protection and inhibition of telomerase-dependent telomere extension (Lipps and Rhodes 2009).

Although differences in telomere structure exist amongst eukaryotes the evolutionary conservation of many components of the telomere highlight the fundamental role they play during the cell cycle and lifespan of a eukaryotic cell. These differences in telomeric composition in different eukaryotes are discussed below

1.2.1 Diptera

Drosophila melanogaster telomeres have a unique telomere structure compared to other eukaryotes. Drosophila telomeres are not maintained by telomerase and therefore lack the short arrays of simple repeat units. Instead they are maintained by two non-LTR reterotransposons; *HeT-A* and *TART* that transpose specifically to chromosome ends resulting in head-to tail arrays of these elements (Pardue and DeBaryshe 2003, Pardue, Rashkova et al. 2005). Despite the variation in telomeric repeat make-up, Drosophila telomeres still share many characteristics with telomeres of other eukaryotes such as homologous telomere binding proteins.

1.2.2 Protozoa

The presence of telomere repeats was first discovered on the ribosomal DNA minichromosome in *Tetrahymena thermophila* (Blackburn and Gall 1978). These protozoan telomeres contained 20-70 tandem copies of a simple hexanucleotide with the sequence TTGGGG. Since that discovery the macronuclear DNA of the ciliates *Stylonychia putulata* and *Oxytricha fallax* were shown be capped with a 20 nucleotide long stretch of TTTTGGGG telomeric repeats with the latter also ending in a 16 nucleotide single stranded 3' overhang (Oka, Shiota et al. 1980, Pluta, Kaine et al. 1982). Certain Trypanosome telomere repeat elements have been characterised such as in *T. cruzi* and *T. brucei*. These protozoan telomeres are much longer consisting of 10-20kb of the repeat array TTAGGG (Blackburn and Challoner 1984, Munoz-Jordan, Cross et al. 2001) with the latter telomeres forming a t-

loop approximately 1kb in size. Both display a 3' overhang ranging from 9-50 nucleotides in *T. cruzi* and 21-250 nucleotides *T. brucei* (Chiurillo, Cano et al. 1999, Munoz-Jordan, Cross et al. 2001).

1.2.3 Fungi

Chromosomes in *Saccharomyces cerevisiae* were originally shown to terminate in tandem irregular repeats of $C_{1-3}A/TG_{1-3}$ (Shampay, Szostak et al. 1984) however it has since been shown that these telomeres display an unusual degree of heterogeneity (Wang and Zakian 1990). The telomeric repeat tract is composed of a terminal sequence of $G_{2-3}(TG)_{1-6}$ repeats and an internal domain of TG_{1-7} repeats. This heterogeneity is experimentally useful as it allows distinction between newly synthesised and pre-existing telomeric DNA (Wang and Zakian 1990). *S. cerevisiae* telomeres terminate with a 3' overhang which are short throughout most of the cell cycle (12-15nt) but which are much longer (30-100nt) in late S/G2 phase (Wellinger, Wolf et al. 1993, Larrivee, LeBel et al. 2004). This increase in 3' overhang is also seen in *Schizosaccharomyces pombe*. These telomeres are composed of 300bp of the repeat sequence $(GTTACA)_n$ (Kibe, Tomita et al. 2003). A higher order looped structure has been identified in both S. *pombe* (Tomaska, Willcox et al. 2004) and S. *cerevisiae* (de Bruin, Zaman et al. 2001).

1.2.4 Plants

The most detailed knowledge of plant telomere biology is found in *Arabidopsis thaliana*. Telomeres in this plant consist of TTTAGGG repeats (Richards and Ausubel 1988) and can range in size from 2-9kb (Richards and Ausubel 1988, Shakirov and Shippen 2004). Similar Arabidopsis-type telomere repeats have since been found in most angiosperms however several studies have revealed that the sequence is absent in the telomerase-negative *Allium cepa* onion and related species (Pich, Fuchs et al. 1996). Many species within Asparagales

possess the vertebrate TTAGGG repeat array whereas others possess variant tandem repeats such as TTGGGG (Sykorova, Lim et al. 2003). Telomere length varies greatly between different plant species ranging from 0.5kb in *C. vulgaris* to 150kb in tobacco (Fajkus, Kovarik et al. 1995). 3' overhangs have been identified in Arabidopsis and *S. latifolia* (Riha, McKnight et al. 2000, Riha and Shippen 2003, Berthiau, Yankulov et al. 2006) however in the latter case these overhangs were only found at half of the telomeres. The only plant to date in which a telomeric t-loop structure has been found is *Pisum sativum* (Cesare, Quinney et al. 2003).

1.2.5 Mammalian telomere structure

TTAGGG was identified as the telomere repeat unit in human cells (Moyzis, Buckingham et al. 1988) and was later shown to be shared by mice (Meyne, Ratliff et al. 1989). The length of this repeat array in mice varies with sub-species and can range from ~12kb in *Mus. spretus* to 200kb in *Mus. musculus* (Kipling and Cooke 1990, Hemann and Greider 2000). At human chromosome ends the range of telomere length is much shorter (5-20kb). In addition to the TTAGGG repeats are degenerate telomere variant repeats such as TCAGGG, TTGGGG and TGAGGG in the proximal 1-2kb of the telomere (de Lange, Shiue et al. 1990, Baird, Jeffreys et al. 1995, Baird, Coleman et al. 2000).

1.2.6 Subtelomeric regions

Subtelomeric regions are located adjacent to the telomere repeat tract DNA. These regions range from 10-300kb in size and consist of unusually dynamic and variable mosaics of sequence arrays (Mefford and Trask 2002). Subtelomeres are structurally similar between species in that they are composed of various repeated elements however the arrangement and composition of these sequences vary greatly among organisms. The structure of subtelomeric regions has been studied in a wide range of organisms including *Plasmodium*

falciparum, *Saccharomyces cerevisiae*, *Drosophila melanogaster*, various plant species and humans.

The subtelomeric regions of parasites and pathogens such as Trypanosoma brucei and *Plasmodium falciparum* have been extensively studied and contain genes encoding surface antigens used in host immune invasion as well as tandem arrays of repetitive sequences (Eid and Sollner-Webb 1995, Pace, Ponzi et al. 1995, Rubio, Thompson et al. 1996). Drosophila subtelomeres also contain tandem repeat arrays which vary in size and sequence composition between chromosome ends (Mason and Biessmann 1995).

Plants subtelomeric regions contain large tracts of tandem repeats which are separated from the telomeric repeat tract by spacer sequences (Ganal, Broun et al. 1992, Pryde, Gorham et al. 1997). Arabidopsis subtelomeric regions are unique: 8 out of the 10 chromosome ends share very little homology between subtelomeres. Furthermore, the sequence directly adjacent to the telomere repeat tract contains no highly repetitive elements (Heacock, Spangler et al. 2004). It is these features of Arabidopsis subtelomeric regions which made them suitable for the development of PETRA (primer extension telomere repeat amplification). PETRA allows the amplification of individual telomeres and is achieved through the use of telomere-specific primers designed around the unique subtelomeric DNA sequence directly adjacent to the telomere repeat tract (Heacock, Spangler et al. 2004).

C. elegans display even less homology between subtelomeric regions. Chromosome ends in this organism lack homology to each other beyond the telomeric repeat array (Wicky, Villeneuve et al. 1996). Like in Arabidopsis, these unique subtelomeric regions in C. Elegans have been exploited for the development of PCR-based telomere-specific length analysis.

STELA (Single Telomere Length Analysis) has allowed the measurement of single telomere length distributions from a single worm (Cheung, Schertzer et al. 2004).

One of the most well characterised subtelomeric regions are those of S. cerevisiae. These subtelomeres contain several gene families, a transposable element family and repetitive elements often referred to as TAS elements (telomere associated sequences) (Pryde, Gorham et al. 1997, Wellinger and Zakian 2012). There are two classes of TAS elements: X and Y'. Y' elements exist in two sizes, Y' long (6.7kb) and Y' short (5.2kb) which differ from each other by multiple insertions and deletions (Louis and Haber 1992). Up to four copies of these Y' elements are present immediately adjacent to the telomere repeat array (Chan and Tye 1983). These Y' elements are only found in approximately half of the subtelomeres in a given strain and the identity of Y'-less subtelomeres differ from strain to strain (Horowitz, Thorburn et al. 1984). The X element is composed of a series of repeats and is located centromere-proximal to the Y' element. X is present at nearly all telomeres although it shows greater variation in size and sequence identity (Louis, Naumova et al. 1994, Wellinger and Zakian 2012). Often a stretch of degenerate telomere repeats separate the 'X' and 'Y'elements (Walmsley, Chan et al. 1984). Centromere-proximal to the X element are blocks of sequence that vary in size from less than 1kb up to 30kb and are shared only between a few chromosome ends (Pryde, Gorham et al. 1997).

In a similar manner to yeast subtelomeric regions, human subtelomeres also contain degenerate telomere repeat tracts. Again the location and size of these (TTAGGG)n like arrays vary between chromosome ends however at the 4p, 16p and 22q subtelomeric regions these arrays appear to separate distinct distal and proximal domains resulting in a subtelomeric structure similar to what is seen in *S. cerevisiae* (Flint, Bates et al. 1997).

More recent studies on human subtelomeres has shed more light on the domain organisation and structure of these highly variable regions. Harold Riethman and co-workers have performed considerable work in mapping human subtelomeric sequence assemblies resulting in reference sequences for all human subtelomeric regions (Riethman, Ambrosini et al. 2004). Analysis of these sequence assemblies has led to the identification of the various elements which constitute a human subtelomeric region. These include single copy DNA, segmentally duplicated DNA tracts which are present in two or more subtelomeres (subtelomeric repeats or Srpts), segmentally duplicated stretches of DNA present at only one chromosome end, satellite sequences, and internal (TTAGGG)n-like sequences. The distribution of these elements varies greatly between chromosome ends giving each subtelomeric region its own unique structure. The chromosome-specific segmental duplications are more variably dispersed throughout each subtelomere whereas the majority of subtelomeric repeats (Srpts) are confined to the most distal region of the subtelomere (Riethman, Ambrosini et al. 2004, Riethman, Ambrosini et al. 2005). The duplicons within the Srpts are found at a number of chromosome ends suggesting the presence of subtelomere families. The 7q, 8q, 11q, 14q, 18q and XpYp chromosome ends contain single-copy DNA sequences immediately adjacent to the TTAGGG repeat tract making them good candidates for Single Telomere Length Analysis (STELA) assay development.

1.3 Telomere-associated proteins

1.3.1 Shelterin

Telomeric DNA associates with the six-protein complex shelterin. Shelterin allows cells to distinguish between natural chromosome ends and DNA breaks, represses DNA repair and

regulates telomerase-based telomere maintenance (Palm and de Lange 2008). Shelterin is made up of Telomeric Repeat binding Factor 1 and 2 (TRF1 and 2), Protection Of Telomeres 1 (POT1), TRF1-Interacting Nuclear protein 2 (TIN2), Rap1 (the human ortholog of the yeast Repressor/Activator Protein 1) and TPP1.

1.3.1.1 TRF1 and TRF2

TRF1 and TRF2 are orthologs of the fission yeast Taz1 protein (Palm and de Lange 2008). They share a common domain structure consisting of a flexible hinge domain which connects C-terminal SANT/Myb domain allowing specific binding for the double stranded sequence 5'YTAGGGTTR3' and a TRF homology (TRFH) domain. It is through the TRFH domain that homodimeization of either TRF1 or TRF2 occur although TRF1 and TRF2 do not directly interact (Broccoli, Smogorzewska et al. 1997, Fairall, Chapman et al. 2001). This domain also provides a site through which other proteins are recruited to telomeres (Chen, Yang et al. 2008). Both TRF1 and TRF2 are highly abundant at the telomere and are estimated to cover each telomere with thousands of dimers (Palm and de Lange 2008). They also have the ability to alter the higher order structure of a telomere: TRF1 can loop and pair stretches of telomeric DNA whereas TRF2 has been shown to form t-loop structures on a model telomere substrate (Stansel, de Lange et al. 2001).

TRF1 is a negative regulator of telomere length: its overexpression leads to progressive telomere shortening whereas a dominant-negative form of TRF1 that removes endogenous TRF1 from telomeres has been shown to result in telomere elongation (van Steensel and de Lange 1997). TRF1 promotes efficient replication of TTAGGG repeats and prevent replication fork stalling (Sfeir, Kosiyatrakul et al. 2009).

TRF2 is important for telomere capping. Deletion of TRF2 results in an ATM-mediated DNA damage signal (Karlseder, Broccoli et al. 1999, Karlseder, Hoke et al. 2004, Celli and de Lange 2005, Denchi and de Lange 2007). TRF2 has also been shown to interact with ATM as well as the Mre11 complex (Zhu, Kuster et al. 2000). TRF2 has been shown to prevent Non-Homologous End-Joining (NHEJ) at telomeres by preventing ERCC1/XPF-mediated removal of the 3' overhang (Zhu, Niedernhofer et al. 2003). Overexpression of TRF2 results in telomere shortening indicating an additional role for the protein as a negative regulator of telomere length (Smogorzewska, van Steensel et al. 2000).

1.3.1.2 RAP1

Little is known about Rap1 however it has been shown to be a binding partner of TRF2 (Li, Oestreich et al. 2000). Unlike yeast Rap1, human Rap1 lacks the ability to directly bind DNA. Instead its localization at the telomere is dependent on TRF2 with which it forms a 1:1 complex (Li and de Lange 2003). Like TRF2, Rap1 is a negative regulator of telomere length (Li and de Lange 2003, O'Connor, Safari et al. 2004). Rap1 also plays a role in suppressing DNA repair pathways: In humans Rap1 is thought to inhibit NHEJ at telomeres. However this view is not supported by studies in mice where Rap1 is dispensable for the suppression of NHEJ and instead appears to suppress homologous recombination (Bae and Baumann 2007, Sarthy, Bae et al. 2009, Sfeir, Kabir et al. 2010).

1.3.1.3 TIN2

TIN2 tethers the shelterin components that bind ssDNA, TPP1/POT1, to the dsDNA-binding components TRF1 and TRF2 (de Lange 2005). The TRFH domains within TRF1 and TRF2 bind the C-terminus and N terminus respectively (Chen, Yang et al. 2008). The recruitment of TPP1-POT1 is achieved through a third protein interaction site in the N terminus of TIN2 (Palm and de Lange 2008). TIN2 also prevents the release of TRF1 from the telomere by

preventing its ADP-ribosylation by tankyrase (Smith, Giriat et al. 1998). Furthermore the TIN2 bridge formed between TRF1 and TRF2 stabilizes TRF2 binding to telomeric DNA (Kim, Beausejour et al. 2004, Ye, Donigian et al. 2004). Loss of TIN2 results in a DNA damage response at the telomere (Kim, Beausejour et al. 2004) and expression of TIN2 with a truncated N-terminus in HT1080 cells causes telomere elongation showing that TIN2 is a negative regulator of telomere length (Kim, Kaminker et al. 1999).

1.3.1.4 POT1

POT1 was first identified through its sequence similarity to TEBPα/β telomeric binding complex in *Oxytricha nova* (Baumann and Cech 2001). Like TEBPα/β, POT1 contains two OB folds in its N-terminus which allows it to bind single-stranded G-strand telomeric sequence *in vitro* (Baumann and Cech 2001, Lei, Podell et al. 2004). POT1 also binds the shelterin component TPP1, thereby connecting it to TIN2, this interaction with TPP1 has been shown to be critical for POT1 association at telomeres (Liu, Safari et al. 2004, Ye, Hockemeyer et al. 2004, Hockemeyer, Palm et al. 2007) however contrasting reports suggest that a TPP1-independent telomeric association of POT1 can occur (Colgin, Baran et al. 2003, He, Multani et al. 2006). Many telomeric functions of POT1 have been revealed: It is thought to stabilize the t-loop by binding to the displacement G-strand in the D-loop (Loayza, Parsons et al. 2004). Reduced loading of POT1 or replacement of the endogenous POT1 with a mutant form lacking the DNA binding domain leads to telomerase-dependent telomere elongation (Loayza and de Lange 2003, Ye, Hockemeyer et al. 2004). POT1 also represses the ATR signalling cascade, protects against telomere-telomere fusions and has a role in generating the correct sequence at human chromosome ends (Veldman, Etheridge et al. 2004, Hockemeyer, Sfeir et al. 2005, Denchi and de Lange 2007).

1.3.1.5 TPP1

As mentioned above TPP1 forms a complex with POT1 through its centrally located POT1 interacting domain (Liu, Safari et al. 2004, Ye, Hockemeyer et al. 2004). This interaction is not only required for telomeric association of POT1 but also proper localisation of POT1 in the nucleus (Chen, Liu et al. 2007). Expression of a non-functional TPP1 results in loss of telomeric POT1 resulting in telomere de-protection and telomere length alterations similar to what is seen after POT1 loss (Liu, Safari et al. 2004, Denchi and de Lange 2007, Xin, Liu et al. 2007). TPP1 also functions to recruit telomerase to telomeres. At the N-terminus of TPP1 is an OB-fold domain which interacts with telomerase and this interaction is necessary for the recruitment of telomerase (Abreu, Aritonovska et al. 2010, Nandakumar, Bell et al. 2012, Zhong, Batista et al. 2012).

Interaction between shelterin components and how the complex associates with telomeric DNA is summarised in fig. 1.1.

1.3.2 Other telomere binding proteins

In addition to shelterin mammalian telomeres contain a large number of other proteins that contribute to the maintenance and protection of chromosome ends. These proteins are less abundant than shelterin and are only transiently associated with the telomere during the cell cycle (Palm and de Lange 2008). Additionally the majority of these factors have non-telomeric roles and are more abundant at other sites in the nucleus or cytoplasm. Paradoxically a number of DNA repair proteins have a telomeric role including the Ku70/80 heterodimer (Hsu, Gilley et al. 1999), XPF/ERCC1 (Zhu, Niedernhofer et al. 2003), the Mre11 complex (Zhu, Kuster et al. 2000) and RAD51D (Tarsounas, Munoz et al. 2004). Other proteins present at the telomere include the DNA replication proteins ORC (Deng, Dheekollu et al. 2007), RecQ helicases (Opresko, von Kobbe et al. 2002) and proteins involved in the maintenance of telomeric chromatin such as HP1 (Garcia-Cao, O'Sullivan et al. 2004).

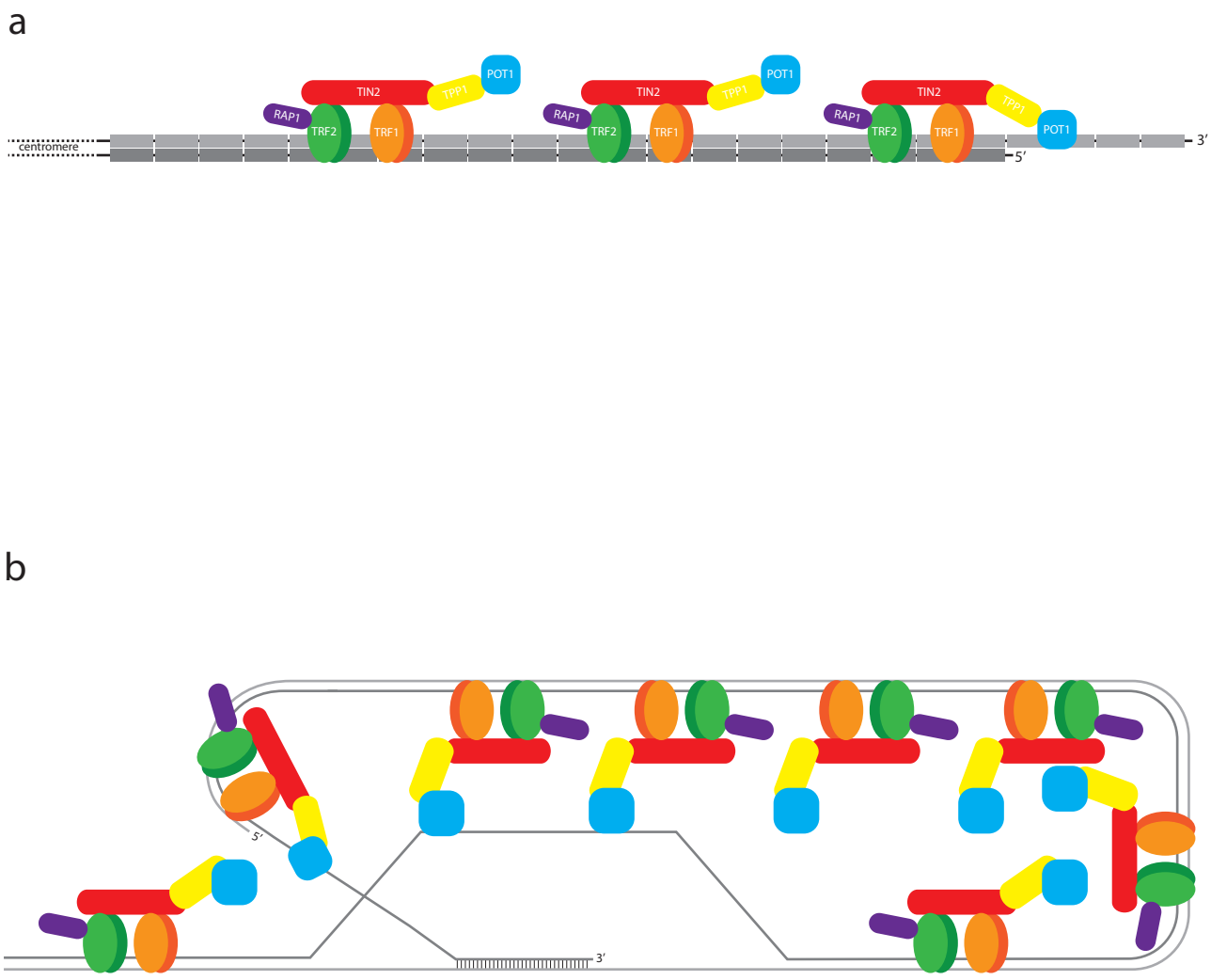

Figure 1.1. The shelterin complex (a) The six protein components in the shelterin complex (b) Representation of the shelterin complex bound to the telomere in a t-loop configuration. TRF1 (orange) and TRF2 (green) independently bind TTAGGG repeats as homodimers. Rap1 (purple) is a binding partner of TRF2. POT1 binds single stranded telomeric DNA and is connected to TIN2 (red) via TPP1 (yellow). TIN2 connects TPP1-POT1 to TRF1 and TRF2-RAP1thereby completing the complex. Adapted from Give me a break: How telomeres suppress the DNA damage response *Denchi. DNA repair 8 1118-1126 (2009).*

1.4 Telomere function

1.4.1 Chromosome capping and DNA damage response

One of the fundamental functions of the telomere is to protect natural chromosome ends from being recognised as DNA double-stranded breaks and consequently prevent fusion between telomeres. Mammalian cells are alerted to DNA lesions in their genome by two phosphatidylinositol 3-kinase-related protein kinases ATM and ATR (Shiloh 2001). The ATM pathway is thought to respond to double-stranded breaks whereas ATR activation requires the formation of ssDNA. Both ATM and ATR phosphorylate histone H2AX in a large chromatin domain around the break site which promotes the local accumulation of other DNA damage response factors such as MDC, 53BP1 and the Mre11 complex. The shelterin components TRF2 and POT1 have been shown to play a key role in preventing telomeres from being recognised as double stranded DNA breaks. Deletion of TRF2 in mouse cells or its inhibition with a dominant-negative form in human cells results in an ATM-mediated DNA damage signal (Karlseder, Broccoli et al. 1999, Celli and de Lange 2005, Denchi and de Lange 2007). Two models have been proposed to explain the TRF2 repression of the ATM pathway: the first suggests that TRF2 maintains the higher order telomere structure which sequesters the telomere terminus away from DNA repair machinery. In support of this argument is the fact that TRF2 has been shown to induce t-loop formation *in vitro* (Stansel, de Lange et al. 2001) however whether t-loops are lost when TRF2 is inhibited is unknown. The second model suggests that TRF2 functions to block a step within the signalling pathway. TRF2 has previously been shown to physically interact with DDR proteins such as the Mre11 complex and ATM and even inhibit ATM activation which supports this second model (Zhu, Kuster et al. 2000, Karlseder, Hoke et al. 2004). POT1 deletion on the other hand results in activation of the ATR pathway (Karlseder, Broccoli et al. 1999, Celli and de Lange 2005, Denchi and de Lange 2007). An identical DNA damage response is seen upon loss of TPP1 and in cells

expressing a mutant POT1 which is incapable of binding TPP1 showing that the interaction between the two proteins is vital for repression of the ATR pathway (Karlseder, Broccoli et al. 1999, Celli and de Lange 2005, Denchi and de Lange 2007, Hockemeyer, Palm et al. 2007, Xin, Liu et al. 2007). It is thought that the POT1/TPP1 complex prevents binding of RPA (replication protein A) to single stranded telomeric DNA.

1.4.2 Telomere position effect

The silencing of telomere-proximal genes or telomere position effect was first identified in Drosophila (Gehring, Klemenz et al. 1984, Hazelrigg, Levis et al. 1984, Levis, Hazelrigg et al. 1985) although it has been most extensively studied in *Saccharomyces cerevisiae.* TPE was first demonstrated in yeast by integration of a URA3 marker gene next to an array of telomeric repeats. Expression of the URA3 gene allows growth of the cells on a medium lacking uracil however on a plate containing 5-FOA (5-fluoro-orotic acid), a drug toxic to URA3 expressing cells, 20-60% cells were still able to grow suggesting that URA3 was silenced in the vicinity of the telomere (Gottschling, Aparicio et al. 1990). Since this initial discovery in yeast the mechanism regulating TPE has been thoroughly investigated. This mechanism consists of an inward spreading of heterochromatin originating from the telomere. Proteins required for TPE include the Sir (Silent Information Regulators) proteins (Aparicio, Billington et al. 1991), the Ku heterodimer components (Ku70 and Ku80) (Boulton and Jackson 1998) and the Rap1 protein (Kyrion, Liu et al. 1993). Rap1 and Ku70/80 are responsible for the recruitment of the Sir proteins to the telomere and thereby initiate the formation of a heterochromatin complex that will propagate towards subtelomeric DNA. This spreading of the heterochromatin complex requires the histone deacetylase activity of Sir2 which allows binding of the Sir3 and Sir4 proteins (Renauld, Aparicio et al. 1993, Hoppe, Tanny et al. 2002). Increasing telomere length improves TPE (Aparicio, Billington et al. 1991, Kyrion, Liu et al. 1993, Renauld, Aparicio et al. 1993). An explanation for this may be due to

the increased number of Rap1 on longer telomeres which allows increased recruitment of Sir proteins thereby promoting formation of the heterochromatin complex. In addition to the Sir histone deacetylases, other histone modifying proteins influence TPE in yeast. Deletion of the histone acetyltransferase Sas2 results in increased TPE and increased spreading of the Sir3 protein (Suka, Luo et al. 2002). Methylation of lysines 4 and 79 on histone H3 by the Set1 and Dot1 histone methyltransferases display anti-silencing properties, mainly by preventing Sir association with the histone H3 tail (Santos-Rosa, Schneider et al. 2002).

A similar silencing of telomere proximal genes was first identified in humans over a decade ago. HeLa clones containing a luciferase reporter gene adjacent to a newly formed telomere were shown to express 10 times less luciferase than control clones generated by random integration of the luciferase gene. Luciferase expression was restored by the histone deactylase inhibitor trichostatin A (TSA) (Baur, Zou et al. 2001). Overexpression of the reverse transcriptase subunit (TERT) and subsequent telomere elongation led to promotion of TPE whereas overexpression of TRF1, which has been shown to regulate telomere length results in re-expression of telomere-proximal genes (Koering, Pollice et al. 2002) indicating the involvement of both telomere length and architecture in human TPE. The human Sir2 homolog SIRT6 was later found to be required for TPE in human cells (Tennen, Bua et al. 2011).

1.4.3 Senescence

Cellular senescence was described more than four decades ago when Hayflick and colleagues demonstrated that cells have a limited proliferative capacity when grown in culture (Hayflick 1965). These experiments showed that the ability of cultured human fibroblasts to proliferate diminishes over time to a point where, although still viable, they fail to grow despite the presence of ample space, nutrients and growth factors in the medium

(Campisi and d'Adda di Fagagna 2007). Since these findings cellular senescence has been shown to play a fundamental role in cancer and aging (Shay and Wright 2005). Senescence can be induced by many stimuli including oncogene overexpression, chromatin perturbation, DNA damage and telomere dysfunction (Campisi and d'Adda di Fagagna 2007). Senescent cells cease to proliferate, become resistant to cell-death signals (apoptosis resistance) and acquire widespread changes in gene expression.

1.4.3.1 Telomere-dependant replicative senescence

The end replication problem results in the progressive loss of telomeric DNA with every cell division until telomeres become short and dysfunctional. These dysfunctional telomeres trigger a classical DNA damage response (DDR) which involves recruitment of DDR proteins such as 53BP1, NBS1 and MDC1 to the chromosome end (d'Adda di Fagagna, Reaper et al. 2003, Takai, Smogorzewska et al. 2003, Herbig, Jobling et al. 2004). The ATM and ATR DNA damage kinases are activated in senescent cells which, in addition to mediating H2AX phosphorylation, activate the Chk1 and Chk2 kinases. These checkpoint kinases then phosphorylate Cdc25, a phosphatase which regulates entry in to and progression through the cell cycle (Gould and Nurse 1989) and p53. p53 stimulates expression of p21, a cyclin-dependent kinase (CDK) inhibitor which in turn inhibits CDK activity, thereby causing cell cycle arrest (Pines 1994). DDR can also induce senescence through the p16-pRB pathway. However this usually occurs secondary to the p53 pathway (Campisi and d'Adda di Fagagna 2007). Telomere-induced replicative senescence can be prevented by ectopic expression of the telomerase catalytic subunit TERT (Bodnar, Ouellette et al. 1998). However telomerase cannot prevent senescence which arises from non-telomeric DNA damage or other senescence inducers (Chen, Ijpma et al. 2001).

1.4.3.2 Telomere independent replicative senescence

In addition to short dysfunctional telomeres, other factors have been shown to induce senescence. One of these factors is DNA damage: like telomere-dependent replicative senescence, DNA damage induced senescence depends strongly on p53 and is usually accompanied by expression of p21. Chromatin perturbation also causes senescence, particularly the promotion of euchromatin formation by histone deacetylase inhibitors (HDACi) (Ogryzko, Hirai et al. 1996, Munro, Barr et al. 2004). The mechanism by which senescence is induced upon HDACi treatment is poorly understood and seems to differ depending on species and cell type: in human fiboblasts HDACi induces expression of p21 and p16 and is dependent on the presence of pRB whereas in mouse fibroblasts the p53 pathway is more important for senescence induction (Ogryzko, Hirai et al. 1996, Munro, Barr et al. 2004). Another senescence-inducing factor is oncogene expression: Expression of oncogenic RAS in normal human fibroblasts results in permanent G1 arrest (Serrano, Lin et al. 1997). Senescence was similarly induced upon overexpression of other members of the RAS signalling pathway such as RAF, MEK and BRAF (Lin, Barradas et al. 1998, Zhu, Woods et al. 1998, Michaloglou, Vredeveld et al. 2005). Since expression of such oncogenes stimulate cell growth it is considered that oncogene-induced senescence is a tumour suppressor mechanism (Braig and Schmitt 2006).

1.4.4 The end replication problem

Another function of the telomere is to provide a solution to the end replication problem. The end replication problem arises during the semi-conservative replication of a linear DNA template (Olovnikov 1973). Due to the ability of DNA polymerases to synthesize DNA only in the 5’ to 3’ direction, the lagging strand must be synthesised in a discontinuous manner using short RNA primers to prime DNA synthesis. Removal of these primers results in the presence of short DNA sequences or Okazaki fragments typically ~100bp in length (Timson,

Singleton et al. 2000) interspersed by gaps 8-12 nucleotides long. These gaps are subsequently filled in by extension of the DNA fragments and ligated. Removal of the terminal primer however leaves in a gap that cannot be filled resulting in a loss of nucleotides with each successive round of replication (Watson 1972). The end replication problem is summarised in fig. 1.2.

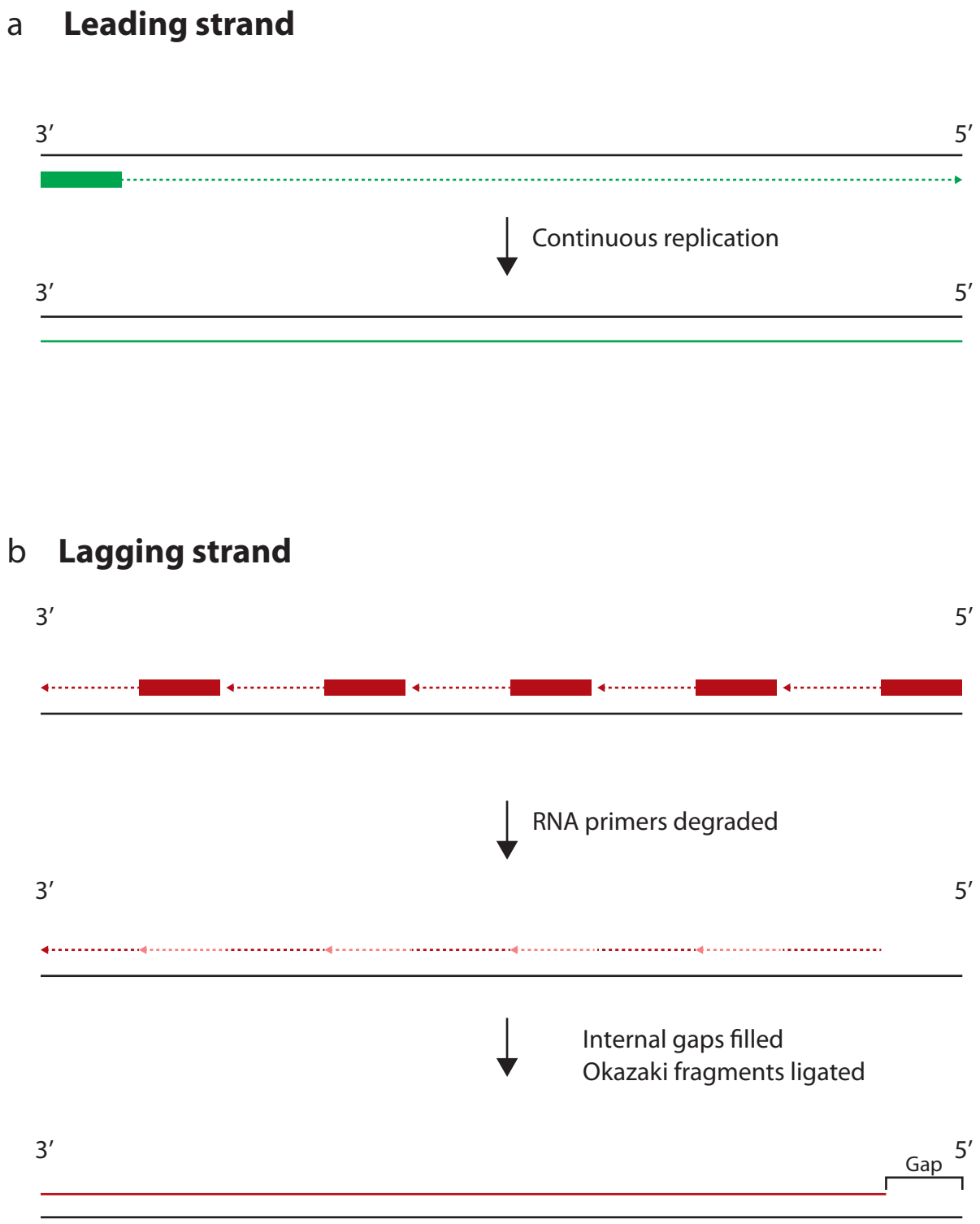

Figure 1.2. Representation of the end replication problem. (a) The 3'–5' leading strand is copied continuously to the end of the DNA molecule using DNA polymerase. (b) The 5'–3' lagging strand is copied in discontinuous Okazaki fragments extended from RNA primers. The RNA primers are then degraded, the internal gaps are filled, and the Okazaki fragments ligated. The 5′ end gap is not filled, leaving an unreplicated terminal region. Adapted from 'The disparity between human cell senescence in vitro and lifelong replication in vivo' *Rubin, Nature Biotechnology 20, 675 - 681 (2002)*

1.5 Telomere elongation

1.5.1 Telomerase

Telomerase is a ribonucleoprotein reverse transcriptase which was discovered in *Tertahymena thermophilia* (Greider and Blackburn 1985) and since been detected in protozoa (Shippen-Lentz and Blackburn 1989, Zahler and Prescott 1989) , fungi (Cohn and Blackburn 1995, Lingner, Cech et al. 1997), and mammals (Morin 1989, Prowse, Avilion et al. 1993).

1.5.1.1 Structure

Telomerase has a dimeric structure, consisting of two copies of a unique catalytic reverse transcriptase protein protein (TERT in humans) and a large RNA component (TERC in humans) from which the telomeric repeats are copied (Lingner, Hughes et al. 1997) and several species-specific telomerase accessory proteins.

TERT consists of three main structural elements: a short C-terminal extension, a central catalytic RT domain and a long N-terminal extension which itself contains a TEN domain and the telomerase RNA-binding domain (TRBD), both of which are involved in binding single stranded nucleic acids (Jacobs, Podell et al. 2006, Rouda and Skordalakes 2007).

TERC consist of three domains, the pseudoknot/template core domain which contains the template for telomere addition, the CR4/CR5 domain and a box H/ACA domain which serves as a binding site for proteins involved in RNA processing and subcellular localisation (Wyatt, West et al. 2010).

In addition to TERT and TERC, several species-specific telomerase accessory proteins are

associated with the complex which regulate its biogenesis, subcellular localisation and functionality (Wyatt, West et al. 2010). Mass spectometric analysis of purified telomerase from HeLa cells identified the pseudouridine synthase dyskerin (DKC1) along with the NTPase proteins NHP2, NOP10, the closely related ATPases pontin/reptin and TCAB1 (telomerase Cajal body protein 1) as integral protein components of the enzyme (Mitchell, Wood et al. 1999, Cohen, Graham et al. 2007, Fu and Collins 2007, Venteicher, Meng et al. 2008, Venteicher, Abreu et al. 2009). Dyskerin, NHP2 and NOP10 are required for the stability and accumulation of TERC (Mitchell, Wood et al. 1999, Cohen, Graham et al. 2007, Fu and Collins 2007, Venteicher, Meng et al. 2008, Venteicher, Abreu et al. 2009). Similarly pontin/reptin are necessary for the stability of TERC (Mitchell, Wood et al. 1999, Cohen, Graham et al. 2007, Fu and Collins 2007, Venteicher, Meng et al. 2008, Venteicher, Abreu et al. 2009). TCAB1 however is thought to exert its influence on telomerase by affecting its subcellular localisation (Mitchell, Wood et al. 1999, Cohen, Graham et al. 2007, Fu and Collins 2007, Venteicher, Meng et al. 2008, Venteicher, Abreu et al. 2009, Stern, Zyner et al. 2012).

1.5.1.2 Function

Telomerase catalyzes the *de novo* addition of TTAGGG repeats onto a telomere end. It is believed that the process is primed by the single-strand 3' telomeric overhangs. New telomeric sequence is synthesised by TERT adding dNTPs onto the 3' end using the TERC component as the template for reverse transcription. When the 5'-template boundary is reached a translocation step repositions the newly synthesised DNA 3' end within the template for a second round of telomere synthesis (Wyatt, West et al. 2010). In a single binding and extension event approximately 60 nucleotides are added to a telomere (Zhao, Abreu et al. 2011). Additionally, telomerase has been shown to preferentially elongate shorter telomeres (Kim, Piatyszek et al. 1994, Britt-Compton, Capper et al. 2009) although

another report has suggested that telomerase extends most chromosome ends during each S phase (Zhao, Sfeir et al. 2009).

1.5.1.3 Telomerase regulation

While TERC expression is ubiquitous, TERT expression appears highly regulated. TERT expression and telomerase activity are often very low or undetectable in somatic cells leading to a loss of ~60-120bp per cell division (Harley, Futcher et al. 1990, Baird, Rowson et al. 2003). This telomere attrition is avoided in long-lived cell types such as germ line cells or stem cells as telomerase is expressed (Kim, Piatyszek et al. 1994). In most cancer cells (85-90%) telomerase activity appears elevated. This high telomerase expression is associated with cancer cell immortality and has a role in tumour development (Kim, Piatyszek et al. 1994, Kolquist, Ellisen et al. 1998). A number of transcriptional regulators have been shown to influence TERT transcription including the transcription factors Sp1 and MZF-2: mutations in the Sp1 binding site completely abolishes TERT promoter activity demonstrating its role as a transcriptional activator of TERT (Kyo, Takakura et al. 2008). Conversely inhibition of MZH-2 binding within the TERT promoter resulted in TERT transcription indicating a repressive role of MZH-2 in TERT transcription (Fujimoto, Kyo et al. 2000). Additionally TERT expression has also been shown to be positively regulated by the oncogene c-Myc (Kyo, Takakura et al. 2008).

TERT can also be regulated in a post translational manner. The ubiquitn ligase MKRN1 interacts with TERT in a yeast-two hybrid assay and its overexpression leads to telomerase degradation, decreased telomerase activity and telomere shortening (Kim, Park et al. 2005).

Finally, shelterin components have been implicated in telomerase regulation. TPP1 binds the TEN domain within TERT and, when in complex with other shelterin components TIN2 and POT1, regulates the recruitment of telomerase to a chromosome end (Xin, Liu et al. 2007, Abreu, Aritonovska et al. 2010, Nandakumar, Bell et al. 2012, Zhong, Batista et al. 2012).

1.5.2 Alternative Lengthening of Telomeres (ALT pathway)

The existence of a telomerase-independent telomere lengthening mechanism was first demonstrated in telomerase-null mutant yeast. The mechanism was found to be dependent on the homologous recombination protein RAD52 (Lundblad and Blackburn 1993). The existence of a similar pathway in humans was first discovered in immortalized human cell lines in which telomere length was shown to be maintained for many population doublings in the absence of telomerase (Bryan, Englezou et al. 1995). It has since been found that in 15% of all human cancers, telomere length is maintained by the ALT pathway (Cesare and Reddel 2010). Although it is agreed that telomere lengthening via the ALT pathway requires a DNA recombination the precise mechanism by which this occurs is unknown. Two models have been proposed to try and explain the process. The first, the Unequal T-SCE model proposes that unequal telomere sister chromatid exchanges (T-SCEs) can result in one daughter cell inheriting a lengthened telomere and a prolonged proliferative capacity and another daughter cell inheriting a shorter telomere and with it a decreased proliferative capacity. The second model involves lengthening of telomeres from recombination-mediated synthesis of new telomeric DNA using an existing telomeric sequence from an adjacent chromosomal telomere as a copy template (Cesare and Reddel 2010). Cells in which telomeres maintain their length via the ALT pathway (or ALT cells) have been shown to possess telomeres extremely heterogeneous in length (Bryan, Englezou et al. 1995). Another phenotypic characteristic of ALT cells include an abundance of extrachromosomal

telomeric DNA which may exist as double stranded telomeric circles (t-circles), partially stranded circles (G or C circles), linear double stranded DNA or very high molecular weight 't-complex' DNA that is likely to contain abnormal, highly branched (Ogino, Nakabayashi et al. 1998, Tokutake, Matsumoto et al. 1998, Cesare, Quinney et al. 2003, Cesare and Griffith 2004, Henson, Cao et al. 2009, Nabetani and Ishikawa 2009). Additionally, a further characteristic of ALT cells is the presence of ALT-associated PML bodies (APBs) (Yeager, Neumann et al. 1999).

1.6 Telomere length analysis

1.6.1 Terminal Restriction Fragment (TRF) analysis

TRF analysis involves digestion of genomic DNA with restriction enzymes (in humans usually a double digest with *Hinf*I and *Rsa*I). These enzymes digest the majority of genomic DNA but not within the telomere repeat tract leaving terminal restriction fragments. These fragments are resolved on an agarose gel and detected by telomere repeat containing probes following southern blot or in-gel hybridization (Baird 2005). TRF analysis has a number of benefits: it is relatively easy and cheap to perform and is also broadly applicable to many different tissue types. Despite these advantages TRF analysis does have its drawbacks: it requires large amounts of DNA which can be a limiting factor when analysing small tissue or cell samples and also severely limit the resolution. Finally there is a telomere length threshold below which TRF analysis will not detect. As the method relies on the degree of hybridization very low hybridization will occur at very short telomeres.

1.6.2 Quantitative fluorescence in situ hybridization (Q-FISH)

Q-FISH, developed by Peter Lansdorp (Lansdorp, Verwoerd et al. 1996), involves the hybridization of fluorescently-labelled nucleic acid probes to metaphase chromosome preparations. Telomere length of individual chromosome ends is represented by Telomere Fluorescence Units (TFUs). Its development revealed the heterogeneity displayed between telomeres of different chromosome ends within the same cell (Lansdorp, Verwoerd et al. 1996). Additionally it showed that some chromosome ends (for example 17p) appear to be shortest in unrelated individuals (Martens, Zijlmans et al. 1998). Q-FISH has a number of advantages over TRF analysis: it has a higher resolution, can be applied when using small populations of cells and it allows telomere-specific length measurements to be made.

However translating TFU accurately into actual DNA length is problematic and, like TRF analysis, it is hybridization-based therefore there is a telomere length threshold below which telomeres cannot be detected by Q-FISH. Furthermore Q-FISH can only be applied to proliferating cells in culture, senescent cells cannot be analysed.

1.6.3 Flow-FISH

Flow-FISH is another telomere length analysis developed from the Lansdorp group. It involves combining telomere FISH with flow cytometry to provide telomere length assessment (Rufer, Dragowska et al. 1998). The development of mulitcolour flow-FISH allows telomere length to be measured in specific haematopoietic subpopulations (Plunkett, Soares et al. 2001) and has become the method of choice when analysing telomere length dynamics of the immune system (Baird 2005).

1.6.4 qPCR

qPCR-based measurement of telomere length was developed by Cawthon (2002). Telomere length is measured using primers which bind telomeric repeats. As telomere length increases the number of sites to which the primer can anneal to increases. The amplification signal generated at the telomere is then compared to signal from a single copy gene within the same sample providing a measurement of relative telomere length. The technique has since been modified by the addition of an oligomer standard which allows measurement of absolute telomere length (O'Callaghan and Fenech 2011). This development has the obvious benefits of allowing a more direct comparison between of telomere length to be made between experiments and between laboratories. The advantages of this technique are the high throughput nature of it and also comparatively small amounts of starting material required compared to other methods of telomere analysis. However like TRF analysis chromosome-specific analysis is not possible.

1.6.5 Single Telomere Length Analysis (STELA)

TRF and other DNA based analyses of telomere length are broadly applicable to numerous cell or tissue samples however they lack resolution. Q-FISH on the other hand provides very high resolution however it is only applicable to certain cell types (Baird 2005). STELA was developed to allow a similarly high resolution analysis of telomere length to Q-FISH but which has the broad application range that TRF analysis allows.

STELA is a single-molecule PCR based telomere length analysis that determines the distribution of telomere lengths at a specific chromosome end (Baird 2005). A linker repeat unit is ligated to the 5' end of the telomere providing a unique sequence tag (fig. 1.3). DNA is diluted such that 4-8 telomeric molecules are amplified in a PCR reaction using a chromosome specific primer and teltail, a primer which specifically anneals to the linker repeat unit. PCR products are resolved with agarose gel electrophoresis and then detected by southern hybridization using a telomere-specific probe. STELA was originally designed at the XpYp chromosome end. By designing primers around the extensive sequence polymorphisms in XpYp telomere-adjacent DNA the individual alleles can be analysed in isolation (Baird, Rowson et al. 2003). The technique has since been further developed for the 2p, 9p, 11q, 12q, 16q, 17p and 18q chromosome ends (Britt-Compton, Rowson et al. 2006) and also to the model organism *C. elegans* (Cheung, Schertzer et al. 2004). STELA has allowed the detailed analysis of telomere loss by the end replication problem and also identified additional mutational mechanisms that are required to create severely truncated telomeres (Baird 2005). Its increased sensitivity compared to TRF analysis was demonstrated by the observation of telomere length in senescent cells: whereas TRF based estimates indicated that telomere length at the point of replicative senescence was around 4kb. However, when measured by STELA, chromosome ends were shown to be virtually devoid of

telomere repeats (Baird, Rowson et al. 2003). This key advantage of STELA to detect very short telomeres has led to the definition of a 'threshold' length below which telomeres have eroded to the point at which they become dysfunctional (Capper, Britt-Compton et al. 2007, Lin, Letsolo et al. 2010). STELA is limited in the fact that it is only applicable to chromosome ends which contain unique telomere-adjacent sequences to design primers around. Additionally it is somewhat labour intensive and due to the requirement of high quality DNA is unlikely to be applicable to degraded or fixed material (Baird 2005).

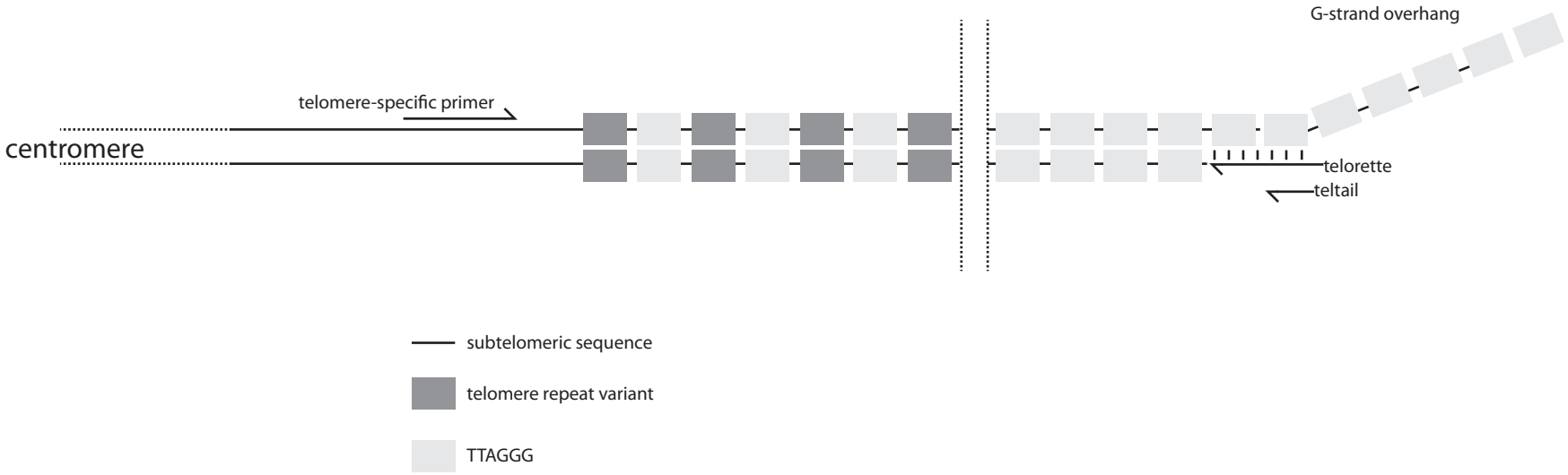

Figure 1.3. Representation of STELA PCR A 'telorette' linker is designed that is complementary to 7bp overhang at the telomere end. The teltail primer binds the telorette linker. Amplification occurs between the teltail primer and the telomere specific primer incorporating polymorphisms specific to the telomere-adjacent sequence of a particular chromosome end. Adapted from 'Extensive allelic variation and ultrashort telomeres in senescent human cells' *Baird et al. Nature Genetics 33, 203 - 207 (2003)*.

1.7 Telomeres and disease

1.7.1 Cancer

Telomere-dependent replicative senescence limits the proliferative capacity of somatic cells however it can be bypassed by inactivation of the p53 and Rb pathways (Lane 1984). Continued cell division eventually leads to 'crisis', a second proliferative barrier characterised by extensive genomic instability and large amounts of cell death (Counter, Avilion et al. 1992). Rare cells emerge from crisis and these cells almost universally express telomerase which maintain the short but stable telomeres and thus promote the formation of cancer (Shay and Wright 2011). Evidence supporting a role of telomerase in cell immortaliztion was provided by Bodnar, Ouellette et al. 1998 who found that constitutive ectopic expression of telomerase in pre-senescent human cells or in cells between senescence and crisis was sufficient to induce immortalization by stabilizing telomere length. Over 90% of human malignancies maintain their telomere length through reactivation of telomerase (Kim, Piatyszek et al. 1994) highlighting its role in cancer cell immortalization. This model of cancer progression suggests that the initiating cell (or cancer stem cell) is likely to have very short telomeres when telomerase is reactivated and recent evidence supports this idea (Marian, Cho et al. 2010, Marian, Wright et al. 2010).

Certain human cancers however do not maintain telomere length through telomerase reactivation but instead regulate telomere length through the ALT pathway (Bryan, Englezou et al. 1997, Dunham, Neumann et al. 2000). Although ALT occurs in common cancers, such as breast carcinomas, it tends to be most prevalent in tumours of mesenchymal origin (Stewart and Weinberg 2006).

1.7.2 Diseases associated with telomere dysfunction

In the past decade a role for telomere dysfunction has been found in a number of diverse degenerative disease states. Telomere dysfunction that drives these syndromes can be brought about through mutations in genes encoding telomerase subunits and its accessory proteins or through mutations in genes encoding other telomere –associated proteins which result in telomere defects.

1.7.2.1 Telomerase dysfunction in disease

Mutations in the genes encoding telomerase or telomerase accessory proteins have been observed in Idiopathic Pulmonary Fibrosis (IPF) and Dyskeratosis Congenita (DKC).

Dyskeratosis Congenita (DC) is a rare inherited syndrome characterised by abnormal skin pigmentation, bone marrow failure, nail dystrophy and leukoplakia (Marrone and Mason 2003). Two distinct forms of DC exist: one is a X-linked form and an autosomal dominant form. The X-linked form is due to mutation in the dyskerin gene at Xq28. The encoded dyskerin protein interacts with the RNA template of the telomerase complex (TERC) as well as a small subgroup of small nucleolar RNAs. Because of this second interaction it was initially difficult to conclude that telomere dysfunction specifically was responsible for the disease (Ruggero, Grisendi et al. 2003). However the discovery that the autosomal dominant form of the disease results from mutation in the TERC gene shows that this disease is due to defects at the telomere. All patients with DKC have very short telomeres (Vulliamy, Marrone et al. 2001).

Idiopathic Pulmonary Fibrosis (IPF) is a fatal lung disease characterised by lung scarring and abnormal gas exchange (Gross and Hunninghake 2001). Two types of the disorder exist; familial IPF and sporadic IPF. Heterozygous mutations in the genes encoding TERT and TERC

have been found in 8-13% of familial IPF cases (Armanios, Chen et al. 2007, Tsakiri, Cronkhite et al. 2007) while TERT mutations have been observed in 3% sporadic IPF. All these mutations result in telomere shortening (Garcia, Wright et al. 2007).

1.7.2.2 Dysfunctional telomere-associated proteins in disease

A number of aging disorders have been directly linked to telomere dysfunction. One of these syndromes is Fanconi anemia (FA), an autosomal recessive disease caused by mutations in the Fanconi genes (Aubert and Lansdorp 2008). Affected individuals display a progressive bone marrow failure and have an increased predisposition to cancer as well as skin, skeletal, genitourinary, gastrointestinal, cardiac and neurological anomalies (Dokal 2006). Telomere shortening is associated with FA as is telomerase activation (Leteurtre, Li et al. 1999). Additionally abnormalities in telomere replication or repair are thought to play a role in the pathogenesis of the disease (Aubert and Lansdorp 2008).

Ataxia Telangiectasia (AT) is another autosomal recessive disease. The responsible mutation for this disease is found in the ATM gene which encodes the ATM kinase protein (Savitsky, Sfez et al. 1995). AT is characterised by neurological deterioration, immunodeficiency and premature ageing. AT sufferers are also predisposed to cancer, particularly T cell leukaemia and lymphoma (Metcalfe, Parkhill et al. 1996). An increased number in telomere-telomere fusions as well as accelerated telomere attrition has been observed in AT patients (Metcalfe, Parkhill et al. 1996).

1.8 Chromatin structure

In eukaryotic organisms, nuclear DNA exists not as naked DNA, but in complex with protein in a structure called chromatin. The most obvious advantage of this DNA:protein complex is that it provides a method of DNA compaction. However the dynamic adjustment of chromatin between a more condensed state (heterochromatin) and a more open, accessible state (euchromatin) also provides another level of regulation acting on the DNA. Whether chromatin exists in either the relaxed euchromatic state or as the inaccessible and highly ordered heterochromatic state depends on a number of factors: The DNA sequence, chromosomal location influences chromatin compaction; repetitive DNA elements found at centromeres and telomeres promote a heterochromatic state. Localization within the nucleus also plays a part in chromatin state but the biggest factor to influence how euchromatic or heterochromatic chromatin is the plethora of proteins that function to alter the chromatin structure. These proteins either act directly on the residues on histone tails altering the interactions between histones and DNA or they utilise the energy derived from the hydrolysis of ATP to physically alter the chromatin structure, these proteins exist in complexes and are referred to as ATP-dependant chromatin remodelling complexes.

1.8.1 Histones and Nucleosomes

The existence of nucleosomes was first suggested based on the observation by electron microscopy that chromatin appeared to adopt a ‘beads on string’ structure (Kornberg 1974, Olins and Olins 1974, Woodcock, Safer et al. 1976). Further evidence was provided by Thomas and Kornberg (1974) who chemically cross-linked histones in chromatin. This experiment demonstrated that H2A, H2B, H3 and H4 form a discrete protein octamer within in the chromatin fibre.

It is this octamer of the core histones H2A, H2B, H3 and H4 which, in complex with DNA, makes up the nucleosomal core particle. The structure of nucleosome reveals a tripartite assembly of the octamer; H3 and H4 are organised into a central $(H3/H4)_2$ tetramer which is flanked by two peripheral H2A/H2B dimers. Nucleosomal assembly is initiated by binding of 121bp DNA around the central H3/H4 tetramer, binding of the two H2A/H2B dimers to either side of the tetramer extends DNA binding up to 147bp (Nemeth and Langst 2004). DNA is wrapped around the nucleosome ~1.65 times, severely distorting the DNA path, and compacting the DNA about 7-fold (Nemeth and Langst 2004). Binding of the linker histone H1/H5 organises an additional 20bp to complete the nucleosome (Robinson and Rhodes 2006). This binding of H1 stabilises the structure of the nucleosome and determines the trajectory of DNA entering and exiting the nucleosome, it is for this reason that it is thought that the linker histones play an important role in the relative positioning of successive nucleosomes and thus the higher order chromatin structure (Robinson and Rhodes 2006). In the 'beads on string' structure the nucleosomes (beads) are separated by linker DNA (string). *In vivo* this linker DNA varies in length from 160bp in yeast to over 220bp in higher organisms (Nemeth and Langst 2004).

1.8.2 Histone Structure

The basic structure of a histone can be divided into two domains: the C terminal histone fold domain and the N- terminal tail domain. Additionally, histones H1 and H2A contains a C-terminal tail domain (Hansen 2002). The histone fold domain is required for the organisation of the histone octamer and DNA binding whereas the tail domains form linker DNA and inter-nucleosomal interactions, thereby modulating the formation of the higher order chromatin structure (Nemeth and Langst 2004). Furthermore residues residing within histone tails are the main target for post-translational modifications such as acetylation, methylation and phosphorylation.

1.8.3 Structure of the Chromatin Fibre

Although much is known about the nucleosomal structure, the arrangement of the higher order chromatin structure remains largely uncharacterized. Nucleosomes are able to compact into tightly folded filamentous structures at physiological salt concentrations. Early work focusing on the higher order chromatin structure was performed using electron micrographs of thin sections of HeLa metaphase chromosomes. It showed the presence of thick 30nm fibres which were dependent on ionic strength and the presence of a linker histone (Marsden and Laemmli 1979, Thoma, Koller et al. 1979). Subsequent studies using X-ray diffraction patterns and electric dichroism have supported this view (McGhee, Nickol et al. 1983, Widom and Klug 1985) however the specific nature of nucleosome-to-nucleosome interactions and the path of linker DNA has remained elusive (Robinson and Rhodes 2006).

Two main models have been proposed to explain the structure of the 30nm chromatin fibre: the one-start helix, or solenoid and the two start helix. The one-start helix proposes that a single 10nm nucleosomal array is arranged in a radial manner by bent linker DNA into a one-start stack and the accumulation of these stacks forms the solenoid 30nm fibre (Finch and Klug 1976). The two-start helix is based on a zigzag arrangement of nucleosomes with straight linker DNA connecting the nucleosomes on the opposite sides of the fibre (Williams, Athey et al. 1986, Woodcock, Grigoryev et al. 1993).

It has been suggested that electrostatic interactions between nucleosomes are the driving force in chromatin fibre compaction (Robinson and Rhodes 2006). These interactions are favoured by increasing salt concentrations which reduce the repulsive forces between linker DNA (Sun, Zhang et al. 2005) and are therefore likely to be altered by post translational modifications that alter the charge of histone tails (Jenuwein and Allis 2001). It has been shown that a key inter-nucleosomal interaction is mediated by the histone H4 tail as its

deletion inhibits chromatin fibre folding (Dorigo, Schalch et al. 2003). Furthermore acetylation of the lysine 16 residue within histone H4 is sufficient to disrupt nucleosome-nucleosome contacts and cause fibre unfolding (Shogren-Knaak, Ishii et al. 2006). The linker histone H1 is also a key mediator in chromatin compaction as its removal leads to de-condensation (Fan, Nikitina et al. 2005).

Higher order structures beyond the 30nm fibre are even less well characterised. Two models (basic radial loop and chromonema) have been proposed to offer an explanation. The basic radial loop model suggests that compacted 30nm fibres form DNA loops of 50-100kb in length fixed to a central protein scaffold (Marsden and Laemmli 1979, Rattner and Lin 1985, Boy de la Tour and Laemmli 1988). In the chromonema model chromosome structures arise from three helical folding levels of chromatin fibres. Fibres of 60-nm in width are further coiled into a 100-130nm fibres which themselves are coiled into the 200-300nm structure of the metaphase chromatid (Belmont, Sedat et al. 1987, Belmont and Bruce 1994).

1.8.4 Heterochromatin and Euchromatin

The terms euchromatin and heterochromatin have been used ubiquitously to refer to the states of compaction of chromatin. Euchromatin describes a relaxed, decondensed state which is associated with actively transcribed regions of the genome whereas heterochromatin describes highly condensed, inaccessible and gene-poor chromatin domains. Heterochromatin can be further divided into two categories: constitutive and facultative. Constitutive heterochromatin remains condensed throughout an organisms lifespan and is usually found in repetitive regions of the genome such as centromeres and telomeres (Craig 2005). Facultative heterochromatin on the other hand is not permanent, it is inducible and can form anywhere in the genome. Its formation is required for mating-type switching in yeast, X-chromosome inactivation and developmental progression in

mammalian cells (Oberdoerffer and Sinclair 2007). Recent evidence however has suggested the existence of four or five heterochromatic states in animals in plants (Roudier, Ahmed et al. 2011, van Steensel 2011), each characterised by different combinations of epigenetic marks.

The dynamic adjustment between euchromatic and heterochromatic states has been demonstrated to be fundamental to many nuclear processes ranging from transcriptional regulation to the repair of DNA damage and even telomere length maintenance. Proteins responsible for this alteration of chromatin structure can be divided into two broad categories: ATP-dependent chromatin remodelers which directly alter the nucleosomal architecture and covalent chromatin remodelers which mediate the addition and removal of chemical groups to residues within the histone proteins.

1.9 Covalent post-translational modifications to histones

Over 60 different residues within the core histones are subject to post-translational modifications including acetylation, methylation, phosphorylation and ubiquitylation (fig. 1.4). These modifications can either function to alter inter-nucleosomal interactions, thereby altering the higher order chromatin structure, or act as binding sites for the recruitment of other chromatin remodelers who can then exert their own chromatin remodelling activity.

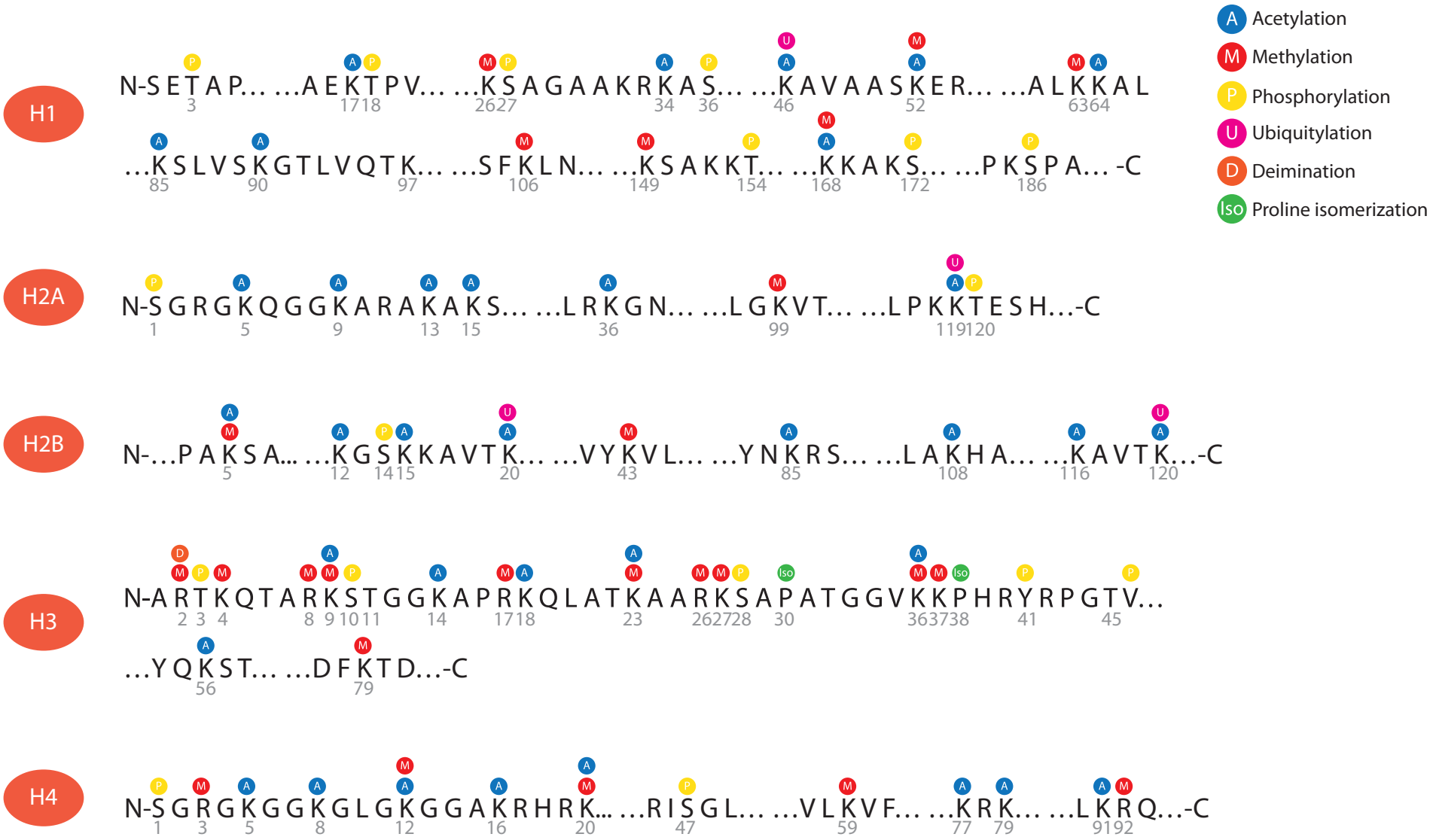

Figure 1.4. Summary of covalent histone modifications on histones H1, H2A, H2B, H3 and H4. The residues subject to post-translational are modifications including acetylation, methylation, phosphorylation, ubiquitylation, deimination and proline isomerization are summarized. The number under each amino acid represents its position in the sequence. Adapted from 'Epigenetic Modifications and Human Disease' P*ortela and Esteller, Nature Biotechnology, 28, 1057-1068 (2010)*

1.9.1 Histone Acetylation

Histone acetylation was the first described histone modification (Phillips 1963). Early studies revealed an association between high levels of histone acetylation and actively transcribed genes indicating a role for histone acetylation in facilitating transcription (Allfrey, Faulkner et al. 1964, Pogo, Allfrey et al. 1966). Subsequent research has suggested that the acetylation of lysine residues neutralizes their positive charge thereby weakening charge-dependent interactions between a histone and nucleosomal DNA, linker DNA or adjacent nucleosomes. Thus accessibility of DNA to transcription machinery is increased (Zentner and Henikoff 2013). Supporting evidence for such a model has been provided with a number of findings: *in vitro* tetra-acetylation of the histone H4 tail substantially reduced its affinity for DNA (Hong, Schroth et al. 1993) and *in vivo* altering the position of lysine on the tail does not alter its effect on the phenotype (Megee, Morgan et al. 1995).

In addition to neutralizing the positive charges of lysine residues, acetylation of lysine residues also provide a binding site for bromodomain-containing proteins. First described in the *Drosophila* brahma chromatin-remodeling enzyme (Tamkun, Deuring et al. 1992), bromodomains have been found in a wide variety of chromatin-associated proteins including histone acetyltransferases and chromatin remodelling proteins (Zeng and Zhou 2002).

1.9.2 Histone Acetyltransferases (HATs)

Histone acetylation is mediated by histone acetyltransferases (HATs). The process involves the transfer of an acetyl group from the acetyl coenzyme A metabolic intermediary to the ε-amino group of lysine residues on the histone tails (Roth, Denu et al. 2001). There are two major classes of HATs: type A and type B. Type B HATs are predominantly cytoplasmic and acetylate free histones including H4 at K5 and K12 (as well as certain sites within H3) but not

histones already deposited into chromatin. This class of HAT is highly conserved, all HATs within this class share sequence homology to yeast Hat1, the founding member of this type of HAT (Bannister and Kouzarides 2011). Type A HATs are more diverse and can be subdivided into three separate groups, GNAT, MYST and CBP/p300 based on amino acid structure and conformational structure (Hodawadekar and Marmorstein 2007). Each of these enzymes modify multiple sites within histone tails and also sites present within the globular histone core such as H3K56 which is acetylated by GCN5 in human cells (Tjeertes, Miller et al. 2009). In common with many histone-modifying enzymes, type A HATs are often found in large multi-protein complexes (Bannister and Kouzarides 2011).

1.9.3 Histone Deacetylases (HDACs)

The functional importance of histone acetylation is due to its highly reversible nature (Sengupta and Seto 2004). This depends on the removal of acetyl groups from histone lysine tails or deacetlyation, a process catalyzed by the histone deacetylase enzymes (HDACs). Mammalian HDACs are divided into four classes based on sequence homology to the yeast HDACs and domain organisation. The class I histone deacetylases include HDAC1, 2, 3 and 8 and have homology to the yeast Rpd3 (reduced potassium dependency 3) HDAC. HDAC4, 5, 7 and 9 belong to class II and have homology to yeast HDA1 (histone deactylase I). HDAC6 and HDAC10 contain two catalytic sites and are classified as class IIa whereas HDAC11 has conserved residues in its catalytic centre shared by both class I and class II HDACs and is sometimes placed in class IV. All these classes of HDACs contain zinc in their catalytic site and are inhibited by HDAC inhibitor compounds such as trichostatin A and vorinostat (Dokmanovic, Clarke et al. 2007). The remaining HDAC class not only differ in their sequence composition to other class HDACs but also in their insensitivity to HDAC inhibitors. Additionally they require the coenzyme NAD+ as a cofactor where the others do not. This class (class III) is made up of the sirtuin proteins (SIRT1, 2, 3, 4, 5, 6 and 7) (Dokmanovic,

Clarke et al. 2007). HDACs have relatively low substrate specificity by themselves, a single enzyme is capable of deacetylating multiple lysine residues within histones (Bannister and Kouzarides 2011). However these enzymes are usually present within multiple distinct protein complexes and the complex a HDAC resides in influences its recruitment and substrate specificity. Additionally several HDAC family members can be present within the same complex: HDAC1 and HDAC2 are present within the NuRD, Sin3a and Co-REST complexes (Bannister and Kouzarides 2011).

1.9.4 Histone methylation

Unlike acetylation and phosphorylation histone methylation does not alter the charge of a histone (Bannister and Kouzarides 2011). Another distinction between histone acetylation and methylation is that whereas histone acetylation generally correlates with transcriptional activation and a more relaxed euchromatic conformation, histone methylation can signal either activation or repression depending on the sites of methylation. Furthermore an extra level of complexity of histone methylation lies in the fact that different forms of methylation can occur: arginine residues can be either mono-methylated and either symmetrically or asymmetrically di-methylated whereas lysine residues can be mono-, di- or tri-methylated. Histidine residues have also shown to be subject to mono-methylation however this modification appears to be rare and is not well characterised (Greer and Shi 2012).

Sites of arginine methylation include H3R2, H3R8, H3R26 and H4R3. However histone methylation research has tended to be focused on the methylation of lysine residues due to the functional importance of this modification. A number of lysine residues throughout all the histone protein have been identified as targets for methylation. The most extensively studied histone lysine methylation sites are H3K4, H3K9, H3K27, H3K36, H3K79 and H4K20.

The classical view of the functional consequences of histone lysine methylation is that H3K4, H3K36 and H3K79 methylation was associated with transcriptional activation and a relaxing of the chromatin structure whereas H3K9, H3K27 and H4K20 methylation mediated transcriptional repression and heterochromatin formation. More recently it has been shown that the effect of histone methylation is not so clear-cut with the degree of methylation (me1, me2 or me3) having a major impact on chromatin structure. For example tri-methylation of H3K9 and H3K27 leads to repression and inactivation however H3K9me1 and H3K27me1 is enriched in actively transcribed genes (Snowden, Gregory et al. 2002, Plath, Fang et al. 2003, Barski, Cuddapah et al. 2007, Kotake, Cao et al. 2007). Furthermore there are instances were the same modification can have opposing activities: H3K9me3 is implicated in the gene silencing and heterochromatin formation by recruiting the further methylating enzymes and heterochromatin protein 1 (HP1) however this mark is also enriched in the coding region of active genes (Vakoc, Mandat et al. 2005). Similarly, H3K4me3 are generally associated with transcriptional activation but they have also been associated with transcriptional repression (Shi, Hong et al. 2006). It is thought that the differing effects of a histone modification are determined by the effector or 'reader' proteins which they bind (Greer and Shi 2012).

Whereas histone acetylation and phosphorylation have direct effects on nucleosome-nucleosome and nucleosome-DNA interactions, histone methylation appears to exert its influence on chromatin structure by the chromatin remodelling proteins it binds. Notably there are more distinct domain types recognising lysine methylation than any other modification. These include the PHD fingers and the Tudor 'royal' family of domains which comprises of chromodomains, Tudor, PWWP and MBT domains (Maurer-Stroh, Dickens et al. 2003, Kim, Daniel et al. 2006, Champagne and Kutateladze 2009). Proteins which posses these domains can bind methylated histone lysine residues and then recruit further

chromatin modifiers. For example H3K4me3 is recognised by the PHD finger within the inhibitor of growth family member 2 (ING2) which tethers the repressive mSin3a-HDAC1 HDAC complex to active proliferation-specific genes following DNA damage (Shi, Hong et al. 2006). A further example is at telomeric chromatin in mice: H3K9me3 provides a high-affinity binding site for heterochromatin protein 1 (HP1). HP1 then interacts with the Suv4-20h1 and Suv4-20h2 histone methyltransferases to promote establishment of telomeric H4K20me3 (Garcia-Cao, O'Sullivan et al. 2004, Benetti, Gonzalo et al. 2007).

1.9.5 Histone methyltransferases

Arginine methylation is performed by a large 11-member family referred to as the PRMTs. All of these enzymes transfer a methyl group from S-adenosylmethionine (SAM) to the ω-guanidino group or arginine (Bannister and Kouzarides 2011). The PRMTs can be divided into two subcatergories: the type-I and type II enzymes. The type-I enzymes monomethylate and asymmetrically di-methylate arginine residues whereas the type-II enzymes mono methylate and symmetrically di-methylate arginine residues.

The methylation of lysine residues within histones is mediated by the histone lysine methyltransferases (HKMTs). Like arginine methyltransferases, all HKMTs catalyse the removal of a methyl group from SAM. This methyl group is then transferred to a lysine's ε-amino group. The first HKMT identified was the suppressor of variegation protein SUV39H1 which targets lysine 9 on histone 3 (H3K9) (Rea, Eisenhaber et al. 2000). Numerous other HKMTs have since been identified. All such enzymes contain a catalytic SET domain. The exception to this is the DOT1L enzyme which methylates H3K79 found in the globular core of histone H3. Unlike other HKMTs DOT1L does not contain a SET domain (Martin and Zhang 2005). Histone methyltransferases appear to be relatively specific enzymes, not only in the lysine residue they methylate but in some cases also the form of methylation they deposit.

For example the human histone methyltransferase SET7/9 can only mono-methylate the H3K4 residue (Xiao, Jing et al. 2003).

1.9.6 Histone demethylases

Histone methylation was originally considered to be irreversible (Byvoet, Shepherd et al. 1972) however the identification of a H3K4 demethylase, lysine-specific demethylase 1A (KDM1A or LSD1) revealed that this was not the case (Shi, Lan et al. 2004). LSD1 was initially thought to demethylate mono- and di-methylated H3K4 residues only, however it has since been demonstrated that it can also demethylate H3K9 when complexed with the androgen receptor (Klose and Zhang 2007). In 2006, the JMJC family of histone demethylases were discovered. Importantly this family of enzymes can demethylate tri-methylated lysines such as H3K9me3 and H3K36me3 as well as mono-, di-methylated lysine residues (Whetstine, Nottke et al. 2006). Additionally one of the JMJC family members, JMJD6 was shown to be capable of performing a demethylation reaction on the arginine residues H3R2 and H4R3 (Chang, Chen et al. 2007).

1.9.7 Other histone modifications

Other histone modifications have also been identified including histone phosphorylation, deimination, ubiquitylation, sumoylation, ADP ribosylation, β-N-acetylglucosamine addition, proline isomerisation and histone tail clipping.

1.9.7.1 Phosphorylation

Histone phosphorylation occurs on serine, threonine and tyrosine residues predominantly found on histone tails. These residues are phosphorylated by kinases which function by transferring a phosphate group from ATP to the hyroxyl group of the target amino-acid side chain (Bannister and Kouzarides 2011). Whereas histone acetylation neutralizes the positive

charge of a histone lysine tail, phosphorylation adds a significant negative charge to the target histone which alters chromatin structure. Removal of phosphate groups from residues within histones in performed by histone phosphatases. Less is known regarding the roles of histone phosphatases. The best known function of histone phosphorylation takes place during the DNA Damage Response (DDR) where histone H2AX is phosphorylated at the Ser139 residue by the ATR and ATM kinases (Burma, Chen et al. 2001, Ward and Chen 2001). In this scenario H2AX phosphorylation spreads up to two megabases from the break site and is required for the accumulation of other DDR proteins such as MRN, MDC1 and 53BP1 (Fernandez-Capetillo, Chen et al. 2002).

1.9.7.2 Deimination

Deimination or citrullination involves converting arginine to a citruline on histones H3 and H4. In mammalian cells this is carried out by the peptidyl deiminase PAD14 and has the potential to antagonize the activating effect of arginine methylation as citrulline prevents arginines from being methylated. There is also evidence that PAD14 can convert mono-methylated arginine to citrulline, thereby, effectively functioning as an arginine demethylase (Cuthbert, Daujat et al. 2004, Wang, Wysocka et al. 2004).

1.9.7.3 Ubiquitunation

The process of ubiquitylation is distinct from all other histone modifications due to the fact that, whereas others result in relatively small molecular changes to amino acid side chains, ubiquitylation results in a much larger covalent modification (Bannister and Kouzarides 2011). The addition of the 76-amino acid polypeptide ubiquitin to histone lysines is mediated by the E1-activating, E2-conjugating and E3-ligating enzymes (Hershko and Ciechanover 1998). Histone lysine residues can be either mono- or poly-ubiquitylated. Sites for ubiquitylation remain largely elusive, however two sites susceptible for ubiquitylation

have been defined in the H2A and H2B histones. Mono-ubiquitylation of H2AK119 has been shown to be involved in gene silencing (Wang, Wang et al. 2004) and mono-ubiquitylation of H2BK123 plays a role in transcriptional initiation and elongation (Lee, Shukla et al. 2007, Kim, Guermah et al. 2009).

1.9.7.4 Sumoylation

Sumoylation is a similar to ubiquitylation in that asimilar group of enxymes (E1, E2 and E3) are required for its deposition on histone lysine residues. Sumoylation by these enzymes involves the addition of a small ubiquitin-like modifier molecule (SUMO) to lysine residues on all four core histones. Although relatively little is known about the function of sumoylation it appears to be a repressive modification and antagonizes the acetylation and ubiquitylation which may otherwise occur on the same lysine residue (Shiio and Eisenman 2003, Nathan, Ingvarsdottir et al. 2006).

1.9.7.5 ADP ribosylation

Arginine and glutamine residues within histones have been shown to be either mono-ADP ribosylated by the MART (Mono-ADP-ribosyltransferase) enzymes or poly-ADP ribosylated by the PARP (poly-ADP-ribose polymerase) enzymes (Bannister and Kouzarides 2011). Additionally, the Sir family of histone deacetylases have also been shown to possess low levels of ADP-ribosylation activity (Hassa, Haenni et al. 2006). Although little is known concerning the function of the modification, levels of poly-ADP ribosylated histones have been correlated with a relaxed chromatin state (Hassa, Haenni et al. 2006). Mono-ADP ribosylation has been detected on all four core histones as well as on the linker histone H1. These modifications have been shown to increase upon induction of DNA damage suggesting a role for this modification in the DNA damage response (Hassa, Haenni et al. 2006).

1.9.7.6 β-N-acetylglucosamine

A recent addition to the list of histone modifications is the addition of β-N-acetylglucosamine (O-GlcNAc) to serine and threonine residues within histones (Sakabe, Wang et al. 2010). All four core histones have been shown to be modified by O-GlcNAc. In mammalian cells the addition of O-GlcNAc is performed by a single enzyme, O-GlcNAc transferase, which transfers the sugar from the donor substrate, UDP-GlcNAc to the histone. Similarly the removal of O-GlcNAc is performed by a single enzyme, β-N-acetylglucosaminidase (O-GlcNAcase) (Sakabe, Wang et al. 2010).

1.9.7.7 Histone proline isomerisation

Prolines exist in either a *trans* or *cis* conformation. The states differ by 180° and changes between the two conformations can severely distort the polypeptide backbone (Kouzarides 2007). Proline isomerases have the ability to facilitate this inter-conversion. Nelson, Santos-Rosa et al. 2006 identified the enzyme FRP4 that can isomerize the proline H3P38 in H3. This activity was shown to regulate the levels of methylation of H3K56. Histone proline isomerisation is not, strictly speaking, a covalent histone modification as no chemical groups are added to histone residues.

1.9.7.8 Histone tail clipping

Like histone proline isomerization, histone clipping is not a 'covalent' histone modification although its action can remove histone modifications from a histone. As the name suggests this process involves the removal of part of the histone tail. Histone tail clipping was first identified in *Tertahymena* where the first 6 amino acids of the H3 tail were removed (Allis, Bowen et al. 1980). It has since been identified in yeast and mice were 21 amino acids of H3 are cleaved (Duncan, Muratore-Schroeder et al. 2008, Santos-Rosa, Kirmizis et al. 2009). The

proteolytic enzyme responsible has yet to be determined in yeast, however in mice it was identified as Cathepsin L (Duncan, Muratore-Schroeder et al. 2008).

1.9.7.9 Cross talk between histone modifications

It is important to note that each histone modification does not function in isolation. Modification of one site may have a promotional or antagonistic influence on other modifications. Furthermore a number of modifications may function collectively to regulate the higher order chromatin structure.

Certain modifications have been shown to have an inhibitory effect on the establishment of other modifications. For example, in yeast and mammals di-methylation of H3R2 is prevented by H3K4me3 and conversely H3R2me2 prevents H3K4me3 methylation (Guccione, Bassi et al. 2007, Kirmizis, Santos-Rosa et al. 2007). On the other hand one modification may be dependent on another: in *S. Cerevisiae the* methylation of H3K4 by COMPASS and of H3K79 by Dot1 is dependent on the ubiquitination of H2BK123 by Rad6/Bre1 (Lee, Villa et al. 2007). This mechanism is conserved in humans (Kim, Guermah et al. 2009). The binding of a protein to a particular modification may be affected by adjacent modifications. An example of this is the binding of heterochromatin protein 1 (HP1) to di- and tri-methylated H3K9 which is disrupted by phosphorylation of H3S10 (Fischle, Tseng et al. 2005). Combined modifications can also result in different functional outcomes to the same modifications acting in isolation. This is due to their recognition by proteins with multiple domains. For example, the chromatin regulator TRIM24 contains a PHD domain and a bromodomain which recognise unmethylated H3K4 and acetylated H3K23 on the same histone tail (Tsai, Wang et al. 2010). Additional histone modification 'cross talk' is seen when numerous modifications are competing for the same residue. This is particularly true for lysine residues that can be acetylated, methylated or ubiquitinated.

1.10 Histone variants

Chromatin structure can also be influenced by the incorporation of histone variants. These variant or 'replacement' histones were identified based on the sequence similarity of the primary sequence which can range from just a few amino acids to differences between whole domains. Of all the core histones only H2A and H3 have corresponding histone variants. The incorporation of histone variants into chromatin requires the action of a histone chaperone and this incorporation plays a role in numerous processes including DNA repair, meiotic recombination chromosome segregation, transcriptional regulation, sex chromosome condensation and sperm chromatin packaging (Talbert and Henikoff 2010).

1.10.1 H2A variants

The H2A histone family has been identified to contain four variants including the canonical H2A, H2A.Z, H2A.X and macroH2A.

1.10.1.1 H2A.Z

H2A.Z-containing nucleosomes are found on either side of a nucleosome-free region (NFR) at transcription start sites were they promote efficient RNA polymerase II recruitment in both yeast and human cells (Zhang, Roberts et al. 2005, Jin, Zang et al. 2009). In addition to its transcriptional regulation role it has also been implicated in DNA repair, heterochromatin formation, suppression of antisense RNAs, embryonic stem cell differentiation and antagonizing DNA methylation in plants (Talbert and Henikoff 2010). Swr1, a member of the SWI/SNF family of ATP-dependent chromatin remodelling complexes, is essential for the incorporation of H2A.Z into chromatin. The histone chaperones Nap1 and Chz1 are thought to be responsible for the transfer of H2A.Z-H2B dimers to Swr1 for the exchange of canonical H2A-H2B dimers (Mizuguchi, Shen et al. 2004, Luk, Vu et al. 2007, Straube, Blackwell et al. 2010).

1.10.1.2 H2A.X

H2A.X shares considerable homology with canonical H2A. As previously mentioned, the C-terminus of H2A.X is phosphorylated at Ser139 by ATM, ATR and DNA-PK in response to DNA damage and this phosphorylation is important for the recruitment of downstream DNA damage repair factors (Fernandez-Capetillo, Celeste et al. 2003). It is thought that canonical H2A-H2B chaperones may also be responsible for the deposition and exchange of H2A.X. The H2A-H2B chaperone FACT has been shown to bind H2A.X and catalyse the exchange of H2A-H2B with H2A.X-H2B (Heo, Kim et al. 2008).

1.10.1.3 Macro H2A

MacroH2A consists of an N terminus, which is similar to H2A and a unique, large C terminus. It is enriched in heterochromatin including X chromosome in female mammals and senescence-associated heterochromatin foci (Costanzi and Pehrson 2001) and plays a role in gene silencing (Angelov, Molla et al. 2003). It is also implicated in chromatin rearrangements during the DNA damage response upon PARP1 activation (Timinszky, Till et al. 2009). Although no macroH2A-specific chaperones have been identified, the apratxin-PNK-like factor (APLF) has been shown to bind macroH2A and loss of APLF results in defects in the recruitment of macroH2A to DNA damage sites (Timinszky, Till et al. 2009).

1.10.1.4 H3 variants

Four main H3 variants have been identified. These include two canonical variants H3.2 and the mammalian-specific H3.1 and two replacement variants: H3.3 which is structurally similar to H3.1 and H3.2 and the centromere-specific CenH3 (or CENP-A in mammals) (Allshire and Karpen 2008). H3.3 and CENPA have been studied most extensively and have been found to carry out distinct functions

1.10.1.5 H3.3

In mouse, human and *Drosophila* the H3.3 protein is encoded by the genes H3F3A and H3F3B. Although H3.3 differs structurally to H3.2 and H3.1 by four and five amino acids respectively, its function in the nucleus differs considerably to its canonical counterparts. H3.3 is expressed throughout the cell cycle allowing histone deposition/exchange through a DNA synthesis-independent pathway during or outside of S phase (Szenker, Ray-Gallet et al. 2011). Studies in *Drosophila* and mammalian cells suggested a role for H3.3 in active chromatin as enrichment of H3.3 is present within the gene body as well as at the promoter of actively transcribed genes (Chow, Georgiou et al. 2005, Schwartz and Ahmad 2005, Wirbelauer, Bell et al. 2005, Daury, Chailleux et al. 2006, Delbarre, Jacobsen et al. 2010, Goldberg, Banaszynski et al. 2010) although H3.3 enrichment has also been observed at inactive genes (Mito, Henikoff et al. 2005, Tamura, Smith et al. 2009). In addition to its presence at active and inactive genes and promoter regions, H3.3 is also located at various heterochromatic regions in the genome: it was found at pericentric chromatin in mouse embryonic fibroblast cells (Drané, Ouararhni et al. 2010, Santenard, Ziegler-Birling et al. 2010) and also in human HeLa cells (Hake, Garcia et al. 2005) as well as at telomeres in mouse ES cells (Wong, Ren et al. 2009). Contrary to the proposal of H3.3 marking active chromatin, its presence at the telomere is required for proper heterochromatin formation and transcriptional repression of telomeric repeats (Goldberg, Banaszynski et al. 2010). The incorporation of H3.3 requires the action of various histone chaperones. The histone regulator A (HIRA) was shown to be the chaperone required for incorporation of H3.3 at promoters and within the body of actively transcribed genes (Goldberg, Banaszynski et al. 2010) whereas H3.3 deposition at pericentric heterochromatin and telomeres requires the death domain-associated protein (DAXX) in complex with ATRX, a SNF2-like ATP-dependent chromatin remodelling factor (Lewis, Elsaesser et al. 2010).

1.10.1.6 CenH3

CenH3 (or CENP-A in mammals) exists in multiple forms all of which share 50-60% sequence identity with canonical H3s in the histone fold domain and no similarities whatsoever it N terminal region (Talbert and Henikoff 2010). CenH3 histones are specific to centromeres were they interact with canonical histones to form CenH3 nucleosomes. In *Drosophila* these nucleosomes consist of one molecule each of CID (CenH3), H2A, H2B and H4 and are proposed to resemble half of an octomeric nucleosome (Dalal, Wang et al. 2007) whereas in yeast CenH3 nucleosomes are thought to comprise of two molecules each of Cse4 (CenH3), H4 and suppressor of chromosome missegregation 3 (Smc3) (Mizuguchi, Xiao et al. 2007). Although CenH3 is localized to centromeres, overexpression of CenH3 can lead to its spreading along the chromosome arm (Sullivan, Hechenberger et al. 1994). Little is known about how CenH3 is deposited to centromeres. However in *S. cerevisiae* loss of the histone chaperones Caf1 and Hira affected Cse4 centromeric association and also altered centromeric structure (Sharp, Franco et al. 2002).

1.11 DNA methylation

The most widely studied epigenetic modification in humans is cytosine methylation. It occurs almost exclusively at CpG dinucleotides which tend to cluster within regions referred to as CpG islands. DNA methylation regulates gene silencing by preventing the binding of transcription factors to DNA (Kuroda, Rauch et al. 2009) and by promoting the recruitment of methyl-CpG-binding domain (MBD) proteins. These MBD proteins in turn recruit histone-modifying and chromatin-remodelling complexes to methylated sites (Lopez-Serra, Ballestar et al. 2008). DNA methylation also plays a key role in genomic imprinting as well as in the maintenance of pericentric and subtelomeric heterochromatin (Lehnertz, Ueda et al. 2003, Gonzalo, Jaco et al. 2006, Kacem and Feil 2009)

DNA methylation is mediated by the DNA methyltransferase (DNMT) family. These enzymes catalyse the transfer of a methyl group from S-adenosyl methionine to DNA (Portela and Esteller 2010). In mammals five members of the DNMT family have been reported (DNMT1, 2, 3a, 3b and 3L) although only three (DNMT1, 3a and 3b) possess methyltransferase activity. DNMT3a and DNMT 3b are classified as *de novo* DNMTs responsible for the establishment of the pattern of methylation during embryonic development whereas DNMT1 is considered the maintenance DNMT as it is required for methylation of hemimethylated sites generated during semi conservative DNA replication (Portela and Esteller 2010).

1.12 Transcription of heterochromatin domains

The notion of heterochromatin being a transcriptionally inactive region has been challenged by the discovery of numerous noncoding RNAs (ncRNAs) derived from heterochromatic loci (Portela and Esteller 2010). In *S. pombe* pericentric repeats are transcribed by RNA polymerase II and subsequently processed by the RNA-dependent RNA polymerase (RdRP) Rdp1, and Dicer (Volpe, Kidner et al. 2002). Small RNAs (22-24 nucleotides) are then assembled into the RNA-induced transcriptional silencing (RITS) complex providing sequence specificity to the complex. The RITS complex is required for H3K9 methylation of centromeric repeats and recruitment of the histone methyltransferase Clr4, which is essential for the spreading of the heterochromatin domains (Portela and Esteller 2010). ncRNA has been shown to play a role in chromatin structure in human cells. The silencing of the inactive X chromosome in females involves the accumulation of the ncRNA transcript *Xist*. This is followed by recruitment of the Polycomb repressive complexes PRC1 and PRC2 which mediate H2AK119 ubiquitination and H3K27 trimethylation respectively (Agrelo and Wutz

2010) thereby maintaining heterochromatic structure. Other heterochromatin regions in the human genome are transcribed including heat shock-induced transcription of satellite III repeats as well as transcription of the telomeric C rich strand at human telomeres giving rise to UUAGGG-repeat containing non-coding RNAs (TERRA or TelRNA) (Rizzi, Denegri et al. 2004, Schoeftner and Blasco 2009).

1.13 ATP-dependent chromatin remodelling

In addition to covalent modification of histones, DNA methylation, ncRNAs and the utilization of histone variants chromatin is subject to structural alteration by the action of large multi-protein complexes. These ATP-dependent chromatin remodelling complexes contain an ATPase subunit which can utilise the energy derived from the hydrolysis of ATP, allowing the complex to mobilize nucleosomes along DNA, evict histones off DNA or promote the exchange of histone variants, which in turn modulate DNA accessibility and alter nucleosomal structure (Wang, Allis et al. 2007). ATP dependent chromatin remodelling complexes can be divided into four families: SWI/SNF, ISWI, NuRD/Mi-2/CHD and INO80.

1.13.1 SWI/SNF

The first chromatin remodelling complex discovered was SWI/SNF. It was identified originally as a regulator of mating type switching (SWI) or as a requirement for growth on energy sources other than sucrose (SNF – sucrose nonfermenting) (Gangaraju and Bartholomew 2007). In yeast, Drosophila and humans there appear to be two versions of the complex: in yeast this is SWI/SNF and the essential RSC complex which itself exists in two functionally distinct complexes (Cairns, Schlichter et al. 1999). In Drosophila the two forms of SWI/SNF are the Brahma associated proteins (BAP) and Polybromo-associated BAP (PBAP) (Mohrmann and Verrijzer 2005). Although human SWI/SNF can be characterized as existing

in two forms, BRG1/hBRM-associated factors (BAF) and Polybromo-associated BAF (PBAF), there are many forms that acquire tissue specific subunits (Wang, Allis et al. 2007). Additionally, sub-complexes exist which consist of SWI/SNF-type remodelers and other factors such as histone methylases (Pal, Yun et al. 2003, Pal, Vishwanath et al. 2004), components of the Sin3 histone deactylase complex (Sif, Saurin et al. 2001) and also BRCA1 (Bochar, Wang et al. 2000, Decristofaro, Betz et al. 2001).

A fundamental role of SWI/SNF complexes is transcriptional regulation. SWI/SNF complexes primarily organise nucleosome positioning to promote accessibility for transcription factor binding and gene activation (Martens and Winston 2003) however they have also been shown to promote transcriptional-repressor binding and gene silencing under certain conditions (Ooi, Belyaev et al. 2006). SWI/SNF complexes have also been implicated in the repair of various forms of DNA lesions: During nucleotide excision repair (NER) SWI/SNF increases the accessibility of DNA to the NER repair factors (Hara and Sancar 2002, Yu, Teng et al. 2005). In *S. cerevisiae* SWI/SNF is recruited to HO-induced double strand breaks where it is thought to play a role in the homologous recombination repair pathway (Osley, Tsukuda et al. 2007). Furthermore, in human cells SWI/SNF appears to play a direct role in the rearrangement of immunoglobin loci during V(D)J recombination (Kwon, Morshead et al. 2000, Morshead, Ciccone et al. 2003, Patenge, Elkin et al. 2004).

1.13.2 ISWI family

The ISWI family was named Imitation Switch due to the similarity between its ATPase subunit, ISWI, and the ATPase subunit in SWI/SNF complexes, SWI2. The first members of the ISWI (Imitation Switch) family, dNURF and dCHRAC were identified in Drosophila (Tsukiyama and Wu 1995, Varga-Weisz, Wilm et al. 1997). Studies since have identified additional ISWI chromatin remodelers in yeast (Tsukiyama, Palmer et al. 1999), Xenopus

(Guschin, Geiman et al. 2000), mice (Lazzaro and Picketts 2001) and humans (Strohner, Nemeth et al. 2001). In humans there are six ISWI family members: ACF/WCRF, CHRAC, RSF, WICH, SNF2/Cohesin and NURF (Wang, Allis et al. 2007). The ISWI ATPase subunit is found in all ISWI family members. In addition to the ISWI subunit ISWI remodelers contain a SANT ('SWI3, ADA2, NCOR and TFIIIB') and a SLIDE (SANT-likeISWI) domain which is believed to play an important role in nucleosome recognition (Boyer, Langer et al. 2002, Grune, Brzeski et al. 2003). The complexes in this family are relatively small (300-800kDa) and generally contain fewer subunits compared to larger complexes in the SWI/SNF, IN80 and Mi-2/NuRD complexes (Gangaraju and Bartholomew 2007).

ISWI complexes play a role in a wide variety of nuclear processes including transcriptional regulation (Corona and Tamkun 2004). ISWI remodelling complexes primarily order nucleosome positioning to induce transcriptional repression (Deuring, Fanti et al. 2000, Goldmark, Fazzio et al. 2000). However there are reported chromatin loci where ISWI remodelers promote transcriptional elongation and transcriptional activation. The ISWI family member NURF is required for activation of *Hox* genes during development (Wysocka, Swigut et al. 2006). This transcriptional regulation is brought about by H3K4me3 which provides a binding site for the bromodomain-containing NURF complex. The human ISWI complexes CHRAC and ACF1 have been implicated in the maintenance of higher order chromatin structures: The ISWI and ACF1 subunits within these complexes have been shown to regulate chromatin folding into loop domains together with the Sin3A/RPD3 deacetylase and the SATB1 (special AT-rich sequence binding 1) transcriptional regulator (Yasui, Miyano et al. 2002). These same ISWI subunits are also required to promote DNA replication through highly condensed heterochromatin (Collins, Poot et al. 2002). RNAi depletion of ACF1 impairs the replication of pericentric heterochromatin whereas depletion of ISWI slows the progression of DNA replication (Collins, Poot et al. 2002).

1.13.3 NuRD/Mi-2/CHD family

In 1998 several different groups simultaneously described the protein composition of a macromolecular histone deacetylase complex variously termed the Mi-2 complex (Wade, Jones et al. 1998), NuRD (Zhang, LeRoy et al. 1998) NURD (Xue, Wong et al. 1998) or NRD (Tong, Hassig et al. 1998). Despite minor differences the protein compositions of these complexes were remarkably similar (Bowen, Fujita et al. 2004): They all possessed a Mi-2 subunit, a member of the SNF2 family of chromatin remodelling ATPases thereby providing a physical link between histone deactylation and ATP-dependent chromatin remodelling (Bowen, Fujita et al. 2004). Several distinct Mi-2/NuRD complexes with highly similar biochemical properties have been identified (Bowen, Fujita et al. 2004). Different isoforms of Mi-2 have been observed in Mi-2/NuRD complexes: (Woodage, Basrai et al. 1997) identified the isoform Mi-2β (CHD4) as the sole Mi-2 present in the complex however later analysis by (Tong, Hassig et al. 1998) revealed the presence of both Mi-2β and Mi-2α. Furthermore the metastasis-associated (MTA) protein family members MTA1, MTA2 and MTA3 have been shown to occupy distinct Mi-2/NuRD complexes (Bowen, Fujita et al. 2004).

The incorporation of unique subunits allows functional specialisation for the complex: only a subset of Mi-2/NuRD complexes contain the methyl-CpG-binding domain protein MBD2 (Feng and Zhang 2001, Humphrey, Wang et al. 2001). The presence of MB2, along with MBD3 that is found in all Mi-2/NuRD complexes, allows recruitment of the complex to methylated DNA. The binding of Mi-2/NuRD complexes to methylated DNA, along with the incorporation of HDAC1 and HDAC2 subunits suggests a role in maintaining a heterochromatic structure and transcriptional repression. Such a role has been found however Mi-2/NuRD has also been shown to promote transcriptional activation (Feng and Zhang 2001, Humphrey, Wang et al. 2001, Williams, Naito et al. 2004).

1.13.4 INO80

The INO80 family is the most recently identified ATP-dependent chromatin remodelling complex family. Members of the family have been identified in *S. cerevisiae* (INO80 and SWR1), *Drosophila* (INO80 and p400) and mammals (INO80, SRCAP (Snf2-related CBP activator protein) and p400) (Morrison and Shen 2009). Of all the chromatin remodelling complex families, INO80 appears to be the most conserved. A high degree of homology is seen in the ATPase subunit and a large number of orthologous subunits are shared between organisms including the RuvB-like, actin, Actin-related protein and YEATS protein subunits. In addition to these conserved subunits, a number of non-conserved, species-specific subunits are present in INO80 family complexes (Morrison and Shen 2009).

Like most chromatin remodelling complexes, INO80 complexes have been identified as transcriptional regulators. In humans this transcriptional regulation is linked to the function of the complex subunit ying yang 1 (YY1), a transcription factor which specifies the genes that are targeted for INO80-mediated chromatin remodelling (Cai, Jin et al. 2007). Complexes within this family however have also been shown to play a key role in the repair of double strand DNA breaks. In *S. cerevisiae* INO80 influences the proximal eviction of nucleosomes surrounding the double strand break which allows association of DNA repair machinery such as the MRE11 nuclease (van Attikum, Fritsch et al. 2004, Tsukuda, Fleming et al. 2005). Other nuclear processes which require INO80 chromatin remodelling activity include DNA replication, centromere stability and chromosome segregation and telomere structure (Morrison and Shen 2009).

1.14 Telomeric Chromatin

Telomeric chromatin structure has been investigated in a number of organisms from lower eukaryotes such as protozoa to mammals and more recently human cells. Although initially telomeres were thought to adopt a heterochromatic state, studies in Arabidopsis and human cells suggest the picture is more convoluted. Histone modifications associated with both repressed heterochromatin and relaxed euchromatic environments have been observed suggesting that telomeric chromatin in these organisms exists in a specialised intermediate conformation. Furthermore the methylation of subtelomeric DNA and presence of long non-coding RNA transcripts (TelRNA or TERRA) have also been shown to influence telomeric chromatin status. A number of chromatin remodelling proteins have been demonstrated to function at the telomere to preserve telomeric chromatin integrity and subsequently telomere length and function

1.14.1 Yeast

Although the telomeric repeat tract in *S. cerevisiae* is devoid of nucleosomes, subtelomeric regions are nucleosomal. As previously mentioned, the formation of a heterochromatin complex containing Rap1, Ku and the Sir proteins within the telomere propagates towards the subtelomeres and establishes a repressive heterochromatin environment which silences telomere-proximal genes (Ottaviani, Gilson et al. 2008). This process is counteracted by the Rpd3 histone deacetylase (De Rubertis, Kadosh et al. 1996). Several chromatin remodelers have also been identified as regulators of telomere length: a genome-wide screen for deletion mutants that affect telomere length identified 35 chromatin remodelling genes which when deleted caused abnormal telomere length phenotypes (Askree, Yehuda et al. 2004). A similar screen for essential yeast genes also revealed that RSC4 and RSC8, subunits of the ATP dependant chromatin remodelling complex RSC as negative regulators of telomere length (Ungar, Yosef et al. 2009). More detailed studies on telomere length

regulation by the remodelling action of chromatin modifying proteins have revealed a role for Ies3, a subunit of the INO80 ATP-dependant chromatin remodelling complex as a negative regulator of telomere length (Yu, Steinberg-Neifach et al. 2007). Mutation of the H3K4 histone methyltransferase Set1 has also been shown to result in telomere shortening confirming it as a positive regulator of telomere length (Roguev, Schaft et al. 2001).

Unlike in S. cerevisiae, loss of Set1 in S. pombe results in telomere elongation and also impaired telomeric silencing (Kanoh, Francesconi et al. 2003) suggesting that methylated H3K4 is an important telomeric chromatin mark. S. pombe telomeres are also enriched in Swi6, the orthologue of *Drosophila* HP1. Swi6 recruitment to telomeres is dependent on telomeric H3K9 methylation by the Clr4 histone methyltransferase (orthologue of mammalian Suv39h1) (Bannister, Zegerman et al. 2001, Nakayama, Rice et al. 2001). Loss of both Swi6 and Clr4 have been shown to affect telomeric silencing (Allshire, Nimmo et al. 1995, Sugiyama, Cam et al. 2007). The multi-enzyme complex SHREC was shown to be recruited to telomeres by redundant pathways involving Taz1 and Ccq1 as well as the RNAi machinery (Sugiyama, Cam et al. 2007). SHREC contains the histone deactylase Clr3 and the chromatin remodelling factor Mit1. The activity of both of these enzymes is required for the silencing of subtelomeric reporter genes (Sugiyama, Cam et al. 2007). Ccq1 is also required, along with Pot1 in an alternative chromosome end maintenance pathway in S. pombe. HAATI (heterochromatin amplification-mediated and telomerase independent) survivor cells lack telomerase and instead preserve chromosome linearity in by amplifying and rearranging heterochromatin sequences which supersede the telomere repeats at chromosome ends (Jain, Hebden et al. 2010).

1.14.2 Drosophila

Drosophila telomeres are enriched in heterochromatin protein 1 (HP1). HP1 is required for telomere length maintenance, transcriptional repression of telomeric sequences and capping of the chromosome end along with HOAP (HP1/ORC-associated protein), the Modigliani(Moi)/DTL and HipHop (HP1-HOAP-interacting protein) (Fanti, Giovinazzo et al. 1998, Savitsky, Kravchuk et al. 2002, Cenci, Siriaco et al. 2003, Gao, Walser et al. 2010, Raffa, Ciapponi et al. 2011). Telomeric binding of HP1 results in the tri-methylation of lysine 9 on the H3 histone (H3K9me3) which promotes the formation of a repressive telomeric chromatin structure thereby regulating the silencing of telomeric sequences and transcription of telomeric retrotransposons (Perrini, Piacentini et al. 2004, Frydrychova, Mason et al. 2008).

1.14.3 Plants

The chromatin organization at Arabidopsis chromosome ends on the other hand appears to be more complex. Arabidopsis subtelomeric regions appear heterochromatin with low levels of H3K4me3 and H3K9 and H4K16 acetylation and high enrichment of H3K27me1. Subtelomeric DNA is methylated by the chromatin remodelling factor DDM1 and the histone methyltransferases suvh4, suvh5 and suvh6 are also required for the deposition of H3K9me2 in subtelomeric regions (Vrbsky, Akimcheva et al. 2010, Vaquero-Sedas, Gámez-Arjona et al. 2011, Vaquero-Sedas, Luo et al. 2012). Telomeric chromatin on the other hand was shown to be enriched in both histone marks usually found in actively transcribed regions including dimethylation of H3K4 as well as acetylation of H3K9 and H4K16 as well as the repressive H3K27me3 mark suggesting an intermediate chromatin structure (Vaquero-Sedas, Luo et al. 2012). Additionally Arabidopsis telomeres also display enrichment of the histone H3 variant H3.3 and are transcribed leading to the formation of TERRA transcripts (Vrbsky, Akimcheva et al. 2010, Vaquero-Sedas and Vega-Palas 2013). Like in Arabidopsis, rice telomeres are also

labelled with H3K4me2, H3K9Ac and H3K27me3 and display low levels of DNA methylation (Vaquero-Sedas, Luo et al. 2012).

1.14.4 Mice

Mammalian telomeric chromatin maintenance has been studied predominantly in mouse Embryonic Stem (ES) cells and Mouse Embryonic fibroblasts (MEFs). A number of proteins have been identified which function in concert to maintain telomeric chromatin integrity and subsequently telomere length homeostasis. Telomeric chromatin in mouse ES and MEF cells has high levels of H3K9me3 enrichment which is mediated by the Suv39h1 and Suv39h2 HMTases. The H3K9me3 modification provides a high-affinity binding site for Cbx1, Cbx3 and Cbx5, homologs of *Drosophila* heterochromatin protein 1 (HP1) which in turn promotes the recruitment of the Suv4-20h1 and Suv4-20h2 HMTases which establish H4K20me3 enrichment. Loss of Suv39h1 and Suv39h2 in SUV39-null mouse embryonic stem (ES) cells and mouse embryonic fibroblasts (MEFs) results in decreased H3K9me2 and H3K9me3 at the telomere and also reduced binding of the chromobox proteins Cbx5, Cbx3 and to a lesser extent Cbx1 (Garcia-Cao, O'Sullivan et al. 2004). Importantly these SUV39-null cells showed abnormally long telomeres. A similar telomere lengthening phenotype was observed in mouse ES and MEFs deficient in Suv4-20 HMTases, along with loss of H4K20me3 at both telomeric and subtelomeric chromatin. These cells also show an increase in sister chromatid recombination both globally and at telomere regions suggesting that the telomere lengthening is via the ALT pathway as opposed to telomerase-mediated lengthening (Benetti, Gonzalo et al. 2007). H4K20me3 enrichment is further enhanced by the Dot1L-mediated H3K79me2 deposition. Dot1L is another HMTase and its reduction results in lower H3K79me2 telomeric enrichment and promotes telomere lengthening via the ALT pathway. (Jones, Su et al. 2008).

Low histone acetylation is another feature of chromatin at mouse telomeres. This is mediated, at least in part by SIRT1, the mammalian homolog of the yeast histone deacetylase Sir2 which, as previously mentioned plays a pivotal role in the telomere position,n effect. Although the yeast Sir2 protein shows no telomere length regulation capacity SIRT1 in mice does: Palacios, Herranz et al. (2010) demonstrated that SIRT1-deficient loss-of-function mouse embryonic fibroblasts (MEFs) showed significantly shorter telomeres than wild-type MEFs as well as a reduction of H3K9me3 and HP1-γ at the telomere. Conversely, MEFs taken from gain-of-function mice with a three-fold increase in SIRT1 expression displayed a reduction in H3K9Ac and also had significantly longer telomeres compared to wild-type MEFs.

In addition to histone modifying proteins, DNA methyltransferases have also been implicated in telomere length maintenance. Subtelomeric DNA is highly methylated by the DNA methyltransferases DNMT1, DNMT3a and DNMT3b. Loss of DNMTs in mouse ES cells results in recombination-based telomere elongation confirming DNMTs as negative regulators of telomere length (Gonzalo, Jaco et al. 2006).

The H3 histone variant H3.3 is enriched at telomeric chromatin in mouse ES cells. Proper deposition of H3.3 is mediated by a complex containing the SWI/SNF family member ATRX and the H3.3 chaperone DAXX (Lewis, Elsaesser et al. 2010). RNAi depletion of H3.3 causes an increase in telomere-dysfunction induced foci (TIFs) (Wong, Ren et al. 2009) as does loss of ATRX along with a dramatic loss of the mammalian heterochromatin protein HP1γ (CBX5) (Wong, McGhie et al. 2010). Loss of either ATRX, DAXX or H3.3 however does not result in any telomere length alterations.

Interestingly, differentiated mouse ES cells display decreased levels of telomeric H3.3 (along with increased H3k9me3 and H4K20me3) suggesting that differing telomeric chromatin structures exist in different cell types. This idea was further explored by a study in which pluripotency was induced in MEFs generating induced pluripotent stem cells (iPSCs), functional equivalents of mouse ES cells (Marion, Strati et al. 2009). Telomeres are shorter in MEFs compared to ES cells however their reprogramming was accompanied by telomerase-dependant telomere elongation which continued to a length similar to what is observed mouse ES cells. Concomitant with this telomere elongation was a change in chromatin structure; reduced levels of H3K9me3 and H4K20me3 were observed as well as upregulation of TERRA. This change in chromatin structure after induced pluripotency shows how cellular context is a key determinant, not only in telomere length, but also in telomeric chromatin structure.

A further feature of mouse telomeric chromatin is the presence of UUAGGG-repeat containing non-coding RNAs (TERRA or TelRNA) (Azzalin, Reichenbach et al. 2007, Schoeftner and Blasco 2009). These molecules can range between 10bp to >9kb in length and form a intermolecular G-quadreplex structure with single stranded telomeric DNA as well as a compact repeated structure containing G-quartets (Azzalin, Reichenbach et al. 2007, Schoeftner and Blasco 2009). It has been suggested that TERRA negatively regulates telomere length by base pairing with the template region of TERC, thereby inhibiting telomerase activity (Luke, Panza et al. 2008, Schoeftner and Blasco 2009). This view is supported by the fact that TERRA expression is low in embryonic stem cells and cancer cells where telomerase activity is high (Azzalin, Reichenbach et al. 2007, Schoeftner and Blasco 2009).

1.14.5 Humans

Telomeric chromatin structure in human cells is a relatively unexplored field. Early evidence of how the chromatin structure contributes towards telomere function in human cells was provided in work in which telomeric silencing was shown to be disrupted upon Trichostatin A (TSA)-induced inhibition of histone deacetylation (Baur, Zou et al. 2001, Koering, Pollice et al. 2002). In subsequent research the deacetylation of H3K9 and H3K56 by SIRT6 was shown to be responsible for this telomeric silencing (Tennen, Bua et al. 2011). SIRT6 loss also leads to an increase in telomere-to-telomere fusions although it has no impact on telomere length (Michishita, McCord et al. 2008).

Very recently a handful of studies have shed light on prominent histone modifications at human chromosome ends. Human telomeres share similarities with Arabidopsis telomeres in that the chromatin environment does not appear to be purely heterochromatic. Human telomeres are enriched in H3K4me3 and H2BK5me1, marks often associated with actively transcribed genes (Rosenfeld, Wang et al. 2009). Furthermore there is an under-representation of H3K9me3 at human telomeres in contrast to the high abundance of H3K9me3 at mouse telomeres, although it is enriched in human subtelomeric chromatin (Rosenfeld, Wang et al. 2009). Similar levels of telomeric H3K9me3 were also observed in IMR90 fibroblasts and HT1080 cells (O'Sullivan, Kubicek et al. 2010, Arnoult, Van Beneden et al. 2012). The repressive H4K20me3 and H3K27me3 marks are also enriched at human telomeres (O'Sullivan, Kubicek et al. 2010, Arnoult, Van Beneden et al. 2012) although again their telomeric enrichment is lower than at mouse telomeres indicating a more open, euchromatic environment at human chromosome ends. Despite these euchromatic histone modifications, several repressive heterochromatic features are also found at human chromosome ends including hypoacetylation of H3K9 and H3K56, methylation of subtelomeric DNA, HP1 enrichment and the presence of TERRA transcripts (Yehezkel, Segev

et al. 2008, Deng, Norseen et al. 2009, Nergadze, Farnung et al. 2009, Deng, Campbell et al. 2010).

TERRA plays a key role in telomere function in human cells. siRNA depletion of TERRA leads to an increase in telomere-dysfunction induced foci, aberrations in metaphase telomeres and loss of telomeric H3K9me3 and origin recognition complex (ORC) which itself prevents telomere dysfunction (Deng, Dheekollu et al. 2007, Deng, Norseen et al. 2009). Not surprisingly, due to the important role TERRA plays at human telomeres it is regulated in a number of ways. Subtelomeric DNA methylation, presumably mediated by the DNMT DNA methyltransferases, negatively regulates TERRA transcription (Yehezkel, Segev et al. 2008, Deng, Norseen et al. 2009, Nergadze, Farnung et al. 2009, Deng, Campbell et al. 2010). TERRA transcription is also down-regulated by increased H3K9me3 and HP1α after telomere elongation (Arnoult, Van Beneden et al. 2012). Several positive regulators of TERRA transcription have been identified including the chromatin organizing factor CTCF (Deng, Wang et al. 2012) as well as the H3K4-specific histone methyltransferas MLL. MLL depletion in human fibroblast cell lines HS68 and IMR90 blocks the usual up-regulation of TERRA following telomere uncapping (Caslini, Connelly et al. 2009).

The proper deposition of H3.3 by the ATRX-DAXX complex is required to maintain telomere structure and function in mice (Wong, Ren et al. 2009, Drané, Ouararhni et al. 2010, Goldberg, Banaszynski et al. 2010, Lewis, Elsaesser et al. 2010, Wong, McGhie et al. 2010) and it is thought that this same pathway plays a similar role at human telomeres as loss of either ATRX, DAXX or H3.3 has been associated with aberrant telomere length phenotypes in a number of cancers. Changes in telomere length reminiscent of the ALT pathway were seen in a panel of human pancreatic neuroendocrine tumours (PanNETs) in which ATRX or DAXX had been mutated (Heaphy, de Wilde et al. 2011). Similar alternative lengthening of

telomeres was observed in glioblastoma multiforme (GBM) tumour samples in which the ATRX-DAXX-H3.3 pathway had been inactivated by somatic mutations (Schwartzentruber, Korshunov et al. 2012). Furthermore ATRX is either undetectable or severely depleted in 90% of ALT cell lines (Lovejoy, Li et al. 2012). RNAi-mediated knockdown of ATRX has been shown in our lab to cause a prominent telomere phenotype consisting of dramatic, stochastic reductions in telomere length (Tankimanova, personal communication). As yet the ATRX-DAXX-H3.3 pathway is the only chromatin remodelling pathway identified in human cells which, when inactivated, leads to alterations in telomere length.

1.15 Project aims

Our lab has previously described extensive allelic and inter-chromosomal telomere length variation, both in the presence or absence of telomerase activity. The primary aim of this project is to investigate whether the chromatin structure of telomeres impacts upon telomere length determination of specific telomeric alleles and chromosome ends in human cells. Two approaches will be taken to address this issue: firstly, the chromatin structure of telomeres of differing lengths will be directly analysed by measuring enrichment of histone modifications known to be prominent at telomeres in other model organisms. Secondly, selected chromatin remodelling proteins will be studied to determine whether they play a role in telomeric chromatin structure and telomere length maintenance.

Past research on telomeric chromatin structure in mammalian cells have identified a role for a number of chromatin remodelers and the histone modifications they deposit at the chromosome end. The vast majority of this work however has relied on TRF analysis and dot blot assays to measure telomere length telomeric occupancy respectively. These approaches lack sensitivity and are unable to differentiate between telomeres. Single Telomere Length Analysis (STELA) provides a high resolution method to measure telomere length distributions at individual chromosome ends. STELA assays have been designed for the 2p, 9p, 11q, 12q, 16p, 17p and 18q telomeres. An allele-specific STELA assay has also been designed for the XpYp chromosome end. The first aim of this project was to develop telomere and telomeric allele-specific qPCR assays for the same chromosome ends. These qPCR assays, when used in conjunction with ChIP, will provide a tool for analysing telomeric chromatin structure at individual chromosome ends. Applying this ChIP-qPCR approach alongside STELA will allow any correlations between telomeric chromatin structure and telomere length to be identified.

Our laboratory has recently identified ATRX as a regulator of telomere length in a keratinocyte holoclone cell population (Tankimanova, personal communication). siRNA knockdown of ATRX results in dramatic reductions in telomere length at a number of chromosome ends. The second aim of the project was to identify more chromatin remodelling proteins which play a role in telomere length maintenance. A selection of proteins were chosen for siRNA knockdown based on a number of criteria including whether they have been shown to play a role at the telomere in other organisms, whether changes in their expression levels was implicated in cancer and also whether they interacted with ATRX. An RNAi screen was performed in which expression of the selected genes was depleted over numerous cell divisions. Any resulting aberrant telomere length phenotypes were then examined at a number of chromosome ends by STELA.

Chromatin remodelers which, when depleted, resulted in telomere defects were investigated further. This included observing telomere length phenotypes after knockdown of the chromatin remodeler in a different cell type to determine whether its telomeric role was universal or restricted to certain cell types. Additionally the mutational mechanism which caused telomere length defects in the absence of a chromatin remodeler was examined.

Chapter 2

Materials and Methods

2.1 Chemicals and reagents

Chemicals and reagents used were obtained from numerous sources including Fisher, Invitrogen, Applied Biosystems, Thermo Scientific, New England Biolabs, Amersham biosciences/GE healthcare, Roche, Sigma-Aldrich and PerkinElmer, Bio-Rad, Abcam and Millipore.

2.2 Plastic lab equipment

Plastic and glass lab equipment used for experiments was obtained from Gilson, Becton Dickinson labware, Eppendorf, Thermo Scientific, Costar, Ambion and SARSTEDT.

2.3 Equipment/machinery

Equipment used during experiments was obtained from Bio-Rad, MJ research, Applied biosystems, Thermo Scientific, Promega, Hybaid, Amersham biosciences and Qiagen.

2.4 Oligonucleotides

Primers were designed based on human DNA sequences obtained from H. Reithman at the Wistar institute (http:/www.wistar.upenn.edu/Reithman) and National Centre for Biotechnology

Information (NCBI). The oligonucleotides were synthesised by MWG-Biotech AG (Ebersberg, Germany). All primers used during this study are listed in table. 2.1.

Application	Primer name	Sequence
STELA PCR	XpYpE2	TTGTCTCAGGGTCCTAGTG
	17pseq1rev	GAATCCACGGATTGCTTTGTGTAC
	18qrev4M	CACAGGGATGGTTAGGTATCTC
	2p2	GAGCTGCGTTTTGCTGAGCAC
	11q13B	CAGACCTTGGAGGCACGGCCTTCG
	12q -197A	GGGAGATCCACACCGTAGCA
	16prev1	CACTTATTAGTTCCAGTCTCTG
	XpYp -427A/415T	GGTTATCAACCAGGTGCTCT
	XpYp -427G/415C	GGTTATCGACCAGGTGCTCC
	teltail	TGCTCCGTGCATCTGGCATC
	Tel2	TGCTCCGTGCATCTGGCATCTAACCCT
Fusion PCR	16p1	TGGACTTCTCACTTCTAGGGCAG
	21q1	CTTGGTGTCGAGAGAGGTAG
	XpYpM	ACCAG GTTTTCCAGTGTGTT
	17p6	GGCTGAACTATAGCCTCTGC
Fusion Reamplification	17p7	CCTGGCATGGTATTGACATG
	16p2	TCACTGCTGTATCTCCCAGTG
	21qseq1	TGGTCTTATACACTGTGTTCCACTGGC
Death-wish reamplification	XpYpC	CAGGGACCGGGACAAATAGAC
	XpYpE	TTGTCTCAGGGTCCTAGTG
	XpYpP	ACCAGGGGCTGATGTAACG
	XpYpG	AATTCCAGACACACTAGGACCCTGA
	teltail	TGCTCCGTGCATCTGGCATC
	Tel2	TGCTCCGTGCATCTGGCATCTAACCCT
qPCR	2p1	CTAAGCCGAAGCCTAACTGGTG
	2p2	GA GCTGCGTTTTGCTGAGCAC
	2p13	AAGCAGCATTCTCCTCAGG
	11q12	CCCTGATTATTCAGGGCTGCAAAG
	11q13B	CAGACCTTGGAGGCACGGCCTTCG
	12qA1	TCAAAAGCCCCTCTGAATCCTGC
	12qB	ATTTTCATTGCTGTCTTAGCACTGCAC
	16pBrev	TTCAGAGGGGCTTTTAGTTTCCCA
	16pC	AAAGGTGGAGCAGCATTCTG
	17pA	GTTTTCACCTGTTTTGGTCTTC

	17pB	GGATCCTTGCACAGGAATAAAC
	18qA	TGACAGTGGTGTCCAGTGGT
	18qC	CACAGGGATGGTTAGGTATCTC
	XpYp -176T	TTTGCGGTGAGTGTCACAGCTCAT
	XpYp -13A	ACCCTCTGAAAGTGGACCT
	XpYp -176G	TTTGCGGTGAGTGTCACAGCTCAG
	XpYp -13A	ACCCTCTGAAAGTGGACCA
	beta-globin FOR	AGGACAGGTACGGCTGTCATC
	beta-globin REV	TTTATGCCCAGCCCTGGCTC
	ZNF554 FOR	CGGGGAAAAGCCCTATAAAT
	ZNF554 REV	TCCACATTCACTGCATTCGT
	alpha satellite FOR	CTGCACTACCTGAAGAGGAC
	alpha satellite REV	GATGGTTCAACACTCTTACA
	GAPDH FOR	TACTAGCGGTTTTACGGGCG
	GAPDH REV	TCGAACAGGAGGAGCAGAGAG
	GAPDH CR FOR	GCCATGTAGACCCCTTGAAGAG
	GAPDH CR REV	ACTGGTTGAGCACAGGGTACTTTAT
Sequencing	XpYpJ	CTAATCTGCTCCCWCCCAC
	XpYp-145agt/ggc	GGACCCAAAGAGTGAGCAGT
	XpYp-30A/T	CTGCTTTTATTCTCTAATCTGCTCCCA
	XpYpseq2	GTTGCTCTGACATGGACACAG
	10q3	AGACACAGGATAGTGGGCTCTG
	17pseq2rev	CCATTAGCCTGTGGGGTCTGAT
	17p2	GCTAGGAATGGAATCATTGACTC
	17p5	TTCATTAGGATCCAGTTTTG
	17p7	CCTGGCATGGTATTGACATG
	17pK1	CATCACTTGTTGAGGACAGG
	17pK2	GTTTTCTGTCTGGACTCC
	17pseq1B	AAGCAGGTTGAGAGGCTGAGG
	21qseq1rev	GCTCTGTTAGAGTAGATAGCTAGCT
	Subtel13B	GTACGCTGTCTTCATGGCAG
	8p1	TGCACAGGACTCTTAGGCTG
Others	XpYpB2	TCTGAAAGTGGACC(A/T)ATCAG

Table 2.1. Oligonucleotide sequences used during the study

2.5 DNA extraction

2.5.1 Phenol/chloroform

Genomic DNA from cell pellets containing over $3X10^6$ cells was extracted by standard phenol/chloroform extraction (Sambrook et al., 1989). Briefly, cells were lysed overnight at 45°C in 300-500µl lysis buffer (10mM Tris-Hcl pH8, 100mM NaCl, 5mM EDTA pH8, 0.5% SDS) containing 30µg RNase A (Sigma; stock 10mg/ml) and 60µg proteinase K (Sigma; stock 20mg/ml). After brief centrifugation 300-500µl phenol/chloroform was added to the cell lysate and rotated for 20mins at room temperature. The mixture was centrifuged at 13000rpm for 5mins to separate the phases, the aqueous and interphase phases were removed and added to an eppendorf containing 300µl phenol/chloroform. This was rotated again for 20mins and then centrifuged (13000rpm) for 5 minutes. The aqueous phase was removed and to this was added 30µl 3M sodium acetate pH5.3 (Sigma) and 900µl ice-cold 100% ethanol to precipitate the DNA. The mix was left at -20°C for at least an hour. After brief centrifugation (13000rpm, 1min) the DNA pellet was washed in 70% ice-cold ethanol and air dried in the micro-flow hood. DNA was then resuspended in 10mM Tris-Hcl pH8.

2.5.2 Magnesil

Genomic DNA was extracted from cells cultured in 96 well plates by using Magnesil paramagnetic particles (Promega). Briefly, cells were washed with 1XPBS and lysed with eLysis buffer (Promega) before the addition of Magnesil particles. After two washes with 1:1 mix of eLysis buffer & alcohol wash (Promega) the Magnesil particles were washed three times with alcohol wash. DNA was eluted from the Magnesil particles with a 10-minute incubation at 65°C in 30µl elution buffer (Promega).

2.5.3 Maxwell

Genomic DNA was extracted from cell pellets using the Maxwell 16 LEV Blood DNA kit (Promega) along with the Maxwell 16 instrument. Cell lysis was achieved through incubation of the cell pellet with 300µl lysis buffer and 30µl proteinase K at 56°C for at least one hour. Cell lysates were then loaded into the cartridges and placed in the Maxwell 16 instrument. The research mode with LEV hardware was ran to extract DNA from the cell lysates. Extracted DNA was eluted into 50 µl elution buffer.

2.5.4 DNA quantification

DNA concentrations were determined in triplicate in a number of ways: either by Hoechst 33258 flurometry as described previously (Baird et al., 2003), using a Nanodrop ND-100 system (Thermo scientific) supplied by the Central Biotechnology Services (CBS) Core Facility in the School of Medicine, Cardiff University (www.cardiff.ac.uk/medic/cbs) or by performing a pilot STELA to determine band number, after which relative DNA quantities to add to reactions were then subsequently calculated.

2.6 PCR

2.6.1 Conventional PCR

DNA (typically 50ng) was added to PCR reactions containing 0.5µM forward primer, 0.5µM reverse primer, 1.2mM dNTPS, 1X Taq buffer (75mM Tris-HCl (pH8.8), 20mM $(NH_4)SO_4$, 0.01% Tween-20) (Abgene), 2mM $MgCl_2$ and 0.5U *Taq* polymerase. PCR reactions were then cycled under the following conditions: 94°C (15 sec) 56-72°C depending on primers used (30 sec) and 72°C (1 min) for 33 cycles.

For primer optimization an annealing temperature gradient ranging from 56°C to 72°C was used across 12 PCR reactions.

2.6.2 STELA PCR

DNA was diluted to 250pg/µl in 10mM Tri-Hcl (pH 8). 0.9 µM Tel2 linker was added to the diluted DNA. Multiple 10µl reactions were set up per sample (typically 6-8) each containing 250pg DNA/tel2 mix, 1X Taq buffer (75mM Tris-HCl (pH8.8), 20mM $(NH_4)SO_4$, 0.01% Tween-20) (Abgene), 2mM $MgCl_{2,}$ 1.2mM dNTPs, telomere-specific primer (0.5µM), teltail primer (0.5µM), and 1U Taq/PWO (Abgene/Roche) at a ratio of 10:1. 1µl DNA/tel2 mix was added to each reaction. These reactions were then cycled in a Bio-Rad DNA Engine Tetrad® Thermal Cycler using the following conditions: 94°C (20 sec), 56-65°C depending on primer used (30 sec), 68°C (10 mins) for 22 cycles.

2.6.3 Fusion PCR

DNA was diluted to 50ng/µl in 10mM Tri-Hcl (pH 8). Multiple 10µl reactions were set up per sample (typically 9) each containing 50ng DNA, 0.5µM telomere-adjacent primers (17p6, XpYpM, 16p1 & 21q1), 1X Taq buffer (75mM Tris-HCl (pH8.8), 20mM $(NH_4)SO_4$, 0.01% Tween-20) (Abgene), 2mM $MgCl_{2,}$ 1.2mM dNTPs and 0.5U Taq/PWO polymerase mix (Abgene/Roche) at a ratio of 10:1. Reactions were then cycled using the following conditions: 94°C (15 sec), 59°C (30 sec) and 68°C (8 mins) for 25 cycles.

2.6.4 Fusion Reamplification PCR

Fusion PCR reactions which amplified a fusion event were diluted 20-fold. 3µl of this dilution was added to a 30µl PCR reaction containing 0.5µM telomere adjacent primers, 1X Taq buffer (75mM

Tris-HCl (pH8.8), 20mM $(NH_4)SO_4$, 0.01% Tween-20) (Abgene), 2mM $MgCl_2$, 1.2mM dNTPs and 0.5U Taq/PWO polymerase mix (Abgene/Roche) at a ratio of 10:1. Reactions were then cycled using the following conditions: 94°C (15 sec), 59°C (30 sec) and 68°C (8 mins) for 33 cycles.

2.6.5 Reamplification of gel-eluted PCR products

Multiple 50µl reactions (typically 6) were set up per gel-eluted PCR product. Each gel-eluted PCR product was diluted 20-fold and 2µl of this dilution was added to the 50µl PCR reaction containing 0.5µM XpYpC and 0.5µM tel2 or teltail, 1X Taq buffer (75mM Tris-HCl (pH8.8), 20mM $(NH_4)SO_4$, 0.01% Tween-20) (Abgene), 2mM $MgCl_2$, 1.2mM dNTPs and 0.5U Taq polymerase (Abgene). The reactions were then cycled using the following conditions: 94°C (15 sec), 60°C (30 sec) and 68°C (8 mins) for 35 cycles.

2.7 Gel Electrophoresis

2.7.1 Gel electrophoresis for STELA and fusion PCR products

DNA fragments were resolved using a 40cm long, 0.5% Tris-acetate-EDTA agarose gel submerged in 1XTAE cooled to 4°C by a circulating cooling system. For STELA 4ul PCR reactions containing 1X ficol-based loading dye (5% bromophenol blue, 5% xylene, 15% ficol) were loaded in the gel and ran through the length of the gel at 120V for 16 hours. 4ul fusion products containing 1X ficol based loading dye were loaded and ran a third to half the length of the 40cm gel using 50V for 16 hours.

2.7.2 For other PCR products

PCR products generated from other types of PCR were either resolved on a 40cm 0.7-1% Tris-acetate-EDTA agarose gel (for large sample numbers) using 120V (1-2 hours) or for fewer sample numbers, on a smaller 10-20cm gels (0.7-1%) using 90V (1-2 hours).

2.7.3 Visualisation of PCR products

Bands stained by ethidium bromide were visualised on a UV-transilluminator.

2.8 Southern Blotting

The resolved STELA or fusion products were depurinated by washing the gel twice in depurination buffer (0.25M HCl) for 6 minutes. After rinsing, the gel was then washed in denaturation buffer (1.5M NaCl/0.5MNaOH) for 15 minutes. The DNA was then transferred onto a positively charged membrane (Hybond XL, Amersham) by alkaline Southern blotting with denaturation buffer for 4-6 hours.

2.9 Probe labelling and hybridisation

2.9.1 Probe synthesis

25ng probe DNA and ladder (1:1 of 1kb:2.5kb) in TE buffer (10mM Tric-Hcl and 1mM EDTA) was labelled using Ready-To-Go DNA labelling beads (GE Healthcare). This kit generates labelled probes using random hexaprime labelling with [α-^{33}P] dCTP.

2.9.2 Hybridisation

After blotting the membranes were rinsed in H_20 before undergoing pre-hybridization for 15 mins in church buffer (0.5M sodium phosphate buffer (1M disodium hydrogen phosphate and 1M sodium dihydrogen phosphate), 1mM EDTA, 1% BSA, 7% SDS, pH 7.2). 25µl of radioactively labelled probe was added to the hybridisation bottles which were then left to hybridize at 60°C overnight.

2.9.3 Removing unbound probe

To remove unbound probes the membrane was washed with 0.1X sodium chloride sodium citrate (SSC)/0.1% sodium dodecyl sulphate (SDS) several times at 60°C. The washed blots were then dried in the hybridization oven at 60°C for ~30mins.

2.9.4 Visualisation of Radiolabelled Blots

Radiolabelled southern blots were placed in a cassette with a phosphoimager screen (Amersham) for 24 hours. The phosphimager screen was then scanned using the Typhoon 9410 biomolecular imager (GE healthcare). STELA and fusion blots were then stripped using boiling 0.1% SDS before being re-probed with a different probe.

2.10 Gel analysis and statistics

Gels scanned using the Typhoon 9410 were subsequently analysed using Molecular dynamics ImageQuant 5.0 (GE). The molecular weights of individual telomeres on each STELA Southern blot were calculated using Phoretix 1D software (Nonlinear dynamics). Telomere length measurements were then exported to Microsoft Excel where the distance between the telomere-adjacent primer

and the telomere repeat array was subtracted giving an accurate measurement of telomere length. Mean telomere length and standard error measurements were then calculated.

Statistics used include Analysis of variance (ANOVA) to compare mean telomere length across numerous samples, Student's t-test to compare telomere means and a chi-squared analysis to measure the statistical significance of the proportion of small telomeres within a population of telomeres.

2.11 Sequencing

PCR products to be sequenced were purified from agarose gel slices using QIAquick gel extraction kit (Qiagen) or the GE healthcare gel extraction kit and purified in 50µl elution buffer. 4.4µl purified PCR product was added to 0.16µM sequencing primer and 4µl BigDye Terminator Cycle sequencing mix (3.1 or 3.0) (Applied Biosystems) and cycled using the following conditions: 96°C (30 sec),56°C (15 sec) and 60°C (4 mins) for 25 cycles. Amplified products from the sequencing PCR were then purified using Dye EX^{TM} 2.0 spin kit (Qiagen) before being sequenced by the Central Biotechnology Service (CBS), School of Medicine, Cardiff University. Sequence data obtained was viewed using Sequence Scanner (version 1.0) (Applied Biosystems) and analysed by using the Basic Local Alignment Search Tool (BLAST) (http://blast.ncbi.nlm.nih.gov/Blast.cgi) to identify the sequence or in the case of testing primer specificity, by comparing sequence data with published subtelomeric sequences from Reithman et al (http://www.wistar.upenn.edu/Riethman).

2.12 Elution of individual PCR products from a STELA blot

Multiple 20µl reactions were set up containing 250pg DNA/tel2 mix, 1X Taq buffer (75mM Tris-HCl (pH8), 20mM $(NH_4)SO_4$, 0.01% Tween-20) (Abgene), 2mM $MgCl_2$, 1.2mM dNTPs, telomere-specific

primer (XpYpC) (0.5µM), teltail primer (0.5µM), and 1U Taq/PWO (Abgene/Roche) at a ratio of 10:1. These reaction were then cycled in a Bio-Rad DNA Engine Tetrad® Thermal Cycler using the following conditions: 94°C (20 sec), 65°C (30 sec), 68°C (10 mins) for 22 cycles. 4µl of these reactions were used to perform a STELA as described earlier. This initial STELA not only allowed identification of small bands to elute from the gel but importantly identified their position on the gel in relation to the DNA ladder. The remaining 16µl of the chosen STELA-PCR reactions were loaded onto a 0.5% TAE agarose gel and ran partially through the gel. The position of the ladders was then examined under a UV transilluminator and the position of the bands was estimated. Wells were cut out of the gel under these positions and dialysis membrane was inserted into the wells. The gel was then re-submerged in 1XTAE buffer and migration of the bands resumed. By examining the migration of the DNA ladder it was possible to determine whether the desired PCR product had migrated onto the dialysis membrane. At this point the membrane was removed from the well and placed in a 1.5 ml tube. The purified products were removed from the membrane by centrifugation and washed in TE.

2.13 Verification of successful elution

20µl PCR reactions were set up containing 2µl eluted PCR product, 1X Taq buffer (75mM Tris-HCl (pH8), 20mM $(NH_4)SO_4$, 0.01% Tween-20) (Abgene), 2mM $MgCl_2$,, 1.2mM dNTPs, XpYpC (0.5µM) and XpYpG (0.5µM), and 1U Taq polymerase (Abgene). PCR reactions were cycled under the following conditions: 94°C (15 sec), 65°C (30 sec) and 68°C (1 min) for 30 cycles. PCR products were then ran on a 1% TAE agarose gel (120V, 1h) and visualised on a transilluminator.

2.14 ChIP

2.14.1 Chromatin extraction

$2x10^6$ cells were seeded in 10mm dishes (BD labware). The following day cells (which had achieved 80% confluency) were cross linked for 10 minutes with shaking using formaldehyde (Sigma) at a final concentration of 1%. Formaldehyde was then quenched using 125mM glycine. Cells were then washed twice with 10ml ice-cold 1XPBS before being detached by scraping in 3ml 1XPBS containing 1XPhenylmethanesulfonyl fluoride (PMSF) (Sigma). After collecting the cells by centrifugation (1200rpm, 5 mins) the 1XPBS was removed by aspiration. Cells were then resuspended in SDS lysis buffer (1% SDS, 10mMEDTA, 50mM Tris-HCl pH8.1) containing 1XPMSF to achieve a final cell concentration of $1x10^4$/µl. To ensure complete cell lysis, the resuspended cells were left on ice for 40 minutes. Chromatin was then divided into 200µl aliquots and sheared by sonication using the Biorupter (Diagenode) at 4°C. 8 cycles of 30s on, 30s off at high power was used to shear chromatin into 200-1000bp fragments. Sonicated samples were then centrifuged for 10 minutes (13000rpm, 4°C) and supernatant was removed. A 50µl aliquot of chromatin was taken to verify chromatin fragment size and the rest of the supernatant was snap frozen using liquid N_2 and stored at -80°C. The 50µl chromatin aliquot was then diluted 1:1 in 50µl TE buffer (10mM Tris-HCl pH8, 1mM EDTA). To this was added 25µl pronase buffer (125mM Tris-HCl pH7.5, 25mM EDTA, 2.5% SDS) and 6.25µl pronase to reverse cross linking. This mix was incubated overnight at 65°C. Following a brief centrifugation 5µl RNase A (10mg/ml) was added to the reverse cross-linked chromatin and incubated for 1 hour at 37°C. DNA was then purified using the QIAquick gel extraction kit (Qiagen) and eluted into 50µl EB buffer. 2µl of ficol-based loading dye was added to 10µl purified DNA before loading the sample onto a small 1.5% TAE agarose gel and ran at 90V for ~30 minutes. The ethidium bromide-labelled chromatin was then visualised on a transilluminator.

2.14.2 Immunoprecipitation

50µl Dynabeads protein G (Invitrogen) per sample were washed 3 times in 1XPBS containing 0.1% BSA before being resuspended in 50µl 1XPBS (0.1% BSA). After addition of antibodies of interest (H3, H3K4me3, H3K9me3, H3K27me3, H4K20me3 (Millipore) and H3.3, TRF1 (Abcam)), the Dynabeads were incubated at 30°C with shaking (1300rpm) for 40 minutes. After washing the beads 3 times with 1XPBS (0.1% BSA) the immunoprecipitation reactions were set up containing antibody conjugated-dynabeads, 100µl chromatin (equivalent 1x106 cells), 100ul 1XPBS (1% BSA) and 750µl 1XPBS. The reactions were incubated with shaking (1300rpm) for 3 hours at 21°C. After incubation the Dynabeads underwent the following wash steps: one wash with FA/SDS buffer (50mM HEPES KOH pH7.5, 150mM NaCl, 1mM EDTA, 1% Triton-X, 0.1% sodium deoxycholate, 0.1% SDS), three washes with FA/SDS containing 500mM NaCl, one wash with LiCl solution (10mM Tris-HCl pH8, 250mM LiCl, 1mM EDTA, 0.5% NP40, 0.5% sodium deoxycholate) and one wash with ice cold TE buffer (1mM Tris-HCl pH8, 1mM EDTA). Chromatin was then eluted from the Dynabeads by adding 1X pronase buffer (25mM Tris-HCl pH7.5, 5mM EDTA, 0.5% SDS) and incubating at 65°C with shaking (1300rpm) for 20 minutes. Eluted chromatin was reverse cross-linked by adding 6.25µl pronase (20mg/ml) and incubating at 65°C overnight. DNA was purified by the same method as described above in 'chromatin extraction'.

2.15 qPCR

2.15.1 ChIP-qPCR

The degree of protein enrichment at a specific region was measured by the absolute quantification method. A standard curve is constructed using 10X serial dilutions of DNA of known quantity. This standard curve is then used to convert to the initial DNA quantity in an immunoprecipitate (IP) sample from the generated Ct value. The Ct value or cycle threshold is the cycle number at which an amplification curve intersects a set threshold. All DNA samples were amplified in triplicate qPCR

reactions. 20µl qPCR reactions were set up containing 0.3µM forward and reverse primers, 1X iQ™ SYBR® green supermix (Biorad) and either IP DNA (5X dilution), input DNA (100X dilution) or input DNA dilutions used for the standard curve (SC): SC1 (3X dilution), SC2 (30X dilution), SC3 (300X dilution) and SC4 (3000X dilution). These reaction were then cycled in an ABI PRISM 7700 (Applied Biosystems) under the following conditions: 94°C (10 mins) followed by 50 cycles of 94°C (20 sec) and 60-66°C (depending on primers used) (1 min). The qPCR reactions were then heated gradually to 95°C for dissociation curve analysis. Raw data was analysed using SDS software v2.3 (Applied Biosystems). DNA quantity at a specific chromosome end was normalised to the quantity of DNA given within the input DNA to give a measure of enrichment (E): E=IP/input. For the telomere-specific analysis of histone methylation marks, the enrichment of these marks was further normalised against enrichment of histone H3 at the same telomere.

2.15.2 qPCR primer optmisation

Amplification efficiency of primer sets was determined by creating a standard curve using 10-fold serial dilutions of gDNA (50, 5, 0.5, 0.05ng). The gradient value from the standard curve was used to calculate the efficiency of the qPCR reaction using the following formulas:

$$E=10^{(-1/\text{gradient})}$$

$$\% \text{ Efficiency}=(E-1)*100.$$

A standard curve gradient of -3.3 indicates complete doubling of PCR product during each cycle: When used in the first of the above formulas a gradient of -3.3 would result in an efficiency (E) of 2:

$$E=10^{(-1/-3.3)}$$

$$E=2$$

This can then be converted into % Efficiency:

$$\% \text{ Efficiency}=(2\text{-}1)*100$$

$$\% \text{ Efficiency}=100$$

When E=2 % the efficiency of the qPCR assay is 100%. The acceptable range for the standard curve gradient is between -3 and -3.6 which would produce qPCR assays of 115% and 90% respectively.

Triplicate 20µl qPCR reactions were set up containing gDNA, 1X iQ™ SYBR® green supermix (Biorad), ddH_20 and 0.3µM forward and reverse primers. qPCR reactions were then cycled in an ABI PRISM 7700 (Applied Biosystems) using the following cycling conditions: 94°C (10 mins) followed by 50 cycles of 94°C (20 sec), 60-66°C (1 min). The qPCR reactions were then gradually heated to 95°C to determine the melting temperature (Tm) of amplified PCR product. Analysis of the qPCR assays was performed on SDS software v2.3 (Applied Biosystems).

2.16 Cell culture

2.16.1 Cells and media

MRC5 cells were obtained from the Coriell cell repository (Institute for Medical Research, Camden, New Jersey, USA). HT1080 and HeLA cells were obtained from Prof. Paul Smith (School of Medicine, Cardiff University) and keratinocyte holoclone populations were provided by Matthew Locke (School of Dentistry, Cardiff University).

Cells were incubated in 5% CO_2 at 37°C. MRC5 cells were cultured in Eagle's minimum essential medium (EMEM, Invitrogen), supplemented 0.1N sodium hydroxide, with sodium bicarbonate (7.5% solution, Gibco), 2X non-essential amino acids, 25mM HEPES, $1X10^5$ U/l penicillin, 100mg/l streptomycin, 2mM L-glutamine (all sigma) and 10% (v/v) foetal calf serum (Autogenbioclear).

HT1080 clones (2, 4, 5, 15, 17, 19) and HeLa cells were cultured in Dulbecco's Modified Eagle's Medium (DMEM, Invitrogen) supplemented with $1X10^5$ U/l penicillin, 100mg/l streptomycin, 2mM L-glutamine (all sigma) and 10% (v/v) foetal calf serum (Autogenbioclear). U87 cells were cultured in U87-MG containing RPMI (Invitrogen), 2X non-essential amino acids $1X10^5$ U/l penicillin, 100mg/l streptomycin, 2mM L-glutamine (all Sigma) and 10% (v/v) foetal calf serum (Autogenbioclear). Keratinocyte holoclone C1B cellswere cultured in HNCC which consisted of Dulbecco's Modified Eagle's Medium (DMEM, Invitrogen) supplemented with Ham's F12 nutrient mixture (Gibco), 89μM adenine, 10^{-4}μM cholera toxin, 400ng/ml hydrocortisone, 10ng/ml epidermal growth factor, 5μg/ml insulin (all Sigma) and 10% (v/v) foetal calf serum (Autogenbioclear). Medium was changed every 3-4 days and cells were passaged when ~80% confluence was reached.

2.16.2 Trypsinising and passaging cells

Cells were washed with HANKs balanced salt solution (Sigma) to remove all remaining serum. To detach the washed cells an appropriate amount of pre-warmed 1Xtrypsin (Life Technologies) was added and the cells were incubated at 37°C until all cells had detached from the plate. After detachment of cells, fresh medium was added to deactivate the trypsin and this cell suspension was transferred to a 15ml falcon tube. For re-plating sufficient numbers of cells and fresh medium was added to a new flask or well.

2.16.3 Counting cells and calculating population doublings

To monitor population doublings cells were counted at every passage. After trypsinisation 10μl cell suspension were counted in a haemocytometer (Impreoved Neubauer, Hawksley). Cell number was then calculated using the following formula:

Total cell no. = (number of counted cells X 10^4) X cell suspension volume (ml)

Population doublings could then be determined using the formula:

PD= [log (total cell number) – log (seeded cell number)]/log2

2.16.4 Cell freezing

Cells to be frozen were pelleted by centrifugation and resuspended in equal volume of growth medium and freezing mixture (4:1 foetal calf serum:dimethylsulfoxide (DMSO)). The suspension was then transferred to freezing ampoules which was placed in a freezing box containing isopropanol. This method ensures gradual freezing and prevents the formation of ice crystals in the cells. Cells were then frozen at 80°C and kept at this temperature for short term storage. For long term storage ampoules were transferred to liquid nitrogen (-196°C).

2.16.5 Cell thawing

Cells were removed from the -80°C freezer or liquid nitrogen and thawed rapidly in a water bath (Grant) at 37°C. Once thawed DMSO was removed by adding 9ml of fresh culture medium drop-wise (the slow dilution minimised cell damage through osmotic shock). The cell suspension was centrifuged (1000rpm, 5 minutes) and supernatant was removed. The cell pellet was then resuspended in the appropriate volume of culture medium and re-plated.

2.16.6 Senescence assay

Senescence of cultured cells was measured by the Senescence Detection Kit (Abcam). Cells cultured in 12-well plate wells were washed with 1XPBS before being fixed in fixative solution for 15 minutes at room temperature. After two washes with 1XPBS the cells were stained overnight at 37°C with a staining solution mix (staining solution, staining supplement, X-gal in DMF (N-N-dimethylformanide) (1mg/ml)). The following day % senescence was calculated by counting the number of blue senescent cells in a total cell number of 500.

2.17 siRNA knockdown

siGENOME SMARTpool siRNA duplexes against all candidate genes encoding chromatin remodelers were obtained (Dharmacon, Thermo Scientific). For each candidate gene, siRNA knockdowns were performed on four independent cell populations. Three successive siRNA transfections were performed for each cell population at intervals of 48h (HT1080 cl. 2) or 96h (Keratinocyte C1B cells). Cells which were not subject to siRNA transfection (untreated) were grown in parallel as were cells that were either subject to transfection with a negative control siRNA or subject to a 'mock' transfection.

2.17.1 Transfection procedure

Keratinocyte holoclone C1B and HT1080 clone 2 cells were cultured in either 24-well or 96-well plate wells. At 70-80% confluency cells were transfected with 25nm siRNA.

siRNA was diluted to a concentration of 250nM in 1XsiRNA buffer (Dharmacon) and optiMEM (Invitrogen). siRNA was then mixed with DharmaFECT transfection reagent and incubated at room temperature for 20 minutes. After incubation the siRNA-DhramaFECT complexes were diluted 10X in antibiotic-free complete medium resulting in a final siRNA concentration of 25nM and a final DharmaFECT concentration of 0.2μl/96-well plate wells or 1μl/24 well plate wells. This transfection mix was then added to the cells (100μl for 96 well plates, 500μl for 24 well plates). Cells were incubated at 37°C in 5% CO_2 for 12 hours after which the transfection mix was replaced by antibiotic-free complete medium. To determine the success of the knockdown RNA was extracted from the cells and copied to cDNA. Expression levels of each gene were then analysed by real-time PCR.

2.17.2 RNA extraction

RNA was extracted from cells using the Cells-to-cDNA™ II kit (Ambion). Cells were washed with 1XPBS before they were lysed by incubation at 75°C for 10 minutes in Cell Lysis II buffer. Following lysis genomic DNA was degraded by the addition of 4U DNase I and incubating at 37°C for 15 minutes. The DNase I was then inactivated at 75°C for 5 minutes. Cell lysates were then stored at -20°C or -80°C for long term storage.

2.17.3 Reverse transcription

To obtain cDNA from the extracted RNA, reverse transcription reactions were set up containing cell lysate containing the RNA template, 625µM dNTPs, 6.25µM random decamers and nuclease-free water. After briefly heating the reaction (70°C, 3 mins) 1X RT buffer, M-MLV Reverse Transcriptase and 10U RNase inhibitor was added. The reaction was then incubated at 42°C for 60 minutes followed by a 10 minute incubation at 95°C to inactivate the reverse transcriptase. Resulting cDNAs were either stored at -80°C or added to qPCR reactions to measure gene expression.

2.17.4 Gene expression analysis

Triplicate qPCR reactions were set up for each cDNA sample containing cDNA (5X diluted), 1X Taqman Fast Universal PCR Master Mix (Applied Biosystems) and 1X Taqman Gene Expression Assay Mix targeted against either the ATRX, DAXX, EZH2 or ACTB (endogenous control) genes. qPCR reaction were then cycled in a ABI PRISM 7700 (Applied Biosystems) under the following conditions: 60°C (1 min) 95°C (20 sec) followed by 4 cycles of 95°C (1 sec) and 60°C (20 sec). Relative gene expression was measured by the ΔΔCt method which compares Ct values derived from amplification

of target genes with the Ct values of an endogenous control (ACTB). This analysis was performed using SDS RQ manager (Applied Biosystems).

Chapter 3

The development of qPCR assays at 2p, 11q, 12q, 16p, 17p, 18q and XpYp telomeres

3.1 Abstract

Differences in telomere length exist between chromosome ends within a cell population and between telomeric alleles at the same chromosome end. Additionally, shorter telomeres are preferentially elongated by telomerase. These observations suggest a mechanism responsible for the maintenance of telomere length and for the targeting of shorter telomeres for elongation. Single Telomere Length Analysis (STELA) assays have previously been developed for a number of different chromosome ends including 2p, 11q, 12q, 16p, 17p, 18q and XpYp (allele-specific). The aim of this chapter was to develop telomere- and allele-specific quantitative PCR (qPCR) assays for these same chromosome ends, which, when used in conjunction with Chromatin Immunoprecipitation (ChIP) will allow the enrichment of histone modifications at the telomere to be measured. Together, analysis of telomere length and patterns of telomeric enrichment of histone modifications will shed light on whether chromatin structure plays a role in telomere length regulation. Past research studying telomeric chromatin has been fruitful in identifying a handful of important histone modifications involved in maintaining proper telomeric chromatin structure. however this work has drawbacks: telomeric enrichment of histone modifications is measured using dot-blot assays which lack telomere specificity therefore measurements of a certain histone modification at a specific telomere cannot be achieved. Similarly methods used to measure telomere length in this work lack telomere specificity; FISH and Terminal Restriction Fragment (TRF) analysis have been the gold standard in recent years when determining telomere length however neither technique can produce such a high resolution, quantifiable, telomere specific measurement of telomere length as STELA. Using telomere-

specific qPCR along with ChIP in parallel with STELA can provide a powerful tool for discovering relationships the chromatin structure of a telomere and its length

3.2 Introduction

3.2.1 qPCR history

The first example of quantification of a polymerase chain reaction (PCR) was described in 1988. This method involved the use of biotin labelled primers to generate 5' biotinylated DNA molecules. After hybridization to a labelled probe, these PCR products were collected on an avidin matrix and the amount of labelled PCR product could be quantified (Syvänen *et al.* 1988). Subsequently other end-point quantification methods were proposed (Becker-André and Hahlbrock 1989; Gilliland *et al.* 1990) however the breakthrough in quantifying PCR was the introduction of real-time quantification of PCR products which allows the simultaneous amplification and detection of PCR products (Higuchi *et al.* 1992). Since the development of real-time PCR (RT-PCR) it has been adapted for numerous molecular biology applications. Not only has it become the standard method used in measuring gene expression, it is also used for pathogen detection (Egli *et al.* 2001; Gut *et al.* 1999; Kato *et al.* 2000), single nucleotide polymorphism (SNP) analysis (Mattarucchi *et al.* 2005; Mhlanga and Malmberg 2001), analysis of chromosome aberrations (Peter *et al.* 1997; Zucman *et al.* 1993) and more recently protein detection (Gillis *et al.* 2011).

3.2.2 Chromatin Immunoprecipitation and qPCR

In addition to the above applications, qPCR is also used for the post-chromatin immunoprecipitation (ChIP) quantification of chromatin-bound protein.

ChIP is a key method used in the study of chromatin structure and dynamics. It can be used to measure the enrichment of chromatin-bound proteins such as transcription factors and chromatin remodelling proteins or it can be used to directly analyse chromatin structure by measuring the degree of enrichment of histone modifications such as histone methylation and histone acetylation. The ChIP process involves an antibody specific to the protein of interest which is used to immunoprecipitate cross-linked chromatin fragmented to ~500bp. DNA immunoprecipitated with the protein of interest is then reverse cross-linked from the protein and purified. QPCR amplifies a specific region designated by the primers from the DNA 'pulled down' with the protein giving a measure of the enrichment of the protein of interest at that region. qPCR has several advantages over other post ChIP enrichment analysis methods; it provides high resolution, sensitive method for analysing enrichment of chromatin bound protein, it is also highly adaptable as enrichment of a particular protein of interest can be measured anywhere in the genome providing primers can be designed to the region. Additionally it requires less starting material than other post-ChIP analysis techniques meaning that protein enrichment within more regions of interest can be studied from a single immunoprecipitation.

The ChIP analysis of protein enrichment at specific genomic loci has been used to study a wide range of cellular processes such as transcriptional activation and repression, the regulation of large chromosomal domains, the DNA damage response and also telomere maintenance.

3.2.3 ChIP and qPCR at the telomere

Quantitative analysis of chromatin-bound protein enrichment at chromosome ends is problematic because of the DNA sequences of telomeric and subtelomeric DNA: The repetitive nature of telomeric DNA impedes the design of functional primers within the telomere and the sequence homology between subtelomeric regions from different chromosome ends means that designing subtelomere-specific primers is also difficult. Despite these challenges, telomeric qPCR has been developed for three chromosome ends in *Saccharomyces cereisiae.* These are based on telomeres with a relatively unique structure that lacks the conserved Y' and X elements found at other chromosome ends.

Specifically, qPCR assays have been designed within the subtelomeric region but which reside close to the telomeric repeat tract at the right arm of chromosome VI (Tel VI-R), the left arm of chromosome I (TelIL) and the left arm of chromosome VII (Tel VII-L) (Fisher *et al.* 2004; Luke et al. 2008; Takata *et al.* 2004; Takata *et al.* 2005; Yu et al. 2007). These qPCR assays are used as standard when measuring telomeric protein enrichment in budding yeast.

In *Drosophila* qPCR and conventional PCR methods have been used with ChIP to analyse telomeric chromatin structure in a small number of studies. (Burgio *et al.* 2011) Conventional PCR has been used to detect presence of telomeric enrichment of various heterochromatin marks including H3K9me3, H3K27me3, H4K40me3 histone H3 and H4 acetylation at the *Het-A* terminal repeat retrotransposon (Burgio et al. 2011). In work studying the telomere capping proteins, HP1/ORC-associated protein (HOAP), HOAP interacting protein (HipHop) and HP1 were shown to be enriched at an artificial model telomere by qPCR (Gao et al. 2010). This model telomere was constructed through I-SceI

endonuclease-induced deletion of a P-element insertion at the tip of chromosome 2R which resulted in the generation of a new telomere. Adjacent to this new telomere was a non-repetitive region which allowed qPCR primer design.

The few examples given above of post-ChIP qPCR analysis of telomeric enrichment demonstrate the difficulty in generating robust qPCR assays at chromosome ends. Considerable effort has been put into obtaining such assays which must reflect the value of qPCR and the benefits in using qPCR over more traditional post-ChIP analysis methods when studying telomeric chromatin.

3.2.4 qPCR at human telomeres

qPCR has previously been utilized at human telomeres as a means of measuring telomere length (Cawthon 2002, 2009; O'Callaghan and Fenech 2011). Telomere length is measured using primers that bind telomeric repeats, as telomere length increases the number of binding sites for the primers also increases. Telomeric copy number is then compared to a single copy reference gene within the same sample to give an indication of relative telomere length. This method has been employed to measure telomere length in a number of varying studies (Aviv *et al.* 2011; Fernandez-Moreno *et al.* 2011; Marcondes *et al.* 2009; Pavesi *et al.* 2009; Wong *et al.* 2011).

Although qPCR has been used with ChIP in human cells to study protein enrichment at various loci throughout the genome for a variety of cellular processes qPCR at human telomeres remains a largely unexplored field.

Due to the inability to design primers to the TTAGGG repeat tract qPCR has not been considered a suitable post-ChIP method to analyse telomeric protein enrichment at human telomeres. An alternative method is to design a qPCR assay within the subtelomeric region immediately adjacent to the TTAGGG repeat tract. This is the approach taken in telomeric ChIP studies in yeast and allows measurement of enrichment of a protein within the telomere repeat tract. This method is also problematic because of two reasons: firstly, a number of human chromosome ends have not been fully sequenced up to the TTAGGG repeats therefore the position of a primer set in relation to the telomere repeats would be unknown. Secondly, the high level of sequence homology shared between different human subtelomeres makes it difficult to design a primer set which will amplify only one subtelomere. There are however nucleotides within telomere-adjacent regions which are specific to that single chromosome end. Exploiting these nucleotides when designing primers is how telomere-specificity can be achieved. Designing qPCR primers around these nucleotides will result in a qPCR assay directly adjacent to the TTAGGG repeats which can be used to detect protein enrichment within the telomere.

Traditionally the method used for analysing chromatin-bound protein enrichment in mammalian cells is chromatin immunoprecipitation followed by dot blots (Benetti et al. 2007b; Garcia-Cao *et al.* 2002; Garcia-Cao et al. 2004a; Jones et al. 2008; Loayza and De Lange 2003). This approach has been taken in a number of studies and although it has been successful it has drawbacks: Firstly, the TTAGGG repeat probe used for detecting immunoprecipitated telomeric DNA detects telomeric DNA from every chromosome end therefore telomere to telomere comparisons cannot be made. Secondly, there are

sensitivity issues with this technique with very subtle differences in enrichment are likely to be missed.

Despite these drawbacks of ChIP-dot blot assays it is important to note that there are advantages of using this system instead of qPCR as a post-ChIP analysis of human telomeric enrichment. A qPCR assay can only detect enrichment of a protein from chromatin fragments which contains the region to which the qPCR assay has been designed to whereas a dot blot can measure enrichment throughout the entire telomere repeat array. This issue becomes problematic when studying telomeres longer than the size of the sonicated chromatin fragments and is particularly relevant at human telomeres which can be up to 15kb in length (de Lange et al. 1990) . Therefore when investigating the role of telomere binding proteins such as the shelterin components or telomerase in telomere length regulation the qPCR assays are not suitable. Extensive evidence indicates that telomere length in humans is evaluated at each chromosome end by the extent of TRF1 binding along the length of the telomere (Smogorzewska et al. 2000; van Steensel and de Lange 1997). Considering that qPCR assays are limited to detecting enrichment only at regions incorporating the qPCR amplicon differences between TRF1 enrichment between telomeres of different length would not be seen.

Using the telomere-adjacent qPCR assays to measure telomeric enrichment in relation to telomere length in yeast is a more pertinent method as telomere length in yeast is ~300bp. Therefore the chromatin fragments amplified by the telomere adjacent qPCR assay would incorporate the entire telomere repeat tract. However there are examples, even in yeast were dot blot assays have been used instead of qPCR as the post-ChIP detection method. One such example is in a study investigating the role of Taz1 and Rap1 in telomere length

regulation in *S. pombe* (Dehe *et al.* 2012). In this study telomerase enrichment at the telomere terminus was analysed in yeast strains *taz1Δ* and *rap1Δ*. Telomere elongation within these strains resulted in telomeres much longer than the size of the sonicated chromatin fragments (0.5kb) therefore the telomere adjacent qPCR assays would not be able to detect telomerase enrichment at the telomere terminus. Because of this limitation of the qPCR assay the authors used the dot blot approach to measure telomerase enrichment.

Despite this drawback of the ChIP-qPCR approach, it is still a suitable method for analysing telomeric chromatin structure at human chromosome ends. Although the enrichment of histone modifications cannot be measured along the entire length of the chromosome such differences may exist at the region detected by the qPCR assays and will reflect differences in chromatin structure at different chromosome ends.

3.2.5 Aims of the project

Single Telomere Length Analysis (STELA) enables the measurement of telomere length distributions at a single chromosome end. Telomere-specificity is achieved through the use of a subtelomeric primer incorporating often only a single nucleotide specific to that chromosome end. The aim of this chapter is to use a similar approach in primer design to generate telomere- and telomeric allele-specific qPCR assays which when used with ChIP will allow the analysis of chromatin structure of an individual chromosome end.

3.3 Results

3.3.1 Telomere-specific qPCR assay development

3.3.1.1 PCR primer design

Because of the sequence homology between different subtelomeres of different chromosome ends and interstitial telomeres, it was necessary to identify nucleotides within a subtelomeric region specific only to that region using published telomere sequences from Reithman et al (http://www.wistar.upenn.edu/Riethman). Once identified, primers were designed around these nucleotides taking into account some key considerations. Firstly the primer designed should be approximately 20 nucleotides in length with a GC content of ~50%. Importantly the telomere-specific nucleotide should reside at the 3' end of the primer. It is this design parameter which gives specificity to one subtelomeric region as a mismatch will occur when the primer anneals to other highly similar subtelomeric sequences from other chromosome ends, resulting in failure of the *Taq* polymerase to extend from the primer in a PCR reaction and hence failure to produce a PCR product from other, undesired subtelomeric regions. Other considerations include ensuring the PCR product is small enough to ensure an efficient qPCR assay (≤250nt) and as close to the telomere repeats as possible. The PCR product also had to include telomere-specific nucleotides to serve as markers during sequencing of the PCR product to confirm whether or not the PCR product generated during the PCR reaction is telomere-specific.

3.3.1.2 Primer optimization and sequencing

Once primers had been designed for a single subtelomeric region they were tested in a conventional PCR reaction. Specifically, a gradient PCR was employed which uses increasing annealing temperature in a single PCR programme across 12 identical reactions ranging from 55-72°C. PCR products were then resolved with a 1% agarose gel. This approach showed whether the primer set generated a correctly sized, robust PCR product. It also allowed identification of the most stringent conditions (i.e. highest annealing temperature) which allowed the generation of this product.

PCR product generated at this annealing temperature was then gel excised and sequenced to determine if the PCR product generated was specific to that subtelomeric region.

3.3.1.3 qPCR assay

Once sequencing of the generated PCR product confirmed specificity to the desired subtelomeric region, the efficiency of the primer set was then tested in a qPCR reaction. qPCR was performed using the annealing temperature which was shown via conventional PCR to amplify only the desired subtelomeric sequence. 10-fold series dilution of genomic DNA (50, 5, 0.5 & 0.05ng) was used as input DNA for triplicate qPCR reactions to create a standard curve. The gradient of the standard curve determines whether differences in Ct values obtained from the different reaction triplicates correspond proportionately to the 10-fold series dilution of gDNA as mentioned in material and methods section 2.15.2. Another factor to consider was whether the qPCR assay was only amplifying the correct PCR product and no other products of differing sizes. The dissociation curve determines how many PCR products of differing sizes are present after the last amplification cycle by measuring the temperature-dependant dissociation between two DNA strands. The PCR product is heated

gradually through their melting temperature (T_m) to 95°C, at the T_m the PCR product dissociates into single-stranded DNA causing a sudden decrease in SYBR green signal which the machine monitors. One PCR product and hence one T_m results in only one peak in the dissociation curve whereas two or more PCR products of differing sizes would be shown by two peaks.

Development of telomere-specific-qPCR assays was carried out for the 2p, 11q, 12q, 16p, 17p and 18q chromosome ends. An allele-specific qPCR assay was also developed within the subtelomeric region of both alleles of the XpYp telomere. The above procedure was applied to the design of primers for all the mentioned chromosome ends (unless otherwise stated) to produce robust, telomere-specific qPCR assays.

3.3.2 2p

Primers 2p1 and 2p2 were previously designed by another lab member. This primer set amplifies an amplicon 190nt in size which extends into the TTAGGG repeats (fig. 3.1a). When tested in conventional PCR using an annealing temperature ranging from 65°C-72°C amplification of the anticipated 190nt PCR product was seen at every annealing temperature without any generation of additional non-specific products (fig. 3.1b). Because of this clean PCR and because 2p-specificity had already been confirmed the primer pair was tested in a qPCR assay with an annealing temperature of 65°C. This amplification efficiency using 2p1 and 2p2 was poor and furthermore, several peaks were present in the dissociation curve showing that several amplicons were being simultaneously amplified (fig. 3.1c,d). In an attempt to stop the amplification of these additional amplicons the annealing temperature was increased to 72°C. Although the peaks in the dissociation curve are less prominent in this qPCR assay they are still present (fig. 3.1f). Also the amplification efficiency is still poor (fig. 3.1e) therefore this primer pair isn't suitable for qPCR. An additional 2p-specific qPCR primer was designed (2p13) which when used in conjunction with 2p1 produces an amplicon of 144nt which extends into the TTAGGG repeats (fig. 3.2a). A conventional PCR using this primer pair amplifies a PCR product of the anticipated size. At lower annealing temperatures (56-60.5°C) additional, larger products are also amplified so for this reason an annealing temperature of 62.8°C was used for subsequent PCR. The 144nt product amplified at a 62.8°C annealing temperature was gel extracted and sequenced using 2p13. The electrophenogram shows that the amplified product was specific to the subtelomeric region of the 2p chromosome end (see the highlighted bases which correspond to the 'marker' bases in (a) (fig. 3.2c). 2p1 and 2p13 were then tested in a qPCR assay. 2p13, when used in tandem with 2p1, produced a better qPCR assay than 2p2 and 2p1: the gradient from the standard curve generated was -4.42 resulting in an amplification efficiency of 68%, however

this is still too low (fig. 3.2d). Additionally, amplification of products of differing sizes occurs when less input gDNA (0.05ng) is present in the qPCR reaction (fig. 3.2e) therefore this assay isn't efficient or robust enough to be used with ChIP to measure enrichment of histone modifications at this chromosome end.

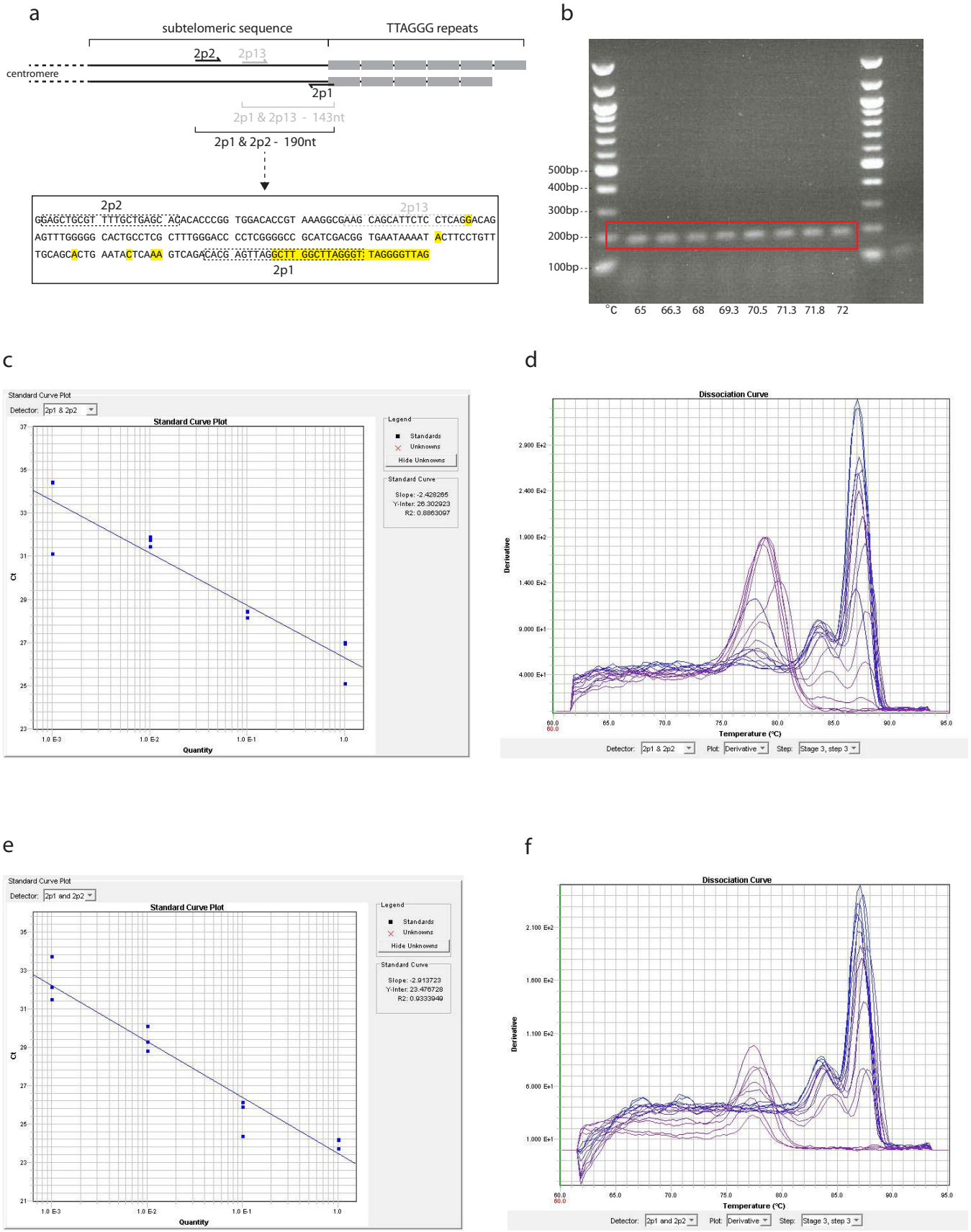

Figure. 3.1 qPCR assay development for 2p subtelomeric region using primers 2p1 & 2p2 (a) 2p1 was designed incorporating a stretch of 2p-specific nucleotides (highlighted in yellow). PCR product generated from 2p1 and 2p2 is 190nt in length, and extends into the TTAGGG repeats. (b) PCR performed using the stated annealing temperature gradient, products generated were ran on a 1% gel and visualized. The red box encircles PCR product of correct size. (c) A standard curve was set up to test the efficiency of the primers 2p1 & 2p2 in a qPCR assay using an annealing temperature of 65°C. The Ct values produced rom qPCR reactions contiaining 10-fold serial dilution of genomic DNA (50, 5, 0.5, 0.05ng) are plotted to create a standard curve with a gradient of –2.43. (d) Dissociation curve showing the temperature at which the PCR products generated from the qPCR amplification dissociates into ssDNA molecules. (e) The same qPCR assay as in (c) was repeated but with an annealing temperature of 72°C, producing a standard curve with a gradient of -2.91. (f) Dissociation curve from the qPCR assay performed with an annealing temperatureof 72°C still shows the presence of multiple product formation

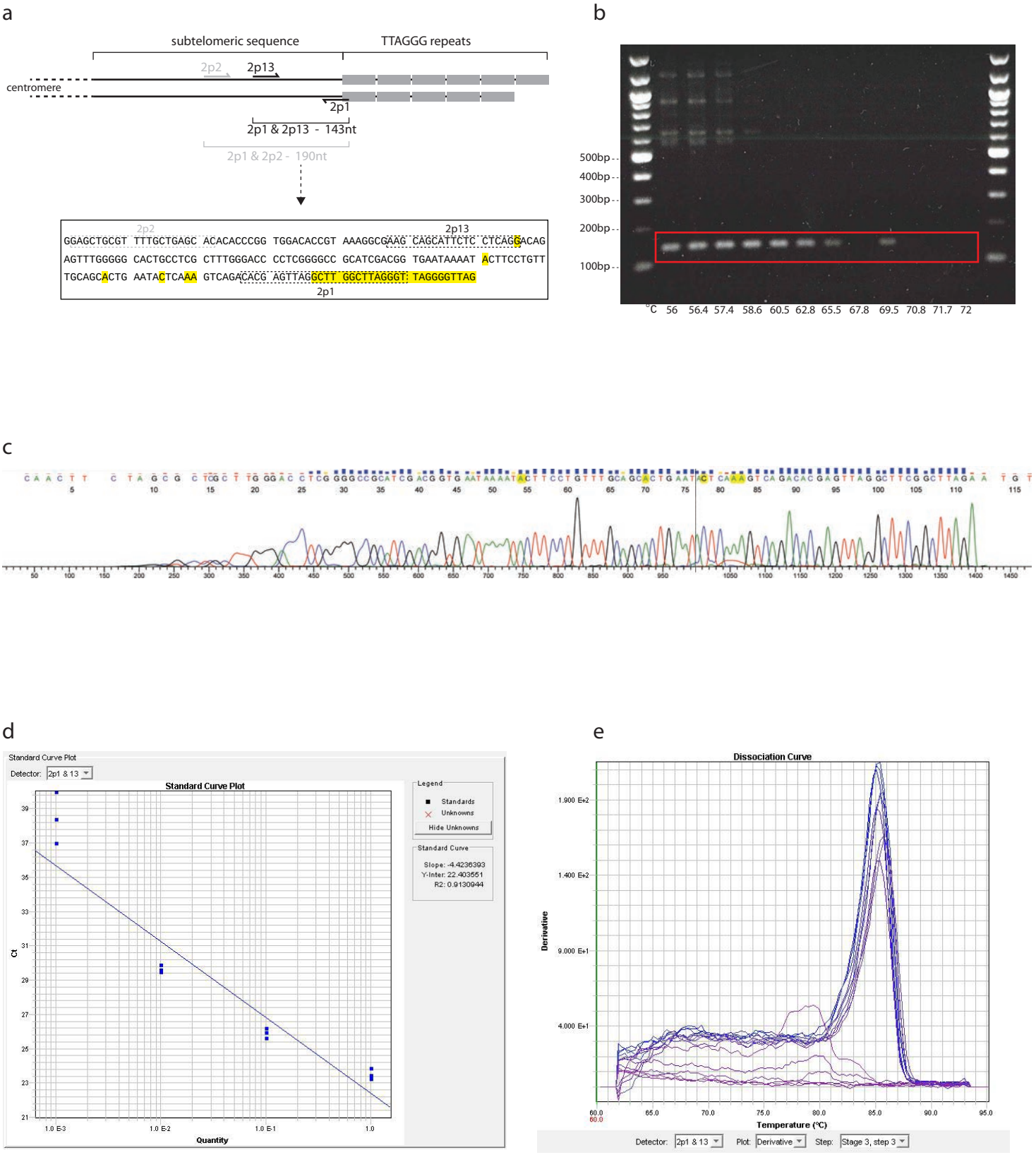

Figure. 3.2 qPCR assay development for 2p subtelomeric region using 2p1 & 2p13 (a) 2p13 was designed incorporating a 2p-specific nucleotide at it's 3' end (highlighted in yellow). PCR product generated from 2p1 and 2p13 is 144nt in length, and extends into the TTAGGG repeats. (b) PCR performed using the stated annealing temperature gradient, products generated were ran on a 1% gel and visualized. The red box encircles PCR product of correct size. (c) Electropherogram from sequencing of PCR product amplified using primers 2p1 & 2p13. 2p-specific nucleotides are highlighted and correspond to the highlighted nucleotides in (a). (d) A standard curve was set up to test the efficiency of the primers 2p1 & 2p2 in a qPCR assay using an annealing temperature of 62.8°C. The Ct values produced rom qPCR reactions contiaining 10-fold serial dilution of genomic DNA (50, 5, 0.5, 0.05ng) are plotted to create a standard curve with a gradient of –4.42. (e) Dissociation curve showing the temperature at which the PCR products generated from the qPCR amplification dissociates into ssDNA molecules.

3.3.3 11q

A previous lab member had also designed 11q-specific primers (11q12 and 11q13B) to generate products for use as a hybridisation probe. A conventional PCR reaction using 11q12 and 11q13B produced a PCR product 95 nucleotides in length 11 nucleotides from the TTAGGG repeats (fig. 3.3a). A PCR product of the correct size was generated at the lower annealing temperatures (65-70.5°C) (fig. 3.3b). The performance of these primers was then tested in a qPCR reaction using an annealing temperature of 66°C. The Ct values generated from the serial dilution produced a standard curve with a gradient of -3.413 meaning that the qPCR efficiency is 96.3% (fig. 3.3c). The dissociation curve shows a single sized product being formed in the qPCR reaction for all the dilutions of gDNA (fig. 3.3d) therefore 11q12 and 11q13B result in the efficient amplification of the 11q subtelomeric region in a qPCR reaction.

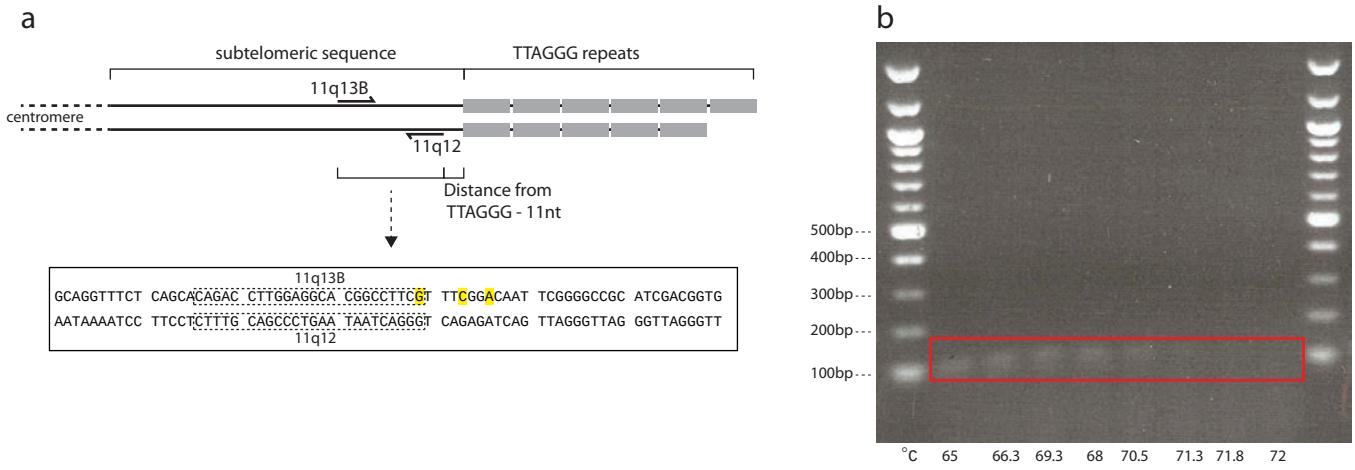

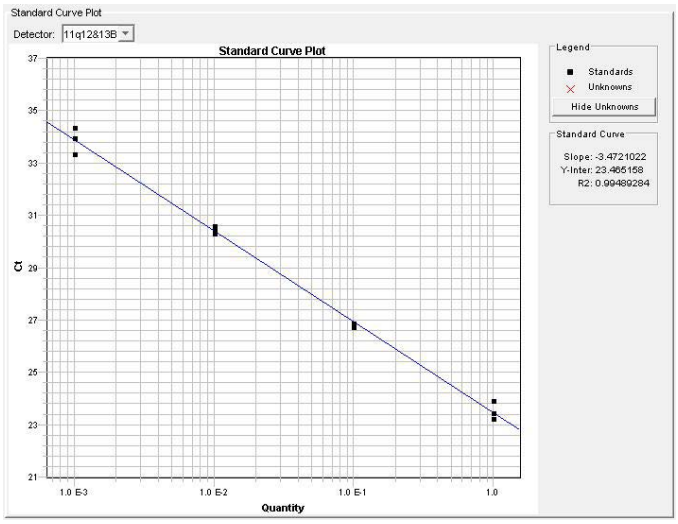

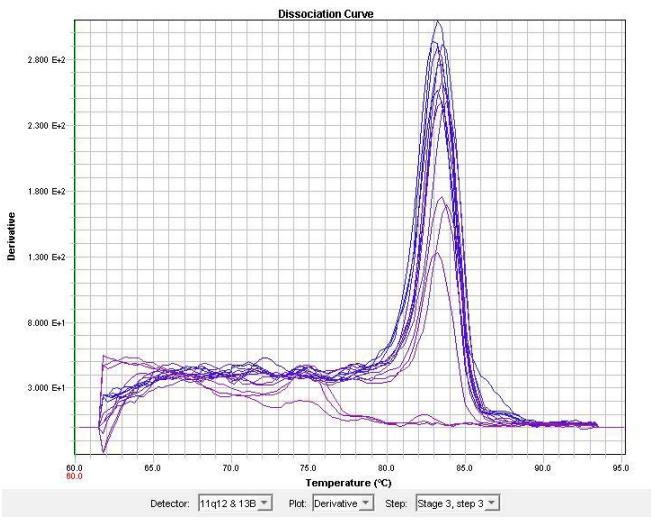

Figure. 3.3 qPCR assay development for 11q subtelomeric region (a) Primers 11q12 and 11q13B were previously designed, 11q13B contains an 11q-specific nucleotide at it's 3' end (highlighted in yellow). These primers generate a PCR product 95nt in length 11nt from away from telomere repeats. (b) PCR was performed using the stated annealing temperature gradient, products generated were ran on a 1% gel and visualized. The red box encircles PCR product of correct size. (c) A standard curve was set up to test the efficiency of the primers 11q12 and 11q13B in a qPCR assay using an annealing temperature of 66°C. The Ct values produced rom qPCR reactions contiaining 10-fold serial dilution of genomic DNA (50, 5, 0.5, 0.05ng) are plotted to create a standard curve with a gradient of -3.413 (d) Dissociation curve showing the temperature at which the PCR product generated from the qPCR amplification dissociates into ssDNA molecules

3.3.4 12q

The subtelomeric sequence of 12q contains two diverged haplotypes (fig. 3.4a) (Baird et al. 2000). In order to develop an assay specific to 12q, but not to differentiate between the haplotypes, it was important to design primers around 12q-specific nucleotides present in both haplotypes. The 12q subtelomere was a good candidate for qPCR assay design, not only due to the relatively high number of 12q-specific nucleotides, but also because of their abundance close to the TTAGGG repeats. Indeed, primers 12qA1 and 12qB each contained three 12q-specific bases within their sequence with one of these nucleotides residing at the primers' 3' end. The resulting product was 254nt in length and 20nt from the TTAGGG repeats (fig. 3.4a). In a conventional PCR 12qA1 and 12qB generated the expected 254nt amplicon with minimal non-specific amplification of PCR products of differing sizes even at lower annealing temperatures (fig 3.4b) To ensure amplification of the 12q subtelomeric region specifically an annealing temperature of 66°C was chosen for future PCR. Sequencing of this product using 12qA1 showed that it was specific to the 12q subtelomere (see the single peaks at the highlighted bases, fig. 3.4c), it also revealed that haplotype B was preferentially amplified: position 192 on the electrophenogram shows a larger peak for the haplotype B-specific base T however there is also a peak for the haplotype A-specific C base showing that this haplotype is also amplified (fig. 3.4c). 12qA1 and 12qB were tested in a qPCR reaction with an annealing temperature of 66°C. The Ct values resulting from the amplification of the 10-fold gDNA dilutions produced a standard curve with a gradient of -3.42, the efficiency of the assay was calculated as 96.1% (fig. 3.4d). The dissociation curve was consistent with the melting of a single amplicon however in reactions containing less gDNA peaks were produced at lower temperatures suggesting the presence of smaller non-specific amplicons or primer-dimer formation (fig. 3.4e). This was seen on a number of occasions and may well limit the functionality of this assay when used to amplify more dilute DNA.

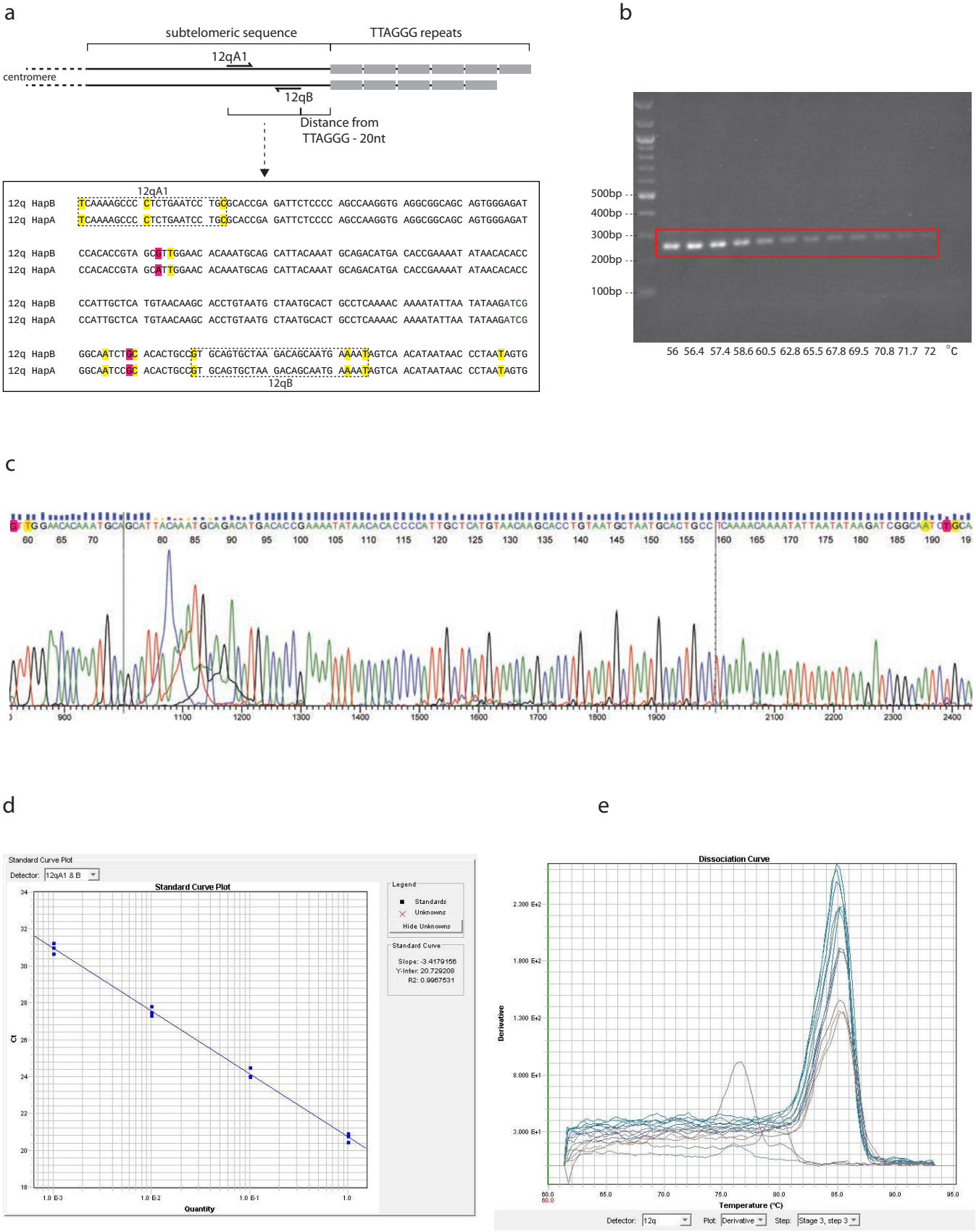

Figure. 3.4 qPCR assay development for 12q subtelomeric region (a) Primers 12qA1 & 12qB were designed incorporating 12q-specific nucleotides (12q-specific nucleotides highlighted in yellow, haplotype-specific bases highlighted in pink). PCR product is 254nt in length, 20nt from TTAGGG repeats. Region to be amplified also contains 12q specific 'marker' nucleotides. (b) PCR performed using the stated annealing temperature gradient, products generated were ran on a 1% gel and visualized. The red box encircles PCR product of correct size. (c) Electrophenogram from sequencing of PCR product amplified using primers 12qA1 and 12qB. 12q-specific and haplotype-specific nucleotides highlighted correspond to marker nucleotides in (a). (d) A standard curve was set up to test the efficiency of the primers 12qA1 and 12qB in a qPCR assay using an annealingtemperature of 66°C. The Ct values of a 10-fold serial dilution of genomic DNA (50, 5, 0.5, 0.05ng) are plotted to create a standard curve with a gradient of –3.417 (e) Dissociation curve showing the temperature at which the PCR product generated from the aPCR amplification dissociates into ssDNA molecules

3.3.5 16p

Primers 16pC and 16pBrev were designed around two 16p-specific nucleotides in the 16p subtelomeric region 190 nucleotides from the TTAGGG repeats (fig. 3.5a). In a conventional PCR reaction a PCR product of the desired 178 nucleotides was generated from 16pC and 16pBrev however at lower annealing temperatures larger, non-specific PCR products were also generated (fig. 3.5b). When an annealing temperature of 62.8°C or above was used these non-specific products failed to amplify leaving only the desired 178nt product. Sequencing of the gel-extracted 178nt PCR product using 16pC revealed that it was 16p-specific as shown by the highlighted 'marker' bases (fig. 3.5c). 16pC and 16pBrev were then tested in a qPCR reaction: Ct values generated from qPCR reactions containing 10-fold dilutions produced a standard curve with a gradient of -3.55 and subsequently a qPCR assay efficiency as 91.2% (fig. 3.5d). A single peak in the dissociation curve shows that the single 16p-specific amplicon is being generated during the assay. However no amplification was seen in the qPCR reactions containing 0.05ng of gDNA suggesting that very small amounts of starting gDNA may be difficult to detect using this 16p qPCR assay (fig. 3.5e).

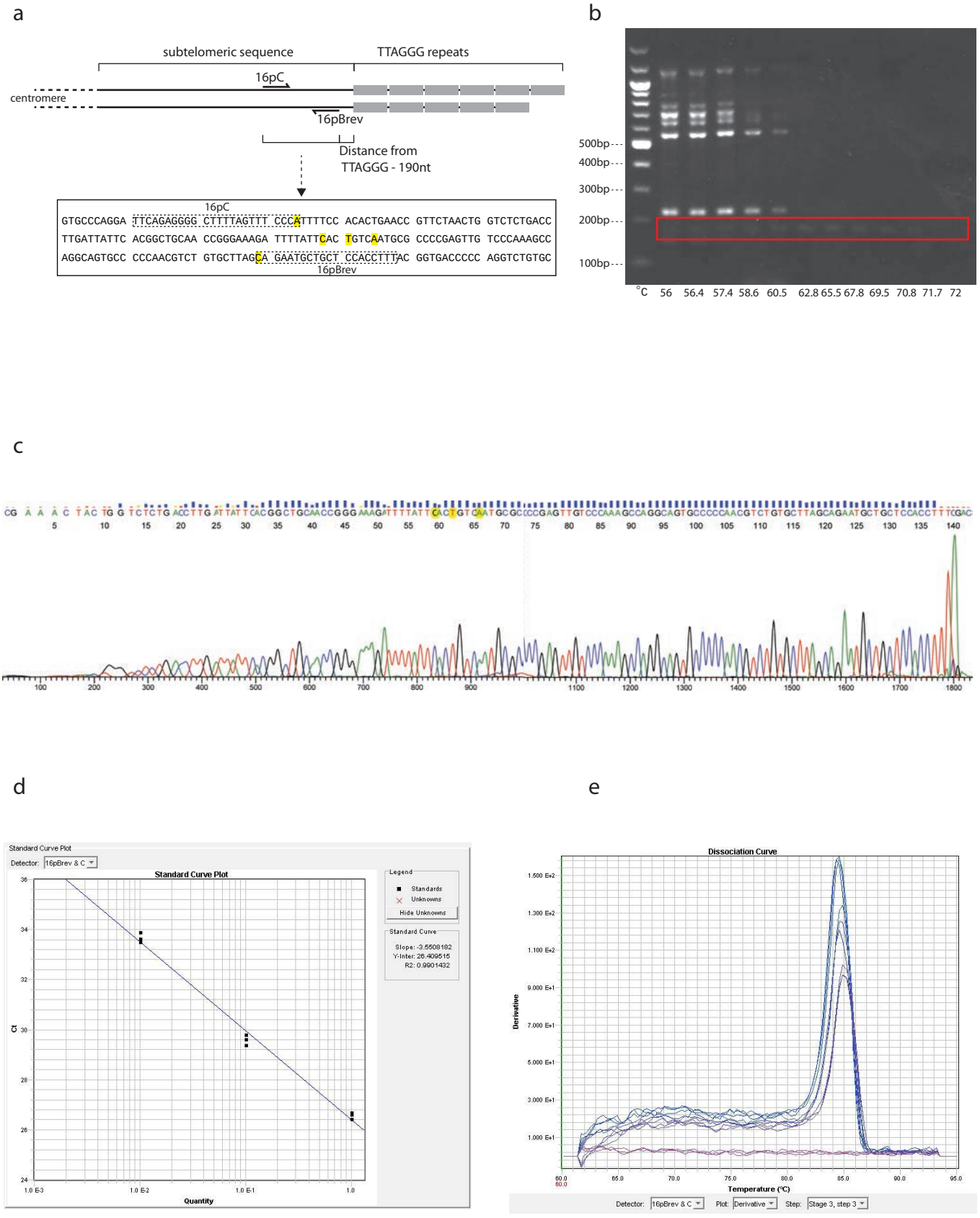

Figure. 3.5 qPCR assay development for 16p subtelomeric region (a) Primers 16pBrev & 16pC were designed incorporating 16p-specific nucleotides (highlighted in yellow). PCR product is 178nt in size and 190nt from TTAGGG repeats. Region to be amplified also contains 16p-specific 'marker' nucleotides. (b) PCR was performed with the stated annealing temperature gradient, products generated were ran on a 1% gel and visualized. The red box encircles PCR product of correct size. (c) Electrophenogram from sequencing of PCR product amplified using primers 16pBrev & 16pC. 16p-specific nucleotides are highlighted and correspond to the highlighted nucleotides in (a).(d)) A standard curve was set up to test the efficiency of the primers 16pBrev & 16pC in a qPCR assay using an annealing temperature of 62.8°C. The Ct values of a 10-fold serial dilution of genomic DNA (50, 5, 0.5, 0.05ng) are plotted, the resulting gradient from the standard curve is –3.55 (e) Dissociation curve showing the temperature at which the PCR product generated from the aPCR amplification dissociates into ssDNA molecules

3.3.6 17p

Designing 17p-specific primers proved particularly difficult due to the paucity of 17p-specific bases in the 17p subtelomeric region. Because of this of the two primers designed (17pA and 17pB) only 17pA possessed one 17p-specific base at its 3' end (fig. 3.6a) and the amplicon was further away from the TTAGGG repeats (426nt). Using this primer set in conventional PCR resulted in strong amplification of a product 245nt in size with minimal amplification of larger, non-specific products even at the lower annealing temperatures (fig. 3.6b). Gel-extracted PCR product was sequenced using 17pA as the sequencing primer revealing that the amplicon was specific to the 17p subtelomeric region (see highlighted 'marker' base fig. 3.6c). Once the specificity of the primer set was confirmed their performance in a qPCR reaction was tested. Initially when an annealing temperature of 67.8°C was used in the cycling conditions the efficiency of the qPCR assay was poor: amplification was weak and the Ct values generated between each point in the standard curve didn't reflect the 10-fold difference in input gDNA. To solve this problem a lower annealing temperature was used (64°C) which greatly improved the amplification efficiency resulting in a standard curve gradient of -3.36 and qPCR efficiency as 98.4% (fig. 3.6d). The dissociation curve shows a single peak indicating the melting of only one PCR product in the qPCR reaction (fig. 3.6e). Therefore using 17pA and 17pB in a qPCR reaction efficiently and specifically amplifies a 245nt amplicon in the 17p subtelomeric region.

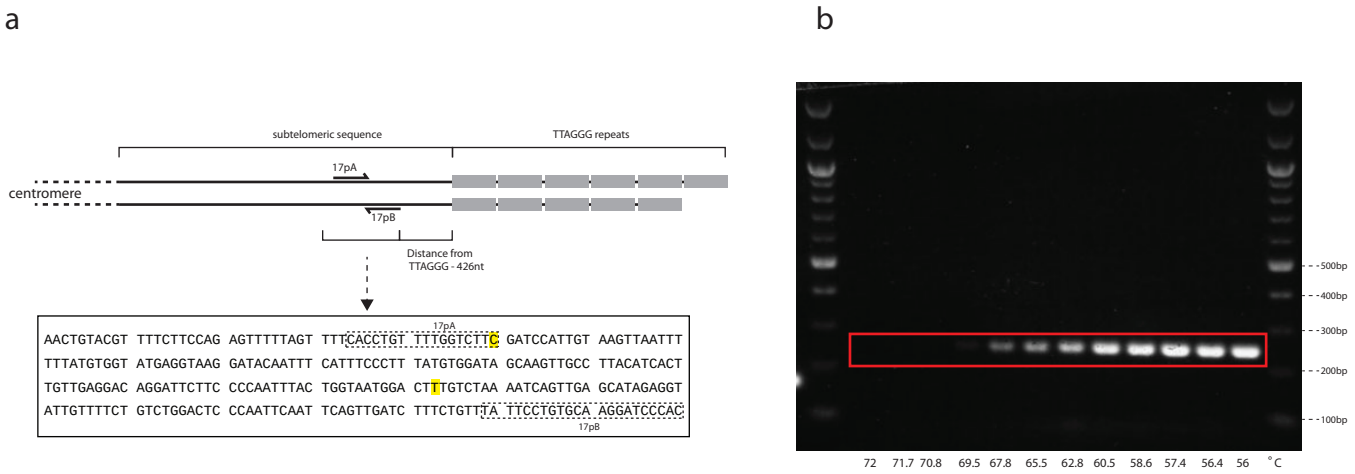

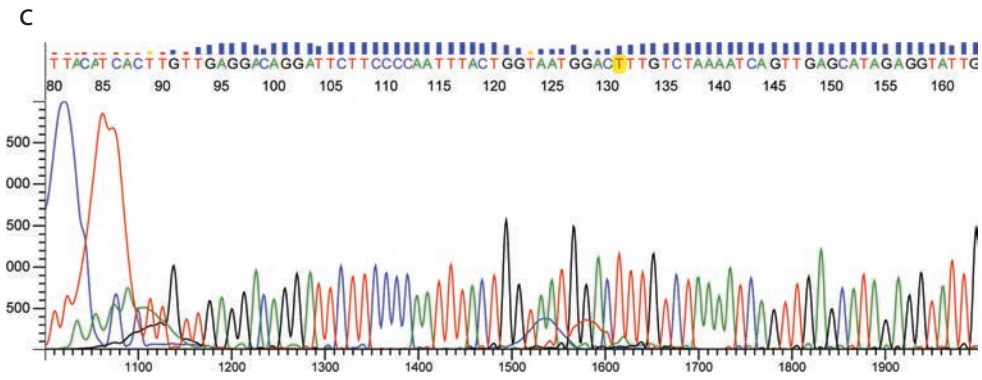

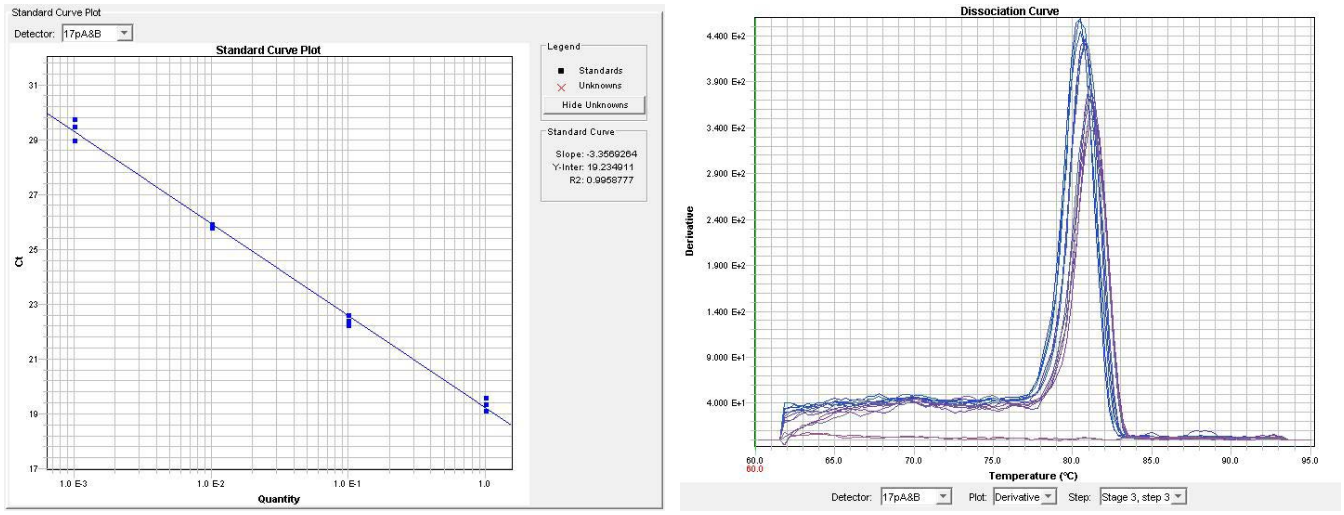

Figure. 3.6 qPCR assay development for 17p subtelomeric region (a) Primer 17pA was designed incorporating a 17p-specific nucleotide at its 3'end. Nucleotides specific to 17p are highlighted in yellow. The PCR product is 245nt in size and 426nt away from telomere repeats . (b) PCR was performed with the stated annealing temperature gradient, products generated were ran on a 1% gel and visualized. The red box encircles PCR product of correct size. (c) Electrophenogram from sequencing of PCR product amplified using primers 17pA and 17pB. 17p-specific nucleotides are highlighted and correspond to the highlighted nucleotides in (a). (d) A standard curve was set up to test the efficiency of the primers 17pA and 17pB in a qPCR assaywith an annealing temperature of 64°C. The Ct values generated from a 10-fold serial dilution of genomic DNA (50, 5, 0.5, 0.05ng) are plotted, the resulting gradient from the standard curve is –3.36. (e) Dissociation curve showing the temperature at which the PCR product generated from the qPCR amplification dissociates into ssDNA molecules

3.3.7 18q

18qA and 18qC were designed 444nt from the TTAGGG repeats to produce a PCR product 190nt in length. The 18qC primer contains no 18q-specific nucleotides however 18qA was designed in a stretch of nucleotides specific to the 18q subtelomere thereby providing the specificity to this region (fig. 3.7a). Amplification using gDNA in a conventional PCR reaction using an annealing temperature of 62.8°C and above resulted in the generation of the expected 190nt amplicon without any non-specific amplification of larger products (fig. 3.7b). Sequencing of this PCR product using 18qC confirmed 18q specificity as demonstrated by the single peaks on the electrophenogram at the highlighted 'marker' bases (fig. 3.7c). qPCR was performed with an annealing temperature of 62.8°C for this primer pair. Ct values derived from amplification of 10-fold gDNA dilutions using these primers produces a standard curve with a gradient of -3.327 (fig. 3.7d). The efficiency of this amplification was 99.7%. The dissociation curve confirms the amplification of the single 18q-specific amplicon in the qPCR reaction when a larger amount of input gDNA was used however slight non-specific amplification was observed at lower gDNA concentrations although this is minimal (fig. 3.7e).

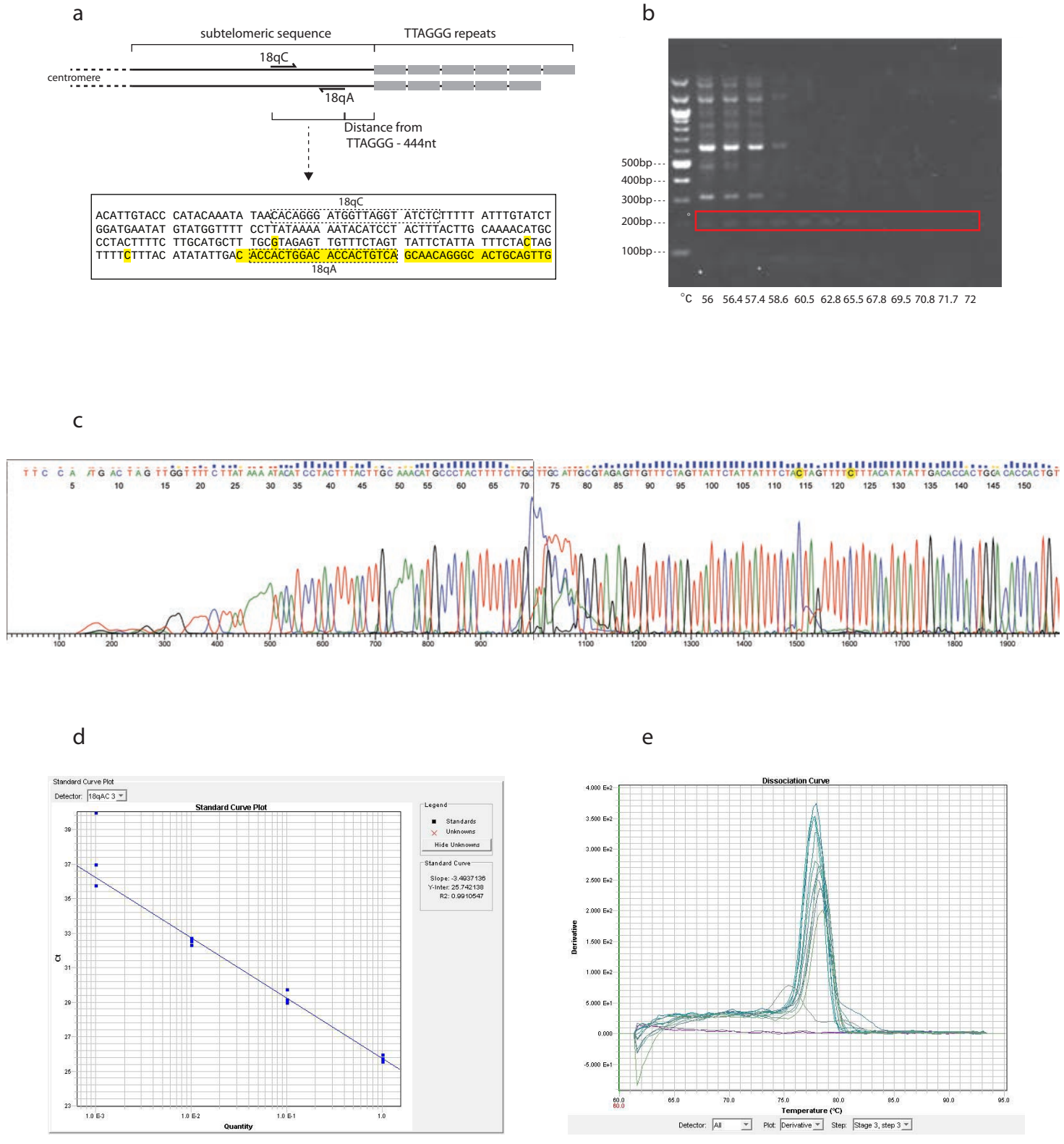

Figure. 3.7 qPCR assay development for 18q subtelomeric region (a) Primers 18qA & 18qC were designed. 18qA is designed within a stretch of 18q-specific nucleotides. Bases specific to 18q are highlighted in yellow. The PCR product is 190nt in size and 444bp away from telomere repeats. Region to be amplified also contains 18q-specific 'marker' nucleotides. (b) PCR was performed using the stated annealing temperature gradient, products generated were ran on a 1% gel and visualized. The red box encircles PCR product of correct size. (c) Electrophenogram from sequencing of PCR product amplified using primers 18qA and 18qC. 18q-specific nucleotides are highlighted and correspond to the highlighted nucleotides in (a). (d) A standard curve was set up to test the efficiency of the primers 18qA and 18qC in a qPCR assay using an annealing temperature of 62.8°C. The Ct values generaated from a 10-fold serial dilution of genomic DNA (50, 5, 0.5, 0.05ng) are plotted, the resulting gradient from the standard curve is –3.49 (e) Dissociation curve showing the temperature at which the PCR product generated from the qPCR amplification dissociates into ssDNA molecules

3.3.8 Allele-specific qPCR assay development (XpYp subtelomeric region)

In addition to the chromosome-specific qPCR assays, an allele-specific qPCR assay was developed at the XpYp telomere. Differences in telomere length between alleles has previously been found at the XpYp telomere (Baird et al. 2003) indicating that differences in telomere length between maternal and paternal alleles is maintained from the zygote throughout development. By developing an allele-specific qPCR assay for the XpYp telomere it will be possible to study the enrichment of different histone modifications at each XpYp allele to see whether chromatin structure is playing a part in the maintenance of the different length telomeric alleles.

3.3.8.1 Genotyping at the XpYp subtelomeric region

Different cell lines were genotyped at the XpYp subtelomeric region to identify them as either heterozygous for both XpYp alleles (TA allele and GT allele), homozygous for the TA allele or homozygous for the GT allele (fig. 3.8a). This was done using primers already known to be allele-specific at the XpYp subtelomeric region (XpYp427A/G, 415T/C and XpYpB2) (Baird et al. 2003). However these primers generate a PCR product of 436 nucleotides in length and are therefore unsuitable for qPCR purposes. The genotyping PCR revealed that of the genomic DNAs tested HT1080, ALTD3, MRC5 genomic DNA was heterozygous at the XpYp subtelomeric region, U87 genomic DNA was homozygous for the TA allele and U138, Hch, CaSki, HeLa, IMR90 genomic DNA was homozygous for the GT allele. A representative from each XpYp genotype was then chosen (MRC5, U87 and HeLa) to be used as a tool for testing the allele-specificity of the primers designed for qPCR.

3.3.8.2 qPCR assay development

Allele-specific primers for the XpYp subtelomeric region were designed in the same way that telomere-specific primers were designed. The sequence immediately adjacent to the XpYp telomere exhibits a high frequency of base substitutional polymorphisms (Baird et al. 1995; Syvänen et al. 1988) allowing great scope when designing primer sets which will specifically amplify only one of the two alleles. Primers were designed which incorporated the polymorphisms present at -13 (A or T) and -176 (T or G) at the 3' end of the primer resulting in two sets of primers: XpYp-13A and XpYp-176T, which should only generate a PCR product from the TA allele and XpYp-13T and XpYp-176G, which should only amplify the GT allele. The primers designed generate a PCR product 202 nucleotides in length which extends into the XpYp telomeric repeats (fig. 3.8b).

In a conventional PCR the most stringent conditions under which a robust, correctly sized PCR product was generated for both allele-specific sets of primers was at an annealing temperature of 65°C (fig. 3.8c). Genomic DNA heterozygous (MRC5) and homozygous (TA allele –U87, GT allele – HeLa) at the XpYp subtelomeric region was then utilized to test whether both sets of the -176, -13 primers were capable of allele-specific amplification. As expected, PCR products were generated by both sets of primers when MRC5 genomic DNA (heterozygous) was used as the template. Importantly, the primer set designed specifically to the TA allele (XpYp-13A,-176T) amplified a PCR product when U87 genomic DNA (homozygous for the TA allele) was used, a PCR product was not generated when HeLa genomic DNA (homozygous for GT allele) was added to the PCR reaction. Likewise XpYp -13T,-176G (designed specifically to the GT allele) only produced a PCR product from HeLa genomic DNA (GT allele-homozygous) (fig. 3.8d). These results confirm that the sets of primers designed were indeed capable of allele-specific amplification in a conventional PCR.

The same process was then repeated in a qPCR reaction to determine if this specificity is maintained.

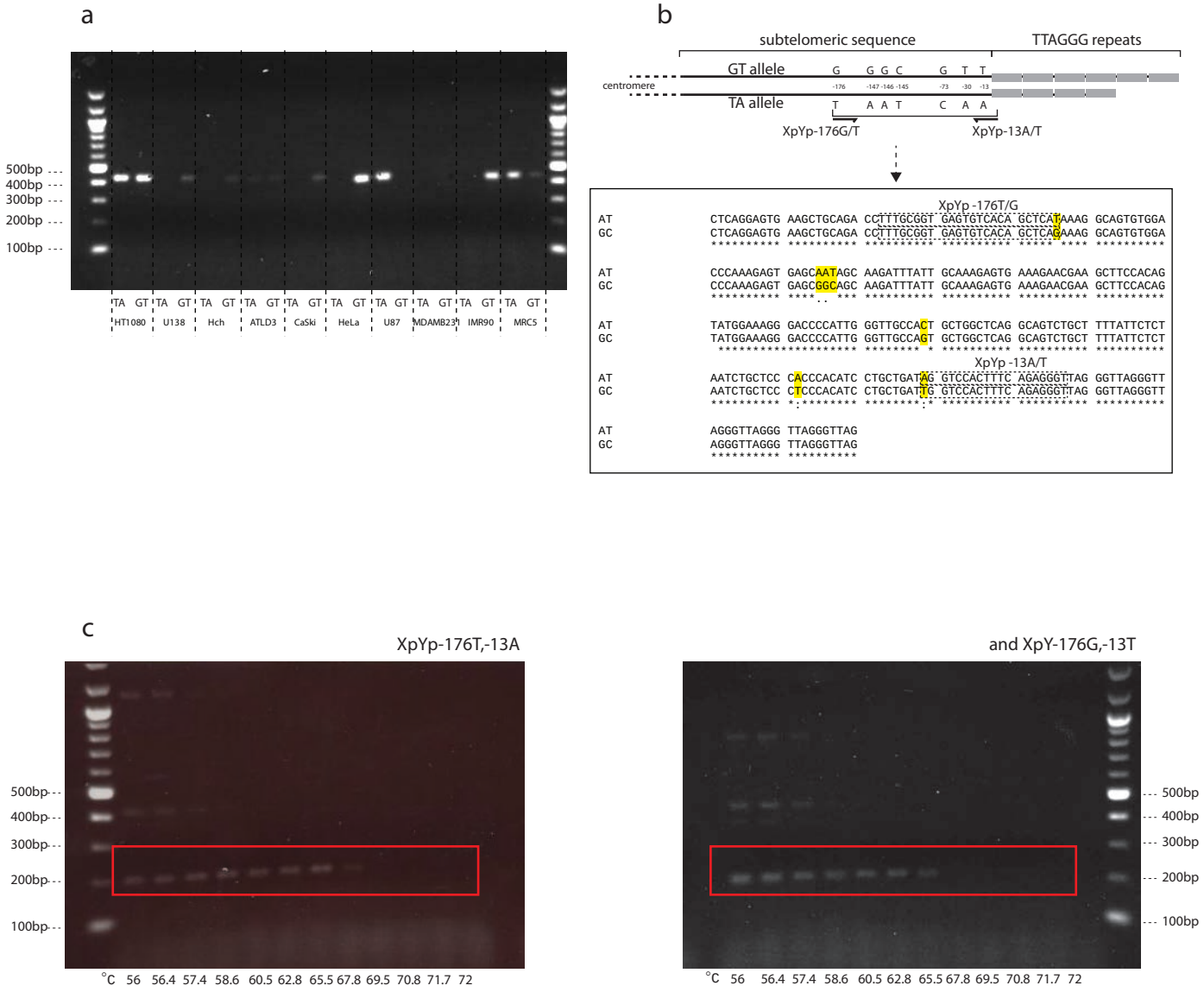

Figure. 3.8 allele-specific qPCR assay development for the XpYp subtelomeric region. (a) gDNA extracted from different cell lines was genotyped at the XpYp subtelomeric region to identify it as either heterozygous for both XpYp alleles (TA allele and GT allele), homozygous for the TA allele or homozygous for the GT allele . This was done using primers already known to be allele-specific at the XpYp subtelomeric region (XpYp427A/G,415T/C and XpYpB2). Pairs of PCR reactions were set up, each pair contained a gDNA, each reaction within the pair contained either XpYp427A, 415T and XpYpB2 or XpYp427G,415C and XpYpB2, PCR products were loaded onto a 1% gel and visualised (b) Primers sets XpYp-176T,-13A and XpY-176G,-13T were designed incorporating the base substitutional polymorphisms at positions -176 and -13 within the XpYp subtelomeric at their 3' ends producing a PCR product 205nt in length which extends into the TTAGGG repeats. (c) Both sets of primers were tested in a conventional PCR using the stated annealing temperature gradient, products generated were ran on a 1% gel and visualized. The red box encircles PCR product of correct size. (d) To test allele-specificity pairs of PCR reaction were set up containing either gDNA heterozygous for both alleles (MRC5), homozygous for the TA allele (U87) or homozygous for the GT allele (HeLa). Withiin each PCR reaction pair, either XpYp-176T,-13A (1) and XpY-176G,-13T (2) were used to amplify the gDNA.

A standard curve was used to determine the efficiencies of the XpYp-13A,-176T and XpYp-13T,-176A reactions as 100% and 92% respectively (fig. 3.9a). The dissociation curves show a single peak indicating the generation of a single PCR product for both sets of primers (fig. 3.9b). It was important to determine whether the single PCR products were amplified the expected allele for each primer pair. U87 (TA-allele homozygous) and HeLa (GT-allele homozygous) genomic DNA was utilised in the same manner as for conventional PCR to determine the allele specificity of the primer sets and the result of this test mirrored what was seen in the conventional PCR: XpYp-13A,-176T primers only produced a PCR product when the TA allele was present in the qPCR reaction (i.e. U87 genomic DNA), no PCR product was generated when HeLa genomic DNA was added to a qPCR reaction containing these primers confirming that this primer set is amplifying allele-specifically (fig. 3.9c(i)). The same can be said for the XpYp-13T,-176G primers but for the opposite allele, there is slight amplification of the TA allele from these primers however this is minimal (fig. 3.9c(ii)).

a

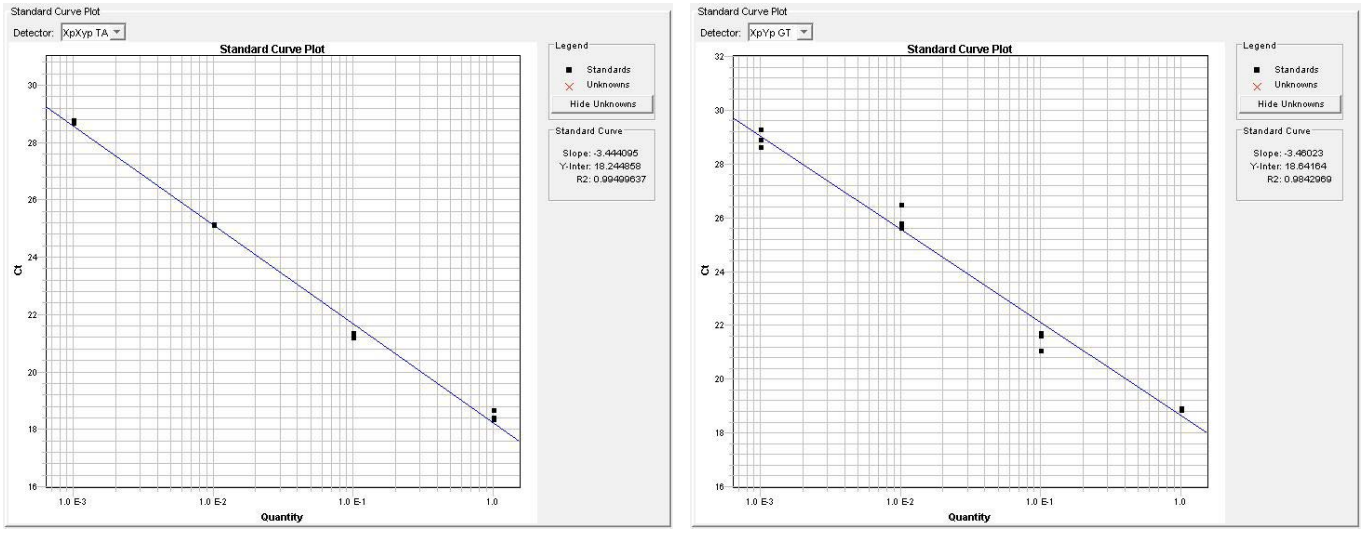

b

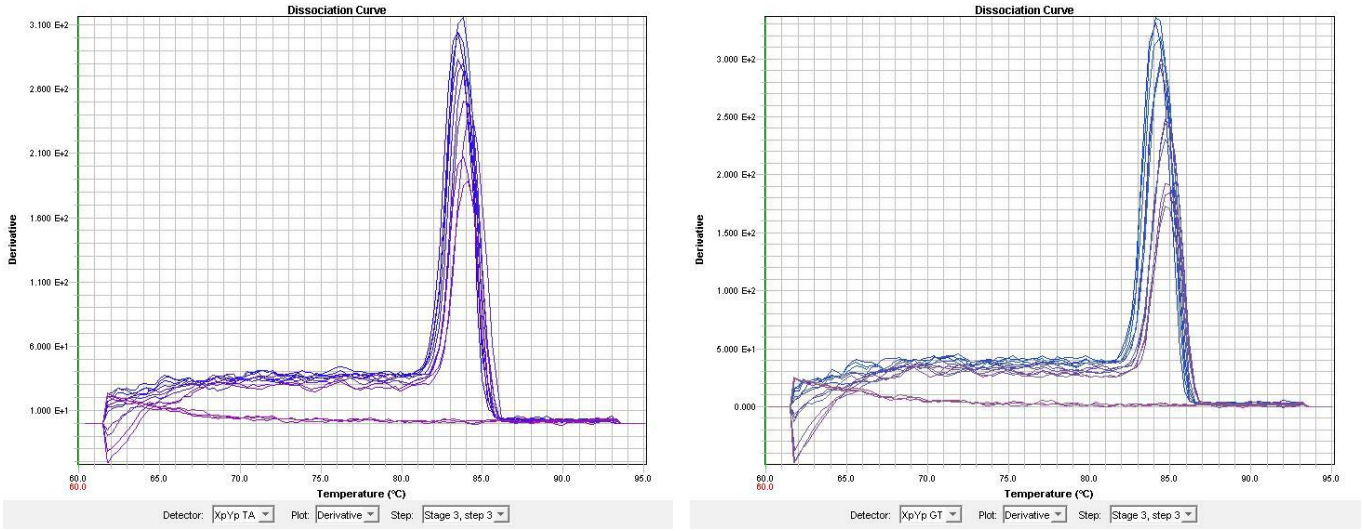

c

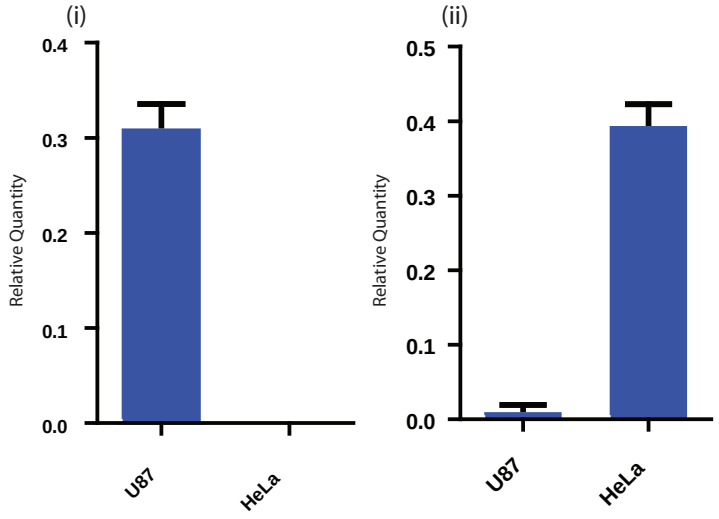

Figure. 3.9 Testing the XpYp allele-specific primers in a qPCR rection. (a) The efficiency of the both primer sets (XpYp-176T,-13A and XpY-176G,-13T) in a qPCR assay was tested using an annealing temperature of 64°C. The Ct values generated from a 10-fold serial dilution of genomic DNA (50, 5, 0.5, 0.05ng) are plotted for XpYp-176T,-13A (left) and XpY-176G,-13T (right) producing standard curves with gradients of -3.44 and -3.46 respectively. (b) Dissociation curve of pYp-176T,-13A (left) and XpY-176G,-13T (right) qPCR assays showing the temperature at which the PCR product generated from the qPCR amplification dissociates into ssDNA molecules. (c) Allele-specificity was tested by using either gDNA homozygous for the TA allele (U87) or homozygous for the GT allele (HeLa) as the input gDNA in triplicate qPCR reactions containing XpYp-176T,-13A (i) orXpY-176G,-13T (ii). The relative quantity of product generated was quantified using the standard curves in (a).

3.3.9 Summary

Using the approaches described above robust qPCR assays have been established for the telomere-adjacent DNA of five chromosome ends. Furthermore a similarly robust assay has been developed to identify the specific alleles adjacent to the XpYp telomere. These assays will provide useful tools to study the chromatin structure of human telomeres and how this may be modulated by telomere length and other factors.

3.4 Discussion

Differences in telomere length between chromosome ends within the same cell population have previously been shown (Britt-Compton et al. 2006). Alleles from the same XpYp telomere have been shown to have differing telomere length distributions (Baird et al. 2003) indicating that differences in telomere length between maternal and paternal alleles is maintained throughout development. Upon ectopic telomerase expression in otherwise telomerase-negative cells, preferential elongation of shorter telomeres is observed (Britt-Compton et al. 2009). These findings raise the question of how these differing telomere lengths are maintained, could it be a chromatin-based mechanism which confers this 'setting' of telomere length and allows shorter telomeres to be targeted for elongation by telomerase?

In this chapter the development of novel telomere-specific qPCR assays for the 11q, 12q, 16p, 17p and 18q chromosome ends as well as allele-specific qPCR assays for the XpYp telomere has been described. When used in conjunction with ChIP, these assays will provide a means to compare the chromatin structure of chromosome ends with differing telomere length distributions. This includes comparisons between different alleles of the same chromosome end, between chromosome ends within the same cell population and also between the same chromosome from different clonal cell populations.

The primers designed for qPCR were based around nucleotides specific to the subtelomeric sequence of interest; this was sometimes a stretch of specific nucleotides but more often it was a single telomere-specific nucleotide. Incorporating this nucleotide at the 3' end of the primer was the key factor in the design which provided telomere or allele-specificity as

when the primer annealed to a highly homologous subtelomeric sequence from a different chromosome end mismatch at the 3' end of the primer would inhibit extension from the template. This method of primer design has been successfully used in the development of telomere-and allele-specific single telomere length analysis (STELA) assays (Baird et al. 2003; Britt-Compton and Baird 2006; Britt-Compton et al. 2006; Capper et al. 2007). The primers designed for these qPCR assays should be more proficient at achieving telomere-specificity as this specificity should be gained from two telomere-specific primers, whereas telomere-specificity in a STELA reaction is reliant on just one primer within the subtelomeric region.

Although telomeric chromatin structure is predominantly studied using ChIP followed by dot blot assays very recent studies have begun to emerge in which telomeric ChIP-qPCR has been developed: ChIP-qPCR was used to determine the enrichment pattern of H3K9me3 in the subtelomeric region of 15q, although the primers designed were quite a distance (7.5kb) from the TTAGGG repeats (Arnoult et al. 2012). A more recent study used ChIP-qPCR to analyse the role of the chromatin organising factor CTCF in chromatin maintenance at human chromosome ends (Deng et al. 2012). The enrichment of a range of histone modifications (H3K4me2, H3K4me3, H3K9me2, H3K9me3) as well as chromatin remodelling proteins (CTCF, SMC3, Rad21) and telomeric binding proteins (TRF1 & TRF2) was studied at several subtelomeric regions. Several sets of primers were designed along the subtelomeric sequence of the 10q, 13q, 15q and XqYq chromosome ends allowing protein enrichment to be analysed from 190 nucleotides to 6.7kb away from the TTAGGG repeats. Having a number of primer sets which collectively span a large area of the subtelomeric region described in their work is an future direction which could be taken in this work. Any interesting histone modification enrichment observed at the telomeres to which qPCR

assays have been designed to could be measured further away from the telomere to determine whether the pattern of enrichment is propagated along the subtelomeric region.

There were certain limitations which couldn't be overcome when designing the qPCR assays: one of the main ones being the lack of sequenced subtelomeres. Some chromosome ends have not been fully sequenced through to the start of the telomeric TTAGGG repeat regions, meaning that the distance between a qPCR assay and the TTAGGG repeats would be unknown for these ends. Another limiting factor for these assays is the number of telomeres to which a functional STELA assay has been designed: Telomere length distributions of 2p, 11q, 12q, 16p, 17p, 18q and XpYp (allele-specific) telomeres can be measured by STELA. The design of qPCR assays was focused on these chromosome ends. Future work could include designing qPCR assays for more chromosome ends in conjunction with the development of STELA assays for these ends.

Amplifying very small amounts of input gDNA (0.05ng) proved problematic for the 12q, 16p and 18q qPCR primers. 16pBrev & 16pC failed to amplify whereas a product of a different size was generated by 12qA1 & 12qB, and to a certain extent 18qA & 18qC, when this amount of gDNA was added to the qPCR reaction (see dissociation curves: fig. 3.4e, 3.5e, 3.7e). The additional product generated by 12qA1 & 12qB could be another PCR product or it could be primer-dimer formation. The presence of additional DNA molecules must be monitored when these assays are applied to ChIP samples by adding a dissociation step to each qPCR assay to ensure that they do not obscure measurements of telomeric enrichment.

Some of the qPCR assays designed targeted a region of the subtelomere which was further from the subtelomere-telomere boundary than anticipated. The challenge lay not only in identifying suitable telomere-specific nucleotides from which a functional primer for qPCR could be designed, but also in ensuring that there were some of these telomere-specific bases present within the PCR product amplified to act as a marker for telomere-specificity during sequencing. Of the qPCR assays designed, the 18q target region was the furthest from the TTAGGG repeats (444nt) meaning that the amount of telomere-repeat containing fragments that could be detected in a ChIP with 18qA and 18qC would be reduced.

The regions analysed using any of these qPCR assays will not be purely telomeric. Designing primers as close to the subtelomere-telomere boundary as possible maximises the amount of immunoprecipitated telomeric DNA measured but considering that the chromatin fragments are sheared to a length of 200-1000bp, the fragments primed by the qPCR primers are going to encompass a large area of telomeric and subtelomeric chromatin. Due to the repetitive nature of telomeric DNA it would be impossible to design a telomere-specific qPCR assay which analysed enrichment in only TTAGGG repeats. The only current method in analysing purely telomeric DNA is by dot blot using a TTAGGG probe which, as previously mentioned, has sensitivity issues and isn't telomere-specific. However the subtelomeric chromatin structure between telomeres of different length is interesting in itself. A similar approach to telomeric qPCR assay design was taken in budding yeast (Fisher et al. 2004; Takata et al. 2004; Takata et al. 2005; Yu et al. 2007) and seems to be an accepted method for measuring telomeric protein enrichment.

In this chapter the development of novel telomere-specific and telomeric allele-specific qPCR assays has been described. The telomeres for which qPCR assays have been designed

to are 11q, 12q, 16p, 17p and 18q. A telomeric allele-specific qPCR assay has also been designed for the XpYp chromosome end. When used in conjunction with ChIP, these assays can provide a sensitive, quantitative method for analysing the chromatin structure of individual telomeres/telomeric alleles. STELA has enabled the high resolution analysis of telomere length distributions of individual telomeres and telomeric alleles. Combining this ChIP-qPCR approach with STELA will allow a detailed analysis of telomeric chromatin structure between chromosome ends which display differing telomere length distributions. Such an approach may help towards answering the question of how telomeric chromatin structure impacts telomere length.

Chapter 4

Telomere-specific chromatin structure analysis in human cells

4.1 Abstract

The nature of telomeric chromatin architecture has been extensively studied in lower eukaryotes such as yeast and *Drosophila*. More recently the chromatin structure at mammalian telomeres has been characterised. This work has been predominantly performed at mouse telomeres and has revealed a heterochromatic environment abundant in repressive marks such as H3K9me3 and H4K20me3. Human telomeric chromatin structure is less well defined but recent reports suggest that unlike mouse telomeres, human telomeres are enriched in both repressive heterochromatin marks and histone modifications usually associated with transcriptionally active euchromatin such as H3K4me3. Although such research has begun to shed light on the chromatin architecture present at human chromosome ends, the chromatin structure at individual human chromosome ends has not yet been studied. Telomere-specific qPCR assays developed in chapter 3 were used in conjunction with Chromatin Immunoprecipitation (ChIP) to allow an analysis of chromatin structure at individual telomeres/telomeric alleles. In this chapter, STELA and telomere-specific ChIP-qPCR were used together to identify any correlation between telomere-specific H3, H3K4me3, H3K9me3 and H4K20me3 enrichment and telomere length. No such correlation was observed between different chromosome ends within a telomerase-negative MRC5 fibroblast population. Telomeric H3, TRF1 and histone methylation enrichment was also compared at the same telomere stably maintained at different lengths in two telomerase positive HT1080 clonal populations: HT1080 cells with longer telomeres showed greater H3 and TRF1 telomeric occupancy, as well as increased enrichment of H3K4me3 and H4K20me3 which suggests a relationship exists between the chromatin structure of a telomere and its length in telomerase-positive cells. Additionally, telomere-specific chromatin

structure was compared between actively proliferating cells and senescent cells. H3, H3K4me3 and H4K20me3 were abundant at the telomeres in a proliferating clonal population of MRC5 cells however when these cells entered senescence their telomeric presence was reduced. The same scenario was observed at 17p and 18q in proliferating and senescent IMR90 fibroblasts. This finding indicates that telomeric chromatin undergoes significant structural changes as a cell ceases to proliferate and enters senescence.

4.2 Introduction

Chromatin structure plays a key role in almost all DNA-related metabolic processes including transcriptional activation and repression, recombination, the sensing and repair of DNA damage and kinetochore and centromere formation (Li *et al.* 2007). Whether chromatin exists in a relaxed, transcriptionally active conformation or a repressive heterochromatic state is influenced by the post-translational modification of the core histones which make up the nucleosome. Over 60 different residues within the core histones are subject to post-translational modifications including acetylation, methylation, phosphorylation and ubiquitination. However this represents a huge underestimate (Bernstein *et al.* 2007; Kouzarides 2007). Although the majority of the modifications remain poorly understood recent studies have provided considerable progress in the understanding of how histone methylation and acetylation contributes to the chromatin environment.

Histone lysine acetylation almost always correlates with an open, accessible chromatin environment. Histone lysine methylation on the other hand can have different effects depending on which residue is modified (Bernstein et al. 2007). Furthermore, extra complexity comes from the fact that methylation of lysine residues may occur in three different forms (mono- di- and trimethyl) and that these forms can elicit different effects on chromatin structure. All three methylation states of H3K4 (H3K4me1, me2 and me3) have been shown to be abundant at transcriptionally active genes in yeast and humans (Heintzman *et al.* 2007; Santos-Rosa et al. 2002). Despite slight differences in where enrichment of the different methylation forms peak within a gene (Pokholok *et al.* 2005) all three forms are considered open euchromatic marks. This is not the case for H3 lysine 9 (H3K9), H3 lysine 27 (H3K27) and H4 lysine 20 (H4K20) methylation. Monomethylation of these residues is enriched in active genes (Barski et al. 2007) whereas trimethylation of these marks is seen in repressive heterochromatin (Kotake et al. 2007; Liu *et al.* 2007; Plath et al. 2003; Snowden et al. 2002). Repressive heterochromatin domains are also characterised by low histone acetylation levels as well

as heavily methylated DNA and are found in non-coding regions of the genome including pericentromeres, gene deserts and at subtelomeres and telomeres.

Telomeric chromatin has generally been considered heterochromatic based on initial studies in budding yeast and *Drosophila* in which the establishment of a heterochromatic state at telomeres and subtelomeres is essential for the protection of chromosome ends and for the silencing of telomere-proximal genes (telomere position effect) (Raffa et al. 2011; Shore 2001). More recently the analysis of telomeric chromatin structure has been extended to higher eukaryotes including mouse cell models and plants. Mouse telomeric and subtelomeric regions are characterized by high levels of the heterochromatic marks H3K9me3, H4K20me3 and H3K79me2 as well as histone hypoacetylation. Mouse subtelomeric DNA is also heavily methylated (Benetti et al. 2007b; Garcia-Cao et al. 2004a; Gonzalo et al. 2006; Jones et al. 2008). Arabidopsis telomeres on the other hand contain a mixture of repressive heterochromatic marks and histone modifications usually associated with actively transcribed regions of the genome such as H3K4me3 and acetylation of the H3K9 and H4K16 residues (Vaquero-Sedas et al. 2011; Vaquero-Sedas et al. 2012; Vrbsky et al. 2010).

Very recently the chromatin structure at human telomeres has begun to be uncovered. In a similar manner to Arabidopsis, human telomeric chromatin does not appear to be enriched in solely heterochromatin-associated marks. H3K4me3 and H2BK5me1, marks often associated with actively transcribed genes, are enriched at the telomere (Rosenfeld et al. 2009). Furthermore, in contrast to the high abundance of H3K9me3 at mouse telomeres, telomeric H3K9me3 is under-represented although it is enriched in subtelomeric chromatin (Rosenfeld et al. 2009). Similar levels of telomeric H3K9me3 were observed in IMR90 fibroblasts and HT1080 fibrosarcoma cells (Arnoult et al. 2012; O'Sullivan et al. 2010). Despite the presence of these active chromatin features, human telomeres

are also enriched in heterochromatin-associated marks including deacetylation of H3K9 and H3K56 and tri-methylation of H3K27 and H4K20me3 although to a lesser extent than was seen at mouse telomeres (Arnoult et al. 2012; Michishita et al. 2008; O'Sullivan et al. 2010; Tennen et al. 2011). Additionally, human subtelomeric DNA is heavily methylated (Nergadze et al. 2009; Yehezkel et al. 2008). The examples of both euchromatic and heterochromatic marks in human telomeric chromatin suggest that it differs from the repressive chromatin environment seen at mouse telomeres. Instead it appears to possess a specialized intermediate structure similar to what is seen at telomeres in Arabidopsis. Clearly the above studies of human telomeric chromatin structure are just the tip of the iceberg and much more work is required to gain a deeper understanding of the intricacies which contribute towards the maintenance of proper telomeric chromatin structure and subsequently ensure telomere function.

Short dysfunctional telomeres are one of the main determinants of replicative senescence. How the telomeric chromatin structure is altered upon senescence is relatively unknown. The accumulation of γH2AX is observed at short dysfunctional telomeres during senescence (d'Adda di Fagagna et al. 2003) as well as at de-protected telomeres devoid of TRF2 and Pot1 (Denchi and de Lange 2007; Takai et al. 2003), this latter process is dependent on the accumulation of H4K20me3 (Dimitrova *et al.* 2008). Telomere-bound H4K20me3 and also H4K16Ac has been shown to be redistributed during the cell cycle in late passage IMR90 celss compared to early passage cells (Rosenfeld et al. 2009). Also observed was a decrease in H3 telomeric occupancy and reduced levels of TRF1 and TRF2 in the late passage cells.

4.2.1 Aims of the chapter

Previous work studying the role of chromatin structure at telomeres has relied upon using chromatin immunoprecipitation in conjunction with dot-blot assays to determine enrichment of specific chromatin modifications. Although this approach has begun to characterise human telomeric chromatin it cannot differentiate between telomeres therefore telomere-specific enrichment of chromatin modifications is not achievable. Single Telomere Length Analysis (STELA) allows the length of individual telomeres to be determined at a range of chromosome ends including 11q, 16p, 17p and 18q. Allele-specific STELA can measure the length of individual telomeric alleles of XpYp chromosome end. Telomere- and telomeric allele-specific qPCR assays have been developed for these same chromosome ends. When used in conjunction with Chromatin Immunoprecipitaion (ChIP), the qPCR assays provide a method for distinguishing the enrichment of histone modifications at individual telomeres. The aim of this chapter is to use STELA and telomere-specific ChIP-qPCR together to determine whether any relationship exists between telomere length and the telomeric enrichment of the histone methylation marks H3K4me3, H3K9me3 and H4K20me3. Any potential relationship between telomere length and telomeric histone methylation will be analysed between different chromosome ends and between different telomeric alleles at the same chromosome end within the same cell population. Histone methylation will also be analysed at a single telomere stably maintained at different lengths in two clonal populations of the telomerase-positive HT1080 fibrosarcoma. Finally telomeric histone methylation patterns will be analysed in actively proliferating and senescent cells to determine whether telomeric chromatin undergoes structural alterations as cells enter senescence. Telomeric enrichment of H4K20 methylation has recently been compared between early (PD30) and late passage IMR90 and WI38 cells (PD75) (O'Sullivan, Kubicek et al. 2010) using the ChIP-dot blot approach. Comparing differences in these histone methylation marks between proliferating and senescent cells in a telomere-specific manner will uncover whether changes in telomeric chromatin structure varies between chromosmoe ends during senescence.

4.3 Results

4.3.1 Analysing the relationship between telomeric histone methylation status and telomere length in MRC5 mixed population

Initially, analysis of telomeric chromatin structure was performed using chromatin extracted from MRC5 mixed population cells. This allowed comparison between telomeric chromatin structure and telomere length at different chromosome ends within a single cell population. STELA was performed to determine the telomere length profiles of 17p, 18q and both alleles of XpYp. The length distributions were then quantified and the mean telomere length calculated for each of the different telomeres. Mean telomere length differs between telomeres/telomeric alleles ranging from 3.197kb for 17p to 5.879kb for 18q (fig. 4.1a).

Before attempting to immunoprecipitate chromatin successful sonication of the chromatin had to be ensured. Chromatin was cross-linked by treating cells with 1% formaldehyde for 10 minutes. After 2 washes in 1XPBS cells were scraped into a falcon tube, centrifuged and resuspended in a SDS-lysis buffer at a concentration of $1X10^6$cells/100μl. Cell lysates were then divided into 200μl aliquots and sonicated for 8 minutes (30s on 30s off) resulting in chromatin fragments within the desired 200-1000bp size (fig. 4.1b).

MRC5 mixed population chromatin was immunoprecipitated with antibodies against histone H3 and TRF1 and qPCR was performed. This acted as a positive control to ensure that the qPCR assays developed in chapter 3 could amplify immunoprecipitated telomeric DNA (fig. 4.1c). Extensive

enrichment of histone H3 was observed in all the telomere/telomeric allele-specific qPCR assays. This degree of H3 enrichment was reasonably consistent across the chromosome ends although there did appear to be a slight decrease at the long XpYp telomeric allele (fig. 4.1c (i)). TRF1 was also successfully immunoprecipitated and detected by the telomere-specific ChIP-qPCR assays although its enrichment was lower at the chromosome ends analysed compared to H3 (fig. 4.1c). Surprisingly considerable variation in telomeric TRF1 occupancy was observed particularly at 17p where TRF1 abundance was significantly lower than at 18q and both XpYp telomeric alleles. The reason for this variation in TRF1 enrichment is unknown but may reflect differences in the telomere variant repeat (TVR) distribution in the proximal 2-3kb of the telomere repeat tract between chromosome ends. TRF1 binds specifically to TTAGGG therefore increased TVR variation could result in less TRF1 binding within the region which is detected by the qPCR assay. 17p has previously been shown to contain an extensive TVR distribution (Letsolo et al. 2010) therefore it is possible that this is the cause of the reduced TRF1 enrichment at 17p. Nevertheless these results show that the ChIP procedure is working and that the developed telomere and telomeric allele-specific qPCR assays is able to measure enrichment of immunoprecipitated DNA at chromosome ends.

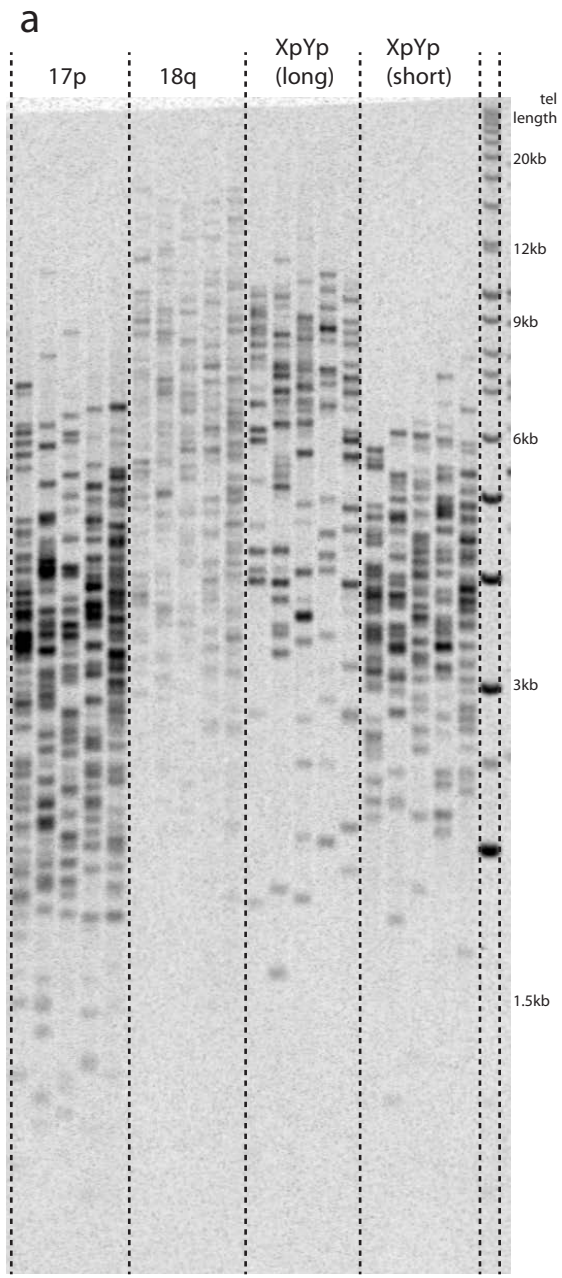

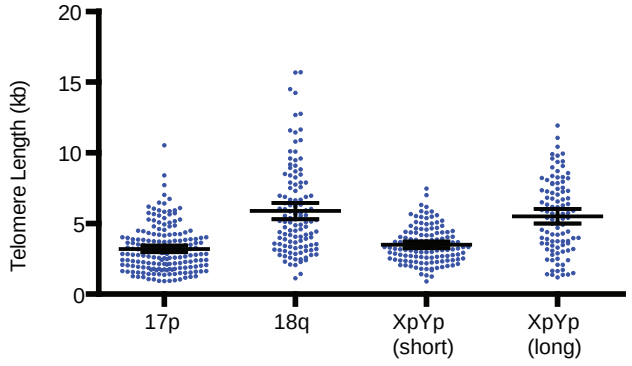

	17p	18q	XpYp (short)	XpYp (long)
Mean tel length (kb)	3.197	5.879	3.489	5.504
Lower 95% CI	2.959	5.300	3.261	4.988
Upper 95% CI	3.434	6.458	3.717	6.020

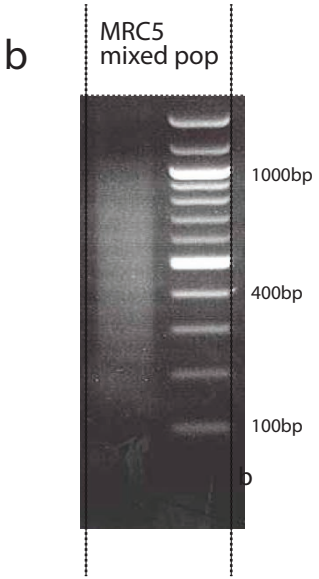

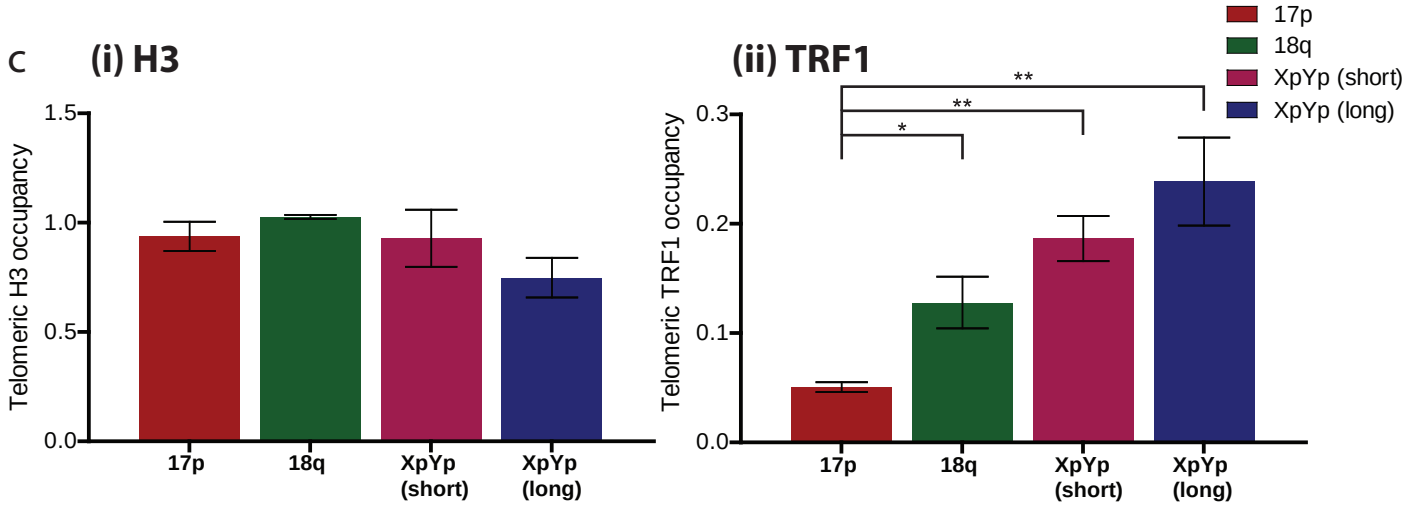

Figure 4.1. Telomere length distributions and telomeric enrichment of H3 and TRF1 at 17p, 18q and XpYp (short and long allele) in a mixed population of MRC5 fibroblast cells. (a) STELA was performed at the 17p,18q and short and long XpYp telomeric alleles using the 17pseq1rev, 18qrev4M, XpYp-433AT and XpYp-433G primers respectively. Telomere length distributions were then quantified using Phoretix software and mean telomere length was calculated (b) chromatin extracted from MRC5 mixed population cells was sonicated for 8 mins (30s o, 30s off). An aliquot of chromatin was taken, reverse cross-linked and DNA was purified. DNA was then electrphoresed on a 1.5% agarose gel to determine fragment size. (c) Relative enrichment of histone (i) H3 and (ii) TRF1 at 17p, 18q and XpYp (long and short allele). Statistically significant differences in enrichment between telomeres/telomeric alleles was measured by t-test, * - P<0.05, ** - P<0.01. Error bars indicate SEM for qPCR reaction replicates, not the SD for internal replicates

MRC5 mixed population chromatin was then immunoprecipitated using antibodies against the histone methylation marks H3K4me3, H3K9me3, H3K27me3 and H4K20me3. Before telomeric occupancy of the marks could be determined the success of the immunoprecipitation had to be verified to ensure that any lack of enrichment of a histone methylation mark at a telomere was biologically relevant and not just a result of a failed IP. This was done by measuring enrichment of the histone methylation marks at their respective positive control loci within the genome where enrichment is expected. For the H3K4me3 histone modification this positive control locus was the GAPDH promoter, for H3K9me3 it was the 3' end of the ZNF554 gene, for H3K27me3 – human α-satellite and for H4K20me3 - β-globin promoter. These loci have previously been shown to be enriched in the mentioned chromatin marks and primers used to amplify these regions were designed by Millipore and provided with the antibody (Frietze *et al.* 2010; Rank *et al.* 2010; Tiwari *et al.* 2008; Wang *et al.* 2009). H3K4me3, H3K9me3 and H4K20me3 showed robust enrichment at their respective control loci compared to a negative control 'no antibody' immunoprecipitation (fig. 4.2a). The antibody against H3K27me3 however failed to immunoprecipitate the histone modification as no differences in enrichment were observed between the test and no antibody control at its positive control loci (fig. 4.2a (iii)). The reason for this failed immunoprecipitation was unknown and attempts made to improve the IP were unsuccessful therefore this histone methylation mark was not analysed further.

Telomere-specific occupancy of the histone methylation marks was then measured at the 17p and 18q telomeres and the short and long XpYp telomeric alleles to determine any potential differences in enrichment of these marks exists and whether these differences correlate with the mean length of the telomeres. Although little variation in H3 abundance was observed between chromosome ends enrichment of each histone methylation mark was normalized to H3 occupancy for each telomere to ensure that any differences observed between telomeres was genuine differences in histone

methylation status and not just as a result of telomeric nucleosomal density. H4K20me3 telomeric enrichment was much higher than H3K4me3 and H3K9me3 enrichment at all the telomeres analysed (fig. 4.2b). H3K4me3 telomeric enrichment was very low, although it was present at 17p and to a lesser extent 18q no enrichment of this mark was detected at either of the XpYp telomeric alleles. Telomeric H3K9me3 was similarly low although it was detected at similar levels at all four telomeres (fig. 4.2b). H4K20me3 telomeric enrichment was also seen at all four telomeres (fig. 4.2b). It was most abundant at the longer 18q telomere however at the longer XpYp telomeric allele, which showed a similar mean telomere length to 18q H4K20me3 enrichment, was at its lowest. No correlation of any kind was seen between the level of telomeric enrichment of any of the histone methylation marks and telomere length.

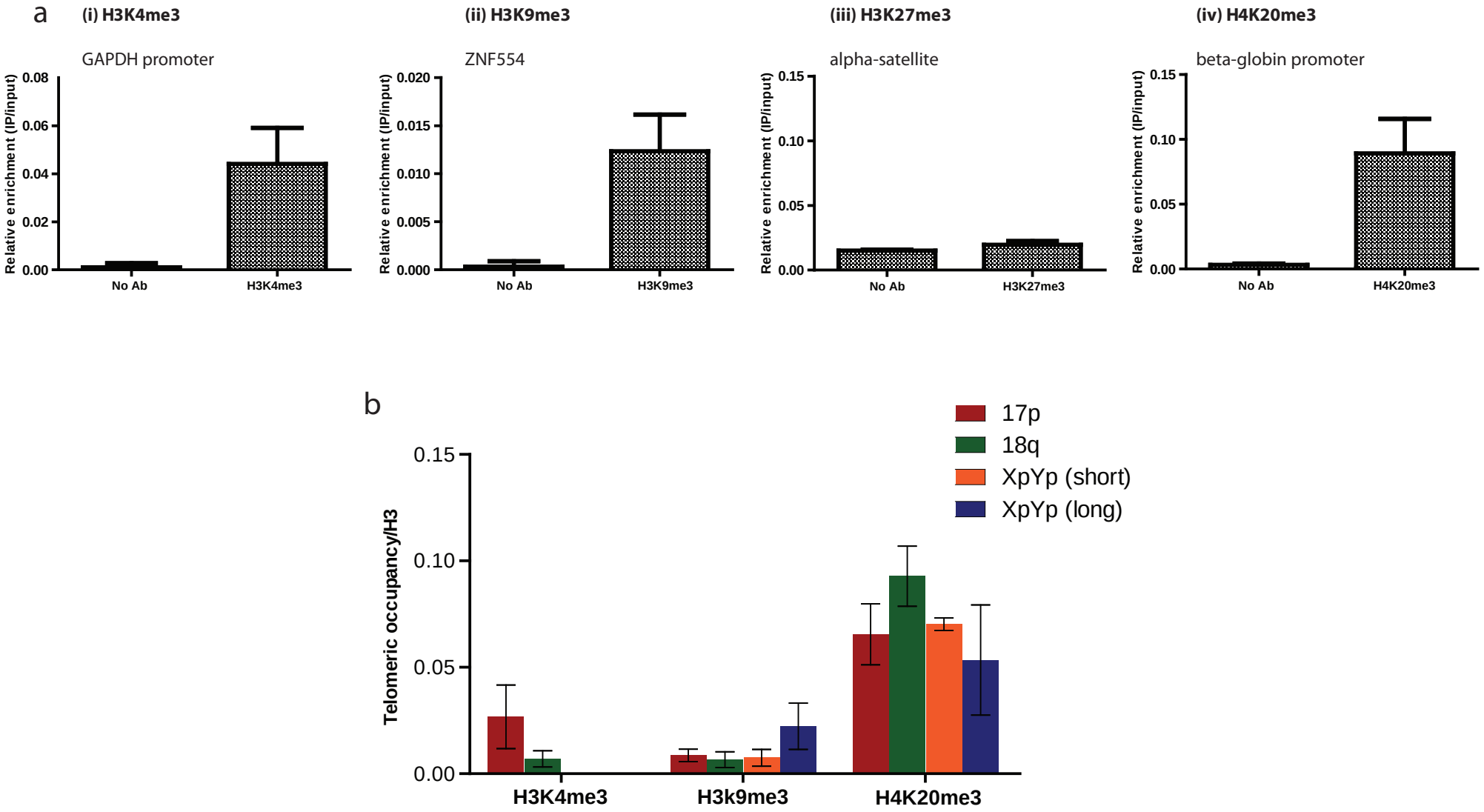

Figure 4.2. ChIP analysis of H3K4me3, H3K9me3, H3K27me3 and H4K20me3 enrichment in a mixed population of MRC5 fibroblasts. (a) Immunoprecipitation efficiency for the histone methylation marks was analysed by measuring their enrichment at the following positive control loci: H3K4me3 - GAPDH promoter, H3K9me3 - ZNF554, H3K27me3 - alpa-satellite and H4K20me3 - beta-blobin promoter. Enrichment of the marks was compared against a no antibody control at the same locus. (b) Telomeric enrichment of (i) H3K4me3, (ii) H3K9me3 and (iii) H4K20me3 at 17p, 18q and XpYp (short and long allele). Error bars indicate SEM for qPCR reaction replicates, not the SD for internal replicates

The STELA length profiles of 17p, 18q and XpYp (short and long alleles) in this mixed population of MRC5 cells show considerable heterogeneity in telomere length at these chromosome ends. Additionally differences in mean telomere length are relatively small (fig. 4.1a) therefore these cells are not the best candidate for attempting to determine any correlation between telomeric histone methylation and telomere length. A better model would involve comparisons between telomeres which vary greatly in length and also possess homogenous telomere length distributions. Such telomeres are more likely to be present in clonal populations of cells therefore clones of MRC5 cells were generated from early passage mixed population MRC5 cells

4.3.2 Generating clonal populations of MRC5 fibroblasts

Early passage MRC5 fibroblasts were diluted in culture medium, 16 individual clones were picked and transferred into separate 96-well plate wells and allowed to expand. After the clonal population had expanded sufficiently an aliquot of each clone was taken and analysed for XpYp telomere length using STELA to observe the differences in telomere length between the two XpYp telomeric alleles (fig. 4.3). Clones 11 and 13 displayed the greatest differential in telomere length between the XpYp telomeric alleles and therefore were chosen to expand further for ChIP analysis.

MRC5 cl.11 and cl.13 cells were cultured to senescence. Unfortunately MRC5 cl.11 cells senesced early and therefore it was not possible to culture enough cells for chromatin extraction. MRC5 cl.13 cells however were cultured continuously and chromatin was extracted from these cells when they were actively proliferating (43 population doublings (PDs) and then again after 49 PDs, at which point the cells had begun to senesce. Senescence was determined by β-galactosidase staining and revealed that of the MRC5 cells which had undergone 49 PDs were 38% senescent.

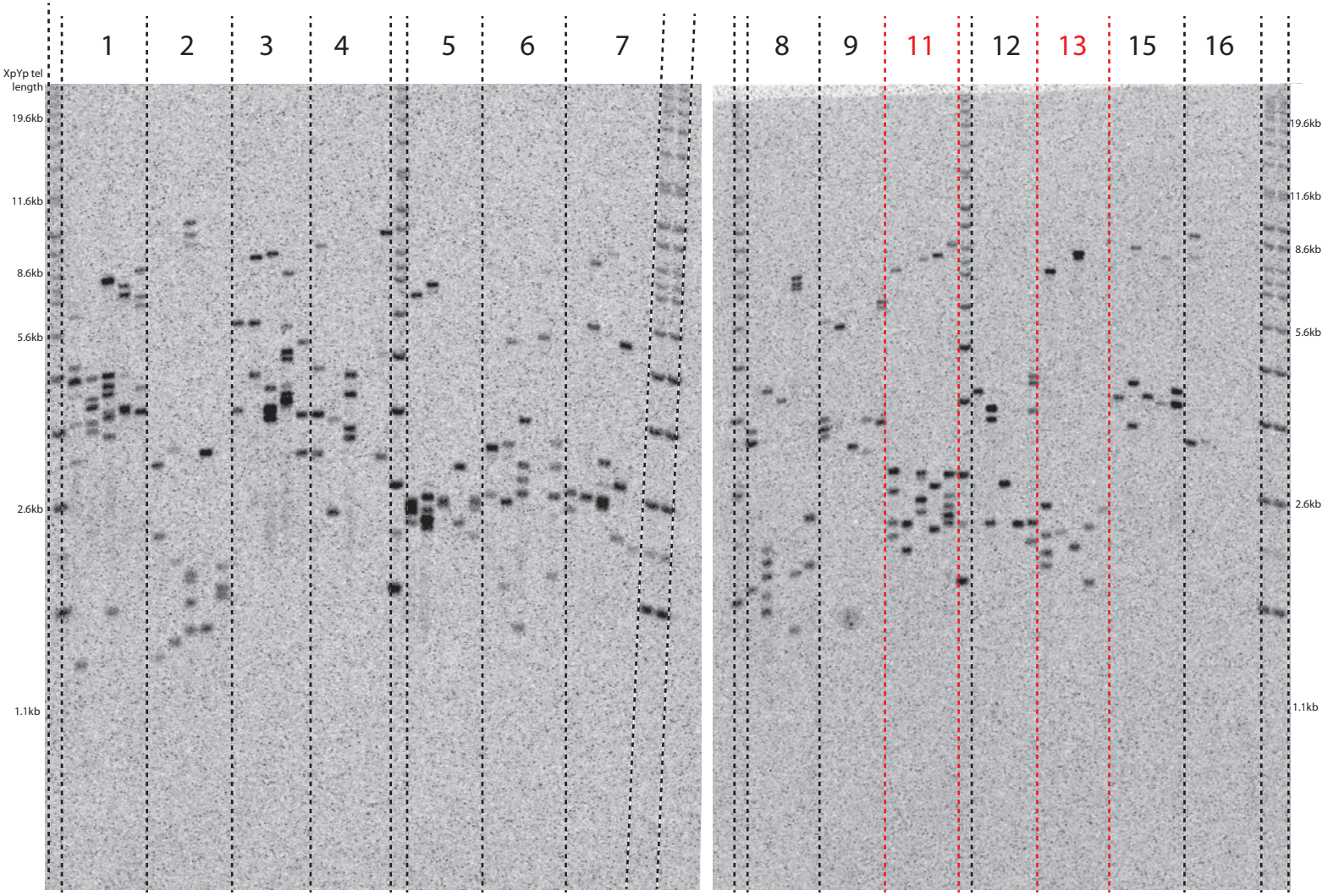

Figure 4.3. MRC5 clone generation MRC5 cells from a mixed population were diluted down to single-cell levels, these single cells were then expanded to produce MRC5 clones. DNA was extracted from these clones and XpYp STELA was performed to determine the clones with the largest disparity between the telomere length of the individual XpYp alleles

4.3.3 Telomere length distributions in MRC5 cl.13 cells

DNA was also extracted from the proliferating and senescent MRC5 cl.13 cells and STELA was performed at 11q, 16p, 17p, 18q and both XpYp telomeric alleles to determine the telomere length profile of the cells as they progress towards senescence (fig. 4.4). Compared to the MRC5 mixed population of cells the proliferating MRC5 cl.13 cells had a greater variation in mean telomere length between chromosome ends ranging from 2.34kb for 17p to 7.069kb for 18q. By the time the cells reached senescence gradual telomere erosion resulted in slight decreases in mean telomere length. This was most noticeable at the shorter XpYp telomeric allele whose mean telomere length decreased by 0.718kb. Homogenous telomere length distributions were seen in both the proliferating and senescent MRC5 cl.13 cells at the 11q, 17p and XpYp telomeres although not at 16p or 18q. 16p telomere length distribution was heterogeneous containing four separate telomeric distributions, consistent with the amplification of at least 2 chromosome ends. This makes it a less suitable candidate when looking at chromatin structure in relation to telomere length although it would still be interesting to determine levels of histone methylation at this telomere to see how it compares to other chromosome ends.

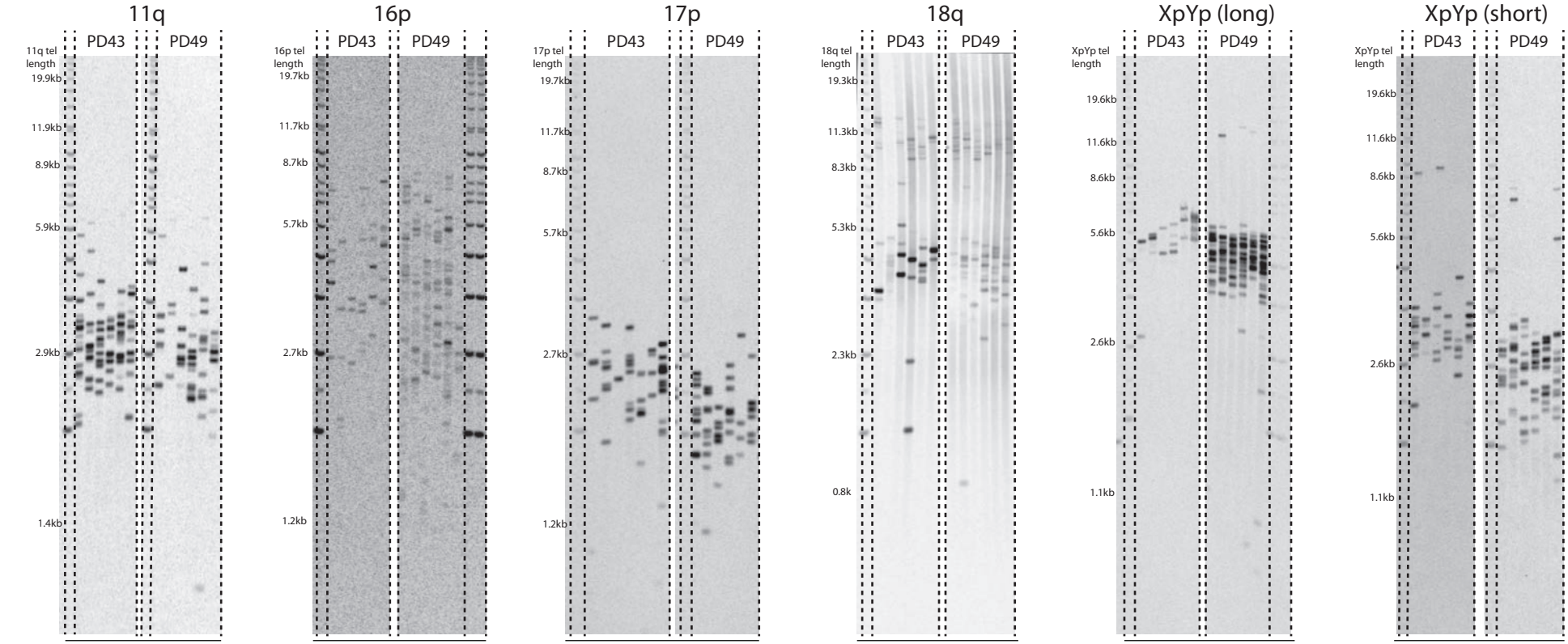

	11q		16p		17p		18q		XpYp (long)		XpYp (short)	
Mean length (kb)	3.201	3.026	4.427	4.19	2.34	1.811	7.069	7.032	5.297	4.608	3.17	2.452
Lower 95% CI	3.010	2.704	3.863	3.768	2.166	1.664	5.989	6.143	4.901	4.425	3.010	2.326
Upper 95% CI	3.392	3.348	4.991	4.613	2.515	1.958	8.148	7.922	5.693	4.790	3.329	2.579

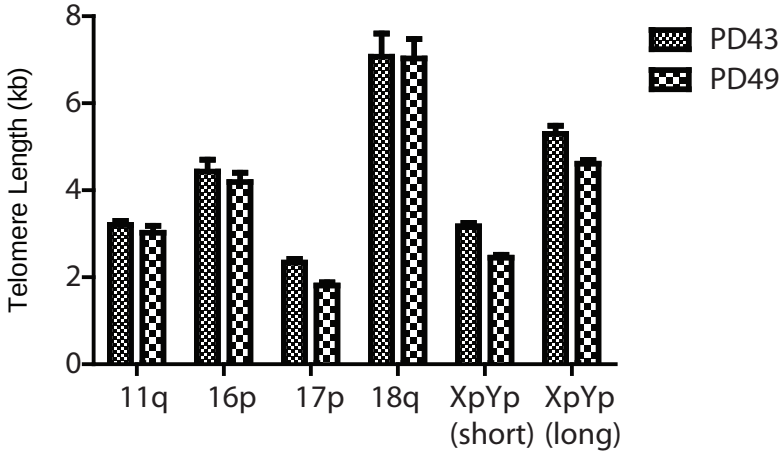

Figure 4.4. Telomere length distributions at 11q,16p,17p,18q and XpYp in a proliferating and senescent clonal MRC5 population MRC5 cl.13 cells were continously cultured, aliquot of cells were taken when the cells were proliferating (43PDs) and when they had begun to senesce (49PDs). DNA was extracted from the proliferating and senescent cell pellets and STELA was performed at the 11q, 16p, 17p, 18q and XpYp (allele specific) telomeres. The resulting telomere length distributions were quantified using Phoretix software and mean telomere length was calculated

4.3.4 Analysis of telomeric chromatin structure in proliferating and senescent MRC5 cl.13 cells

Using the chromatin extracted from the MRC5 cl.13 cells it is possible to make several comparisons: Firstly telomeric chromatin structure can be compared between different telomeres/telomeric alleles of different lengths. Secondly any changes in the chromatin structure at the same telomere in proliferating and senescent cells can be determined. The telomere-specific approach will also uncover whether there are differences in the degree of telomeric chromatin structural change between chromosome ends as cells enter senescence.

Sonication efficiency of the MRC5 cl.13 chromatin was confirmed: Like the MRC5 mixed population chromatin 8 minutes of sonication (30s off, 30s on) sheared the MRC5 cl.13 chromatin to the desired 200-1000bp size range (fig. 4.5a).

Enrichment of H3 and TRF1 were then measured at 11q, 16p, 17p and the two XpYp telomeric alleles (fig. 4.5b&c). Telomeric H3 enrichment in the MRC5 mixed population was fairly consistent across the chromosome ends, but in the MRC5 cl.13 cells, significant variation in H3 enrichment was observed between chromosome ends both in the proliferating cells ($P<0.0001$) and in the senescent cells ($P=0.0007$) (fig. 4.5b). Significant differences in telomeric H3 enrichment existed between the proliferating and senescent cells at the same chromosome end, this was observed at 16p, 18q and the short XpYp telomeric allele. Similar variation was seen in TRF1 enrichment between chromosome ends in the proliferating cells ($P=0.0014$) and in senescent cells ($P<0.0001$) (fig. 4.5c). There was a dramatic loss of TRF1 as cells underwent senescence at 11q, 16p, 17p, 18q and the shorter XpYp telomeric allele.

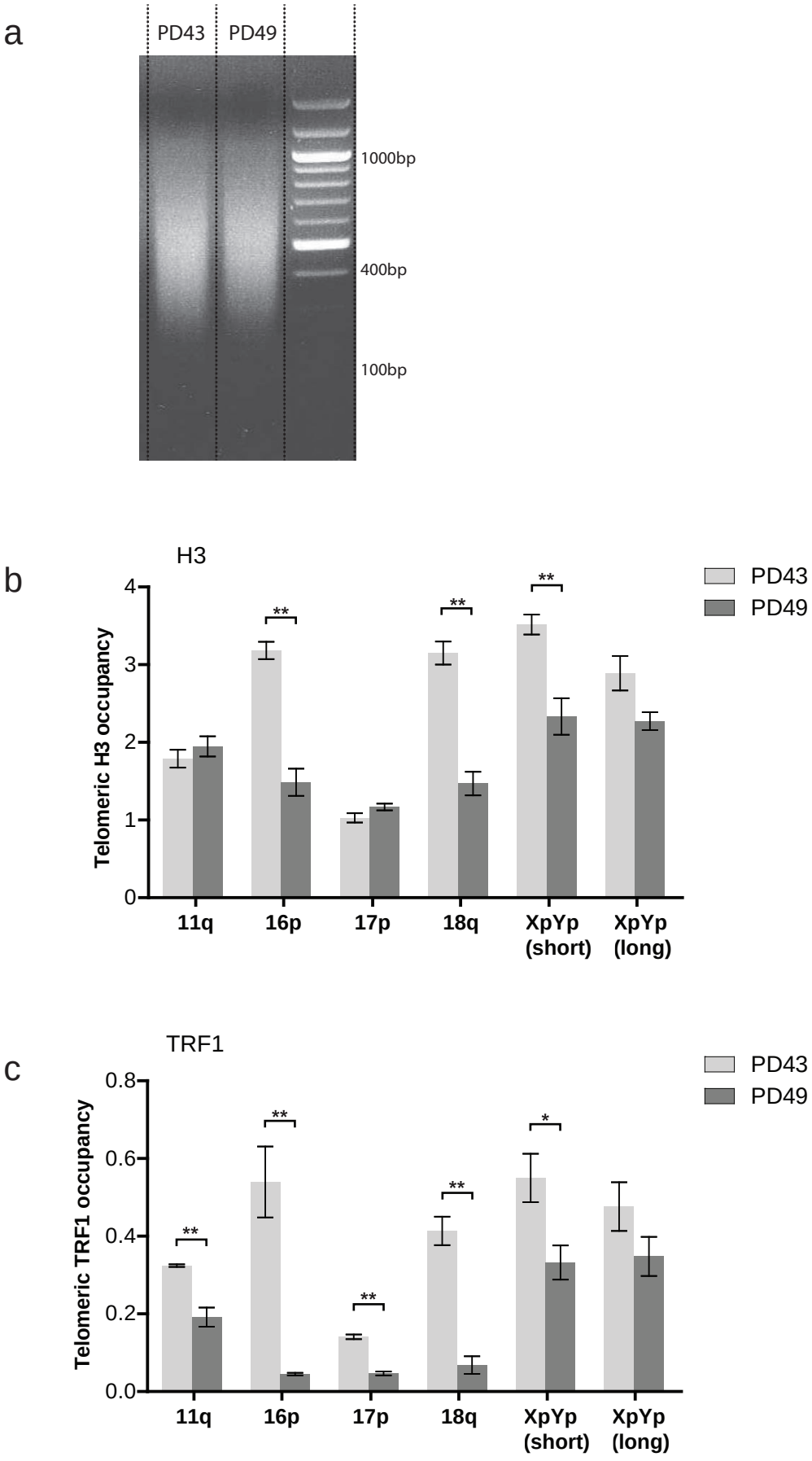

Figure 4.5. Verfication of chromatin fragment size and H3 and TRF1 telomeric enrichment in MRC5 cl.13 cells. (a) chromatin extracted from PD43 and PD 49 MRC5 cl.13 cells was sonicated for 8 mins (30s o, 30s off). An aliquot of chromatin was taken, reverse cross-linked and DNA was purified. DNA was then electrphoresed on a 1.5% agarose gel to determine fragment size. (b) Summary of mean telomere length in the proliferating and senescent MRC5 cl.13 cells at 11q, 16p, 17p, 18q and the short and long XpYp telomeric alleles. (b&c) Relative enrichment of histone H3 (b) and TRF1 (c) was measured at the 11q, 16p, 17p, 18q and XpYp (long and short allele). Statistically significant differences in enrichment was measured by t-test, * - P<0.05, ** - P<0.01. Error bars indicate SEM for qPCR reaction replicates, not the SD for internal replicates

Chromatin extracted from the proliferating and senescent cells was immunoprecipitated using antibodies against H3K4me3, H3K9me3 and H4K20me3. The enrichment of these marks was measured at their respective positive control loci. In the proliferating MRC5 cl.13 cells robust enrichment of all three marks was observed (fig. 4.6). In the senescent cells H3K4me3 was enriched at its positive control loci however this enrichment was reduced ~2.6-fold compared to the proliferating cells (fig. 4.6a). A greater reduction in H3K9me3 and H4K20me3 was seen at their positive control loci in the senescent cells; compared to proliferating cells enrichment of these marks was ~10-fold and ~7-fold lower respectively (fig. 4.6b&c).

The telomeric enrichment H3K4me3, H3K9me3 and H4K20me3 was compared between the different length telomeres within the proliferating (PD43) and senescent (PD49) MRC5 cl.13 cell populations A further comparison of telomeric occupancy was then made at the same chromosome end between the proliferating and senescent cells. In a similar manner to the MRC5 mixed population telomeric chromatin structure analysis telomeric histone methylation status in the MRC5 cl.13 cells was normalised against telomere-specific H3 occupancy.

The abundance of H3K4me3 differed significantly between the chromosome ends analysed in the proliferating cells (P=0.0068) however it did not correlate with telomere length (fig. 4.7a). Less variation was seen between chromosome ends in the senescent cells, again these differences did not correlate with the length of the telomeres. Upon senescence loss of telomeric H3K4me3 was observed. This was seen at 11q, 16p, XpYp short telomeric allele and most strikingly the 17p telomere but not at the long XpYp allele were telomeric H3K4me3 was comparable between proliferating and senescent cells. Interestingly no H3K4me3 was detected at all at the 18q telomere

in the proliferating cells and very little in the senescent cells suggesting that this telomere adopts a more heterochromatic structure.

A similar senescence-induced loss of telomeric H3K9me3 was observed in the MRC5 cl.13 cells. This was seen at all the chromosome ends but was particularly prominent at 17p and at 18q and the long XpYp telomeric allele were no H3K9me3 was detected at all in the senescent cells (fig. 4.7b). Variation in telomere-specific H3K9me3 abundance between chromosome ends was observed in both the proliferating and senescent cells however this wasn't shown to be statistically significant by an Analysis of Variance (ANOVA) and, like telomeric H3K4me3, didn't appear to correlate with telomere length.

Although significant differences in H4K20me3 enrichment was seen between telomeres/telomeric alleles in the proliferating cells ($P>0.0001$) and senescent MRC5 cl.13 cells ($P=0.0004$) these differences failed to correlate with telomere length in (fig. 4.7c). Like H3K4me3 and H3K9me3 enrichment there was a trend towards H4K20me3 loss as cells entered senescence. Again this was most prominent at 17p suggesting that this telomere is more susceptible to changes in its chromatin conformation than the other chromosome ends analysed.

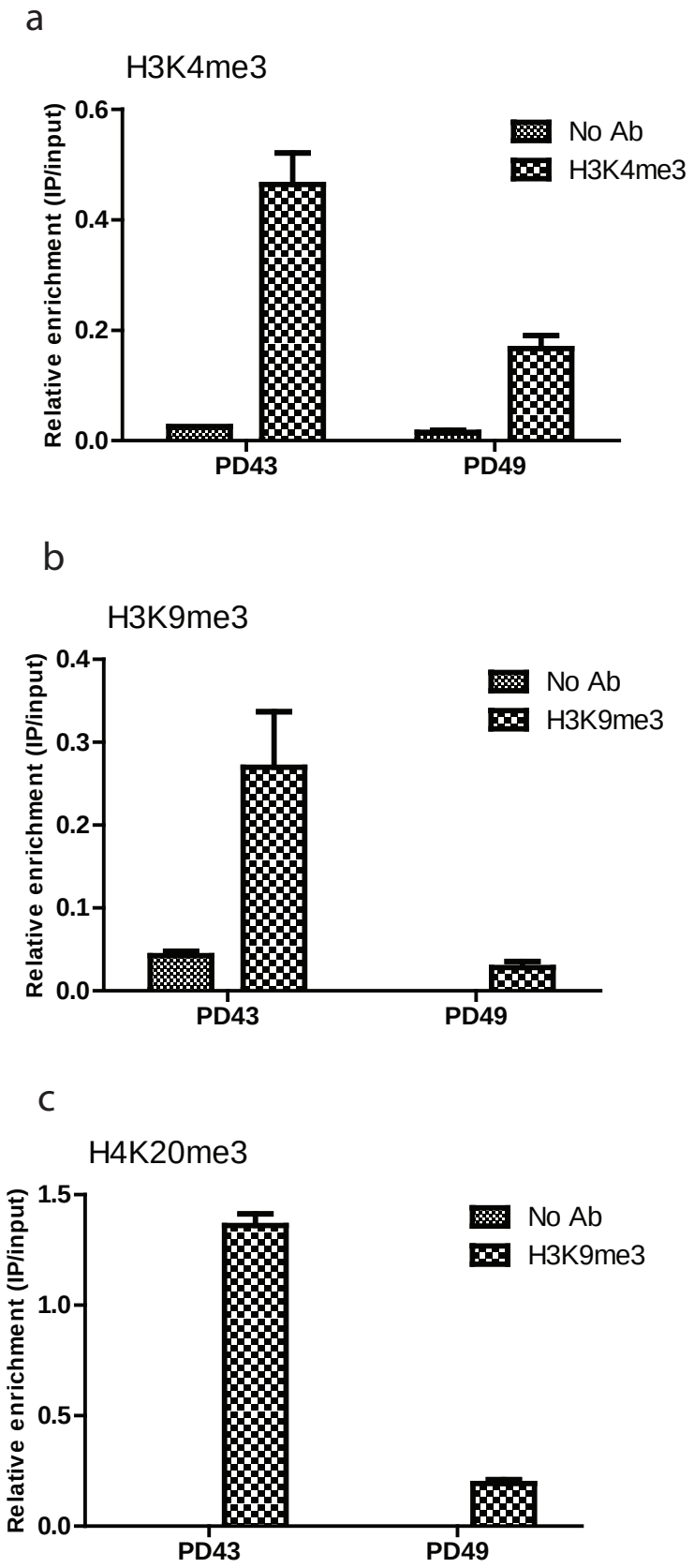

Figure 4.6. Enrichment of H3K4me3, H3K9me3, H3K27me3 and H4K20me3 at their respective positive control loci in MRC5 cl.13 cells. Immunoprecipitation efficiency for the histone methylation marks was analysed in both proliferating and senescent MRC5 cl.13 cells by measuring their enrichment at the following positive control loci: (a) H3K4me3 - GAPDH promoter, (b) H3K9me3 - ZNF554, and (c) H4K20me3 - beta-blobin promoter. Enrichment of the marks was compared against a no antibody control at the same locus. Error bars indicate SEM for qPCR reaction replicates, not the SD for internal replicates

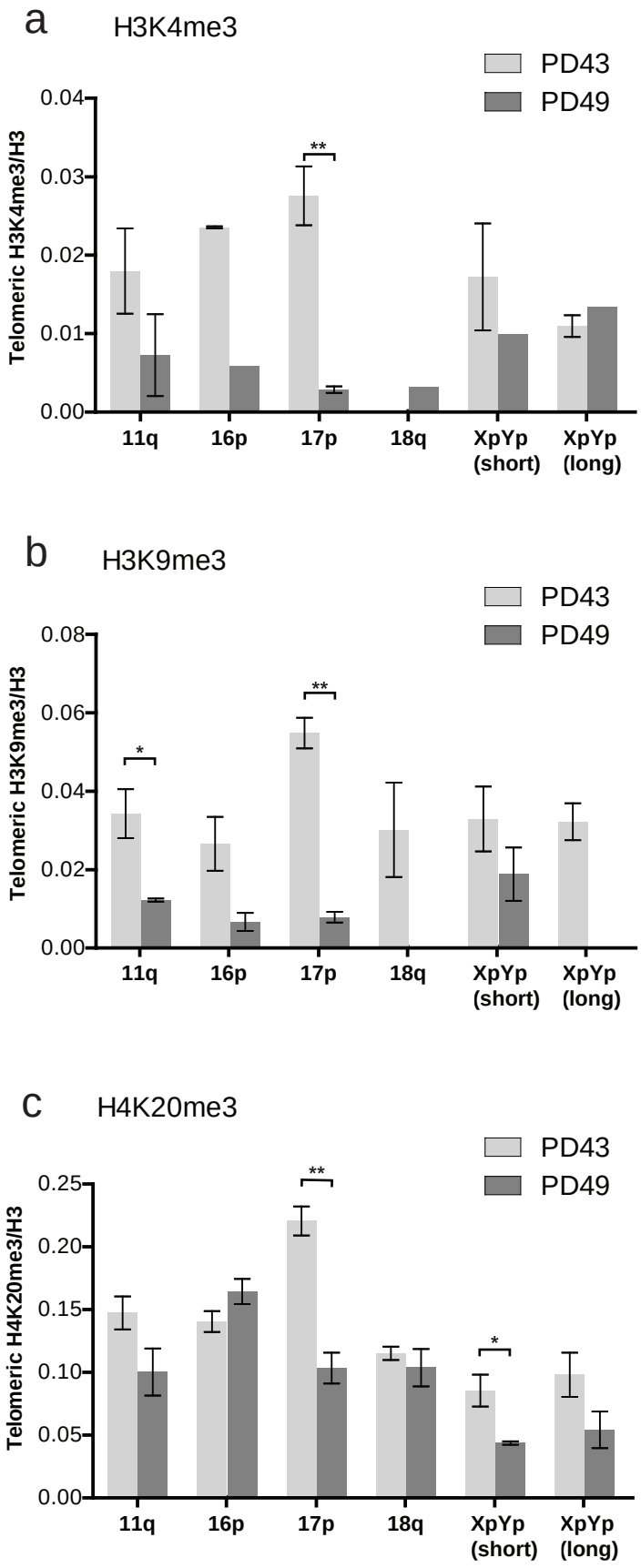

Figure 4.7. Enrichment of H3K4me3, H3K9me3 and H4K20me3 at the 11q, 16p, 17p and 18q telomeres and at the short and long XpYp telomeric alleles in proliferating and senescent MRC5 cl.13 cells. (a) Summary of mean telomere length in the proliferating and senescent MRC5 cl.13 cells at 11q, 16p, 17p, 18q and the short and long XpYp telomeric alleles. (b,c&d) Chromatin extracted from proliferating (PD43) and senescent (PD49) MRC5 cl.13 fibroblasts was immuno-precipitated using antibodies against the histone methylation marks (a) H3K4me3, (b) H3K9me3 and (c) H4K20me3. This DNA was then added to triplicate qPCR reactions for each telomere-specific assay. Amplification signal generated at each telomere was normalised to the amplification signal generated by input DNAand to teloere-specific H3 occupancy. Statistically significant differences in enrichment was measured by t-test, * - P<0.05, ** - P<0.01. Error bars indicate SEM for qPCR reaction replicates, not the SD for internal replicates

4.3.5 Differences in telomeric H4K20me3 enrichment in proliferating and senescent IMR-90 fibroblasts

The changes in the H4K20me3 mark in senescent cells was further investigated using IMR-90 fibroblasts. Specifically, telomeric enrichment of this mark was compared between proliferating (PD32) and senescent (PD86) IMR90 cells. The H4K20me3 immunoprecipitates from these cells were a kind gift from Professor Peter Adams (University of Glasgow) therefore H3, H3K4me3 and H3K9me3 enrichment was not analysed in these cells, also telomere length analysis could not be performed. Also, due to the small amount of IP DNA available, it was only possible to analyse enrichment of H4K20me3 in these cells at 17p and 18q. Telomeric enrichment of H4K20me3 was analysed in three independent ChIP assays. In all three assays telomeric H4K20me3 was significantly higher at 17p in proliferating cells compared to the senescent cells (fig. 4.8a). This observation was most noticeable in ChIP 2 where senescent cells displayed a ~10 fold reduction of 17p-assocaited H4K20me3 compared to the proliferating cells (fig. 4.8a(ii)). H4K20me3 enrichment at 18q was also shown to be significantly reduced in the senescent IMR-90 fibroblasts in all three CHIP experiments although this reduction is less pronounced than at 17p (fig. 4.8b).

It is important to note that the H4K20me3 ChIP-qPCR data for these IMR-90 fibroblasts was not normalised to telomeric H3 levels. It is therefore possible that the loss of H4K20me3 in senescent cells may result from an altered nucleosomal density. However even if this was the case an altered nucleosomal structure still represents a change in chromatin structure as cells enter senescence. Taken together these data along with the loss of H3, H3K4me3, H3K9me3 and H4K20me3 in the senescent MRC5 cl.13 cells, suggest a change in telomeric chromatin structure as fibroblasts enter senescence.

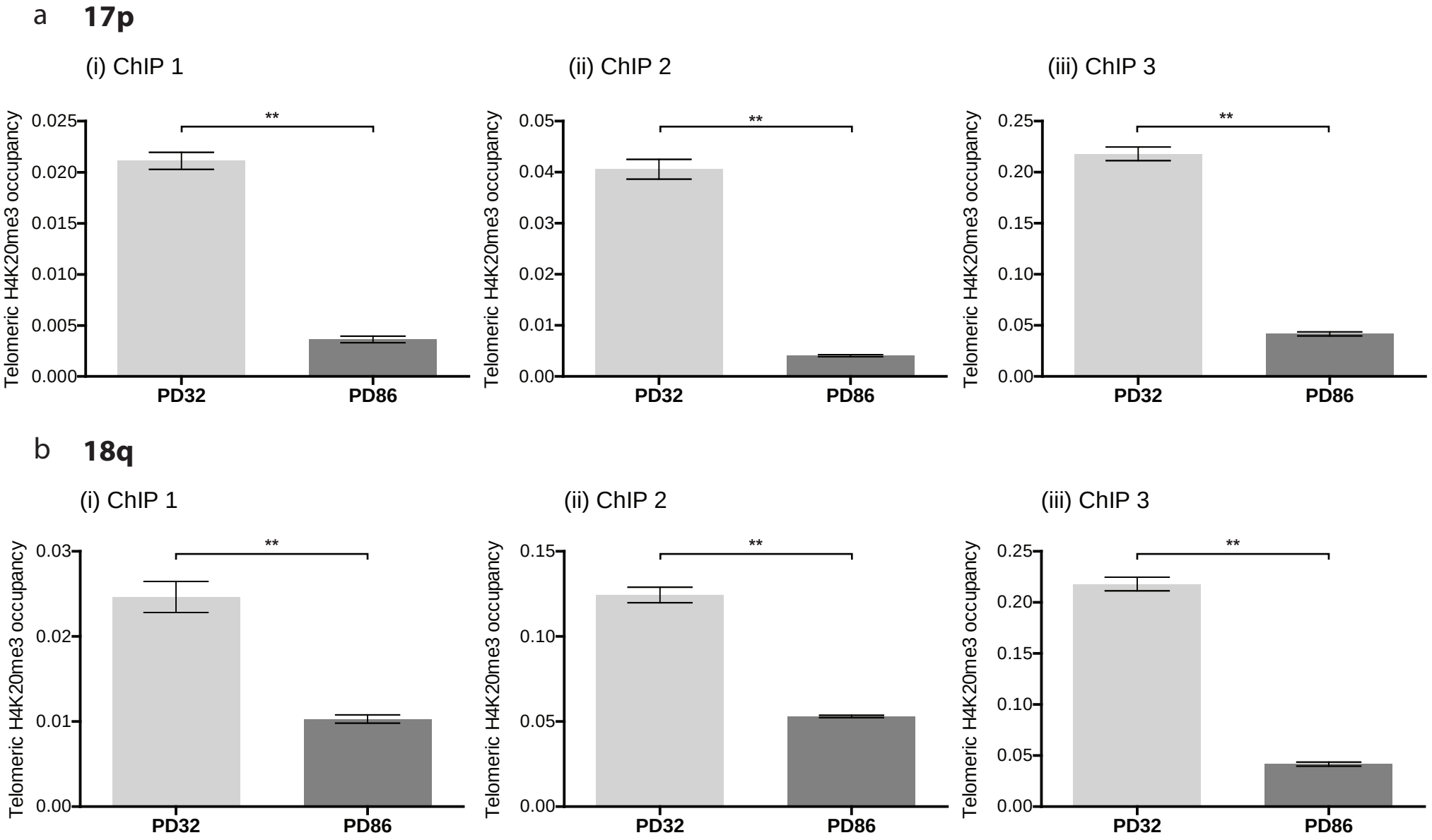

Figure 4.8. Enrichment of H4K20me3 at the 17p and 18q telomeres in proliferating and senescent IMR-90 fibroblasts. Chromatin was extracted from proliferating (PD32) and senescent (PD86) IMR-90 fibroblasts and immunoprecipitated using an antibody against the histone methylation mark H4K20me3 in three independant experiments (ChIP#1, #2 and #3). Telomere specific enrichment of these marks was analysed using qPCR assays designed to the 17p and 18q telomeres. Immunoprecipitated DNA was added to triplicate qPCR reactions for each telomere-specific assay. Statistically significant differences in enrichment was measured by t-test, * - P<0.05, ** - P<0.01. Error bars indicate SEM for qPCR reaction replicates, not the SD for internal replicates

4.3.6 Analysis of telomeric chromatin structure in two HT1080 clonal populations

In addition to analysing telomeric histone methylation enrichment patterns in MRC5 and IMR90 telomerase-negative fibroblasts, the same procedure was carried out using chromatin from clonal populations of the telomerase-positive HT1080 fibrosarcoma cell line. The rationale behind using these cells was that it would allow comparison between histone methylation patterns at the same chromosome end stably maintained at different lengths in the two different clonal populations.

4.3.7 HT1080 cl.2 and cl.4 telomere length distributions

Firstly differences in telomere length at the same chromosome end between different HT1080 clones were determined. HT1080 cl.2 and cl.4 showed large differences in telomere length at a range of chromosome ends analysed by STELA including 11q, 16p, 17p, 18q and XpYp (fig. 4.9). For all the chromosome ends analysed HT1080 cl.2 cells had a greater mean telomere length than HT1080 cl.4 cells with the differences between mean telomere length for a given chromosome end ranging from 3.114kb for 11q to 4.434kb for 18q. These large differentials in telomere length distributions between the two HT1080 clones make them a good candidate for identifying any relationship between telomere length and telomeric chromatin structure.

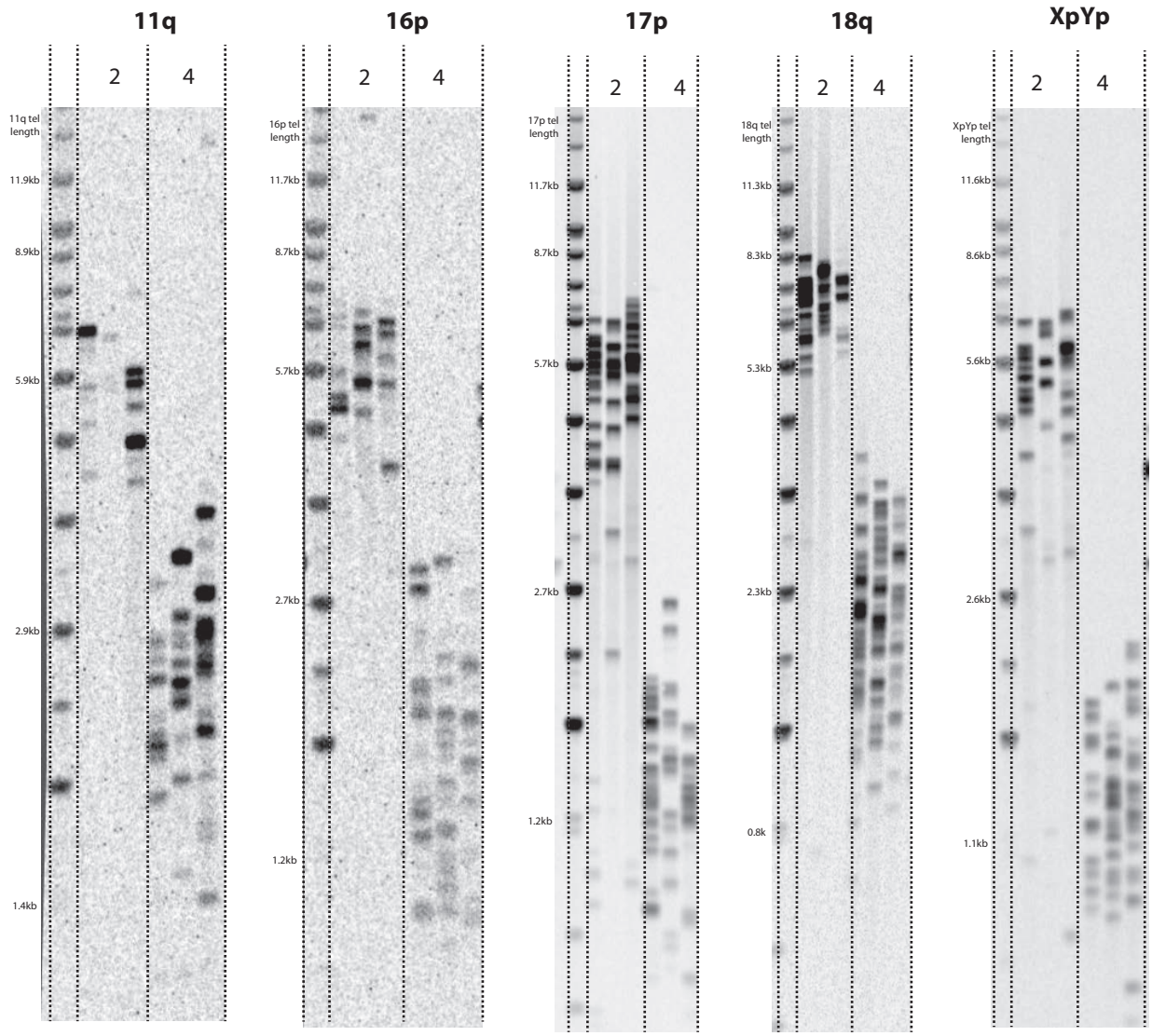

Mean tel length (kb)	5.534	2.420	5.898	1.753	4.806	1.389	6.528	2.094	4.843	1.276
Lower 95% CI	4.995	2.209	5.426	1.526	4.232	1.234	6.021	1.897	4.361	1.163
Upper 95% CI	6.072	2.631	6.370	1.981	5.381	1.545	7.035	2.290	5.325	1.389

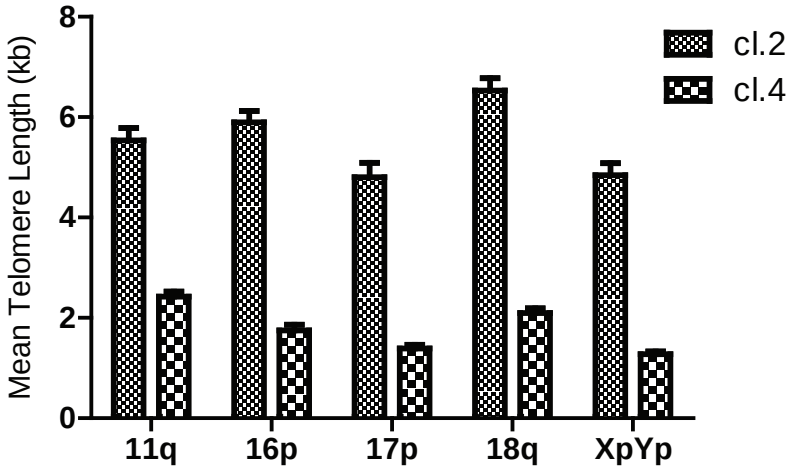

Figure 4.9. Telomere length distribution at the 11q, 16p, 17p, 18q and XpYp chromosome ends in two HT1080 clonal populations DNA was extracted from two clonal populations (cl.2 & cl.4) of the fibrosarcoma HT1080 cell line. STELA was performed at the 11q, 16p, 17p, 18q and XpYp telomeres. The resulting telomere length distributions were quantified using Phoretix software and mean telomere length was calculated

Before measuring the enrichment of telomeric chromatin marks it was necessary to ensure that the ChIP procedure used for the MRC5 cells would also be successful for the HT1080 cl.2 and cl.4 cells. The extracted HT1080 cl.2 and cl.4 chromatin was sonicated for 8 minutes (30s on, 30s off) and successfully generated fragments within the desired 200-1000bp range (fig. 4.10a).

The abundance of telomere-associated histone H3 and TRF1 was then measured in both HT1080 cl.2 and cl.4 cells. Telomeric H3 occupancy varied significantly between chromosome ends within both the clonal populations (cl.2 – $P<0.0001$, cl.4 – $P=0.0002$) (fig. 4.10b). The most striking observation of this result however was the clear differences in telomeric H3 occupancy at the same telomere maintained at different lengths in the two clones. Across all the chromosome ends analysed there was significantly less H3 enrichment at the shorter cl.4 telomeres compared to the longer cl.2 telomeres (fig. 4.10b). Although TRF1 telomeric enrichment was lower than H3 its enrichment pattern across the chromosome ends mirrored what was seen for H3, particularly in the cl.2 cells. Like H3 enrichment the variation in TRF1 between telomeres was highly significant in this clone ($P<0.0001$) and also in the cl.4 cells ($P=0.0039$) (fig. 4.10c). The difference in telomere-specific TRF1 enrichment between clones was even more dramatic than for H3. Robust enrichment of TRF1 was observed for all the telomeres analyzed in the HT1080 cl.2 cells however when these same telomeres were stably maintained at a lower length in the HT1080 cl.2 cells telomeric TRF1 enrichment was significantly lower (fig. 4.10c)

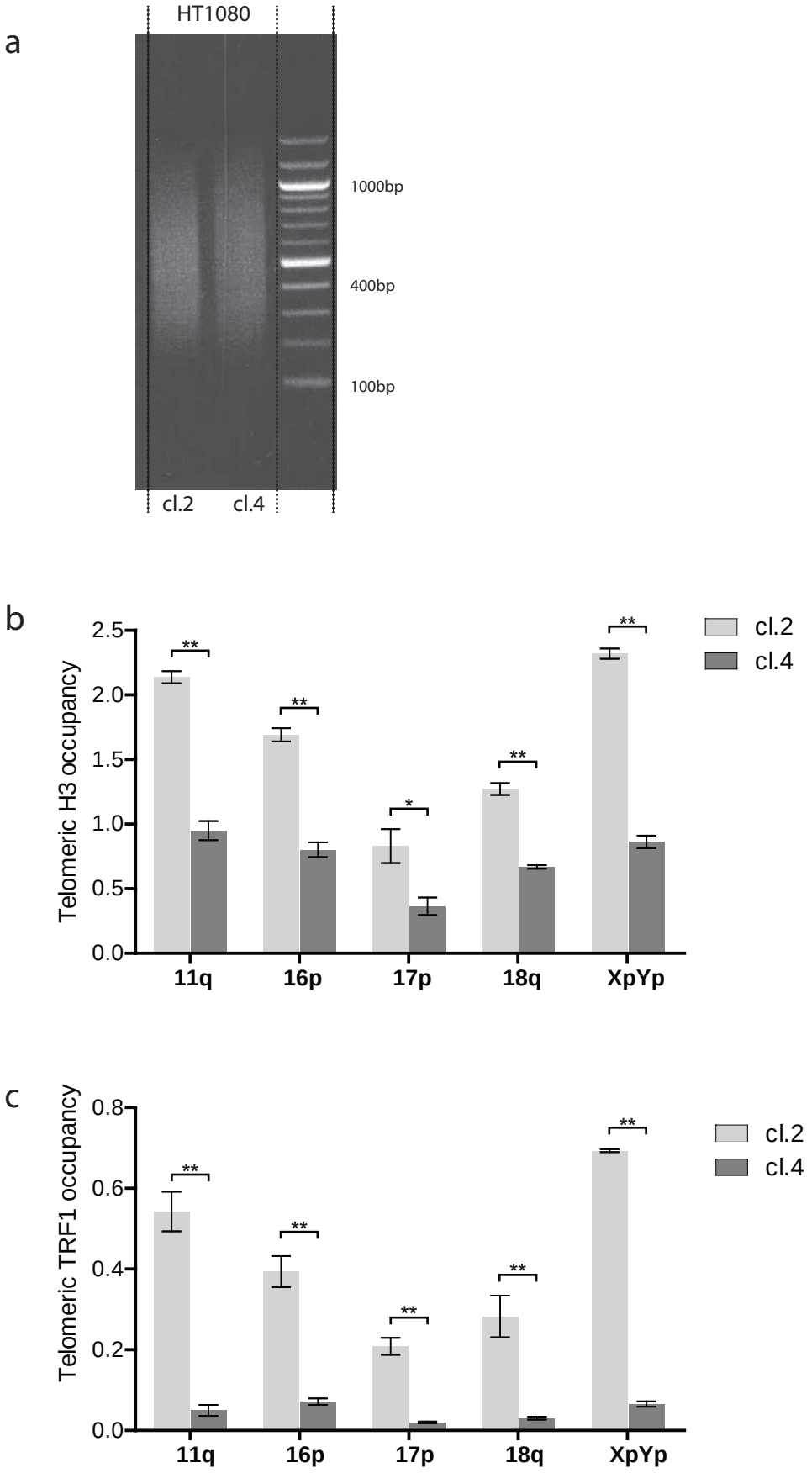

Figure 4.10. Verification of chromatin fragmentsize and telomeric enrichment of histone H3 and TRF1 at the 11q, 16p, 17p, 18q and XpYp chromosome ends in two HT1080 clonal populations. (a) chromatin extracted from HT1080 cl.2 and cl.4 cells was sonicated for 8 mins (30s o, 30s off). An aliquot of chromatin was taken, reverse cross-linked and DNA was purified. DNA was then electrphoresed on a 1.5% agarose gel to determine fragment size. (b) Summary of mean telomere length at 11q, 16p, 17p, 18q and XpYp in HT1080 cl.2 and cl.4 cells. (b&c) Chromatin extracted from HT1080 cl.2 and cl.4 cells was immunoprecipitated using antibodies against (b) H3 and (c) TRF1. The immunoprecipitated DNA was then added to triplicate qPCR reactions specific to the 11q, 16p, 17p, 18q and XpYp telomeres. Amplification signal generated at each telomere was normalised to the amplification signal generated by input DNA and then normalised to telomere-specific H3 occupancy. Statistically significant differences in enrichment was measured by t-test, * - P<0.05, ** - P<0.01. Error bars indicate SEM for qPCR reaction replicates, not the SD for internal replicates

Immunoprecipitation efficiency of H3K4me3, H3K9me3 and H4K20me3 was determined by measuring the enrichment of these marks at their respective positive control loci. Enrichment of H3K4me3 was observed at the GAPDH promoter in the HT1080 cl.2 and also in the HT1080 cl.4 cells although to a lesser extent (fig. 4.11a). Similarly H4K20me3 was shown to be abundant at its positive control loci, β-globin in the HT1080 cl.2 cells however at the same locus in the HT1080 cl.4 cells this enrichment was reduced (fig. 4.11c). H3K9me3 enrichment was weak: in the HT1080 cl.2 cells enrichment of H3K9me3 was low and in the HT1080 cl.4 cells was comparable to the no antibody control (fig. 4.11b).

There was little or no amplification of the H3K9me3 immunoprecipitated DNA from the telomere-specific qPCR assays. Although this mark has been previously shown to be under-represented at HT1080 telomeres (Arnoult et al. 2012), its enrichment at its positive control loci (ZNF554) was also low suggesting that the immunoprecipitation was not successful (fig. 4.11b) therefore telomeric H3K9me3 levels were not analysed for these cells.

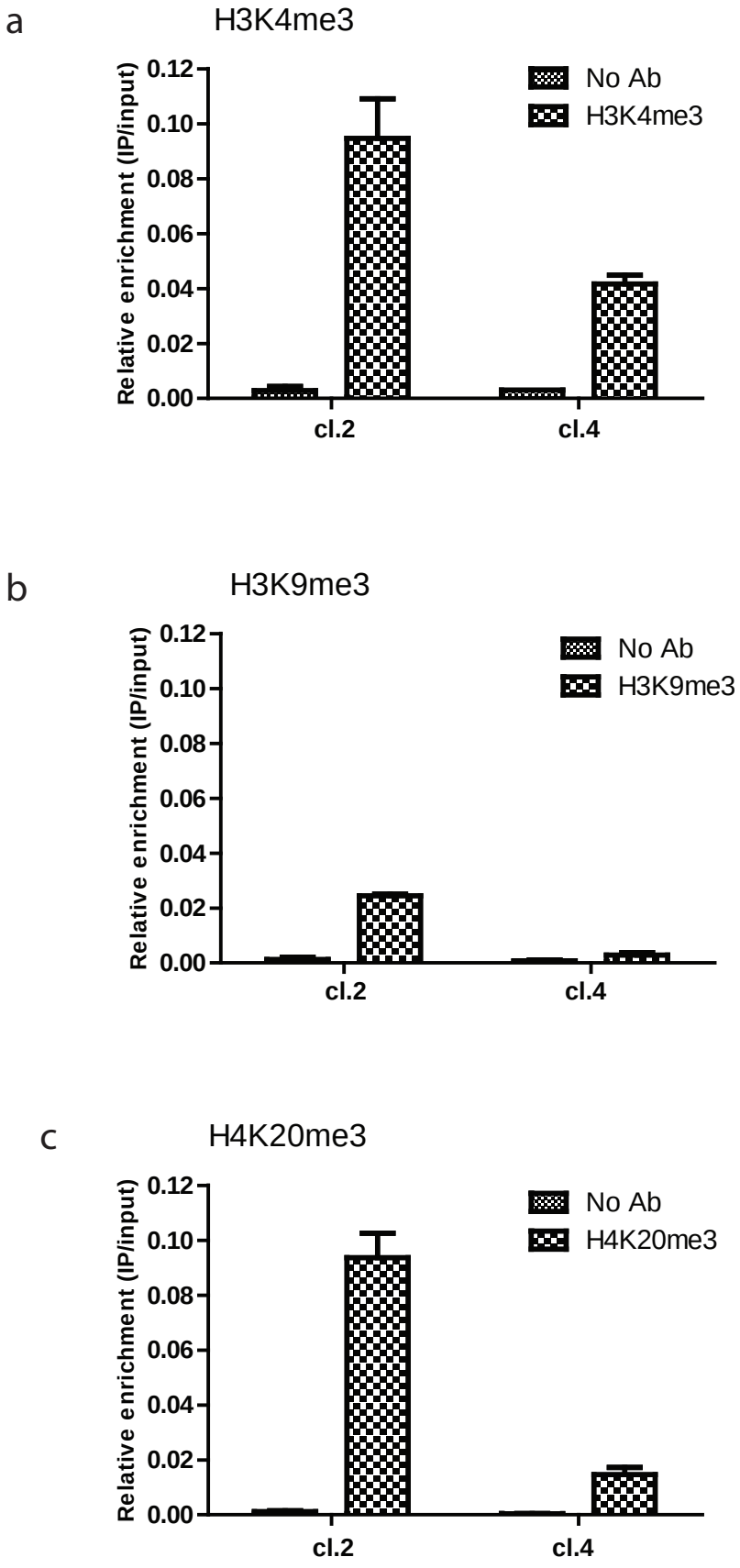

Figure 4.11. Enrichment of H3K4me3, H3K9me3, H3K27me3 and H4K20me3 at their respective positive control loci in HT1080 cl.2 and cl.4 cells. Immunoprecipitation efficiency for the histone methylation marks was analysed in both clonal HT1080 cell populations by measuring their enrichment at the following positive control loci: (a) H3K4me3 - GAPDH promoter, (b) H3K9me3 - ZNF554, and (c) H4K20me3 - beta-blobin promoter. Enrichment of the marks was compared against a no antibody control at the same locus. Error bars indicate SEM for qPCR reaction replicates, not the SD for internal replicates

Telomeric H3K4me3 enrichment was low at all chromosome ends analysed. Within the same clonal population the differences in enrichment of H3-normalised H3K4me3 did not reflect the subtle variation in telomere length seen between the different chromosome ends. However when comparison of H3K4me3 enrichment was made between the same chromosome end maintained at different lengths in the two HT1080 clones a positive correlation between telomeric H3K4me3 and telomere length was observed for four of the five telomeres analysed. The XpYp telomere in the HT1080 cl.2 cells had a mean telomere length of 4.843kb and also showed robust enrichment of H3K4me3. HT1080 cl.4 cells however displayed a mean XpYp telomere length of 1.276kb and H3K4me3 enrichment was minimal (fig. 4.12a). The same scenario was observed at the 16p, 17p and 18q chromosome ends however not at 11q were H3K4me3 abundance was comparable in the two clonal populations.

H4K20me3 was far more abundant at each telomere analysed compared to H3K4me3. Although significant variation in H4K20me3 enrichment existed between telomeres within the cl.2 cells (P=0.0018) telomeric H4K20me3 levels were much more uniform across the chromosome ends in cl.4 cells (P=0.4854) (fig. 4.12b). In either case no correlation was observed between telomeric H4K20me3 and telomere length between different chromosome ends within the same clonal population. However differences were observed at the same chromosome ends between clones. Robust H4K20me3 enrichment was observed at the longer telomeres in the HT1080 cl.2 cells at each chromosome end however the reduction in mean telomere length seen in the HT1080 cl.4 cells was accompanied by a dramatic loss of telomeric H4K20me3 (fig. 4.12b).

Telomeres in HT1080 cl.4 cells were stably maintained at a lower length than in the HT1080 cl.2 cells. Concomitant with this reduced telomere length was a dramatic reduction in H3 telomeric

occupancy, reduced tri-methylation of H4K20, and to a lesser extent, H3K4 and lower TRF1 levels. These combined observations suggest that telomeric chromatin structure does play a role in the maintenance of telomere length at least in a telomerase-positive context.

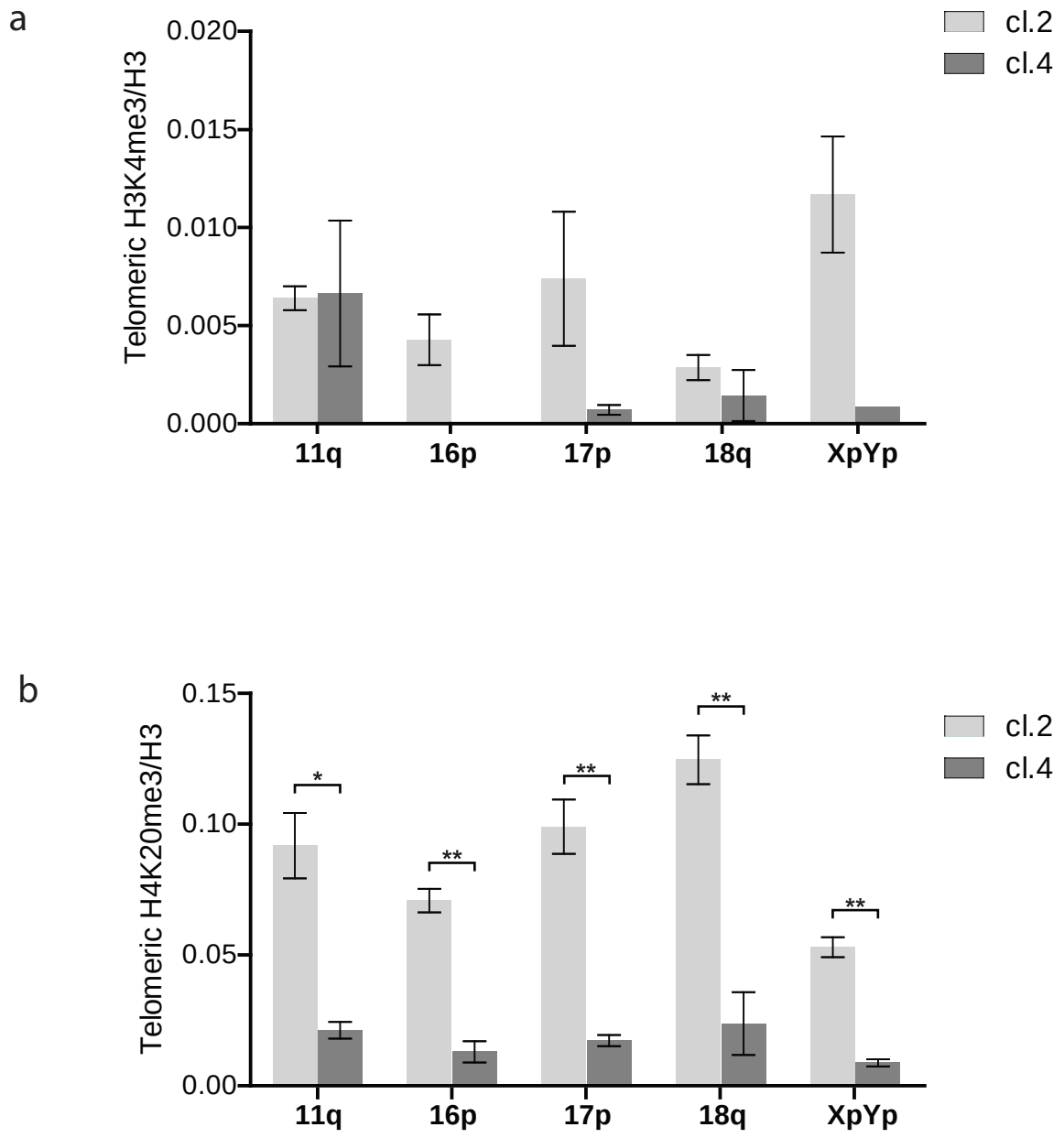

Figure 4.12. Telomeric enrichment of histone H3K4me3 and H4K20me3 at the 11q, 16p, 17p, 18q and XpYp chromosome ends in two HT1080 clonal populations. Chromatin extracted from two HT1080 clonal populations (cl.2 & cl.4) was immunoprecipitated using antibodies against (a) H3K4me3 and (b) H4K20me3. Immunoprecipitated DNA was then added to triplicate qPCR reactions specific to the 11q, 16p, 17p, 18q and XpYp telomeres. Amplification signal generated at each telomere was normalised to input DNA and to telomere-specific H3 occupancy. Statistically significant differences in enrichment was measured by t-test, * - $P<0.05$, ** - $P<0.01$. Error bars indicate SEM for qPCR reaction replicates, not the SD for internal replicates

4.4 Discussion

In this chapter telomeric chromatin structure has been analysed in a number of different scenarios; between telomeres/telomeric alleles of different lengths within the same cell population, between the same chromosome end maintained at different lengths in two different clonal populations of the same cell line and between proliferating and senescent cells. Potential correlation between telomere length and telomeric chromatin structure has been identified in telomerase-positive HT1080 cells. Additionally changes in telomeric histone methylation patterns have been observed between actively proliferating and senescent cells.

Despite the success of measuring telomere/telomeric allele-specific enrichment of the histone methylation marks there are a number of shortcomings to the approach taken which if rectified would provide a more robust analysis of telomeric chromatin structure. Firstly, aside from the IMR-90 ChIP-qPCR data, the data presented is from single ChIP experiments. It is preferable to repeat a ChIP experiment several times and calculate the average enrichment of a protein. Additional experiments were not possible due to time constraints and therefore the data in this chapter must be viewed as preliminary. It will be necessary to repeat these ChIP assays to confirm whether the results seen in this chapter are biologically relevant.

A further potential criticism of the approach taken in this chapter is that the ChIP-qPCR assays detect chromatin fragments containing both telomeric and subtelomeric DNA, therefore differentiating between the two is not possible. Subtelomere/telomere chromatin boundaries have been shown to exist in Arabidopsis and in budding yeast (Altaf *et al.* 2007; Grunstein 1998; Vaquero-Sedas et al. 2011). Such a boundary has also been suggested in human cells (O'Sullivan et al. 2010). In this study a TTAGGG repeat containing probe and a probe specific to the 17p subtelomere were used to

analyse chromatin structure in the subtelomere and telomere. They observed higher levels of histone H3, H4K16 acetylation and H3K79 di-methylation in 17p subtelomeric regions compared to telomeric regions. A drawback of the approach taken in this study however is that the 17p subtelomere probe used would not be able to distinguish between the 17p subtelomeric sequence and the five interstitial telomeric sequences found elsewhere in genome, therefore the enrichment measured by this probe will reflect predominantly non-subtelomeric chromatin structure. In defence of the approach taken in this chapter the qPCR assays were designed immediately adjacent to the TTAGGG repeats where possible and considering that subtelomeres can range in size from 10-300kb (Mefford and Trask 2002) the amount of subtelomeric DNA detected by the ChIP-qPCR assays is relatively small.

An issue which required careful consideration throughout the analyses was the method in which amplification signals generating at each chromosome end were normalised. The most widely used method of normalizing ChIP-qPCR data is the IP/INPUT method. This method was employed in this chapter. When comparing ChIP-qPCR data generated from different chromatin samples erroneous differences in enrichment of a chromatin-bound protein can result because of differences in the starting amount of chromatin between samples. By normalising to the input chromatin this source of variation is nullified. A limitation of this method of normalisation however is that it cannot normalise against variation arising due to differences in immunoprecipitation efficiency between chromatin samples. Normalising qPCR-data to an internal control sequence can cancel out immunoprecipitation efficiency differences between chromatin samples. However this method relies upon the assumption that the chromatin structure at the control sequence does not differ between samples (Haring *et al.* 2007). It is because of this assumption that this normalisation strategy was not used when analysing telomeric histone methylation between proliferating and senescent MRC5 cells and IMR90 cells. It has been shown that when cells enter senescence their global chromatin landscape is altered

(O'Sullivan et al. 2010). Although no specific changes in chromatin structure at the positive control loci (GAPDH promoter, ZNF554 and β-globin promoter) have been documented it cannot be ruled out therefore this data was not normalised in this manner. Instead, in addition to normalising to input chromatin, telomere-specific ChIP-qPCR data was normalised to telomeric H3 occupancy. This method is advantageous because it ensures that any differences in the enrichment of a histone methylation mark are not just a result of altered telomeric H3 occupancy. The downside of the method of normalisation used in this chapter is that it is impossible to say whether the changes seen in telomeric enrichment of histone methylation marks between proliferating and senescent cells or between HT1080 clonal populations is specific to telomeres or just a result of global alterations of the enrichment of a mark.

Although considerable research has identified certain histone modifications as influencing factors on telomere length at mouse chromosome ends very little research has been undertaken identifying any relationship between a length of a telomere and its chromatin structure in human cells. In a recent study telomerase was ectopically expressed in HT1080 cells resulting in HT1080+TT cells with an average telomere length of 36.2kb, 24.9kb longer than the average telomere length in the parental cell line (HT1080) (Arnoult et al. 2012). Concomitant with this dramatic increase in telomere length was an increase in telomeric H3 occupancy and increased H3K9me3. H3K9me3 immunopreipitation was unsuccessful in the HT1080 cells in this chapter therefore no comparisons between its enrichment and telomere length could be made however there did appear to be a correlation between telomeric H4K20me3, and to a lesser extent H3K4me3 and telomere length.

Changes in telomere structure have previously been observed between different developmental stages of a cells life span. Pluripotent stem cells have been shown to possess a more relaxed

telomeric chromatin conformation than differentiated cells in mice (Marion et al. 2009). Changes in telomere chromatin structure between proliferating and senescent cells however are less well defined, particularly in human cells. Loss of telomeric H3 occupancy as well as reduced TRF1 and TRF2 abundance has been shown in IMR90 cells entering senescence (O'Sullivan et al. 2010). The data presented in this chapter is somewhat consistent to this work. TRF1 levels were lower at all the chromosome ends tested in senescent MRC5 cl. 13 cells compared to the same cells when proliferating. However differences in H3 occupancy are far less clear: although the senescent cells have lower levels of telomeric H3 at 16p, 18q and, to a lesser extent, the XpYp telomeric alleles than the proliferating cells, 11q and 17p H3 occupancy is comparable. This highlights the advantage of using the telomere-specific ChIP-qPCR assays as the dot blot system of detection is unable to distinguish protein occupancy between chromosome ends. Telomeric H3K4me3 and H3K9me3 levels were reduced in senescent MRC5 cl.13 cells. H4K20me3 was also lower in the telomeres in these senescent cells as well as at 17p and 18q in senescent IMR90 fibroblasts. The senescence-induced loss of telomeric H3K4me3 and H4K20me3 are previously unreported. Very recently reduced H3K9me3 within the 7q and 11q subtelomeric regions was reported in senescent human WI-38 fibroblasts (Thijssen *et al.* 2013). H3K9me3 levels were 2-3 fold lower in senescent cells compared to proliferating cells. This difference was observed 4kb away from the telomere but is similar to the difference seen at 11q in the MRC5 cl.13 cells at the telomere/subtelomere boundary were a 2.8 fold loss in H3K9me3 occupancy was seen in the senescent cells.

An unexpected finding during this chapter was the differences in TRF1 enrichment between chromosome ends within the same cell population. The aim was to design the qPCR assays as close to the TTAGGG repeat tract as possible however due to the limited number of telomere-specific nucleotides to design primers around the qPCR PCR products were more subtelomeric than would have been preferable. The most extreme case is the qPCR assay for the 18q chromosome end which

amplifies a region 444nt away from the TTAGGG repeat tract. The upshot of this is that of the chromatin fragments immunoprecipitated, less telomeric DNA will be amplified by these primers compared to other chromosome ends. Given that TRF1 binds only TTAGGG repeats and not to subtelomeric DNA it would be reasonable to assume that the distance from the qPCR assay to the TTAGGG repeat at each chromosome end would have been reflected by the differences in telomere-specific TRF1 enrichment. Such differences have recently been observed (Deng et al. 2012). In this study six sets of primers were designed at increasing distances from the TTAGGG repeat tract within the XqYq subtelomere and TRF1 and TRF2 abundance was analysed at these sites. Whereas robust TRF1 and TRF2 enrichment was observed at the most telomere-proximal site (109nt from TTAGGG), enrichment of the two proteins was approximately 4-fold lower at the next primer site (966nt from TTAGGG). TRF1 and TRF2 binding was then minimal further into the subtelomere. No such correlation was observed in experiments in this chapter. Although differences in TRF1 enrichment existed between chromosome ends in all the cell types tested these differences didn't reflect the distance between the qPCR assay and TTAGGG repeat tract. This is best exemplified in the proliferating MRC5 cl.13 cells (fig. 4.5c). The qPCR assays at 17p and 18q were 426nt and 444nt away from the telomeric repeat tract respectively. Despite the similar qPCR assay position TRF1 enrichment varies considerably between the two ends: 17p TRF1 enrichment is low whereas 18q TRF1 enrichment is higher and almost at a similar level to TRF1 enrichment at XpYp whose qPCR assay extends into the telomeric repeats. A potential cause of this variation could be the presence of telomere variant repeats (TVRs). TVRs have been shown to occur in the proximal 2-3kb of telomere repeat arrays (Baird et al. 2000; Baird et al. 1995). Considering that TRF1 binds solely to TTAGGG repeats TVR variation between chromosome ends may result in differing amounts of TRF1 binding in the proximity of the qPCR assays.

The telomere-specific ChIP-qPCR assays could be used to analyse telomeric chromatin structure in a number of different contexts including at different stages of the cell cycle, after depletion of a chromatin remodeler of interest or in cells ectopically expressing telomerase to name but a few. More specific future directions which would directly follow on from this work would include analyzing the telomere-specific enrichment of different histone modifications at different length telomeres and in proliferating and senescent cells. Such marks would include the alternative methylation forms (mono- and di-methylation) of the histone methylation marks studied in this chapter and also H2BK5me1, H3K79me2 and H4K16Ac all of which have been shown to be present at telomeres in various human cell types (O'Sullivan et al. 2010; Rosenfeld et al. 2009).

The aim of this chapter was to determine whether telomeric chromatin structure differs between telomeres of different length. The telomere-specific enrichment of three histone methylation marks (H3K4me3, H3K9me3 and H4K20me3) as well as histone H3 and TRF1 was analysed at individual chromosome ends with differing telomere length distributions. Although slight differences in telomeric H3K4me3, H3K9me3 and H4K20me3 were observed between different chromosome ends in a telomerase-negative MRC5 fibroblasts these differences didn’t correlate with telomere length. When the same marks/proteins were analysed at the same chromosome ends stably maintained at different lengths in two telomerase-positive HT1080 clonal populations a positive correlation between telomeric chromatin structure and telomere length was observed: HT1080 cells with longer telomeres showed increased enrichment of H3K4me3 and H4K20me3 as well as greater H3 telomeric occupancy suggesting the existence of a relationship between the chromatin structure of a telomere and its length in telomerase-positive cells.

A further aim of the chapter was to determine whether the chromatin structure of individual chromosome ends differs between actively proliferating cells and senescent cells. Telomeric H3K4me3, H3K9me3 and H4K20me3 were reduced in a clonal population of MRC5 cells as they entered senescence. Loss of H4K20me3 was also observed in IMR90 fibroblasts as they enter senescence at 17p and 18q. The changes in chromatin structure as cells entered senescence differed between chromosome ends: whereas some telomeres appeared more susceptible to loss of a particular histone methylation mark other telomeres did not. The identification of such differences highlights the benefits of using the telomere-specific ChIP-qPCR approach over the more traditional ChIP-dot blot assays which would not be able to differentiate between the chromatin structure of different chromosome ends.

Chapter 5

Identification of human chromatin remodelers with a role in telomere length maintenance

5.1 Abstract

Telomere length is a key determinant of telomere function and is affected by various factors including telomerase-mediated extension, the ALT (Alternative Lengthening of Telomeres) pathway, oxidative stress and also telomeric chromatin structure. A number of chromatin remodelling proteins have been identified as regulators of telomere length in yeast and in recent years several mammalian proteins have been identified which, through their ability to maintain the chromatin structure at telomeres, contribute to telomere length homeostasis. The emerging model for telomeric chromatin regulation is one in which telomeric chromatin is maintained through an ordered sequence of events mediated through the actions of a number of nucleosome-altering proteins, DNA methyltransferases and long non-coding RNAs (TERRA). It also appears likely that the telomeric chromatin structure is not universal but may differ depending on the cellular context. It is highly probable that additional chromatin remodelers with telomeric roles are yet to be found, particularly in human cells were examples are scarce. The aim of this chapter was to identify other chromatin remodelling proteins which may play a role in telomere length maintenance.

A clonal population of the human HT1080 fibrosarcoma cell line was selected because it contained homogeneous telomere length distributions that would allow subtle changes to be detected. A novel 96-well plate based RNAi knockdown screen was performed using siRNAs targeting 15 selected chromatin remodeler-encoding genes. Aberrant telomere length phenotypes resulting from loss of a chromatin remodelling protein were then identified by Single Length Telomere Length Analysis (STELA) at the 17p, 18q and XpYp chromosome ends. siRNA mediated knockdown of the histone methyltransferase (HMTase) EHMT2 resulted in an increase in very short 17p telomeres whereas

loss of another HMTase, DOT1L caused a divergence in the 17p telomere length distribution suggesting the presence of two subpopulations each with differing telomere length distributions. Subtle alterations in mean telomere length was observed after siRNA mediated knockdown of the HMTases MLL and EZH2, the histone deacetylases (HDACs) HDAC1 and SIRT6, the SWI/SNF subunit BAF155 and the H3.3 histone chaperone DAXX. However due to certain limitations of the RNAi screen the robustness of these observations is questionable and more work would have to be performed to confirm these chromatin remodelers as regulators of telomere length.

5.2 Introduction

In eukaryotes epi-genetic information is stored in the DNA-protein complex chromatin. Nucleosomes, the fundamental unit of chromatin, have an octomeric structure consisting of two copies of each of the four core histones (H2A, H2B, H3 and H4) around which 147bp of DNA is wrapped. Nucleosome core particles are linked by the H1 'linker' histone to form a 'beads-on-a-string' structure, which itself, is further folded into higher order structures. This 'folding' is a necessary function of chromatin to fit the entire genome (~2m DNA in humans) within a single nucleus (~5µm). Chromatin also serves another purpose within the nucleus, which is to provide another layer of regulation acting on the DNA. The dynamic modulation of chromatin structure controls access to the DNA sequence for non-histone nuclear proteins and is a highly conserved process throughout eukaryotes. It is achieved through chromatin remodelling activity of proteins which covalently modify histones, ATP-dependant chromatin remodelling complexes, utilization of histone variants and also DNA methylation. The role of chromatin remodelling has been implicated in a wide range of cellular processes including the regulation of gene expression, DNA replication, the DNA damage response and more recently telomere maintenance.

5.2.1 The importance of telomere length

Telomere length plays a central role to the functionality of a telomere. One of the primary functions of the telomere is to protect linear chromosomes from damage and degradation. Due the incomplete nature of semi-conservative DNA replication (the end replication problem) (Harley, Futcher & Greider, 1990; Olovnikov, 1971) telomeres are required to act as a buffer at the ends of chromosomes to prevent the loss of genetic information. The telomere erosion observed with every cell division in telomerase-negative cells can also act as a 'counter' of cell division to provide a mechanism of tumour suppression. With on-going cell division continued telomere erosion

eventually results in the loss of telomeric function, which triggers recruitment of the DNA damage response apparatus, leading to a p53-dependant G1-S cell cycle arrest (replicative senescence) (Baird, 2005). Consistent with this idea of cell division 'counting' by telomere erosion is the observation is the high level of telomerase expression in immortal cell lines and over 90% of human malignancies (Harle-Bachor & Boukamp, 1996; Kolquist et al., 1998) suggesting that telomerase expression and consequently stable telomere length prevents telomere erosion-induced replicative senescence.

Telomeres also function to prevent the natural end of a chromosome from being recognised as a double stranded DNA break. This is achieved through the higher order 'T-loop' structure (Griffith et al., 1999; Stansel, de Lange & Griffith, 2001) that acts as a protective cap and sequesters chromosome ends away from the DNA repair apparatus. Dysfunctional short telomeres lose this 'capping' property which can result in fusion of a telomere with either another telomere or with a non-telomeric DNA double strand break. These fusion events have the potential to promote genomic instability which drives tumour progression (O'Hagan et al., 2002).

Due to the central role telomere length plays in telomere function considerable effort has been made to identify determinants of telomere length including telomerase and other telomeric proteins, recombination-based mechanisms, oxidative stress and also environmental effects such as smoking and obesity (Bryan et al., 1995; Greider & Blackburn, 1985; Petersen, Saretzki & von Zglinicki, 1998; Smogorzewska et al., 2000; Valdes et al., 2005; van Steensel & de Lange, 1997). The role of chromatin in telomere length maintenance has however been a largely unexplored field until recent years.

5.2.2 Telomeric chromatin and chromatin remodelers at the telomere

Telomeric chromatin shares characteristic features with other repeat-containing heterochromatic regions of the genome such as pericentric repeats (Schoeftner & Blasco, 2010), namely low levels of histone acetylation, high levels of histone methylation and DNA methylation. Maintenance of telomeric chromatin structure is a tightly regulated process. Disruption of the telomeric chromatin structure can result in a number of aberrant telomere phenotypes including increased telomere-to-telomere fusions, increased telomere dysfunction-induced foci (TIFs) and alterations in telomere length. Chromatin remodelers which play a role in maintaining telomeric chromatin structure have been studied in various organisms including yeast, mice and more recently in human cell lines.

Compared to model organisms the role of chromatin remodelers at human telomeres is less well defined. Interestingly several studies have reported opposing enrichment patterns of certain histone modifications to what was observed in mouse ES and MEF cells. H3K27me3 enrichment was not observed at mouse telomeres however it is present at human telomeres. Conversely, whereas H3K9me3 levels are high at mouse telomeres, it was only detected at low levels at telomeres in HT1080 and HeLa cells (Arnoult, Van Beneden & Decottignies, 2012; O'Sullivan et al., 2010; Rosenfeld et al., 2009). The fact that human telomeres have a different chromatin structure compared to mice telomeres suggests that alternative chromatin remodelers are required at the telomere in humans. Given the scarcity of known chromatin remodelers which function at human telomeres there is a need to shed more light on telomeric chromatin structure maintenance in human cells and how this impacts upon telomere length.

5.2.3 Aims of the chapter

The aim of this chapter was to identify chromatin remodelling proteins which have an impact upon telomere length. This was done by using a novel 96-well plate-based RNAi screen in which selected chromatin remodelling genes were targeted for knockdown in a clonal population of the HT1080 fibrosarcoma cell line. Resulting aberrant telomere length phenotypes were characterised with Single Telomere Length Analysis (STELA).

5.3 Results

5.3.1 Selecting chromatin remodelling genes

The selected genes all encoded a protein with chromatin remodelling function and have all been implicated in some form of cancer. Deletion or knockdown of some of the genes has also been shown to result in telomere dysfunction in different organisms such as yeast or mice. Additionally, due to data generated in our lab where siRNA-mediated knockdown of the SWI/SNF family member ATRX resulted in a striking loss of telomere length, chromatin remodelers that interacted with ATRX were also were also included on the list. A summary of the genes selected is presented in Table 5.1.

Remodeler class	Symbol	Name	Other Aliases	Involvement in cancer?	Role at telomere?	Interacts with ATRX?
Histone Deacetylase (HDAC)	HDAC1	histone deacetylase 1	HD1; RPD3; GON-10; RPD3L1; DKFZp686H12203; HDAC1	✓		✓
	HDAC4	histone deacetylase 4	HD4; HDACA; HA6116; HDAC-A; KIAA0288; HDAC4	✓		✓
Sirtuin protein	SIRT1	sirtuin (silent mating type information regulation 2 homolog) 1 (S. cerevisiae)	SIR2L1; SIRT1	✓	✓	
	SIRT6	sirtuin (silent mating type information regulation 2 homolog) 6 (S. cerevisiae)	SIR2L6; SIRT6	✓	✓	
Histone Methyltransferase (HMT)	EHMT2	euchromatic histone-lysine N-methyltransferase 2	G9A; BAT8; NG36; KMT1C; C6orf30; FLJ35547; DKFZp686H08213; EHMT2	✓	✓	
	EZH2	enhancer of zeste homolog 2 (Drosophila)	ENX1; EZH1; KMT6; ENX-1; KMT6A; MGC9169; EZH2	✓	✓	✓
	DOT1L	DOT1-like, histone H3 methyltransferase (S. cerevisiae)	DOT1; KMT4; KIAA1814; DKFZp586P1823; DOT1L	✓	✓	
	MLL	myeloid/lymphoid or mixed-lineage leukemia (trithorax homolog, Drosophila)	HRX; TRX1; ALL-1; CXXC7; HTRX1; KMT2A; MLL1A; FLJ11783; MLL/GAS7; TET1-MLL; MLL	✓	✓	
Histone Demethylase	JARID1C	lysine (K)-specific demethylase 5C	MRXJ; SMCX; MRXSJ; XE169; JARID1C; DXS1272E; KDM5C	✓		
	UTX	lysine (K)-specific demethylase 6A	UTX; MGC141941; bA386N14.2; DKFZp686A03225; KDM6A	✓		
ATP-dependent chromatin remodeler	BAF155	SMARCC1 (SWI/SNF related, matrix associated, actin dependent regulator of chromatin, subfamily c, member 1)	Rsc8; SRG3; SWI3; BAF155; CRACC1; SMARCC1	✓	✓	
	LSH	helicase, lymphoid-specific	HELLS; PASG; SMARCA6; Nbla10143	✓		
Histone Chaperone	DAXX	death-domain associated protein	DAP6; EAP1; BING2	✓	✓	✓
Histone variant	H3F3A	H3 histone, family 3A	H3F3; H3.3A	✓	✓	✓
	H3F3B	H3 histone, family 3B	H3.3B	✓	✓	✓

Table 5.1. Candidate genes encoding chromatin remodelers chosen for RNAi knockdown in HT1080cl. 2 cells. Genes were chosen based on thier ability to fulfill certain criteria: the encoded protein has chromatin remodeling activity, the protein has been shown to have a role at the telomere and the up- or down-regulation of the gene has been implicated in cancer

5.3.2 Optimization of RNAi knockdown procedure

To allow rapid analysis of any aberrant telomere phenotypes resulting from knockdown of the candidate genes, the RNAi knockdown screen was performed on a 96-well plate scale using a clonal cell population of the HT1080 fibrosarcoma cell line (clone 2). HT1080 cl.2 was selected from a panel of clones because it displayed a homogeneous telomere-length distribution at all three of the chromosome ends to be analysed (17p, 18q and XpYp) which will allow subtle telomere phenotypes to be more easily identified.

By seeding differing amounts of HT1080 cl.2 cells per well, it was determined that 4500 cells seeded the night prior to transfection gave the optimal cell confluence (~70%) for the knockdown (data not shown). siRNA transfections were then performed using the recommended conditions (Dharmacon).

The premise for this experiment was to maintain low mRNA levels of a candidate gene over a number of cell divisions, thereby maximizing the chance of observing any subtle, gradual telomere elongation/erosion processes. To maintain low mRNA level of a given gene three successive transfections were carried out, however, it was necessary to determine the time points upon which these transfections should be performed. This was determined in a pilot experiment in which the HT1080 cl.2 cells were transfected with a siRNA targeting GAPDH. GAPDH mRNA levels were then measured at 24-hour intervals over a period of 72 hours (fig. 5.1). GAPDH mRNA level fell to its lowest level 48 hours after the initial transfection (~23%) before recovering to 67% by 72 hours. With the caveat that different genes will exhibit differing kinetics of knockdown and protein half-life it was considered that for this particular clone, successive transfections 48 hours apart, should maintain a low mRNA level.

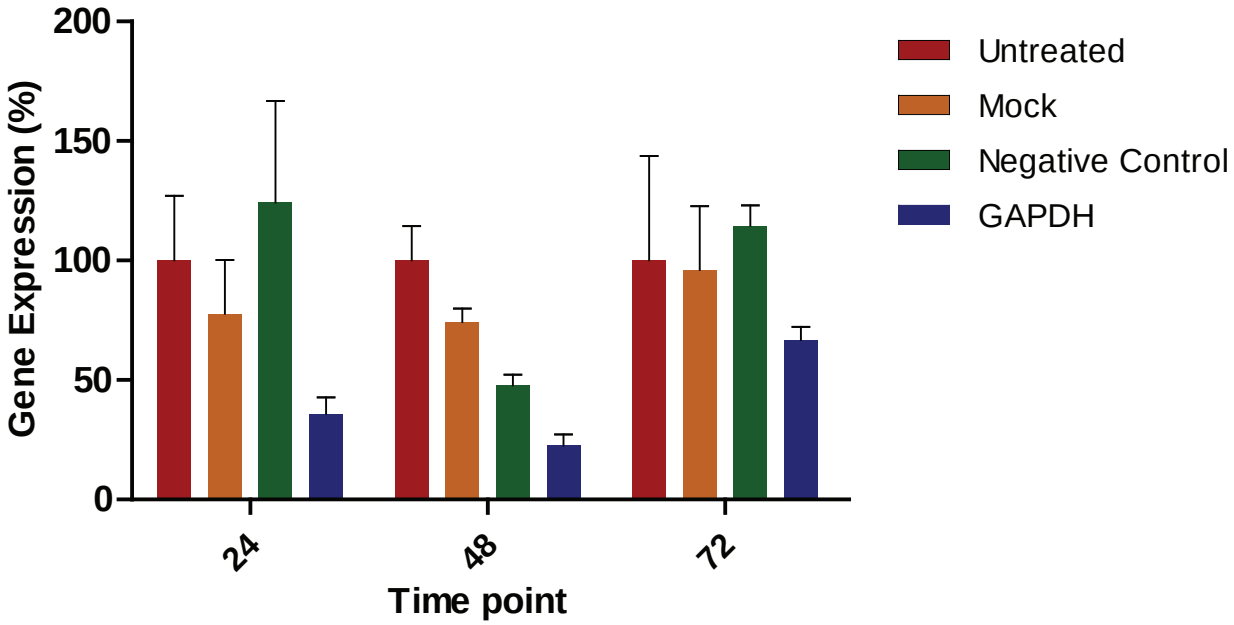

Figure 5.1. GAPDH mRNA levels reach their lowest levels 48 hours post-transfection with GAPDH siRNA. 4500 HT1080 cl. 2 cells cultured in 96 well plate wells were either transfected with siRNA targeting GAPDH or non-targeting siRNA (negative control), subject to DarmaFECT 4 without siRNA (mock) or untreated. RNA was then extracted from the cells at 24 hour intervals post-transfection. Following reverse trancription relative gene expression was measured by RT-PCR using Taqman gene expression assays (Applied Biosystems) specific to GAPDH and ACTB (endogenous control)

5.3.3 Clonal drift

Before initiating the RNAi screen it was necessary to perform a 'mock' knockdown to determine whether changes in telomere length observed in HT1080 cl.2 cells grown in the 96-well plates could occur as a consequence of clonal drift in culture. Eight independent cell populations of HT1080 cl. 2 were seeded into 96-well plate wells; the replicates were then cultured for the same amount of time as during the RNAi knockdown screen (6 days). DNA was then extracted and STELA was performed at 17p, 18q and XpYp to determine the telomere length profiles of the 8 replicates (fig. 5.2). Band quantification revealed that the 17p telomere length ranged from 4.775kb to 5.319kb in length in the eight replicates. Importantly an analysis of variance showed that these small differences in telomere length were not statistically significant (P=0.5778) (fig. 5.2a). A similar scenario was found at the XpYp telomere; telomere length ranged from 4.606kb to 4.969kb and again, these differences in length were not significant (P=0.6593) (fig. 5.2c). More variation was observed at the 18q telomere at this chromosome end telomere length ranged from 6.136kb to 6.697. Although an analysis of variance showed no significant difference overall between the replicates (P=0.2441), because of the increased variation between replicates and lower ANOVA P-value, t-tests were performed between individual replicates. Significant differences were found between replicate 2 and 6 (P=0.0381) and between replicate 5 and 6 (P=0.0146) (fig. 5.2b). Therefore any changes in mean 18q telomere length observed after gene knockdown were only considered biologically relevant if they were outside of this range (below 6.136kb or above 6.697kb).

Clonal drift

a

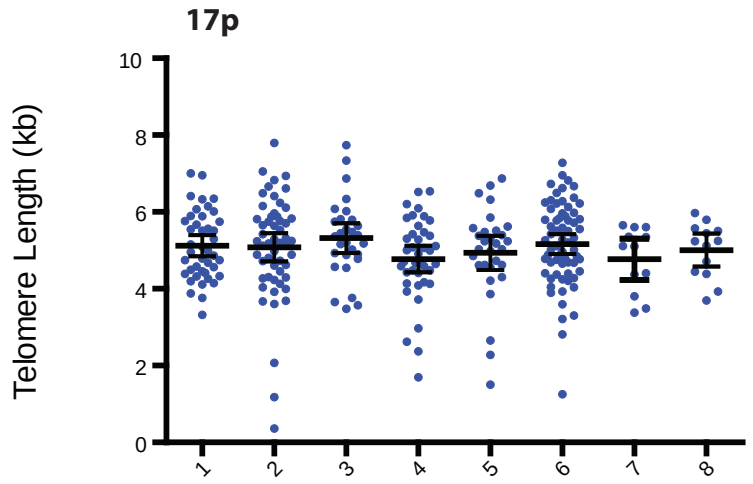

Mean tel length (kb)	5.117	5.079	5.319	4.775	4.934	5.164	4.768	5.006
Lower 95% CI	4.842	4.710	4.931	4.432	4.490	4.904	4.231	4.575
Upper 95% CI	5.392	5.447	5.706	5.117	5.378	5.424	5.306	5.437

ANOVA - P=0.5788

b

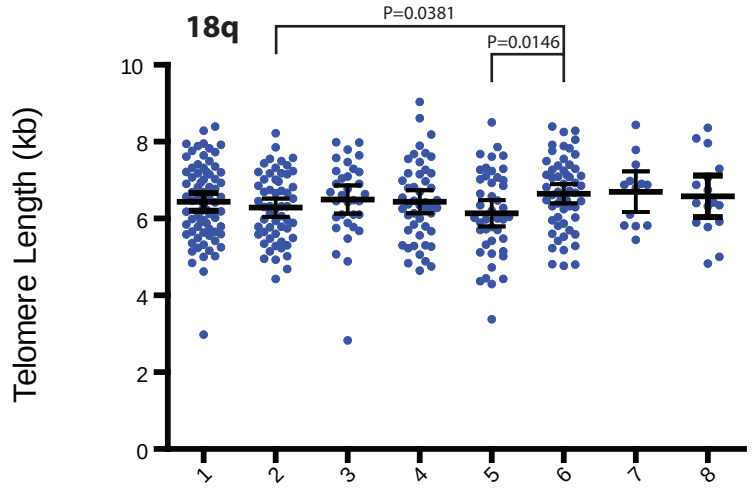

Mean tel length (kb)	6.435	6.287	6.497	6.436	6.136	6.648	6.697	6.582
Lower 95% CI	6.205	6.050	6.130	6.137	5.794	6.398	6.168	6.041
Upper 95% CI	6.665	6.525	6.864	6.735	6.478	6.898	7.225	7.123

ANOVA - P=0.2441

c

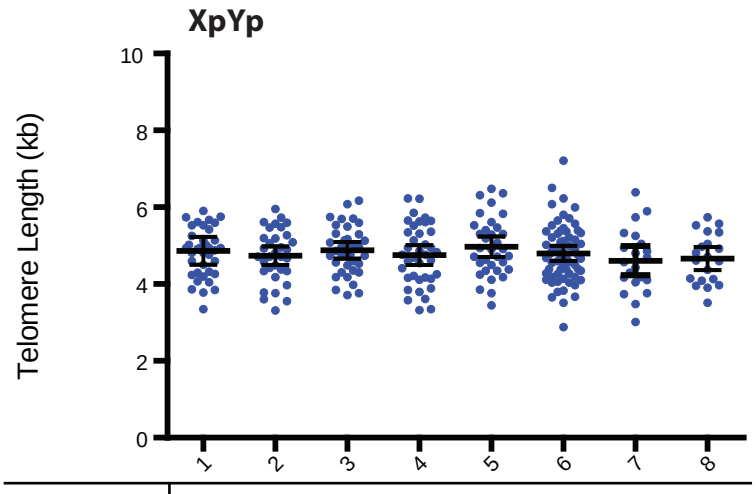

Mean tel length (kb)	4.865	4.737	4.878	4.755	4.969	4.797	4.606	4.665
Lower 95% CI	4.502	4.495	4.663	4.496	4.702	4.602	4.227	4.364
Upper 95% CI	5.228	4.979	5.093	5.014	5.236	4.992	4.985	4.967

ANOVA - P=0.6593

Figure 5.2. Clonal drift of HT1080 cl. 2 cells grown in 96 well plate. Eight cell populations of HT1080 cl. 2 cells were maintained in the same manner as in the siRNA mediated knockdown protocol. Briefly 4500 HT108 cl.2 cells were seeded in 96 well plate wells and cultured for 6 days, after which DNA was extracted using Magnesil paramagnetic particles and used in a STELA reaction for the 17p, 18q and XpYp chromosome ends. Telomere length was then quantified using Phoretix 1D software (Nonlinear dynamics) and any and statistically significant differences in mean telomere length was determined by one way Analysis of Variance and t-test

5.3.4 Telomere phenotypes observed in the RNAi screen

From the screen several abnormal telomere phenotypes were observed. Differences in mean telomere length occurred between untreated cells and cells deficient in a particular chromatin remodeler. In other cases deficiency in certain chromatin remodelers resulted in changes in the pattern of telomere length distributions including an increase in frequency of very short telomeres suggesting compromised telomere stability and also the presence of two distinct populations of telomere length. In most cases the telomere length defects observed through loss of a certain chromatin remodeler was specific to only one of the three telomeres studied however in some instances two or even all three telomeres (17p, 18q and XpYp) were affected. For each gene targeted for knockdown four independent transfections were performed (e.g. TERT-1, -2, -3 and -4), the same telomere length phenotype was not observed in all four biological replicates, it was only present in one to three of the replicates.

Below the aberrant telomere length phenotypes found from the RNAi screen are summarised. The screen has certain limitations which may affect the robustness of the conclusions drawn from the results presented. These issues are discussed in detail in the following discussion chapter (5.4).

5.3.5 TERT

In every replicate of TERT-deficient HT1080 cl.2 cells a reduction in mean telomere length, compared to untreated controls was observed. These differences were small and did not reach statistical significance at the 17p and 18q telomeres (fig. 5.3a&b); however at the XpYp telomere the reductions in mean length were larger and statistically significant (fig. 5.3c). TERT-1 mean XpYp telomere length was 4.523kb, 375bp shorter than the untreated XpYp telomere (P=0.0153), whereas TERT-3 had an even shorter mean telomere length of 4.177kb, 721bp shorter than untreated cells

($P<0.0001$). This experiment provided a proof of principle that subtle changes in telomere length, following the knockdown of a telomere specific gene in this clonal population, can be identified after just 6 days of culture.

a

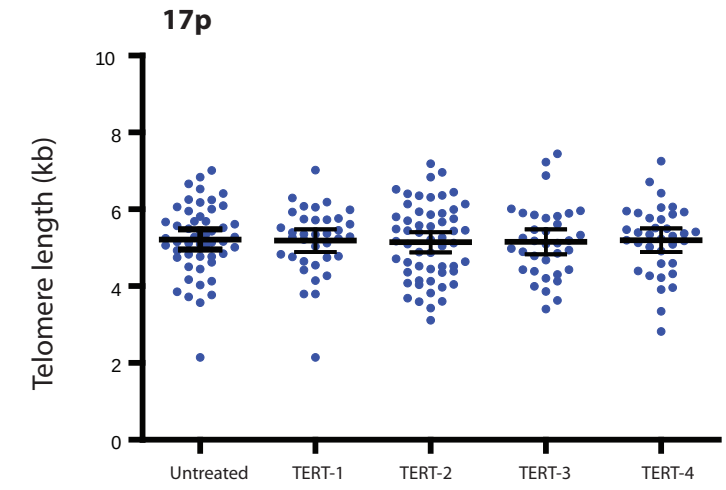

Mean tel length (kb)	5.215	5.183	5.144	5.153	5.199
Lower 95% CI	4.954	4.886	4.879	4.829	4.891
Upper 95% CI	5.476	5.481	5.408	5.476	5.506

b

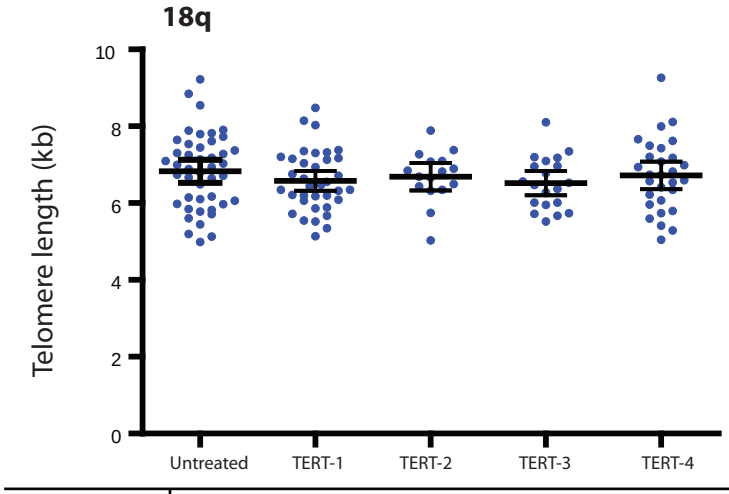

Mean tel length (kb)	6.829	6.578	6.688	6.523	6.719
Lower 95% CI	6.530	6.318	6.333	6.205	6.361
Upper 95% CI	7.128	6.838	7.043	6.841	7.076

c

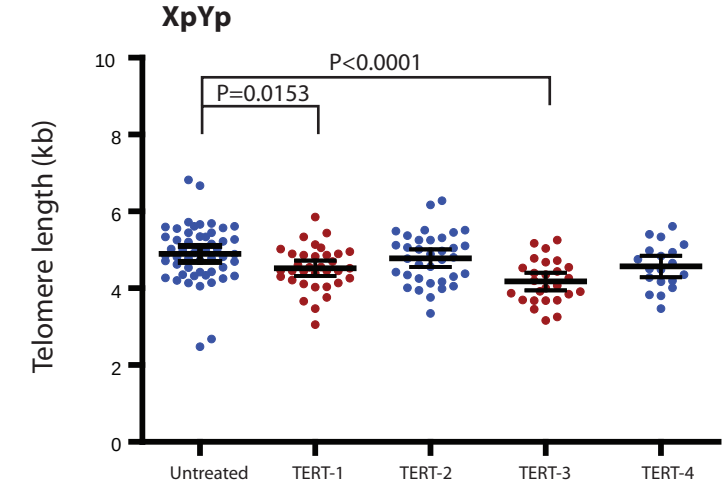

Mean tel length (kb)	4.898	4.523	4.783	4.177	4.567
Lower 95% CI	4.688	4.325	4.554	4.094	4.310
Upper 95% CI	5.108	4.721	5.012	4.482	4.743

Figure 5.3. The effect of siRNA-mediated knockdown of TERT on the telomere length distribution at 17p, 18q and XpYp. HT1080 cl. 2 cells were transfected with 25nm siRNA targeted against TERT mRNA using DharmaFECT 4. TERT-1, -2, -3 & -4 represent four biological replicates independently transfected. Each replicate was successively transfected three times at 48h intervals. 48 hours after the third transfection DNA was extracted using Magnesil paramagnetic particles. STELA was then performed at 17p (a), 18q (b) and XpYp (c) using the 17pseqrev1, 18qrev4M and XpYpE respectively. Telomere length distributions were then quantified using Phoretix software. Any significant differences in mean telomere length between untreated cells and cells targeted for TERT knockdown as measured by t-test are stated

5.3.6 SIRT6

siRNA knockdown of SIRT6 caused a significant decrease in mean telomere length at the 17p and XpYp chromosome ends. In untreated cells the mean 17p telomere length was 5.215kb. In the SIRT6-2 and SIRT6-3 replicates telomere length was shorter than in untreated cells however this was not statistically significant (fig. 5.4a). The SIRT6-4 replicate did show a significant loss of 17p telomere length (P=0.0401) (fig. 5.4a). All four SIRT6 replicates showed a small reduction in telomere length at 18q although this wasn't statistically significant (fig. 5.6b). Similarly small reductions were observed at XpYp in the SIRT6-2, -3 and -4 replicates however SIRT6-1 showed a greater degree of telomere loss which was significantly different to untreated XpYp mean telomere length (P=0.0432) (fig. 5.4c).

5.3.7 EHMT2

Loss of EHMT2 appeared to result in an increase in the frequency of very short 17p telomeres compared to untreated cells (fig. 5.5). This phenotype was only present at 17p. In an attempt to determine the statistical significance of this observation a X-squared test was performed. The proportion of telomeres below 3kb in size within the whole population of telomeres was compared between the four EHMT2-deficient replicates and untreated cells (fig. 5.5). EHMT2-1, -2 and -4 had a significantly increased percentage of 17p telomeres below 3kb in length compared to untreated cells (fig. 5.5c). The mean 17p telomere length was slightly lower in all four EHMT2 knockdown replicates compared to the untreated cells however these differences were not statistically significant (fig. 5.6a). Similar reductions in 18q mean telomere length were observed in the EHMT2 knockdown replicates compared to untreated cells however again these differences were small and not statistically significant (fig. 5.6b). No aberrant telomere phenotypes were observed at XpYp where the mean telomere length of the untreated and EHMT2 replicate cells was very similar (fig. 5.6c).

a

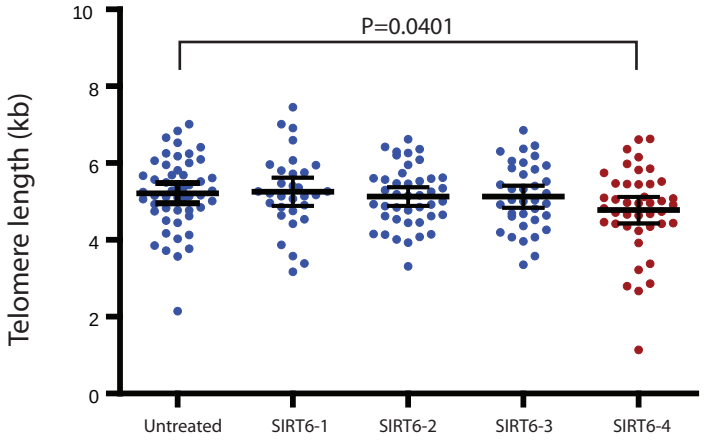

Mean tel length (kb)	5.215	5.252	5.131	5.127	4.775
Lower 95% CI	4.954	4.887	4.888	4.837	4.430
Upper 95% CI	5.476	5.618	5.375	5.417	5.121

b

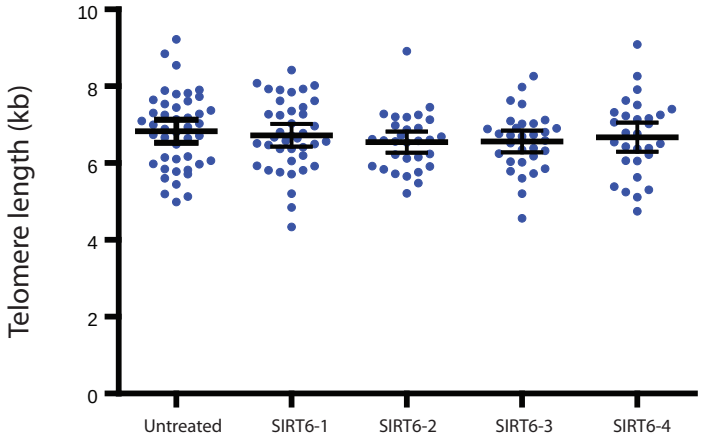

Mean tel length (kb)	6.829	6.724	6.544	6.564	6.675
Lower 95% CI	6.530	6.428	6.267	6.280	6.295
Upper 95% CI	7.128	7.019	6.821	6.848	7.054

c

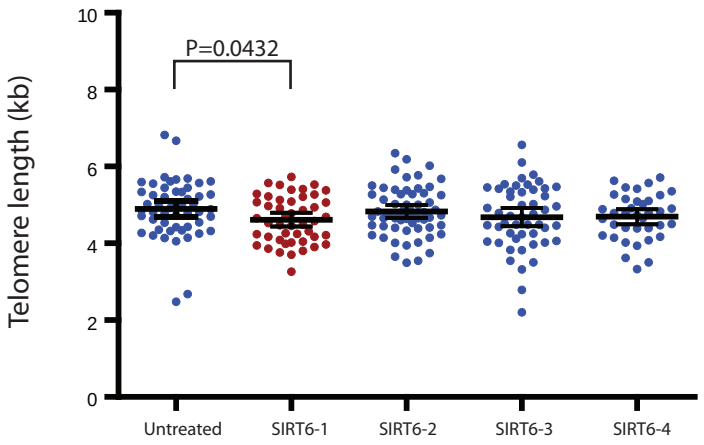

Mean tel length (kb)	4.898	4.614	4.831	4.682	4.692
Lower 95% CI	4.688	4.436	4.663	4.443	4.494
Upper 95% CI	5.108	4.792	4.998	4.921	4.890

Figure 5.4. The effect of siRNA-mediated knockdown of SIRT6 on the telomere length distribution at 17p, 18q and XpYp. HT1080 cl. 2 cells were transfected with 25nm siRNA targeted against SIRT6 mRNA using DharmaFECT 4. SIRT6, -2, -3 & -4 represent four biological replicates independently transfected. Each replicate was successively transfected three times at 48h intervals. 48 hours after the third transfection DNA was extracted using Magnesil paramagnetic particles. STELA was then performed at 17p (a), 18q (b) and XpYp (c) using the 17pseqrev1, 18qrev4M and XpYpE respectively. Telomere length distributions were then quantified using Phoretix software. Any significant differences in mean telomere length between untreated cells and cells targeted for SIRT6 knockdown as measured by t-test are stated.

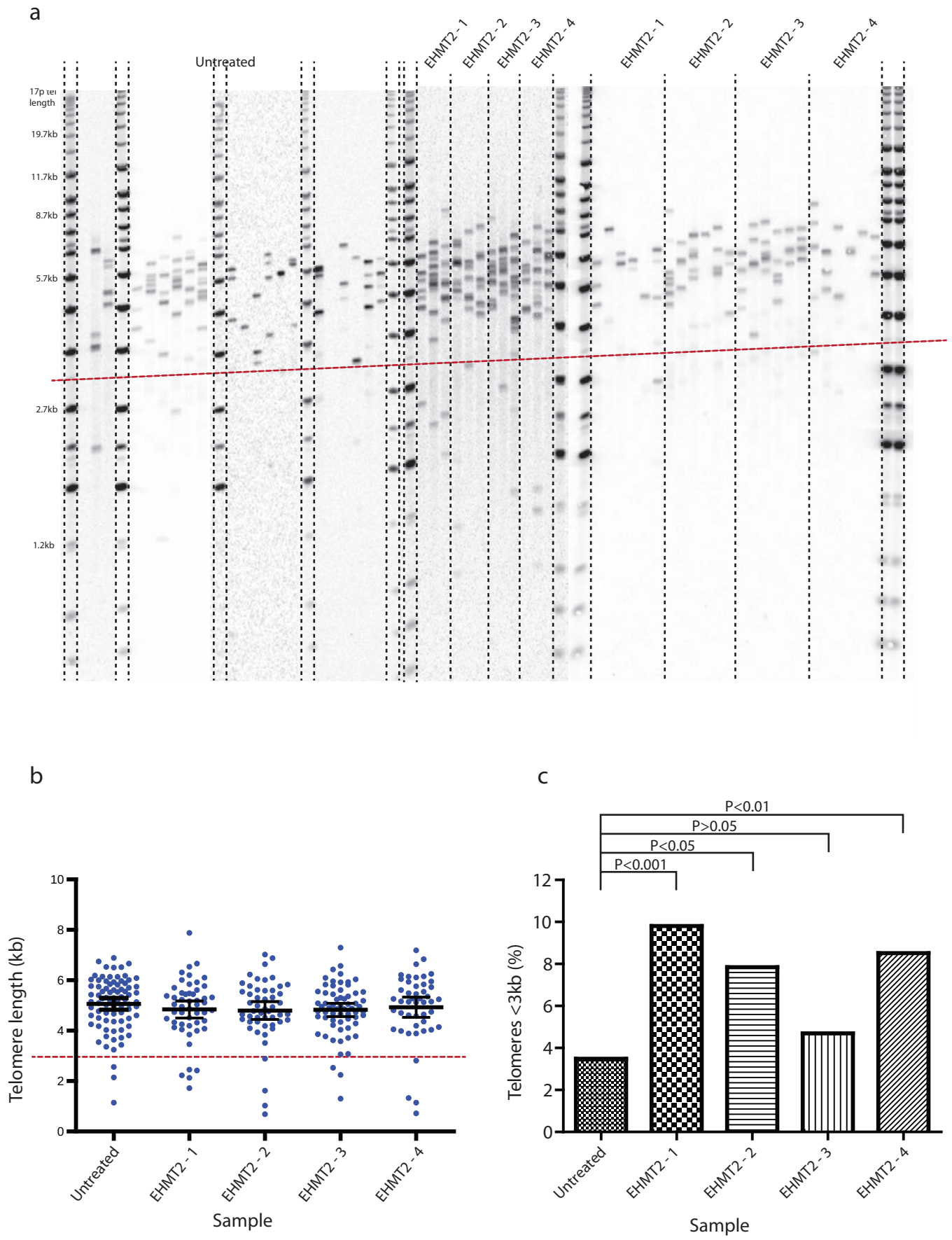

Figure 5.5. siRNA-mediated knockdown of EHMT2 results in increased presence of very short 17p telomeres. (a) The 17p telomere length distribution of four independant EHMT2-deficient cell populations was determined by STELA. Bands below the red line were considered short telomeres. (b) Dot blot of quantified telomere length distributions of the four EHMT2 knockdown replicates. Telomere length from the above STELA blot was quantified using Phoretix software and diplayed as dot blots, significant differences in mean telomere length between any of the replicates and untreated cells was determined by t-test and are displayed. (c) The proportion of small telomeres (<3kb) was calculated for all replicates. Significant differences between the proportion of small 17p telomeres in the EHMT2 knockdown replicates and untreated cells was determined by a chi-squared test

a

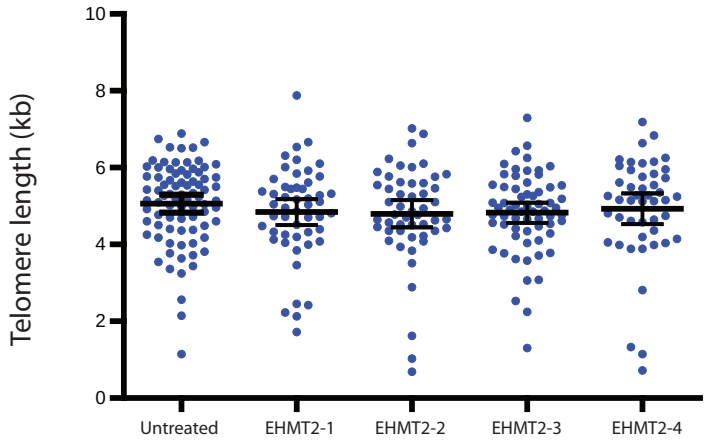

Mean tel length (kb)	5.064	4.843	4.797	4.825	4.93
Lower 95% CI	4.829	4.505	4.444	4.565	4.533
Upper 95% CI	5.299	5.182	5.151	5.086	5.327

b

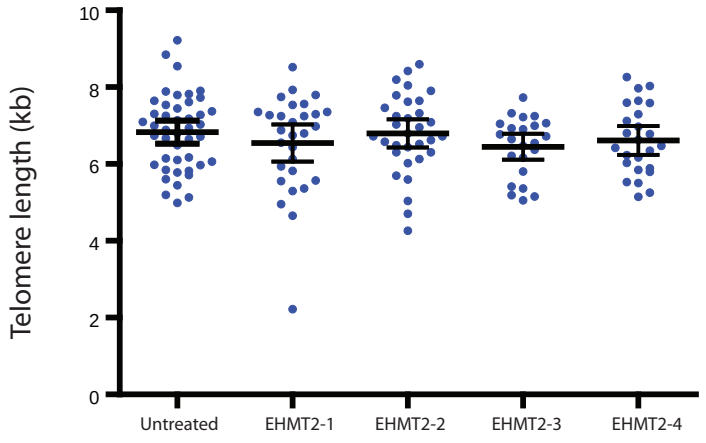

Mean tel length (kb)	6.829	6.546	6.796	6.45	6.613
Lower 95% CI	6.530	6.060	6.425	6.113	6.241
Upper 95% CI	7.128	7.032	7.166	6.787	6.985

c

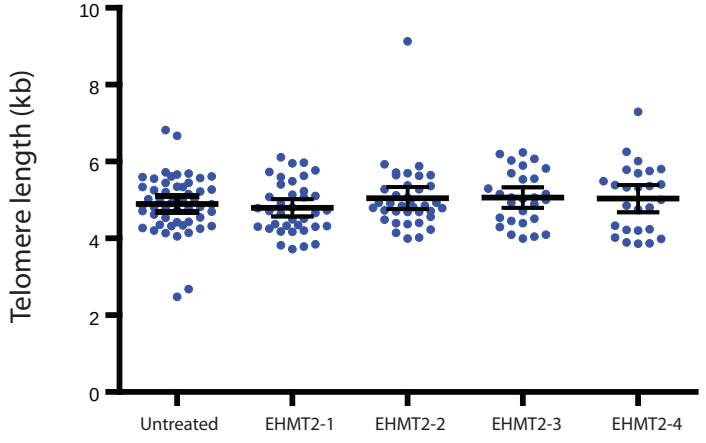

Mean tel length (kb)	4.898	4.797	5.047	5.063	5.036
Lower 95% CI	4.688	4.574	4.759	4.794	4.682
Upper 95% CI	5.108	5.019	5.334	5.333	5.390

Figure 5.6. The effect of siRNA-mediated knockdown of EHMT2 on the telomere length distribution at 17p, 18q and XpYp. HT1080 cl. 2 cells were transfected with 25nm siRNA targeted against EHMT2 mRNA using DharmaFECT 4. EHMT2-1, -2, -3 & -4 represent four biological replicates independently transfected. Each replicate was successively transfected three times at 48h intervals. 48 hours after the third transfection DNA was extracted using Magnesil paramagnetic particles. STELA was then performed at 17p (a), 18q (b) and XpYp (c) using the 17pseqrev1, 18qrev4M and XpYpE respectively. Telomere length distributions were then quantified using Phoretix software. Any significant differences in mean telomere length between untreated cells and cells targeted for EHMT2 knockdown as measured by t-test are stated.

5.3.8 SIRT1

Quantification of 18q telomere length after siRNA knockdown of SIRT1 revealed a possible telomere shortening phenotype, in all four replicates one of which was significantly lower than in untreated cells (P=0.0349) (fig. 5.7b). However the variation observed in this experiment is within the bounds of variation observed in the clonal drift experiment (fig. 5.2)

5.3.9 DOT1L

DOT1L deficiency resulted in a reduction in mean telomere length at XpYp and at the 18q telomere (fig. 5.8b&c). The mean 18q telomere length in DOT1L-4 cells was 6.125kb, a 704bp loss compared to the untreated mean 18q mean telomere length. This reduction in telomere length is significant (P=0.01) and below the lower mean 18q telomere length threshold (6.136kb) determined in the clonal drift experiment (fig. 5.2). The same DOT1L knockdown replicate also displayed shorter XpYp telomeres than untreated cells although the difference was less pronounced (513bp loss, P=0.0345) (fig. 5.8c). A similarly significant XpYp telomere shortening phenotype was observed for DOT1L-3 which had a mean telomere length of 4.551kb compared to 4.898kb for untreated cells (P=0.0211). DOT1L-1 cells also displayed a reduction in mean XpYp telomere length compared to untreated cells however this difference was smaller and not statistically significant. Additionally loss of DOT1L appeared to cause a divergence of telomere length in 17p telomeres in the DOT1L-1 replicate resulting in two distinct populations of telomeres with different length (fig. 5.8a & 5.9). Whereas the 17p telomeres from untreated cells had a mean telomere length of 5.192kb, the two populations of telomeres in the DOT1L-1 replicate had mean telomere length of 5.879kb and 4.329kb respectively. This phenotype was only observed in one of the four knockdown replicates for DOT1L and wasn't observed at 18q or XpYp.

a

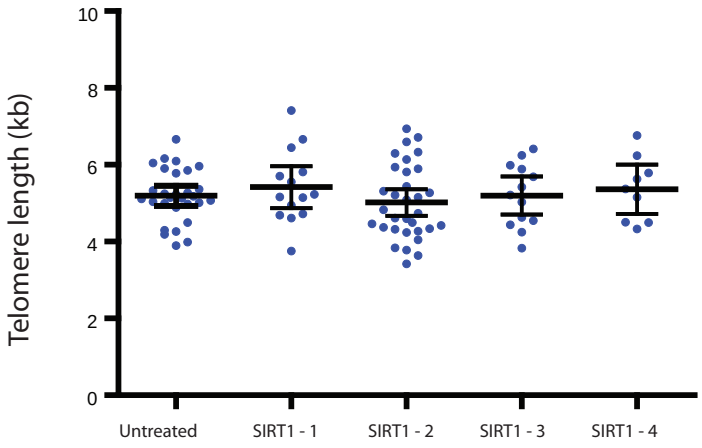

Mean tel length (kb)	5.192	5.418	5.018	5.196	5.363
Lower 95% CI	4.932	4.870	4.672	4.700	4.721
Upper 95% CI	5.453	5.965	5.364	5.693	6.005

b

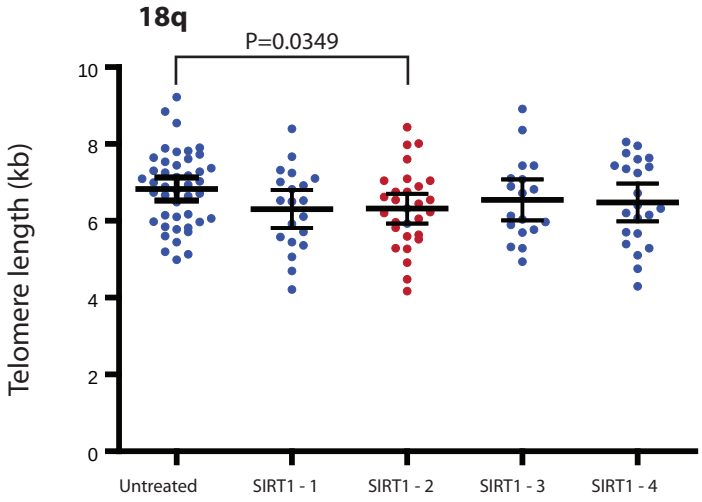

Mean tel length (kb)	6.829	6.308	6.317	6.564	6.479
Lower 95% CI	6.530	5.813	5.932	6.014	5.987
Upper 95% CI	7.128	6.804	6.702	7.078	6.972

c

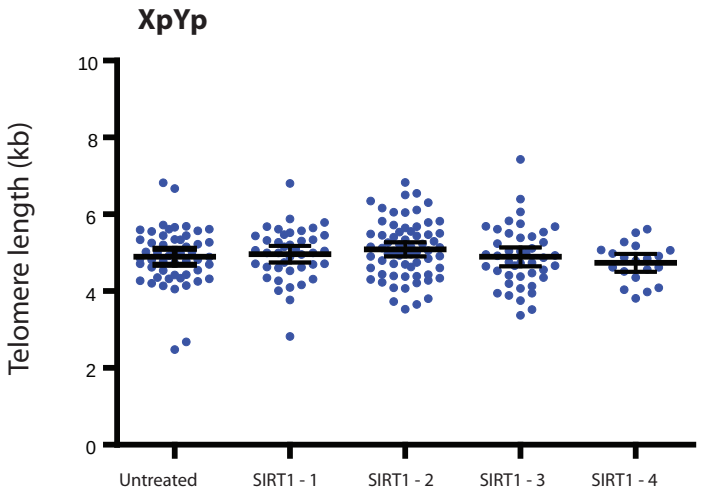

Mean tel length (kb)	4.898	4.964	5.09	4.892	4.736
Lower 95% CI	4.688	4.748	4.906	4.647	4.501
Upper 95% CI	5.108	5.180	5.275	5.137	4.971

Figure 5.7. The effect of siRNA-mediated knockdown of SIRT1 on the telomere length distribution at 17p, 18q and XpYp. HT1080 cl. 2 cells were transfected with 25nm siRNA targeted against SIRT1 mRNA using DharmaFECT 4. SIRT1-1, -2, -3 & -4 represent four biological replicates independently transfected. Each replicate was successively transfected three times at 48h intervals. 48 hours after the third transfection DNA was extracted using Magnesil paramagnetic particles. STELA was then performed at 17p (a), 18q (b) and XpYp (c) using the 17pseqrev1, 18qrev4M and XpYpE respectively. Telomere length distributions were then quantified using Phoretix software. Any significant differences in mean telomere length between untreated cells and cells targeted for SIRT1 knockdown as measured by t-test are stated.

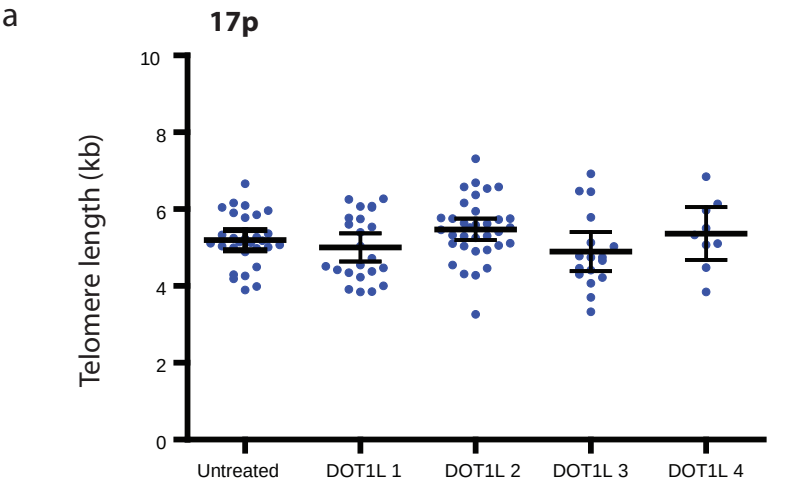

Mean tel length (kb)	5.192	5.003	5.475	4.895	5.366
Lower 95% CI	4.932	4.635	5.195	4.384	4.677
Upper 95% CI	5.453	5.371	5.755	5.406	6.056

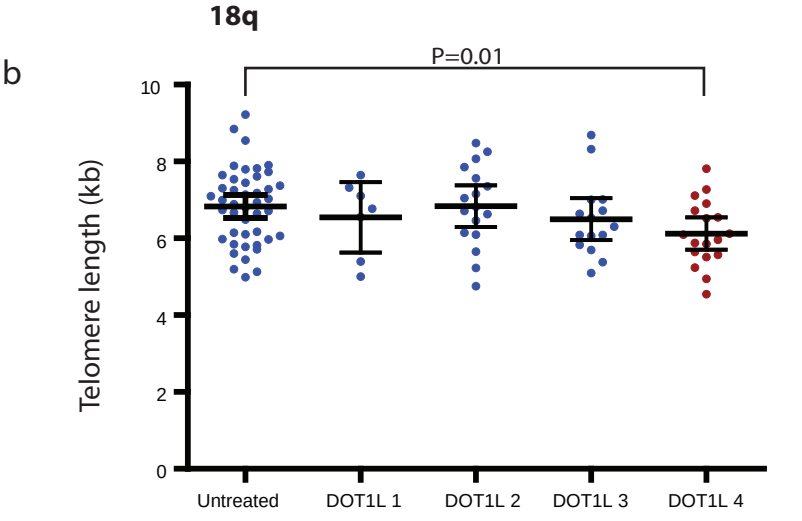

Mean tel length (kb)	6.829	6.543	6.84	6.497	6.125
Lower 95% CI	6.530	5.628	6.299	5.950	5.704
Upper 95% CI	7.128	7.458	7.381	7.043	6.546

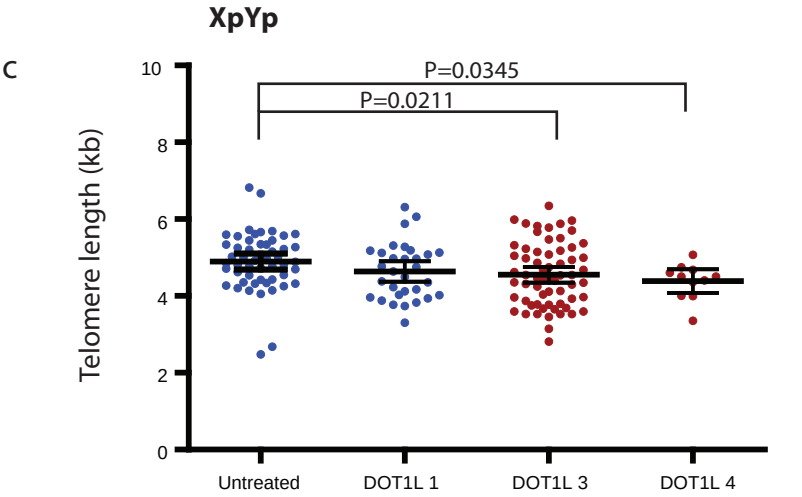

Mean tel length (kb)	4.898	4.64	4.551	4.385
Lower 95% CI	4.688	4.372	4.343	4.076
Upper 95% CI	5.108	4.907	4.758	4.695

Figure 5.8. The effect of siRNA-mediated knockdown of DOT1L on the telomere length distribution at 17p, 18q and XpYp. HT1080 cl. 2 cells were transfected with 25nm siRNA targeted against DOT1L mRNA using DharmaFECT 4. DOT1L-1, -2, -3 and -4 represent four biological replicates independently transfected. Each replicate was successively transfected three times at 48h intervals. 48 hours after the third transfection DNA was extracted using Magnesil paramagnetic particles. STELA was then performed at 17p (a), 18q (b) and XpYp (c) using the 17pseqrev1, 18qrev4M and XpYpE respectively. Telomere length distributions were then quantified using Phoretix software. Any significant differences in mean telomere length between untreated cells and cells targeted for DOT1L knockdown as measured by t-test are stated.

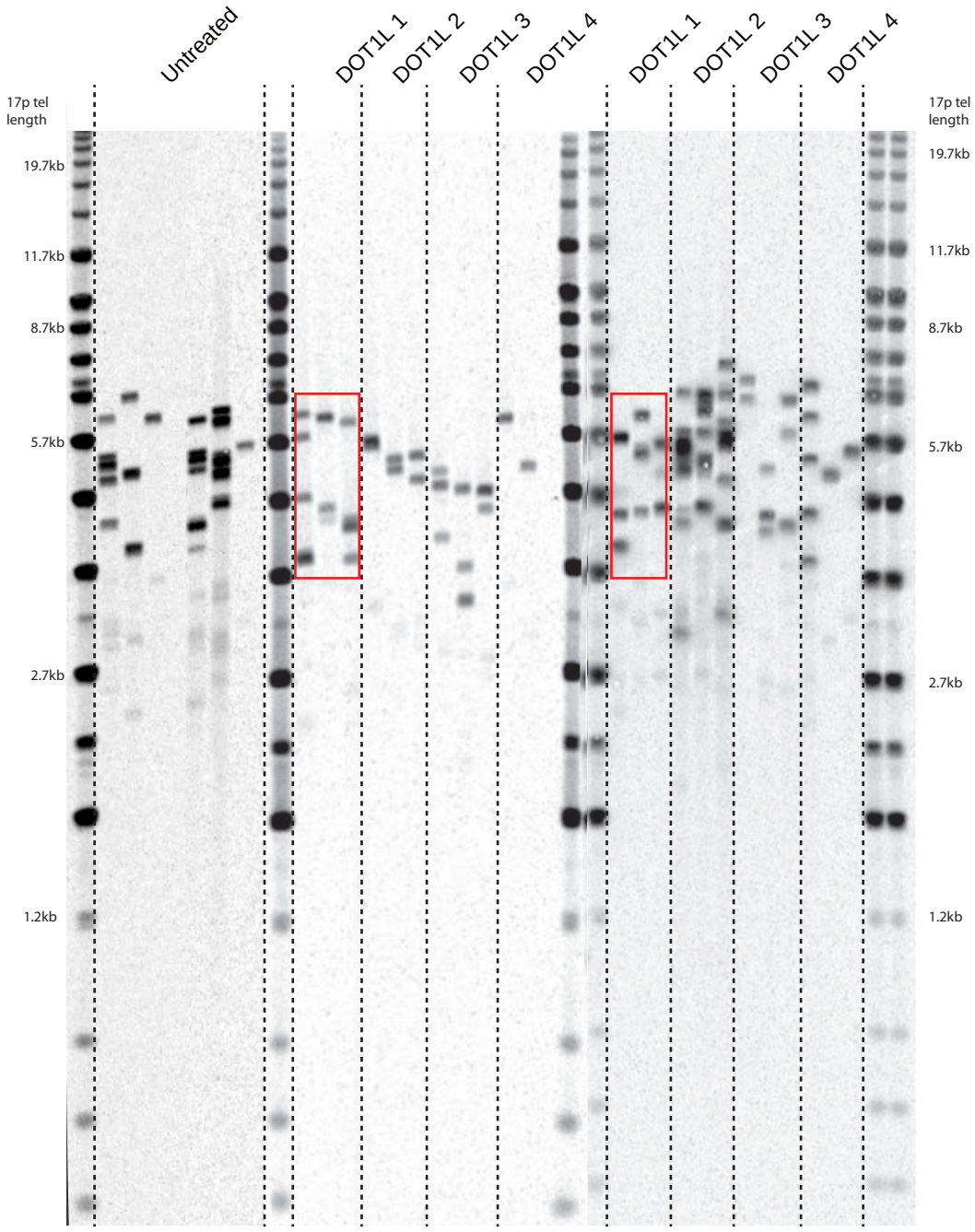

Figure 5.9. siRNA-mediated knockdown of DOT1L reaults in the divergence of two populations of telomeres with differing telomere length distributions. Four HT1080 cl. 2 cell populations (DOT1L-1, -2, -3 & -4) were subject to three successive transfections with siRNA targeted against DOT1L at 48h intervals. Untreated cells were grown in parallel with the DOT1L knockdown replicates. 48 hours after the third transfection DNA was extracted from the cells uisng Magnesil paramagnetic particles. 17p telomere length was then measured using STELA

5.3.10 EZH2

EZH2-deficient HT1080 cl.2 cells showed aberrant telomere length phenotypes at 17p and XpYp (fig. 5.10). EZH2-1 and EZH2-3 replicates had mean 17p telomere length of 4.976kb and 4.997kb respectively which did not significantly differ from the 17p telomeres from untreated cells (telomere length of 5.192kb). EZH2-2 however showed a statistically significant increase in mean 17p telomere length of 0.491kb (P=0.0095). EZH2-4 also displayed a significant alteration in mean telomere length however in this replicate mean telomere length was reduced compared to untreated 17p telomeres (mean – 4.673, P=0.0386) (fig. 5.10a). The mean 18q telomere length in EZH2-3, -3 and -4 was significantly lower than in untreated cells (fig. 5.10b) however this variation in length was within the bounds of variation observed in the clonal drift experiment therefore it is impossible to say whether EZH2 loss resulted in telomere shortening at 18q. The EZH2-4 replicate displayed a reduced telomere length phenotype at XpYp; mean telomere length at this chromosome end was 4.471kb, a 0.427kb reduction compared to XpYp telomeres form untreated cells (mean: 4.898kb) (fig. 5.10c).

5.3.11 BAF155

No aberrant telomere length phenotype was observed at 17p and 18q in the HT1080 cl.2 cells targeted for BAF155 knockdown (fig. 5.11a&b) however at the XpYp chromosome a reduction in mean telomere length was observed. BAF155-1 cells had a slight reduction in mean XpYp telomere length compared to the untreated cells however this was not statistically significant. Greater XpYp length losses were observed in the other two BAF155 knockdown replicates (fig. 5.11c). BAF155-2 and -3 had mean XpYp telomere lengths of 4.518kb and 4.444kb which, when compared to the mean XpYp telomere length in the untreated cells (4.898kb), represented a significant reduction in length (BAFF155-2 – P=0.0235, BAFF155-3 – P=0.0441).

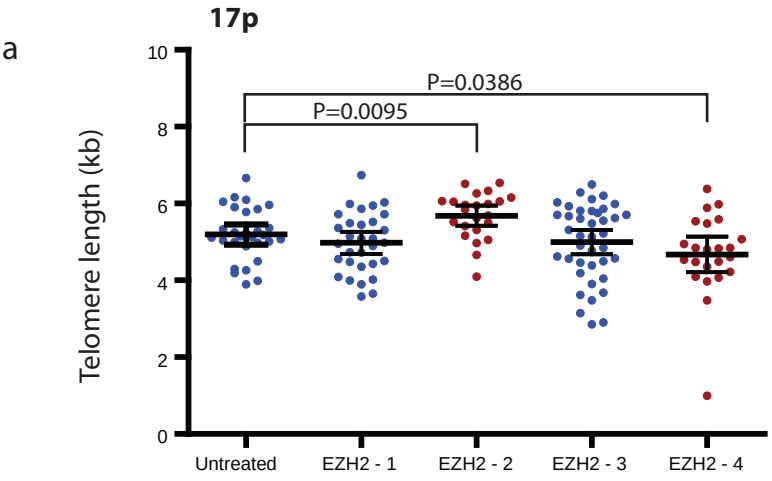

Mean tel length (kb)	5.192	4.976	5.683	4.997	4.673
Lower 95% CI	4.932	4.691	5.421	4.682	4.211
Upper 95% CI	5.453	5.262	5.944	5.311	5.135

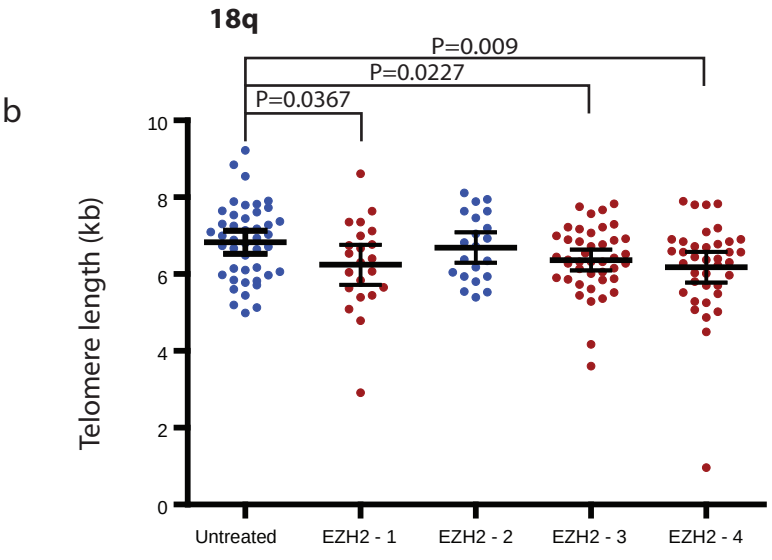

Mean tel length (kb)	6.829	6.244	6.69	6.364	6.18
Lower 95% CI	6.530	5.723	6.296	6.093	5.783
Upper 95% CI	7.128	6.765	7.085	6.635	6.578

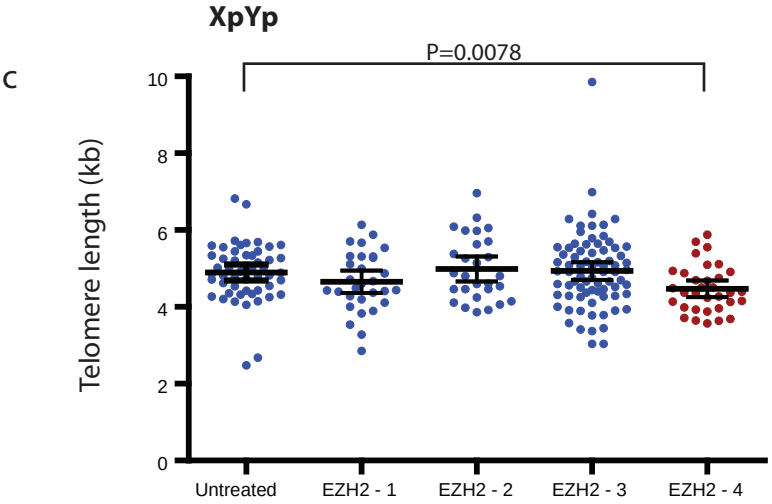

Mean tel length (kb)	4.898	4.655	4.991	4.934	4.471
Lower 95% CI	4.688	4.363	4.665	4.705	4.253
Upper 95% CI	5.108	4.947	5.316	5.163	4.689

Figure 5.10 The effect of siRNA-mediated knockdown of EZH2 on the telomere length distribution at 17p, 18q and XpYp. HT1080 cl. 2 cells were transfected with 25nm siRNA targeted against EZH2 mRNA using DharmaFECT 4. EZH2-1, -2, -3 and -4 represent four biological replicates independently transfected. Each replicate was successively transfected three times at 48h intervals. 48 hours after the third transfection DNA was extracted using Magnesil paramagnetic particles. STELA was then performed at 17p (a), 18q (b) and XpYp (c) using the 17pseqrev1, 18qrev4M and XpYpE respectively. Telomere length distributions were then quantified using Phoretix software. Any significant differences in mean telomere length between untreated cells and cells targeted for EZH2 knockdown as measured by t-test are stated.

a

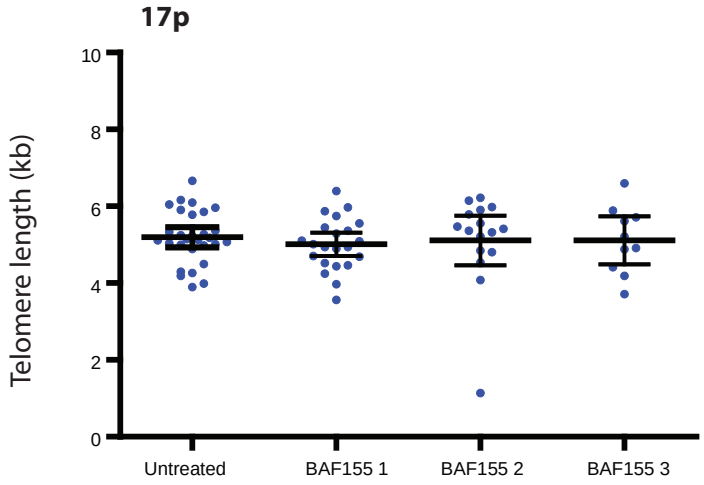

Mean tel length (kb)	5.192	5.009	5.112	5.114
Lower 95% CI	4.932	4.708	4.466	4.490
Upper 95% CI	5.453	5.310	5.757	5.737

b

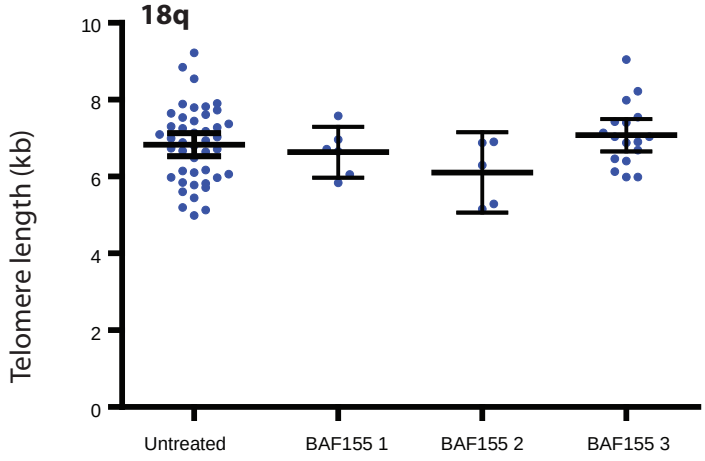

Mean tel length (kb)	6.829	6.634	6.106	7.076
Lower 95% CI	6.530	5.975	5.060	6.653
Upper 95% CI	7.128	7.294	7.152	7.498

c

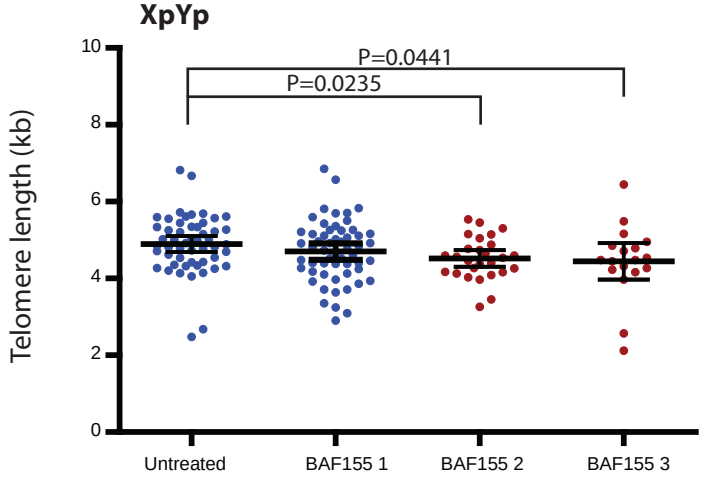

Mean tel length (kb)	4.898	4.703	4.518	4.444
Lower 95% CI	4.688	4.490	4.301	3.968
Upper 95% CI	5.108	4.916	4.736	4.919

Figure 5.11. The effect of siRNA-mediated knockdown of BAF155 on the telomere length distribution at 17p, 18q and XpYp. HT1080 cl. 2 cells were transfected with 25nm siRNA targeted against BAF155 mRNA using DharmaFECT 4. BAF155-1, -2 and -3 represent three biological replicates independently transfected. Each replicate was successively transfected three times at 48h intervals. 48 hours after the third transfection DNA was extracted using Magnesil paramagnetic particles. STELA was then performed at 17p (a), 18q (b) and XpYp (c) using the 17pseqrev1, 18qrev4M and XpYpE respectively. Telomere length distributions were then quantified using Phoretix software. Any significant differences in mean telomere length between untreated cells and cells targeted for BAF155 knockdown as measured by t-test are stated.

5.3.12 HDAC1

17p STELA analysis showed no differences significant differences in telomere length between the untreated and HDAC1-knockdown replicate cells although there was a slight increase in the generation of very small telomeres particularly in HDAC1-1, -2 and -3 (fig. 5.12a). Mean 18q telomere length in the HDAC1 knockdown replicates was lower compared to untreated cells however these differences were small and did not reach statistical significance (fig 5.12b). A telomere lengthening phenotype was observed at XpYp: Untreated cells had a mean XpYp telomere length of 4.898kb however XpYp telomeres in the HDAC1-4 knockdown replicate had significantly lengthened resulting in a mean telomere of 5.391kb (P=0.0146) (fig. 5.12c). This phenotype was not observed for any of the other knockdown replicates, indeed there was very little deviation in mean XpYp telomere length between HDAC1-1, -2 and -3 and untreated (fig. 5.12c).

5.3.13 MLL

Some differences in mean 17p telomere length exists between the untreated and MLL knockdown replicate cells however this variation is not statistically significant (fig. 5.13a). 18q telomeres were significantly shorter in three of the MLL knockdown replicates tested (MLL -2 – mean: 6.363kb, P=0.0316, MLL-3 – mean: 6.25kb, P=0.0098, Mll-4 - mean: 5.936, P=0.0063) compared to 18q telomeres from untreated cells (mean: 6.829kb) (fig. 5.13b) although only the reduction in mean 18q telomere length in the MLL-4 was outside the bounds of variation observed in the clonal drift experiment. The reliability this observation however may be compromised due to the relatively low number of telomeres quantified for MLL-4 at this chromosome end (n=11). Despite this, the fact that this same telomere shortening phenotype occurs in three out of the four knockdown replicates suggests that this result may be significant. MLL-3 also showed a significant reduction of 0.388kb in mean XpYp telomere length compared to untreated cells (P=0.0489) (fig. 5.13c).

a

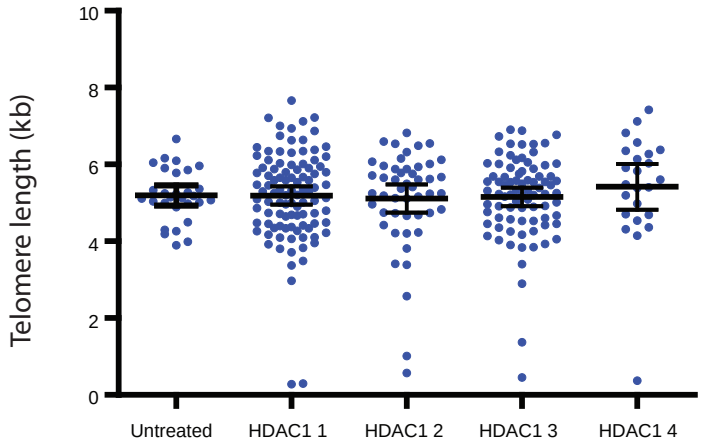

Mean tel length (kb)	5.192	5.189	5.112	5.154	5.417
Lower 95% CI	4.932	4.951	4.748	4.916	4.822
Upper 95% CI	5.453	5.428	5.476	5.392	6.012

b

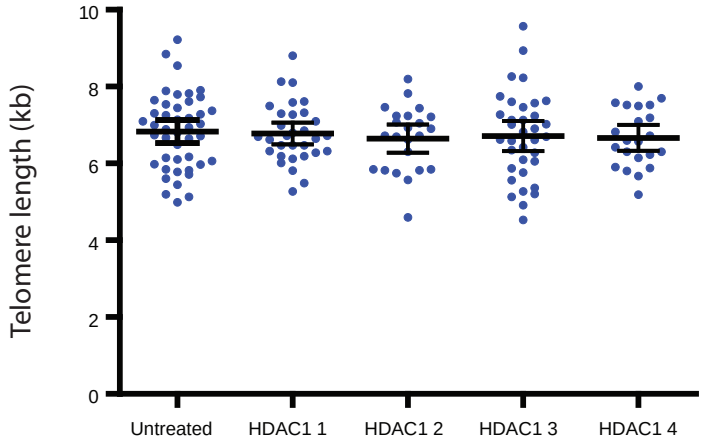

Mean tel length (kb)	6.829	6.779	6.646	6.711	6.666
Lower 95% CI	6.530	6.495	6.283	6.321	6.327
Upper 95% CI	7.128	7.064	7.010	7.101	7.005

c

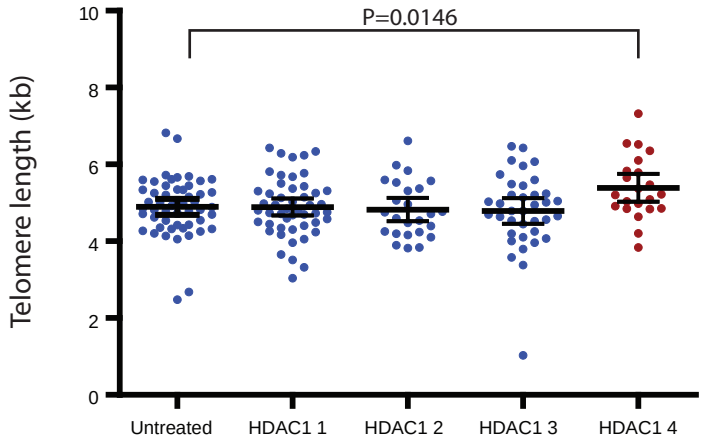

Mean tel length (kb)	4.898	4.891	4.823	4.786	5.391
Lower 95% CI	4.688	4.670	4.517	4.455	5.027
Upper 95% CI	5.108	5.112	5.128	5.117	5 755

Figure 5.12. The effect of siRNA-mediated knockdown of HDAC1 on the telomere length distribution at 17p, 18q and XpYp. HT1080 cl. 2 cells were transfected with 25nm siRNA targeted against HDAC1 mRNA using DharmaFECT 4. DOT1L-1, -2, -3 and -4 represent four biological replicates independently transfected. Each replicate was successively transfected three times at 48h intervals. 48 hours after the third transfection DNA was extracted using Magnesil paramagnetic particles. STELA was then performed at 17p (a), 18q (b) and XpYp (c) using the 17pseqrev1, 18qrev4M and XpYpE respectively. Telomere length distributions were then quantified using Phoretix software. Any significant differences in mean telomere length between untreated cells and cells targeted for HDAC1 knockdown as measured by t-test are stated.

a

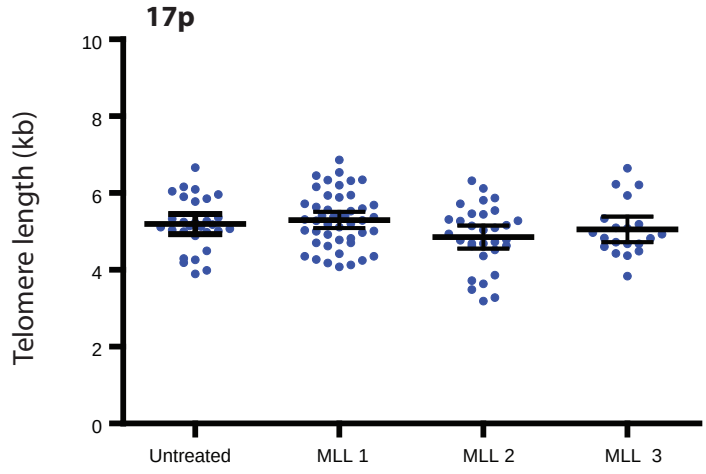

Mean tel length (kb)	5.192	5.298	4.856	5.054
Lower 95% CI	4.932	5.086	4.557	4.722
Upper 95% CI	5.453	5.510	5.155	5.386

b

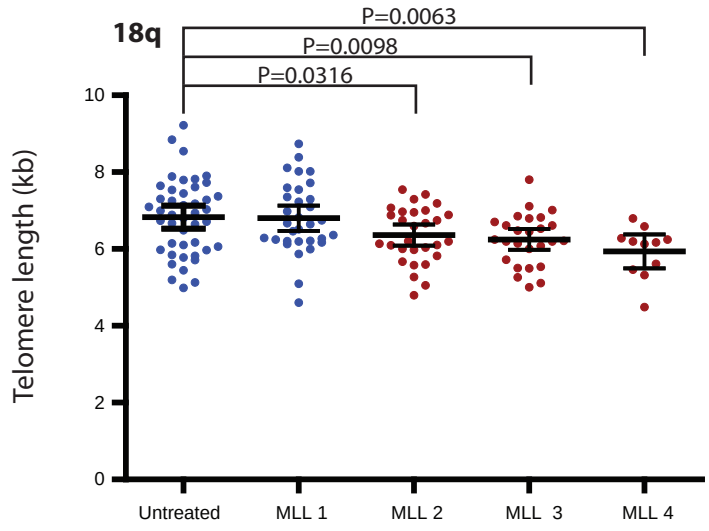

Mean tel length (kb)	6.829	6.8	6.363	6.25	5.936
Lower 95% CI	6.530	6.468	6.088	5.979	5.494
Upper 95% CI	7.128	7.133	6.637	6.520	6.379

c

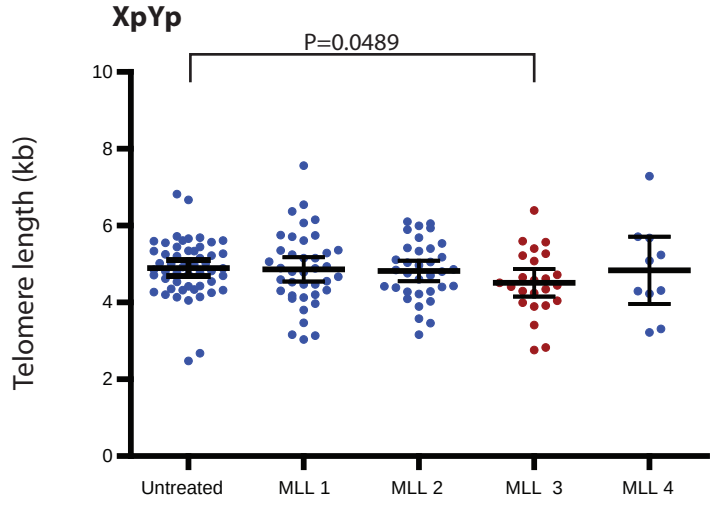

Mean tel length (kb)	4.898	4.861	4.823	4.51	4.838
Lower 95% CI	4.688	4.547	4.556	4.151	3.959
Upper 95% CI	5.108	5.175	5.090	4.869	5.717

Figure 5.13. The effect of siRNA-mediated knockdown of MLL on the telomere length distribution at 17p, 18q and XpYp. HT1080 cl. 2 cells were transfected with 25nm siRNA targeted against MLL mRNA using DharmaFECT 4. MLL-1, -2, -3 and -4 represent four biological replicates independently transfected. Each replicate was successively transfected three times at 48h intervals. 48 hours after the third transfection DNA was extracted using Magnesil paramagnetic particles. STELA was then performed at 17p (a), 18q (b) and XpYp (c) using the 17pseqrev1, 18qrev4M and XpYpE respectively. Telomere length distributions were then quantified using Phoretix software. Any significant differences in mean telomere length between untreated cells and cells targeted for MLL knockdown as measured by t-test are stated.

5.3.14 JARID1C

RNAi-mediated depletion of the histone demethylase JARID1C did not result in any significant aberrant 17p telomere length phenotypes (fig. 5.14a). JARID1C-3 showed a slight increase in mean 17p telomere length compared to untreated cells however this did not reach statistical significance. Statistically significant differences in mean 18q telomere length were observed between untreated cells and JARID1C-2 and -3 cells (fig. 5.14b). 18q telomeres from untreated cells had a mean telomere length of 6.829kb whereas JARID1C-2 and JARID1C-3 displayed significantly shorter telomeres (JARID1C2 – mean: 6.342kb, P=0.0273, JARID1C-3 – mean: 6.299kb, P=0.0236). However mean telomere lengths for these replicates is higher than the lower mean 18q telomere length threshold determined in the clonal drift experiment (6.136kb) so the biological relevance of this result is questionable. No significant differences in mean XpYp telomere length was observed between the untreated and JARID1C replicate cells (fig. 5.14c).

5.3.15 DAXX

RNAi-mediated depletion of DAXX resulted in a decrease in the mean telomere length at 17p (fig. 5.15a). The mean 17p telomere length in DAXX-1 and -2 cells was very similar to in untreated cells (5.192kb). DAXX-3 cells displayed a slightly reduced mean 17p telomere length (5.044kb) although this did not reach statistical significance. DAXX-4 however had a significantly shorter mean 17p telomere length of 4.656kb (P=0.0109). Some variation in mean 18q telomere length was observed between untreated and DAXX-knockdown replicate cells however this was small and not statistically significant (fig. 5.15b). Even less variation in mean XpYp telomere length was observed between cell populations (fig. 5.15c).

a

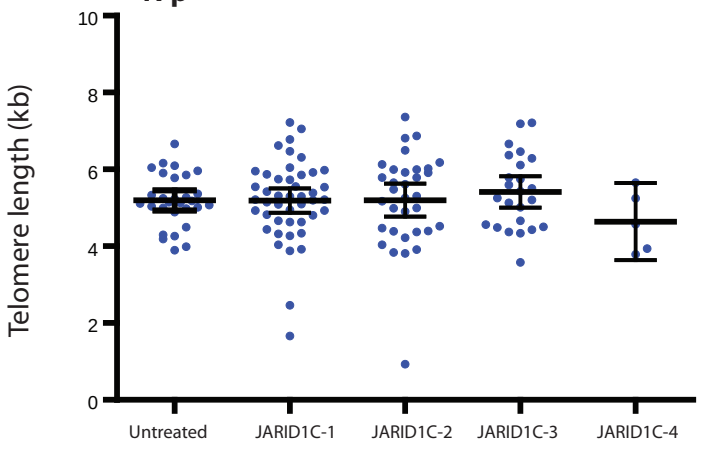

Mean tel length (kb)	5.192	5.19	5.198	5.412	4.639
Lower 95% CI	4.932	4.874	4.769	5.005	3.634
Upper 95% CI	5.453	5.505	5.627	5.819	5.644

b

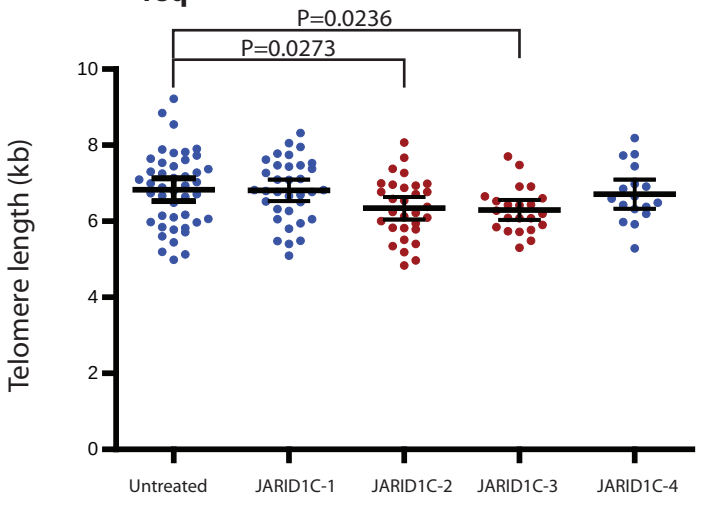

Mean tel length (kb)	6.829	6.812	6.342	6.299	6.713
Lower 95% CI	6.530	6.526	6.044	6.033	6.330
Upper 95% CI	7.128	7.099	6.640	6.564	7.096

c

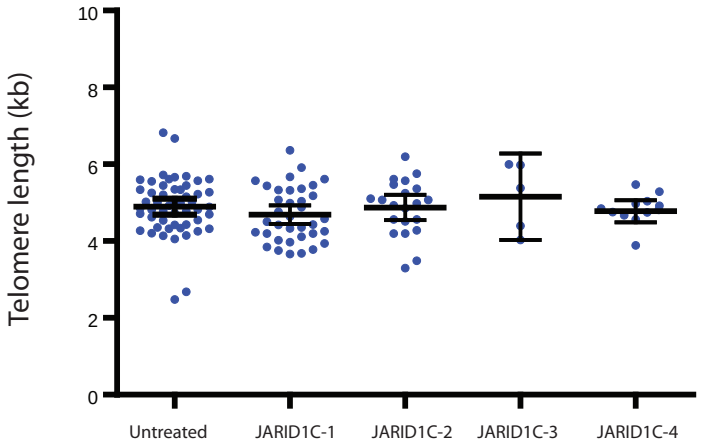

Mean tel length (kb)	4.898	4.690	4.872	5.154	4.776
Lower 95% CI	4.688	4.450	4.543	4.028	4.490
Upper 95% CI	5.108	4.930	5.202	6.280	5.062

Figure 5.14. The effect of siRNA-mediated knockdown of JARID1C on the telomere length distribution at 17p, 18q and XpYp. HT1080 cl. 2 cells were transfected with 25nm siRNA targeted against HDAC4 mRNA using DharmaFECT 4. JARID1C-1, -2, -3 and -4 represent four biological replicates independently transfected. Each replicate was successively transfected three times at 48h intervals. 48 hours after the third transfection DNA was extracted using Magnesil paramagnetic particles. STELA was then performed at 17p (a), 18q (b) and XpYp (c) using the 17pseqrev1, 18qrev4M and XpYpE respectively. Telomere length distributions were then quantified using Phoretix software. Any significant differences in mean telomere length between untreated cells and cells targeted for JARID1C knockdown as measured by t-test are stated.

a

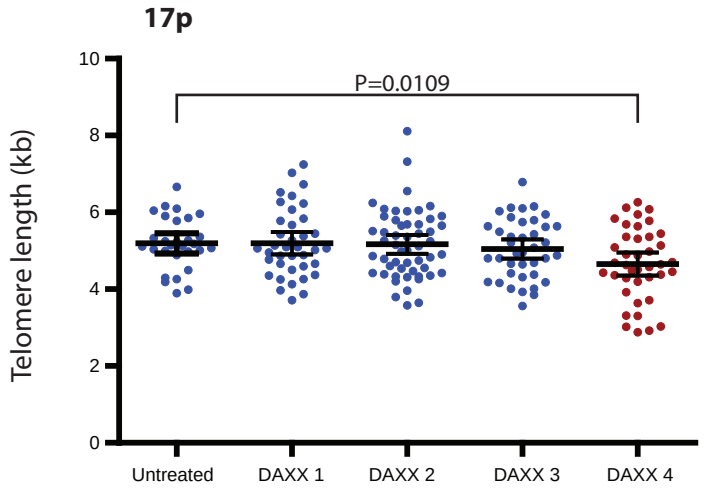

Mean tel length (kb)	5.192	5.197	5.168	5.044	4.656
Lower 95% CI	4.932	4.906	4.923	4.792	4.356
Upper 95% CI	5.453	5.489	5.413	5.296	4.955

b

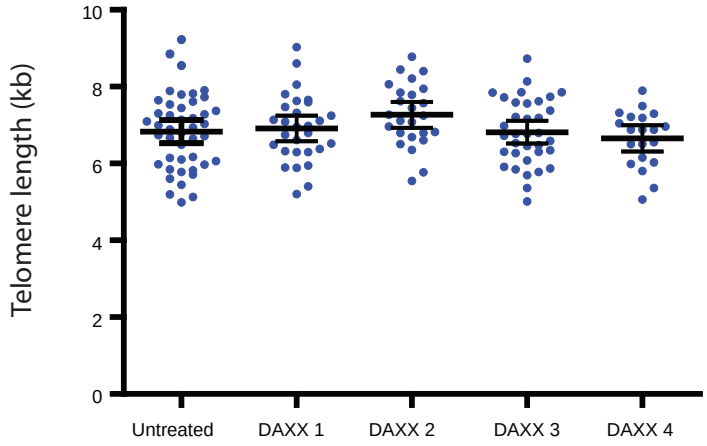

Mean tel length (kb)	6.829	6.913	7.267	6.814	6.651
Lower 95% CI	6.530	6.578	6.930	6.518	6.309
Upper 95% CI	7.128	7.248	7.603	7.109	6.994

c

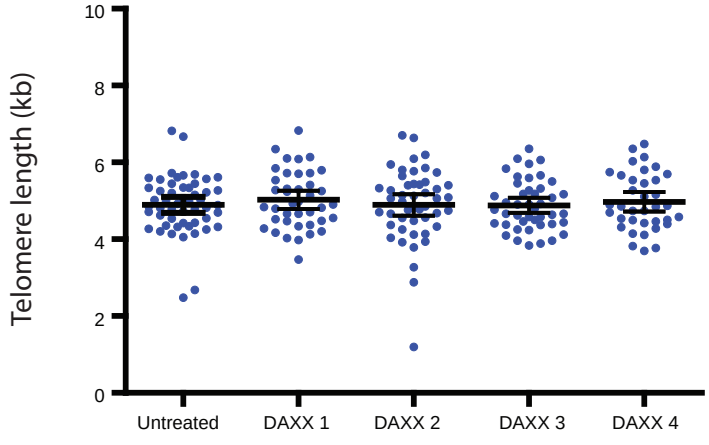

Mean tel length (kb)	4.898	5.026	4.895	4.881	4.974
Lower 95% CI	4.688	4.787	4.616	4.685	4.721
Upper 95% CI	5.108	5.265	5.175	5.078	5.226

Figure 5.15. The effect of siRNA-mediated knockdown of DAXX on the telomere length distribution at 17p, 18q and XpYp. HT1080 cl. 2 cells were transfected with 25nm siRNA targeted against DAXX mRNA using DharmaFECT 4. DAXX-1, -2, -3 and -4 represent four biological replicates independently transfected. Each replicate was successively transfected three times at 48h intervals. 48 hours after the third transfection DNA was extracted using Magnesil paramagnetic particles. STELA was then performed at 17p (a), 18q (b) and XpYp (c) using the 17pseqrev1, 18qrev4M and XpYpE respectively. Telomere length distributions were then quantified using Phoretix software. Any significant differences in mean telomere length between untreated cells and cells targeted for DAXX knockdown as measured by t-test are stated.

Above, the aberrant telomere length phenotypes observed in the RNAi screen are summarised, siRNA mediated knock down of the other candidate genes (HDAC4, LSH, UTX, H3F3A and H3F3B) did not result in telomere length defects, the telomere length distributions of the 17p, 18q and XpYp telomeres after knockdown of these genes are summarised in figures 5.16-20.

a

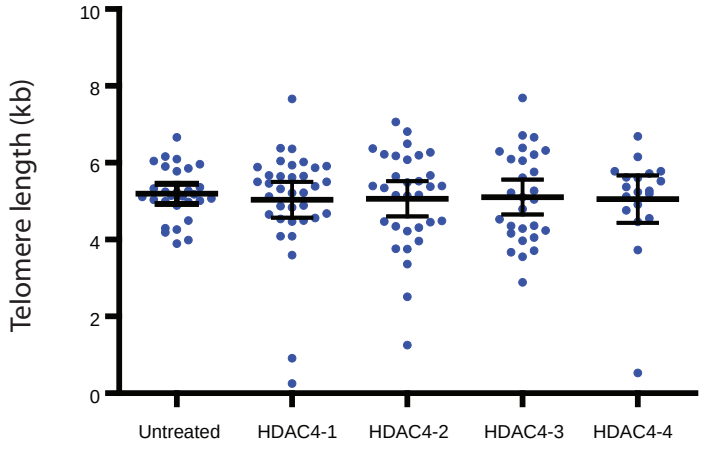

Mean tel length (kb)	5.192	5.038	5.059	5.108	5.054
Lower 95% CI	4.932	4.570	4.601	4.650	4.439
Upper 95% CI	5.453	5.505	5.517	5.566	5.670

b

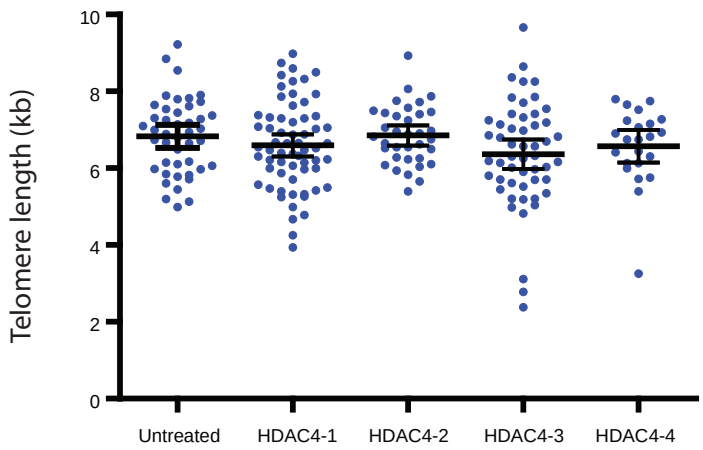

Mean tel length (kb)	6.829	6.594	6.852	6.36	6.571
Lower 95% CI	6.530	6.308	6.590	5.976	6.144
Upper 95% CI	7.128	6.881	7.113	6.745	6.998

c

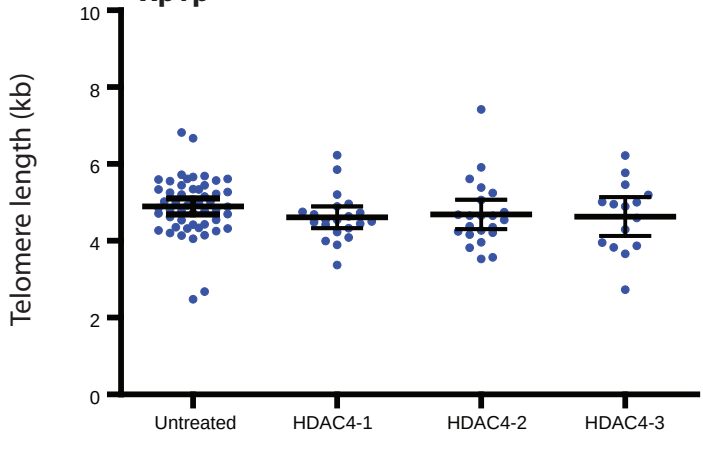

Mean tel length (kb)	4.898	4.611	4.684	4.63
Lower 95% CI	4.688	4.326	4.300	4.126
Upper 95% CI	5.108	4.895	5.068	5.135

Figure 5.16. The effect of siRNA-mediated knockdown of HDAC4 on the telomere length distribution at 17p, 18q and XpYp. HT1080 cl. 2 cells were transfected with 25nm siRNA targeted against HDAC4 mRNA using DharmaFECT 4. HDAC4 -1, -2, -3 and -4 represent four biological replicates independently transfected. Each replicate was successively transfected three times at 48h intervals. 48 hours after the third transfection DNA was extracted using Magnesil paramagnetic particles. STELA was then performed at 17p (a), 18q (b) and XpYp (c) using the 17pseqrev1, 18qrev4M and XpYpE respectively. Telomere length distributions were then quantified using Phoretix software. Any significant differences in mean telomere length between untreated cells and cells targeted for HDAC4 knockdown as measured by t-test are stated.

a

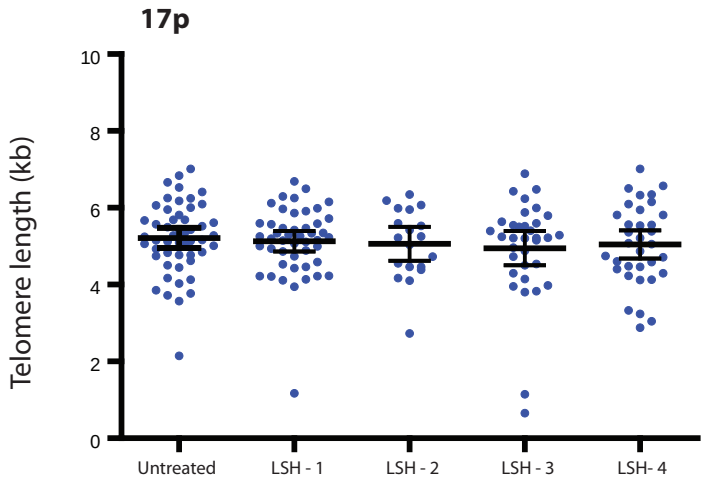

Mean tel length (kb)	5.215	5.128	5.063	4.949	5.044
Lower 95% CI	4.954	4.863	4.623	4.501	4.677
Upper 95% CI	5.476	5.393	5.502	5.397	5.411

b

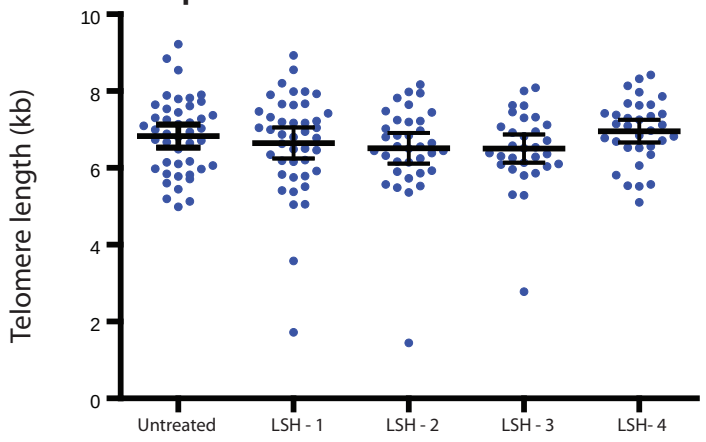

Mean tel length (kb)	6.829	6.649	6.511	6.503	6.955
Lower 95% CI	6.530	6.248	6.111	6.139	6.659
Upper 95% CI	7.128	7.051	6.911	6.867	7.252

c

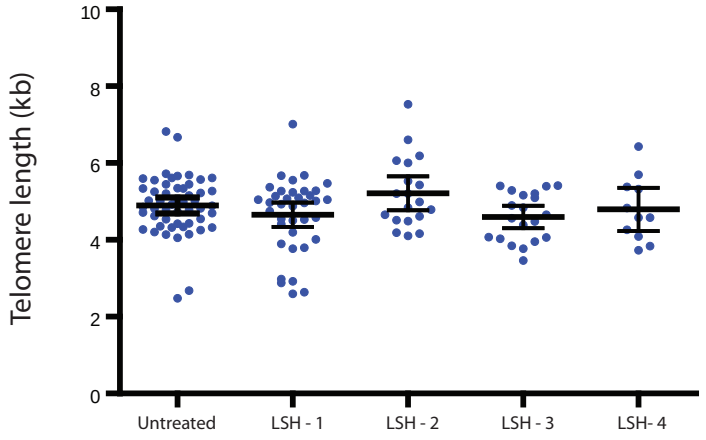

Mean tel length (kb)	4.898	4.652	4.699	4.497	4.524
Lower 95% CI	4.688	4.333	4.446	4.268	4.355
Upper 95% CI	5.108	4.970	4.951	4.727	4.692

Figure 5.17. The effect of siRNA-mediated knockdown of LSH on the telomere length distribution at 17p, 18q and XpYp. HT1080 cl. 2 cells were transfected with 25nm siRNA targeted against LSH mRNA using DharmaFECT 4. TERT-1, -2, -3 & -4 represent four biological replicates independently transfected. Each replicate was successively transfected three times at 48h intervals. 48 hours after the third transfection DNA was extracted using Magnesil paramagnetic particles. STELA was then performed at 17p (a), 18q (b) and XpYp (c) using the 17pseqrev1, 18qrev4M and XpYpE respectively. Telomere length distributions were then quantified using Phoretix software. Any significant differences in mean telomere length between untreated cells and cells targeted for LSH knockdown as measured by t-test are stated.

a

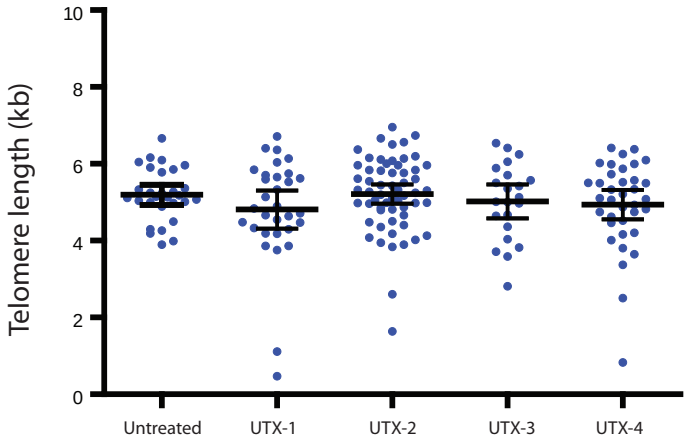

Mean tel length (kb)	5.192	5.809	5.212	5.02	4.936
Lower 95% CI	4.932	4.315	4.959	4.581	4.552
Upper 95% CI	5.453	5.304	5.465	5.459	5.320

b

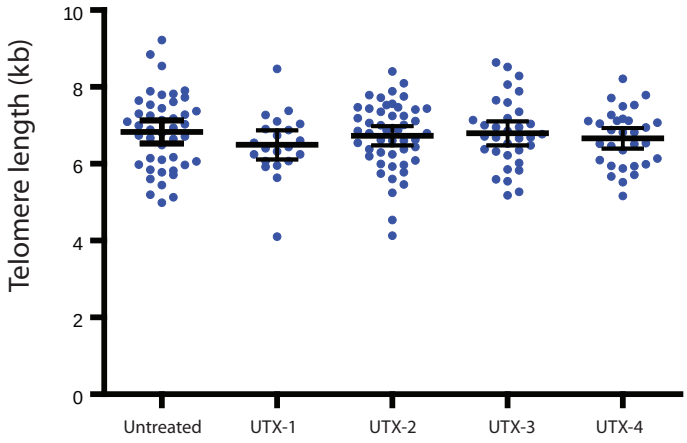

Mean tel length (kb)	6.829	6.493	6.729	6.795	6.663
Lower 95% CI	6.530	6.112	6.479	6.481	6.392
Upper 95% CI	7.128	6.873	6.980	7.108	6.933

c

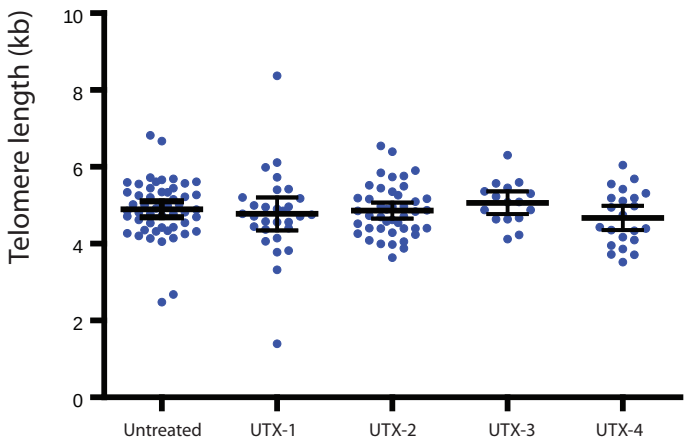

Mean tel length (kb)	4.898	4.775	4.862	5.064	4.67
Lower 95% CI	4.688	4.348	4.657	4.770	4.352
Upper 95% CI	5.108	5.202	5.067	5.359	4.988

Figure 5.18. The effect of siRNA-mediated knockdown of UTX on the telomere length distribution at 17p, 18q and XpYp. HT1080 cl. 2 cells were transfected with 25nm siRNA targeted against UTX mRNA using DharmaFECT 4. UTX-1, -2, -3 and -4 represent four biological replicates independently transfected. Each replicate was successively transfected three times at 48h intervals. 48 hours after the third transfection DNA was extracted using Magnesil paramagnetic particles. STELA was then performed at 17p (a), 18q (b) and XpYp (c) using the 17pseqrev1, 18qrev4M and XpYpE respectively. Telomere length distributions were then quantified using Phoretix software. Any significant differences in mean telomere length between untreated cells and cells targeted for UTX knockdown as measured by t-test are stated.

a

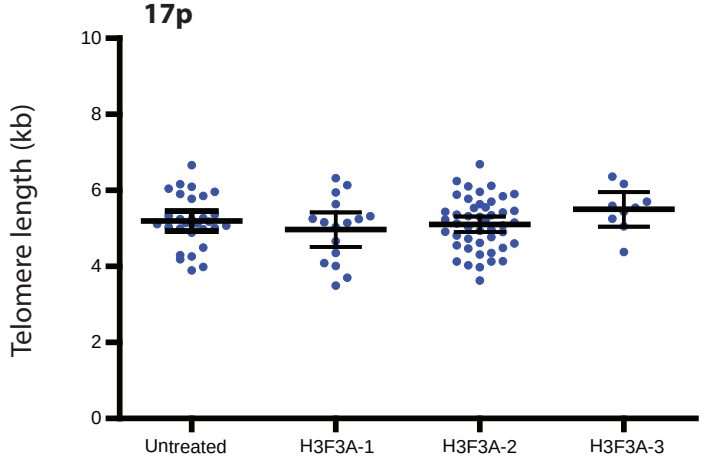

Mean tel length (kb)	5.192	4.969	5.108	5.501
Lower 95% CI	4.932	4.515	4.904	5.050
Upper 95% CI	5.453	5.424	5.311	5.952

b

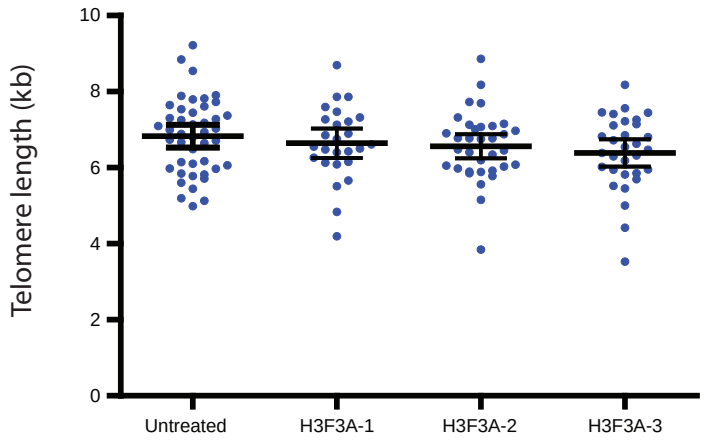

Mean tel length (kb)	6.829	6.644	6.559	6.389
Lower 95% CI	6.530	6.257	6.242	6.032
Upper 95% CI	7.128	7.031	6.876	6.746

c

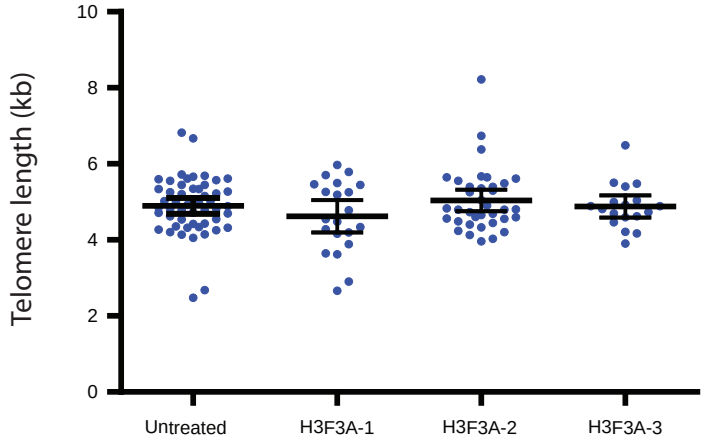

Mean tel length (kb)	4.898	4.622	5.04	4.878
Lower 95% CI	4.688	4.195	4.756	4.585
Upper 95% CI	5.108	5.048	5.324	5.171

Figure 5.19. The effect of siRNA-mediated knockdown of H3F3A on the telomere length distribution at 17p, 18q and XpYp. HT1080 cl. 2 cells were transfected with 25nm siRNA targeted against H3F3A mRNA using DharmaFECT 4. H3F3A-1, -2, -3 and -4 represent four biological replicates independently transfected. Each replicate was successively transfected three times at 48h intervals. 48 hours after the third transfection DNA was extracted using Magnesil paramagnetic particles. STELA was then performed at 17p (a), 18q (b) and XpYp (c) using the 17pseqrev1, 18qrev4M and XpYpE respectively. Telomere length distributions were then quantified using Phoretix software. Any significant differences in mean telomere length between untreated cells and cells targeted for H3F3A knockdown as measured by t-test are stated.

a

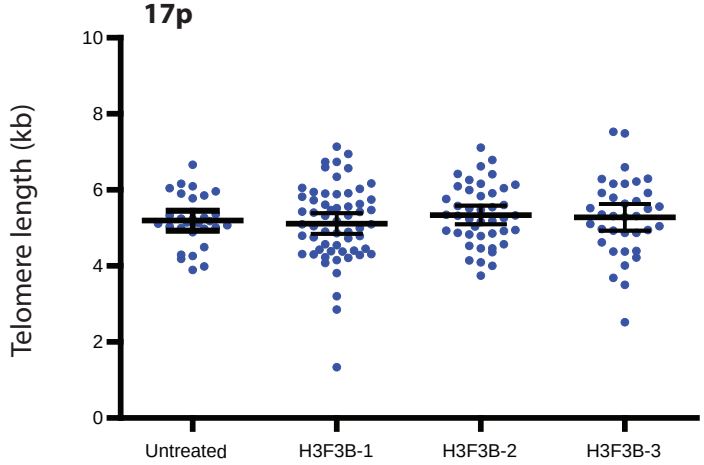

Mean tel length (kb)	5.192	5.116	5.342	5.279
Lower 95% CI	4.932	4.848	5.097	4.929
Upper 95% CI	5.453	5.384	5.586	5.628

b

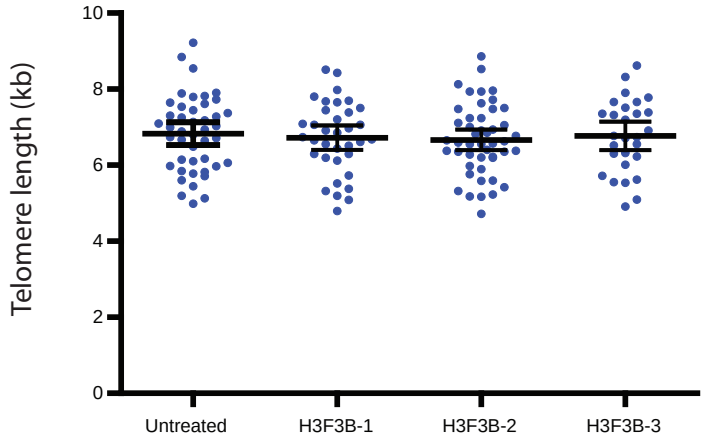

Mean tel length (kb)	6.829	6.144	6.725	6.666
Lower 95% CI	6.530	6.403	6.393	6.398
Upper 95% CI	7.128	7.047	6.939	7.144

c

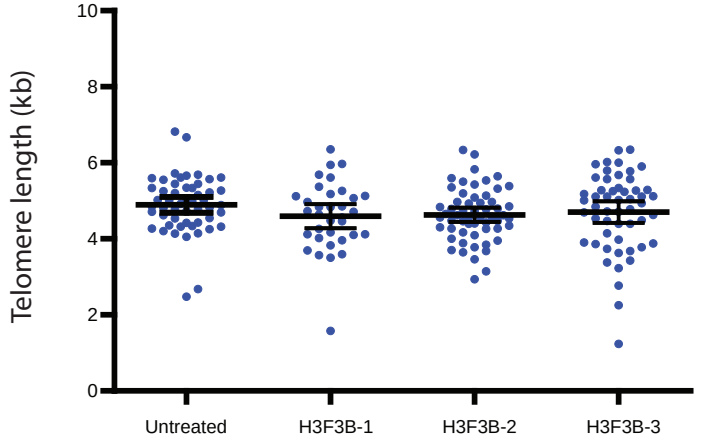

Mean tel length (kb)	4.898	4.597	4.719	4.632
Lower 95% CI	4.688	4.281	4.447	4.423
Upper 95% CI	5.108	4.914	4.817	4.991

Figure 5.20. The effect of siRNA-mediated knockdown of H3F3B on the telomere length distribution at 17p, 18q and XpYp. HT1080 cl. 2 cells were transfected with 25nm siRNA targeted against H3F3B mRNA using DharmaFECT 4. H3F3B-1, -2, -3 and -4 represent four biological replicates independently transfected. Each replicate was successively transfected three times at 48h intervals. 48 hours after the third transfection DNA was extracted using Magnesil paramagnetic particles. STELA was then performed at 17p (a), 18q (b) and XpYp (c) using the 17pseqrev1, 18qrev4M and XpYpE respectively. Telomere length distributions were then quantified using Phoretix software. Any significant differences in mean telomere length between untreated cells and cells targeted for H3F3B knockdown as measured by t-test are stated.

5.4 Discussion

Various chromatin remodelers have previously been shown to contribute to telomere length maintenance through their ability to modify chromatin in mouse Embryonic Stem (ES) and Embryonic Fibroblast (MEF) cells (Benetti et al., 2007; Garcia-Cao et al., 2004; Gonzalo et al., 2006; Jones et al., 2008; Palacios et al., 2010). however such examples at human telomeres are scarce with ATRX, DAXX and H3.3 representing the only chromatin remodelling pathway which regulates telomere length (de Wilde et al., 2012; Heaphy et al., 2011; Schwartzentruber et al., 2012)

Single Telomere Length Analysis (STELA) allows high-resolution analysis of individual telomere length distributions at several chromosome ends and when used in combination with the 96-well plate based RNAi screen presented here provides a novel high throughput method for analysing telomere length at individual chromosome ends in cells targeted for gene knockdown. The sensitivity STELA provides allows subtle aberrant telomere length phenotypes to be identified. This is particularly relevant in cases were deficiency in a chromatin remodeler causes a gradual erosion of telomeric repeats over successive cell divisions. The likelihood of identifying these subtle telomere length phenotypes was also increased by using the HT1080 clonal population with the homogenous telomere length distribution profiles for 17p, 18q and XpYp.

Despite the benefits of the approach taken there are a number of drawbacks which means that conclusions of the effect of the selected chromatin remodelers on telomere length cannot be made with confidence. Firstly the knockdown of TERT did not result in a widespread telomere shortening phenotype. Across all three telomeres analysed only two of the twelve comparisons between untreated and TERT knockdown replicate cells displayed a statistically significant telomere shortening phenotype (both at XpYp). The fact that there was a lack of a robust telomere shortening

phenotype in the absence of TERT shows that under the conditions used the approach taken lacked sensitivity. It would have been beneficial to know the rate at which telomere shortening was expected to occur in these cells. An analysis of telomere shortening in HT1080 cells after RNAi-mediated knockdown of TERT has not previously been performed. However overexpression of the helicase Pif1 reduces telomerase activity in HT1080 cells by 85%. Concomitant with this inhibition of telomerase activity is a progressive telomere shortening phenotype (Zhang et al., 2006). The rate of telomere shortening upon telomerase inhibition observed was 10-27bp per PD. In this chapter the HT1080 cl.2 cells were subject to TERT knockdown over 6 days. The growth rate of the cells was 1.225PD/day therefore over 6 days the population doublings for these cells was 7.225 PD. If a similar rate of telomere length loss occurs in these cells as in the HT1080 cells in which Pif1 was overexpressed then the total telomere length loss expected would be 73-195bp. This telomere length loss is smaller than the variation in telomere length between the untreated replicates in the clonal drift experiment. Therefore such losses would not be seen as the system is not sensitive under the conditions used in this chapter.

Telomere shortening after inhibition of telomerase activity by Pif1 overexpression was obvious after 15-35PDs (Zhang et al., 2006). After 55PDs telomere length losses amounted to 0.5-1.5kb. Similarly robust telomere length losses needed to be observed in this screen to give confidence that the differences in telomere length observed between the TERT-depleted and untreated cells were genuine telomere shortening events due to loss of TERT and not just the product of variation within the system. Therefore in future screens the cells would have to be subject to TERT depletion for a much longer period of time. Obviously if the screen was not sensitive enough to detect telomere length defects in the absence of TERT then the same will be true for mean telomere length alterations in the absence of the selected chromatin remodelers. Again performing the knockdown of these genes over a longer period of time will allow gradual telomere erosion/elongation

phenotypes to manifest themselves and give confidence that these phenotypes are not just due to variation in the system.

The assay was designed to uncover very subtle deviations in telomere length and as such the difference between a genuine telomere length defect and just variation within the system is very small. The clonal drift experiment was designed to demonstrate the bounds of variability within the assay. Any differences in telomere length within the knockdown replicate cells that fell within the bounds of variability defined by the clonal drift experiment were discarded. The problem with the clonal drift experiment is that the number of untreated replicates chosen to analyse may have influenced the variation bounds within the system. Measuring telomere length in more independent untreated cell populations may have shown greater variation within the system and this would have an adverse effect on the interpretation of the results from the candidate genes. The variation observed within the system is exemplified in the 17p telomere length analysis in the EZH2 knockdown replicates (fig. 5.10). In this example one of the cell populations transfected with EZH2 targeting siRNA showed an increase in telomere length whereas another showed a decrease in telomere length. This must reflect variation within the system. Pooling the telomere length distributions from all four individual knockdown replicates may have eradicated some of this variation however by doing this the differences in the knockdown efficiency within each independent replicate are not taken into consideration.

The lack of verification that the selected chromatin remodelling genes were actually being sufficiently depleted in the cells is another problem with the assay. The high throughput format of the screen is advantageous because the effect of a large number of chromatin remodelers on telomere length regulation can be investigated in a short space of time. However it was not possible

to determine the extent of knockdown for all 16 genes as it would have been too costly and time consuming. Although it would have been beneficial to know the extent of the knockdown for each gene, this screen was used as a tool to look for chromatin remodelling proteins which, when depleted, potentially caused an aberrant telomere length phenotype. Any such chromatin remodelers could then be further investigated which would include verifying expression levels of these genes after knockdown. The initial optimization of the technique in which the extent of knockdown of the GAPDH gene showed that the technique could successfully knock down expression of a gene, it also determined the best time point at which to do successive knockdowns (fig. 5.1). However a criticism of this initial experiment is that RNA levels were measured after GAPDH knockdown, not protein level. Measuring protein levels after knockdown is beneficial as protein levels within a cell are determined not only by RNA levels but also by the level of protein degradation. Additionally knockdown of a gene would depend somewhat on the gene in question and the siRNA duplex designed against that gene, however the same procedure has since been used to knockdown gene expression in clonal populations of keratinocyte cells and was shown to achieve >70% gene knockdown. Additionally, each gene targeted for knockdown was targeted in four independent knockdowns to maximise the chance of success. Despite this GAPDH optimization experiment it still would have been better to validate siRNA knockdown efficiency by western analysis for each gene, especially because the phenotypes that were searched for were so subtle and the margin between a genuine telomere length defect due to depletion of a chromatin remodeler and telomere length alterations due to variation within the system was so fine.

Perhaps in future investigations using a similar approach fewer genes should be targeted. By focusing on a smaller number of chromatin remodelers it would be easier to verify the knockdown efficiency and the screen could also be performed on a larger scale which would allow the isolation of protein for western analysis. A larger screen would also enable more DNA to be extracted which

would result in a more robust STELA analysis with more quantifiable bands and also allow the analysis of any telomere-to-telomere fusion events. Obtaining enough DNA from the cells from the 96 well plate was an issue during the screen. On some occasions there simply wasn't enough DNA to perform STELA at all three chromosome ends. In other cases very little DNA was recovered which resulted in only very few bands on the STELA blots which impeded statistical analysis of telomere length distributions.

RNAi-mediated knockdown of the histone methyltransferase EHMT2 resulted in a significant increase in very short 17p telomeres (fig. 5.5&5.6). EHMT2 is a HMTase similar to the Suv39h1 and Suv39h2 HMTases responsible for maintaining telomeric chromatin structure and length in mouse ES cells. Although EHMT2 was initially proposed to target transcriptionally active sites (Tachibana et al., 2001; Tachibana et al., 2002) it has recently been found that it can exert transcriptional repression *in vitro* via its HMTase activity suggesting a role in heterochromatin formation (Tachibana et al., 2002). EHMT2 has recently been implicated in a role in the maintenance of telomere length: an investigation into genes involved in DNA and histone methylation revealed that the minor allele of EHMT2 rs558702 G>A was associated with shorter telomeres (Kim et al., 2012). The loss of telomere length in the EHMT2-deficient cells in this chapter does not appear to be the result of impaired telomerase activity as these length changes are rapid and dramatic, whereas after telomerase loss the changes would be small and cumulative. An alternative explanation for the generation of very small telomeres could be defects in the restarting of stalled replication forks. Loss of DNA replication and DNA damage proteins implicated in the restarting of stalled replication forks within telomeric DNA has been shown to lead to exposure of ssDNA that is susceptible to degradation. This results in dramatic telomere shortening (Crabbe et al., 2007; Pandita et al., 2006). The contribution of EHMT2 on telomeric chromatin structure could facilitate the binding of such proteins allowing successful restart of stalled replication forks. Another explanation could be that loss of EHMT2 promotes

recombination-based telomere rapid deletion (TRD) events. TRD are single-step intrachromosomal events which have been shown to cause dramatic loss in telomere length in yeast, Arabidopsis and human cells (Iyer, Chadha & McEachern, 2005; Wang, Smogorzewska & de Lange, 2004; Watson & Shippen, 2007). It has been suggested that in human cells the higher order t-loop structure of a telomere resembles an intermediate in the homologous recombination repair pathway and is therefore at risk of inappropriate processing by the HR machinery. Expression of a truncated form of TRF2, TRF2$^{\Delta B}$ in human primary fibroblasts results in homologous recombination at the telomere causing dramatic telomere shortening and the formation of t-loop-sized circular DNAs suggesting that TRF2 represses this pathway to maintain telomere length (Wang et al., 2004). EHMT2 could perform a similar function by altering the telomeric chromatin structure and impeding the telomeric binding of HR machinery.

Loss of DOT1L, another HMTase which protects against recombination-based telomere shortening in mouse ES cells (Jones et al., 2008), was also shown to cause aberrant telomere length phenotypes in the screen although this phenotype did not suggest a recombination-based mechanism was responsible. The presence of two populations of telomeres of different lengths was observed at 17p in the DOT1L-1 replicate. The reason behind this divergence in telomere length is not clear but this could be due to the coexistence of two sub-populations of DOT1L-1 cells; one sub-population may have derived from cells which were successfully transfected with DOT1L-specific siRNA and whose telomeres were resultantly shortened and the other sub-population may represent cells in which DOT1L levels were not reduced and so had telomeres of normal length. It seems likely that this result is a true reflection of the 17p telomere length within these cells as STELA was performed on two separate occasions using DOT1L-1 replicate DNA and on both occasions the same divergence in 17p telomere length was observed.

Knockdown of other chromatin remodelers appeared to result in subtle alterations in the mean telomere length however as mentioned above the robustness of these results are questionable due to the limitations in the approach taken during the screen. These included the HMTases MLL and EZH2, the HDACs HDAC1 and SIRT6, the ATP-dependent chromatin remodelling complex subunit BAF155 and the H3.3 chaperone DAXX.

A slight reduction in 18q and XpYp telomere length was observed in the MLL knockdown replicate cells (fig. 5.13). The deposition of H3K4me3 by MLL at telomeres in HS68 and IMR90 fibroblasts was shown to be essential for telomere transcription and capping however no telomere length regulation role has previously been found (Caslini et al., 2009). Set1, the MLL homolog in budding and fission yeast has been shown to be a regulator of telomere length (Kanoh et al., 2003; Roguev et al., 2001).

Depletion of another HMTase, EZH2, showed a significant alteration in mean telomere length at 17p, 18q and XpYp suggesting a potential role for the HMTase in telomere length maintenance. A number of previous reports on EZH2 and the H3K27 methylation mediated by EZH2 raise the intriguing possibility of a role for EZH2 at human telomeres. Firstly EZH2 has been shown to be implicated in TPE in *Drosophila* and yeast (Laible et al., 1997) although a telomere length regulatory role has not been reported. Secondly, H3K27 methylation has long been considered a repressive heterochromatin mark; it has been implicated in the silencing of HOX gene expression (Jones & Gelbart, 1990; Struhl, 1981) as well as silencing of the inactive X chromosome (Heard, 2005) and H3K27me3 enrichment has recently been reported at human telomeres (Arnoult et al., 2012; Rosenfeld et al., 2009; Vaquero-Sedas, Luo & Vega-Palas, 2012). Additionally, EZH2 physically interacts with a number of chromatin remodelling complexes which have already been reported to play a role at mammalian telomeres: The DNA methyltransferases (DNMTs), which prevent

recombination-based telomere lengthening in mouse ES cells (Gonzalo et al., 2006), not only physically interact with EZH2 but require EZH2 for binding to target regions in osteosarcoma cells (Fuks et al., 2006), the SWI/SNF family member ATRX, responsible for proper H3.3 deposition at the telomere in mouse ES cells, also physically interacts with EZH2.

EZH2 also physically interacts with the histone deacetylase HDAC1 (van der Vlag & Otte, 1999) as does ATRX (Zoltewicz et al., 2004). siRNA mediated knockdown of HDAC1 resulted in a telomere lengthening phenotype at XpYp in one of the four knockdown replicates. A role for HDAC1 in regulating human telomeric chromatin maintenance has not been reported although given that the *Drosophila* orthologue to HDAC1, Rpd3 has been shown to be required for prevention of telomere fusions on polytene chromosome ends (Burgio et al., 2011) and *Drosophila* and yeast Rpd3 counteracts the silencing of telomeric-proximal genes (De Rubertis et al., 1996) HDAC1 may well have a role in the maintenance of human telomeric chromatin.

The histone deacetylase activity of SIRT6 has previously been shown to be required for preventing the establishment of telomere dysfunction induced foci (TIFs) and telomere-to-telomere fusions in human WI-138 fibroblasts (Michishita et al., 2008). It is also essential for the silencing of telomere proximal genes (TPE) (Tennen et al., 2011). Despite these reported telomeric functions of SIRT6, it has not been shown to be involved in maintenance of telomere length. Fig. 5.4 shows that loss of SIRT6 in the HT1080 cl. 2 cells leads to a reduction in telomere length suggesting a previously unidentified role for SIRT6 in human telomere length maintenance.

BAF155, encoded by the *SMARCC1* gene is one of 12 BAFs (BRG1-associated factors) found in mammalian SWI/SNF complexes. BAF155 deficiency in the HT1080 cl.2 cells caused a subtle

reduction in mean XpYp telomere length in two of the three BAF155 knockdown replicates (fig. 5.11) This protein, along with another BAF; BAF170 is a homolog of Rsc8, a subunit found in the RSC ATP-dependant chromatin remodelling complex in *Saccharomyces cerevisiae*. A genome-wide screen searching for essential yeast genes that affected telomere length maintenance revealed that, contrary to what was observed in the BAF155-deficient HT1080 cl. 2 cells, the absence of Rsc8 resulted in telomere elongation (Ungar et al., 2009). A similar screen performed by (Askree et al., 2004) identified another RSC subunit, Rsc2 which functioned to maintain telomere length. Loss of Rsc2 resulted in a telomere shortening phenotype. These observations give support to the idea that BAF155 is a regulator of telomere length in HT1080 cells

siRNA-mediated knockdown of DAXX caused a significant reduction in the mean telomere length of only one of the four knockdown replicates and only at the 17p telomere (fig. 5.15). The limited aberrant telomere length phenotype resulting from loss of DAXX was surprising considering DAXX and ATRX were shown to be associated with alternative lengthening of telomeres in human pancreatic neuroendocrine tumours (PanNETs) (Heaphy et al., 2011) and glioblastoma multiforme (GBM) tumour samples (Schwartzentruber et al., 2012). In addition RNAi-mediated knockdown of ATRX in a keratinocyte holoclone cell population has been shown in our lab to cause a prominent telomere phenotype consisting of dramatic, stochastic reductions in telomere length (Tankimanova, personal communication). siRNA knockdown of H3F3A and H3F3B, the genes encoding the histone H3 variant H3.3, did not result in any aberrant telomere length phenotypes. Seeing as DAXX functions to maintain telomeric chromatin structure by ensuring proper telomeric deposition of H3.3 along with its complex partner ATRX, it was expected that telomere length defects observed in DAXX-deficient cells would also be present in the H3F3A and H3F3B knockdown cells. The fact that this is not the case may be due to one of a number of reasons: It is possible that the significant reduction in DAXX-4 knockdown replicate cells was due to variation in the system and not because

of DAXX loss. It is also possible that H3F3A and H3F3B expression may have only been partially knocked down and sufficient H3.3 protein remained in the HT1080 cl.2 cells to perform its telomeric function. An alternative explanation is that there may be an additional pathway through which DAXX functions to maintain telomere length which is independent of H3.3 deposition.

In this chapter an RNAi screen was performed in an attempt to identify chromatin remodelling proteins which, when depleted, result in aberrant telomere length phenotypes. Depletion of a number of chromatin remodelling proteins appeared to cause alterations in mean telomere length. These include the histone methyltransferases EZH2 and MLL, the histone deacetylases HDAC1 and SIRT6, the ATP-dependant chromatin remodelling complex subunit BAF155 and the H3.3 histone chaperone DAXX. However due to limitations in the sensitivity of the screen under the conditions used the robustness of these mean telomere length alterations are questionable as they may reflect variation within the system. Depletion of the histone methyltransferases EHMT2 and DOT1L caused a change in the pattern of telomere length distributions. Loss EHMT2 caused a significant increase in very small 17p telomeres (<3kb) compared to untreated cells. DOT1L depletion resulted in a divergence in the 17p telomere length distribution suggesting the presence of two subpopulations each with differing telomere length distributions. The screen provides a good starting point for identifying chromatin remodelers with a role in telomere length regulation however a number of issues need to be resolved in order for robust conclusions can be made with confidence. These issues would include performing the screen over a longer period of time to allow aberrant telomere length phenotypes to manifest themselves. This is particularly relevant to the TERT knockdown positive control experiment where a robust telomere shortening phenotype would have to be observed. Using shRNA to stably knockdown expression of the selected genes over more population doublings would also be beneficial. Verification of knockdown would also have to be performed by western analysis to give confidence that changes in telomere length were due to loss of the

chromatin remodeler in question. Extracting protein from the cells would be achieved by performing the screen on a larger scale. This would also allow the extraction of more DNA for better STELA analysis of telomere length and also allow identification of any telomere-to-telomere fusion events occurring in the absence of a particular chromatin remodeler.

Chapter 6

The role of DAXX at the telomere in keratinocyte holoclone cells

6.1 Abstract

A number of mammalian chromatin remodelling proteins have been shown to maintain telomeric chromatin structure and consequently prevent telomere dysfunction. Of the proteins identified the histone H3.3 chaperone DAXX has been shown to form a complex with the SWI/SNF family member ATRX and that this interaction is necessary for the proper H3.3 deposition within telomeric chromatin in mouse embryonic stem cells (ESCs). Loss of either member of this ATRX-DAXX-H3.3 pathway in these cells results in telomere dysfunction. Mutations in this pathway have also been implicated in telomere length changes in human tumour samples and in several human cell lines in which the ALT (Alternative Lengthening of Telomeres) pathway is activated. Recently, a member of our lab has identified ATRX as a regulator of telomere length in a keratinocyte holoclone population (Tankimanova, personal communication). In the previous chapter the RNAi screen revealed potential telomere length defects after knockdown of EHMT2, EZH2 and DOT1L and, to a lesser extent, DAXX in a clonal population of the HT1080 fibrosarcoma cell line. The aim of this chapter is to further investigate the roles of these proteins at the telomere in a population of keratinocyte holoclone (kC1B) cells. Successive siRNA-mediated knockdown of DAXX over a number of cell divisions in kC1B cells promotes telomere shortening at a number of chromosome ends and telomere-to-telomere fusion events. EHMT2 deficiency in these cells also caused telomere shortening. Loss of EZH2, DOT1L and ATRX did not result in any aberrant telomere phenotypes. To provide insight into the mechanism by which telomere shortening was occurring, attempts were made to sequence short telomeres

generated in DAXX deficient cells. Although this was unsuccessful the development of methods to isolate, reamplify and sequence telomeres may prove to be a useful tool to study telomeric DNA in the future.

6.2 Introduction

The maintenance of telomeric chromatin structure in mammalian cells is a tightly regulated process; its disruption can lead to alterations in telomere length as well as telomere dysfunction and the formation of telomere-to-telomere fusions. A number of chromatin remodelers have been shown to preserve telomere structure and integrity through their ability to maintain telomeric chromatin in mouse cell models (Benetti et al. 2007b; Garcia-Cao et al. 2004a; Gonzalo et al. 2006; Jones et al. 2008; Lewis et al. 2010; Palacios et al. 2010; Wong et al. 2010; Wong et al. 2009) however such examples at human telomeres are rare (Caslini et al. 2009; Michishita et al. 2008; Tennen et al. 2011). The RNAi screen performed in a clonal population of the human HT1080 fibrosarcoma cell line described in the previous chapter revealed a potential telomeric role for a handful of proteins implicated in chromatin remodelling including the histone methyltransferases (HMTases) EHMT2, DOT1L and EZH2 and, to a lesser extent, the histone H3.3 chaperone DAXX.

These HMTases have previously been shown to have a role at the telomere in various organisms: Reduction of EHMT2 expression has been suggested to associate with shorter telomeres in human blood samples (Kim et al. 2012) whereas the EZH2 HMTases has been implicated in the maintenance of telomere position effect in yeast and *Drosophila* (Laible et al. 1997). DOT1L has been identified as a repressor of the Alternative Lengthening of Telomeres (ALT) pathway in mouse embryonic stem cells (ESCs) as its loss in these cells results in recombination-based telomere elongation along with loss of the heterochromatin-associated marks H3K79me2 and H4K20me3 (Jones et al. 2008). Of all the chromatin remodelers identified in the screen DAXX has been the most studied in regards to its role at the telomere in mammalian cells

6.2.1 The death-domain-associated protein (DAXX)

DAXX was originally identified through its binding with the death domain of the transmembrane death receptor FAS which enhances apoptosis through the induction of the c-Jun NH_2–terminal kinase (JNK) pathway (Yang *et al.* 1997). It has since been shown that aside from its function at the plasma membrane, DAXX is mainly a nuclear protein which associates with a number of different proteins involved in a range of diverse nuclear functions (Salomoni and Khelifi 2006). One of the main functions of DAXX however, is its role as a histone chaperone, specifically to the histone H3.3 replacement variant.

Aside from the canonical H3.1 and H3.2 variants, mammalian chromatin is also enriched in a histone H3 replacement variant H3.3. H3.3 differs by only four amino acids to its canonical counterparts however this difference has been shown to be necessary for H3.3 replication-independent incorporation into chromatin (Ahmad and Henikoff 2002; Tagami *et al.* 2004). Whereas H3.1 and H3.2 are deposited within chromatin in replication coupled manner by the CAF1 complex (Verreault *et al.* 1996) H3.3 is subject to replication-independent deposition into actively transcribed regions by the HIRA complex (Ray-Gallet *et al.* 2002; Tagami et al. 2004) and by DAXX in complex with the SWI/SNF family member ATRX complex at pericentric repeats (Drané et al. 2010) and at telomeres (Lewis et al. 2010). The telomeric deposition of H3.3 by the ATRX-DAXX complex is essential for maintaining telomeric chromatin structure: Mutation of the ATRX-DAXX-H3.3 pathway in mouse ESCs results in telomere dysfunction as well as reduced binding of the heterochromatin associated protein CBX5 (Lewis *et al.* 1999; Wong et al. 2010; Wong et al. 2009). It was shown that the precise role for DAXX within the complex is to physically interact with H3.3 via its globular domain however ATRX levels were reduced in Daxx-/- ESCs suggesting that DAXX is also required for ATRX protein stability or expression.

6.2.2 The role of the ATRX-DAXX-H3.3 pathway at human telomeres

Although a role in telomere length regulation for the ATRX-DAXX-H3.3 pathway was not implicated in mouse ESCs, such a role has been implicated in numerous human tumour samples: In a recent study telomere-specific fluorescence in-situ hybridization (FISH) was used to determine telomere length in pancreatic neuroendocrine tumours (PanNETs) with mutations in either the ATRX or DAXX genes (Heaphy et al. 2011). All 19 PanNETs with these inactivated mutations displayed ultra-bright telomere FISH signals, an indicator of the alternative lengthening of telomeres pathway. A similar correlation between alternative lengthening of telomeres and mutations in the ATRX-DAXX-H3.3 pathway was observed in glioblastoma multiforme brain tumour samples (Schwartzentruber et al. 2012). Furthermore, characterisation of genetic alterations in 22 human ALT cell lines revealed that ATRX was either undetectable or severely depleted in 90% of ALT cell lines (Lovejoy et al. 2012). Results from our lab also indicate an important role for ATRX at human telomeres in a keratinocyte holoclone cell population: siRNA-mediated knockdown of ATRX in these cells resulted in a striking stochastic loss of telomere length (Tankimanova, personal communication) which further supports the idea of the ATRX-DAXX-H3.3 pathway functioning to repress the ALT mechanism. This dramatic phenotype however was not seen in other cell types suggesting that the telomeric chromatin structure is particularly susceptible to recombinational mechanisms in these keratinocyte holoclone cells.

6.2.3 Differing telomeric chromatin structure in pluripotent and differentiated cells

Keratinocyte holoclone cells are one of three types of keratinocyte cells. They form large, smooth rapidly growing colonies with fewer than 5% of the colonies terminally

differentiating and aborting. It is believed these holoclones are stem cells. The other two types are meroclones and paraclones (Barrandon and Green 1987). Paraclones are terminally differentiating cells that from small and abortive colonies whereas mereclones consist of an intermediate mixture of holoclones and paraclones. The finding that loss of ATRX caused dramatic telomere shortening in only the 'stem cell' holoclone population of keratinocyte cells (Tankimanova, personal communication) is consistent with findings in mouse embryonic stem cells (ESCs) in which the ATRX-DAXX-H3.3 pathway was studied: H3.3 is enriched at the telomere in pluripotent mouse ESCs and embryonic germ cells (EGs) but not in other non-pluripotent mouse and human cell types (Wong et al. 2009). Furthermore, upon differentiation of these mouse ESCs, H3.3 was delocalised from the telomeres, H3K9me3 and H4K20me3 levels increased and MNase sensitivity decreased as the telomeric chromatin became more condensed and heterochromatic. These observations strongly suggest that the role of the ATRX-DAXX-H3.3 pathway in ensuring telomeric chromatin integrity is restricted to stem cells.

Differences between telomeric chromatin status between pluripotent stem cells and differentiated cells has been elegantly illustrated in a study in which telomeric chromatin structure was analysed in mouse embryonic fibroblasts (MEFs) which had undergone nuclear reprogramming to produce induced pluripotent stem cells (iPSCs) which were the functional equivalents of mouse ES cells. During reprogramming dramatic telomerase-dependent telomere elongation is observed which continues until ES cell telomere length is reached. Concomitant to telomere lengthening is a loss of the heterochromatin-associated H3K9me3 and H4K20me3 resulting in a more open, relaxed telomeric chromatin conformation (Marion et al. 2009). The opposing changes in chromatin structure seen upon differentiation and

induced pluripotency highlight the differences in telomeric chromatin structure between stem cells and differentiated cells.

6.2.4 Aim of the chapter

In light of the differing chromatin states in stem cells and differentiated cells it would be interesting to determine whether the chromatin remodelers identified during the RNAi screen in the HT1080 clonal population play a role in maintaining telomeric chromatin structure and telomere length in the keratinocyte holoclone stem cells. This is particularly relevant to DAXX as loss of its complex partner ATRX was shown to have a dramatic effect on telomere length in these cells. DAXX, as well as the HMTases EHMT2, DOT1L and EZH2, were subjected to siRNA-mediated knockdown in a keratinocyte holoclone (kC1B) cell population and any resulting aberrant telomere length profile was analysed with Single Length Telomere Analysis (STELA) at a number of chromosome ends. Telomeric dysfunction was further analysed by studying the nature of any telomere-to-telomere fusions resulting from depletion of a chromatin remodeler. Finally the mechanism underpinning any telomere length alterations was studied using novel mutational analysis methods.

6.3 Results

6.3.1 Optimization of knockdown procedure

A similar screen was performed in the keratinocyte holoclone C1B (kC1B) cells as in the HT1080 clone cells with some alterations. The screen was performed on a larger scale (24 as opposed to 96 well plate-format) to allow the harvest of more cells and subsequently the extraction of more DNA. This allows a larger scale STELA and also single molecule telomere fusion assays to be performed. The time points at which the cells were transfected with siRNA were also changed: the expression level of a targeted RNA was at its lowest level 48 hours after transfection in the HT1080 clone cells therefore the three transfections were performed at 48 hour intervals. Similar optimization performed in the keratinocyte holoclone C1B cells revealed that siRNA transfection at 96-hour intervals maintained low RNA levels of the targeted gene over numerous cell divisions and so this time interval was used.

6.3.2 Verification of knockdown efficiency

Before analysing any potential changes to telomere length after knockdown of the chromatin remodeler the efficiency of the knockdown had to be determined. kC1B cells were transfected with siRNA targeted against DAXX, EZH2, or ATRX (positive control) using DharmaFECT 1, 96 hours later RNA was extracted and RNA expression levels of the encoding genes were examined. Knockdown of all of the target genes was achieved with varying degrees of success (fig. 6.1); ATRX knockdown efficiency was highly efficient (>80%) for all four biological replicates (fig. 6.1a (i)). DAXX knockdown efficiency was also good with a ~70% reduction in DAXX expression in all four of the replicates (fig. 6.1a (ii)) Knockdown of

EZH2 was similarly efficient (~70% gene expression) for three of the four replicates however EZH2-4 only a 50% reduction in EZH2 expression levels (fig. 6.1a (iii)). It is unclear as to why this is the case but highlights the importance of including more than one replicate for each siRNA transfection. As expected the cells subjected to only dharmaFECT 1 (mock) and the cells transfected with a scrambled non-specific siRNA sequence (negative control) showed no great deviation in the expression of any of the target genes compared to the untreated cells (fig. 6.1a).

6.3.3 The effect of chromatin remodeler depletion on cell growth

To determine any potential effect on the growth rate kinetics of the kC1B cells after loss of the chromatin remodelling proteins, cells were counted when passaged 24h after transfection and population doublings were calculated. Loss of ATRX or DAXX did not appear to have any impact on the growth rate of the cells, this can be seen when all four knockdown replicates for each gene knockdown are combined and an average growth rate is calculated (fig. 6.1b (i)) or when each individual ATRX or DAXX-deficient replicate is compared against untreated cells (fig. 6.1b (ii & iii)). Loss of EZH2 however did result in a slight reduction in growth rate compared to untreated cells; each replicate underwent fewer population doublings, particularly at the day 8 time point (fig. 6.1b (iv)).

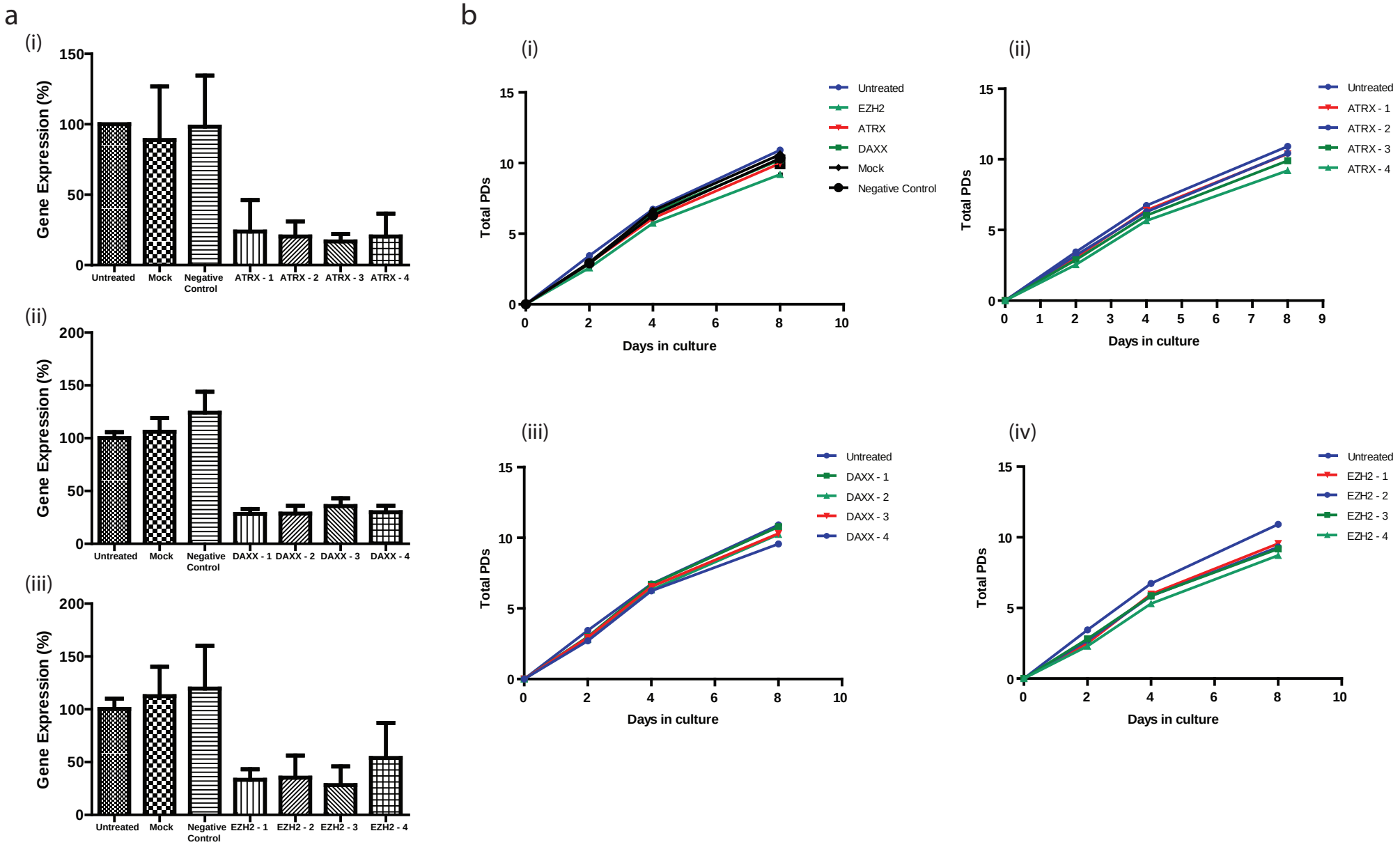

Figure 6.1. Verification of knockdown efficiency and growth rate of kC1B cells after siRNA knockdown. (a) RNA was extracted from either untreated cells, cells subjected to DharmaFECT 1 (mock), cells transfected with a non-specific siRNA (negative control) or cells transfected with a siRNA targeted against ATRX (i), DAXX (ii) or EZH2 (iii) using a cells-to-cDNA kit™II kit (Ambion). RNA level was then analyzed by RT-PCR using Taqman gene expression assays specific to each targeted gene and ACTB (endogenous control).(b) 24h after each siRNA transfection cells were passaged and counted. Population doublings of each cell type was then calculated to determine whether deficiecy of the chromatin remodelers affected the growth rate of these cells. (i) the average rate of population doubling for all four biological replicates within one knockdown experiment (ii-iv) the population doublling rate of the (ii) ATRX , (iii) DAXX and (iv) EZH2 knockdown replicates.

a **17p**

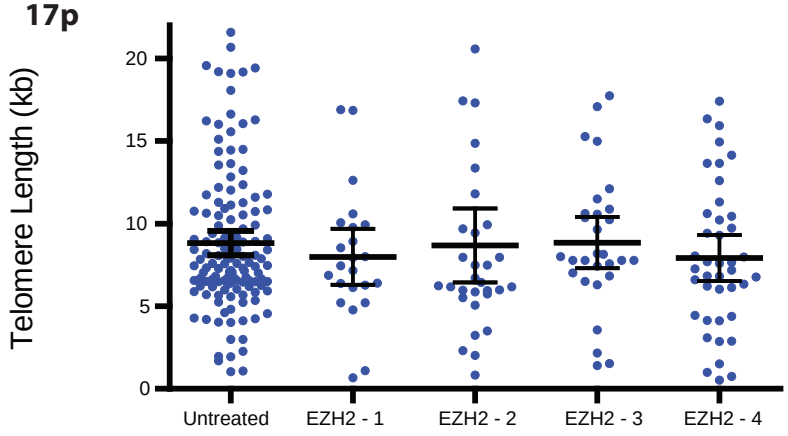

Mean tel length (kb)	8.831	7.987	8.677	8.852	7.915
Lower 95% CI	8.647	6.289	6.439	7.295	6.521
Upper 95% CI	10.17	9.685	10.91	10.41	9.309

b **18q**

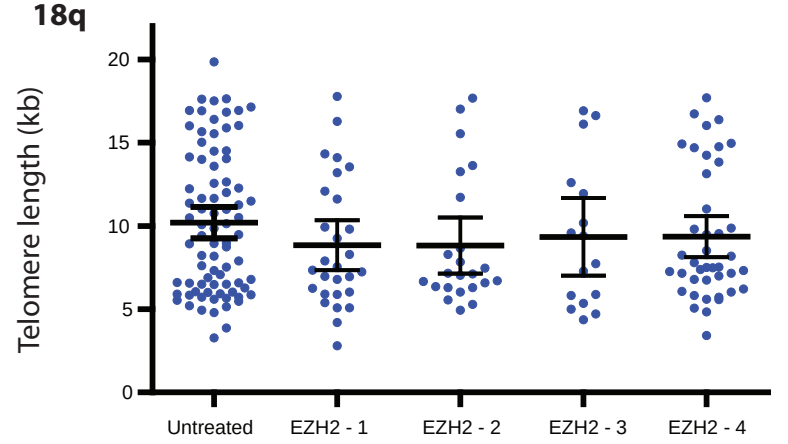

Mean tel length (kb)	10.19	8.843	8.83	9.346	9.356
Lower 95% CI	8.225	7.344	7.147	7.017	8.117
Upper 95% CI	10.46	10.34	10.51	11.68	10.59

c **XpYp**

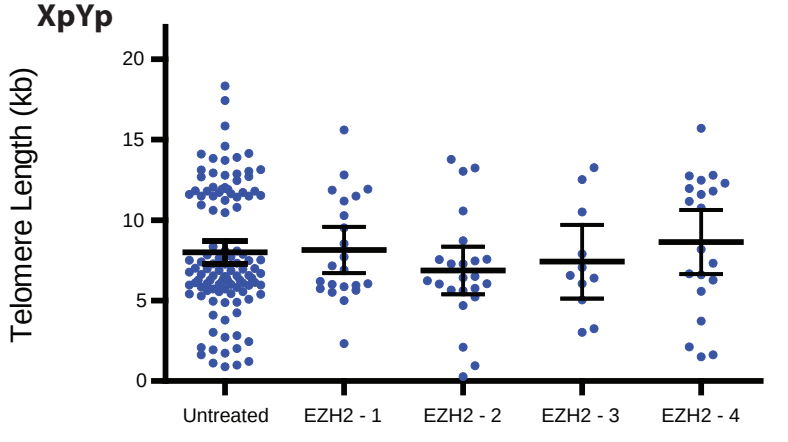

Mean tel length (kb)	7.992	8.149	6.87	7.419	8.645
Lower 95% CI	7.552	6.711	5.384	5.131	6.653
Upper 95% CI	8.787	9.586	8.356	9.707	10.64

Figure 6.2. The effect of siRNA-mediated knockdown of EZH2 on the telomere length distribution at 17p, 18q and XpYp. kC1B cells were transfected with 25nm siRNA targeted against EZH2 mRNA using DharmaFECT 1. EZH2-1, -2, -3 & -4 represent four biological replicates independently transfected. Each replicate was successively transfected three times at 96h intervals. 96 hours after the third transfection DNA was extracted. STELA was then performed at 17p, 18q and XpYp using the 17pseqrev1, 18qrev4M and XpYpE primers respectively. Telomere length distributions were then quantified using Phoretix software (Nonlinear dynamics)

6.3.4 Telomere length defects caused by siRNA mediated knockdown of DAXX

Once efficient gene knockdown was confirmed the effect of the chromatin remodeler depletion on telomere length in the kC1B cells was analyzed using STELA at the 17p, 18q, and XpYp chromosome ends. Firstly the telomere length profiles of untreated cells that were grown in parallel to the cells subject to knockdown were analyzed at 17p, 18q and XpYp (Appendix fig. A1). 17p had a mean telomere length of 8.831kb whereas 18q and XpYp had mean telomere lengths of 10.19kb and 7.992kb respectively. The kC1B telomere length distributions were much more heterogeneous than the HT1080 cl. 2 telomere length distributions at all three chromosome ends analysed.

In contrast to the aberrant telomere length phenotypes seen in HT1080 cl.2 cells, siRNA-mediated depletion of the HMTase EZH2 in the kC1B cells did not cause any alterations in telomere length (fig. 6.2). Mean 17p telomere length did not differ between any of the EZH2 knockdown replicates and untreated cells as determined by an analysis of variance (ANOVA (P=0.7708) (fig. 6.2a). Similarly mean 18q and XpYp telomere length in the EZH2 knockdown replicates did not differ from what as seen in the untreated cells (18q – P=0.4551, XpYp – P=0.5828) (fig. 6.2b&c). Images of the 17p, 18q and XpYp STELA blots for the EZH2 knockdown replicates are presented in Appendix figures 2-4.

Telomere length distributions in ATRX-deficient cells were analysed as a positive control for the assay as ATRX depletion in another keratinocyte holoclone caused a striking loss of telomere length. Surprisingly in kC1B cells loss of ATRX did not result in any significant telomere length alterations (fig. 6.3). All the ATRX knockdown replicates displayed a lower

mean 17p telomere length compared to the untreated cells however none of these differences were statistically significant (P=0.8117) (fig. 6.3a). A more pronounced difference in mean 18q telomere length was observed, particularly between the untreated and ATRX-4 knockdown replicate cells where the difference in mean telomere length was 1.109kb however, like at the 17p telomere, these differences were not significant (P=0.4215) (fig. 6.3b). This was also the case at the XpYp telomere were negligible, insignificant differences in telomere length was observed between replicates (P=0.4744) (fig. 6.3c). Images of the 17p, 18q and XpYp STELA blots for the ATRX knockdown replicates are presented in Appendix figures 5-7.

In contrast, the depletion of DAXX in the kC1B cells caused significant alterations in telomere length at 17p, 18q and XpYp (fig. 6.4). There was an abundance of 17p telomeres greater than 15kb in length in the untreated cells however after siRNA-mediated depletion of DAXX the presence of these very long telomeres was greatly diminished. Furthermore there was a greater frequency of very short telomeres in three of the DAXX knockdown replicates (DAXX-1, DAXX-3 & DAXX-4) (fig. 6.4a). These alterations in the 17p telomere length distributions caused a striking reduction in mean 17p telomere length: DAXX-1, DAXX-3 & DAXX-4 show a loss in telomere length of 2.203kb, 2.964kb and 1.898kb respectively. When compared to the mean 17p telomere length in the untreated cells this reduction in length is highly significant (DAXX-1 – P=0.0003, DAXX-3 – P<0.0001, DAXX-4 – P=0.0037). The same DAXX deficient replicates showed a similarly reduced frequency of very long 18q telomeres and an increase in very short 18q telomeres (fig. 6.4b). Again this caused a highly significant reduction in mean 18q telomere length compared to untreated 18q telomeres: DAXX-1 showed a mean 18q telomere length reduction of 3.442kb (P<0.0001) whereas DAXX-3 and DAXX-4 showed loss of 2.387kb and 2.765kb respectively (DAXX-3: P=0.0011, DAXX-4:

P=0.0004). Although DAXX-2 cells displayed a subtle telomere shortening phenotype at 17p, this was not statistically significant (P=0.0958). At 18q however a striking 3.661kb loss in telomere length was observed in these cells (P<0.0001). This same replicate also showed significant telomere shortening at XpYp where a loss of 2.701kb was observed (P=0.0002) (fig. 6.4c), this phenotype was not present in DAXX-1, -3 and -4.

a

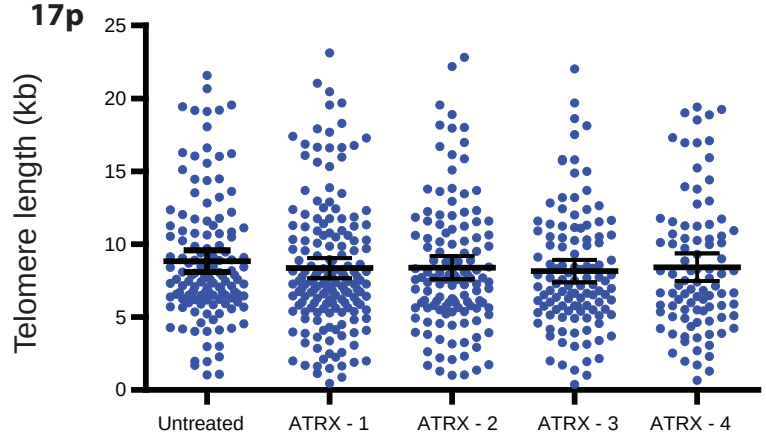

Mean tel length (kb)	8.831	8.358	8.397	8.159	8.426
Lower 95% CI	8.647	7.675	7.602	7.399	7.477
Upper 95% CI	10.17	9.042	9.193	8.919	9.374

b

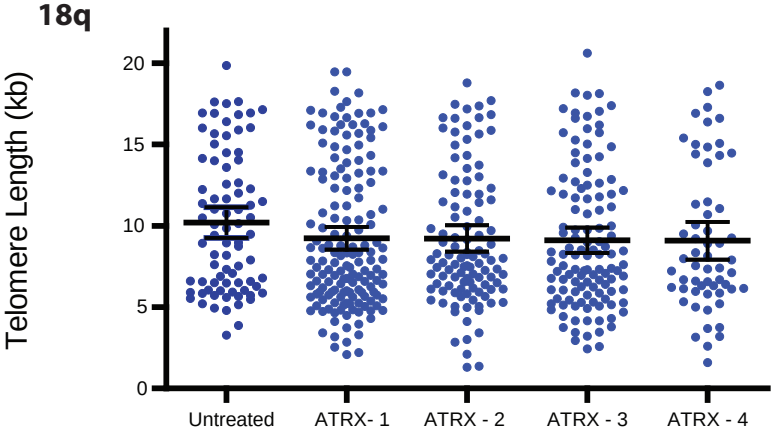

Mean tel length (kb)	10.19	9.233	9.222	9.113	9.081
Lower 95% CI	8.225	8.538	8.413	8.338	7.923
Upper 95% CI	10.46	9.927	10.03	9.887	10.24

c

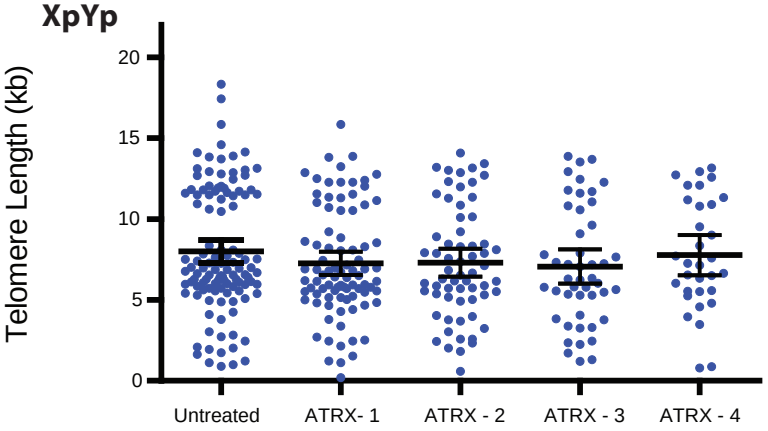

Mean tel length (kb)	7.992	7.268	7.304	7.066	7.773
Lower 95% CI	7.552	6 548	6.436	6.005	6.529
Upper 95% CI	8.787	7.989	8.171	8.127	9.016

Figure 6.3. The effect of siRNA-mediated knockdown of ATRX on the telomere length distribution at 17p, 18q and XpYp. kC1B cells were transfected with 25nm siRNA targeted against ATRX mRNA using DharmaFECT 1. ATRX-1, -2, -3 & -4 represent four biological replicates independently transfected. Each replicate was successively transfected three times at 96h intervals. 96 hours after the third transfection DNA was extracted. STELA was then performed at 17p, 18q and XpYp using the 17pseqrev1, 18qrev4M and XpYpE primers respectively. Telomere length distributions were then quantified using Phoretix software (Nonlinear dynamics)

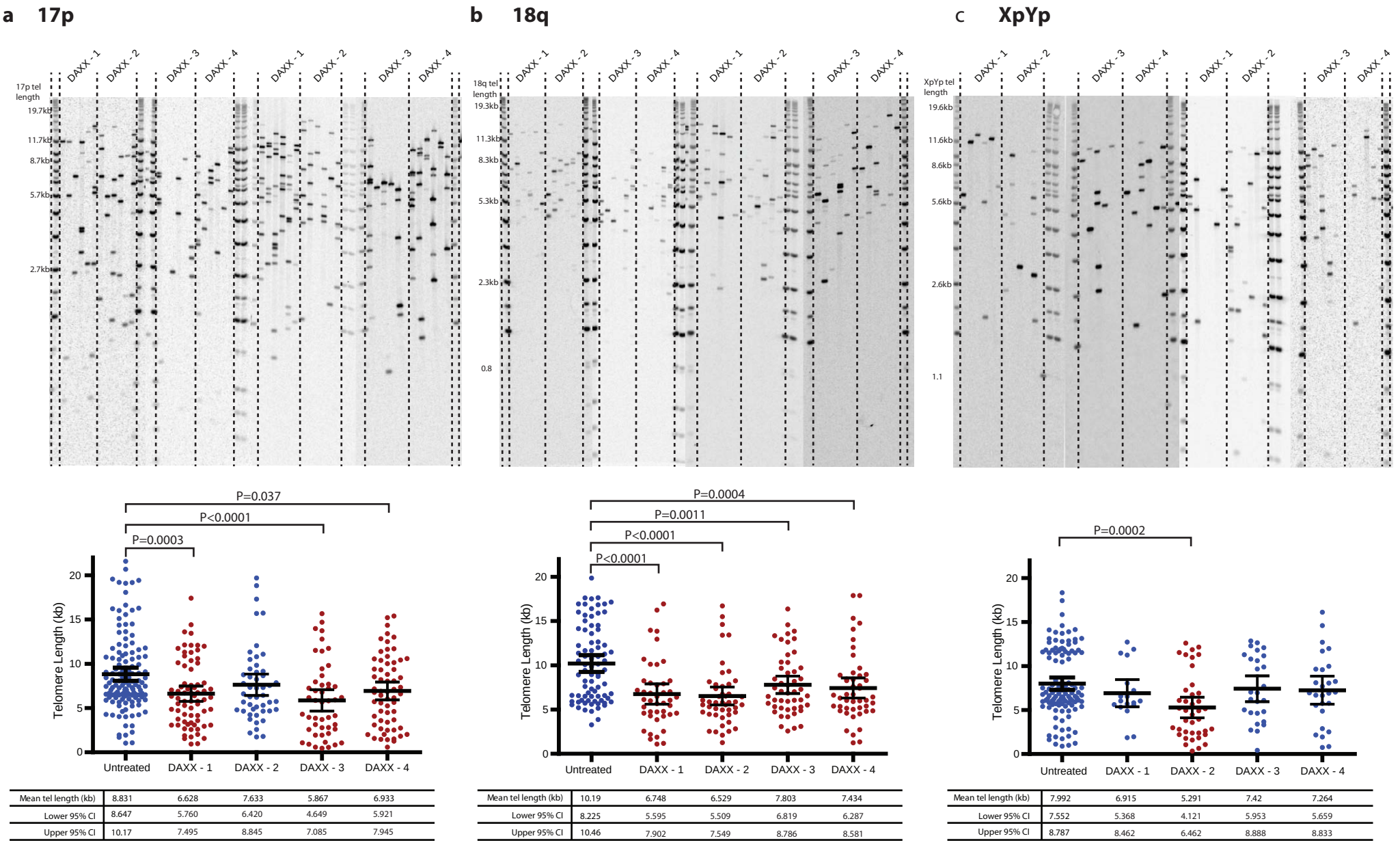

Mean tel length (kb)	8.831	6.628	7.633	5.867	6.933
Lower 95% CI	8.647	5.760	6.420	4.649	5.921
Upper 95% CI	10.17	7.495	8.845	7.085	7.945

Mean tel length (kb)	10.19	6.748	6.529	7.803	7.434
Lower 95% CI	8.225	5.595	5.509	6.819	6.287
Upper 95% CI	10.46	7.902	7.549	8.786	8.581

Mean tel length (kb)	7.992	6.915	5.291	7.42	7.264
Lower 95% CI	7.552	5.368	4.121	5.953	5.659
Upper 95% CI	8.787	8.462	6.462	8.888	8.833

Figure 6.4. The effect of siRNA-mediated knockdown of DAXX on the telomere length distribution at 17p, 18q and XpYp. kC1B cells were transfected with 25nm siRNA targeted against DAXX mRNA using DharmaFECT 1. DAXX-1, -2, -3 & -4 represent four biological replicates independently transfected. Each replicate was successively transfected three times at 96h intervals. 96 hours after the third transfection DNA was extracted. STELA was then performed at (a)17p, (b) 18q and (c) XpYp using the 17pseqrev1, 18qrev4M and XpYpE primers respectively. Telomere length distributions were then quantified using Phoretix software (Nonlinear dynamics)

6.3.5 Telomere shortening in DAXX deficient cells is less pronounced at the 2p and 16p chromosome ends

Because of the dramatic telomere shortening phenotype observed at all three telomeres tested, the effect of DAXX deficiency at other chromosome ends was analysed. 2p and 16p STELAs were performed in the same manner as for 17p, 18q and XpYp. Mean 2p telomere length was lower in all of the DAXX deficient replicates, the most pronounced and only significant shortening phenotype was in the DAXX-4 replicate were a 0.98kb loss in 2p telomere length was observed (P=0.0143) (fig. 6.5a). No telomere shortening phenotype was seen at 16p. Slight differences in length were present but these were negligible (fig. 6.5b).

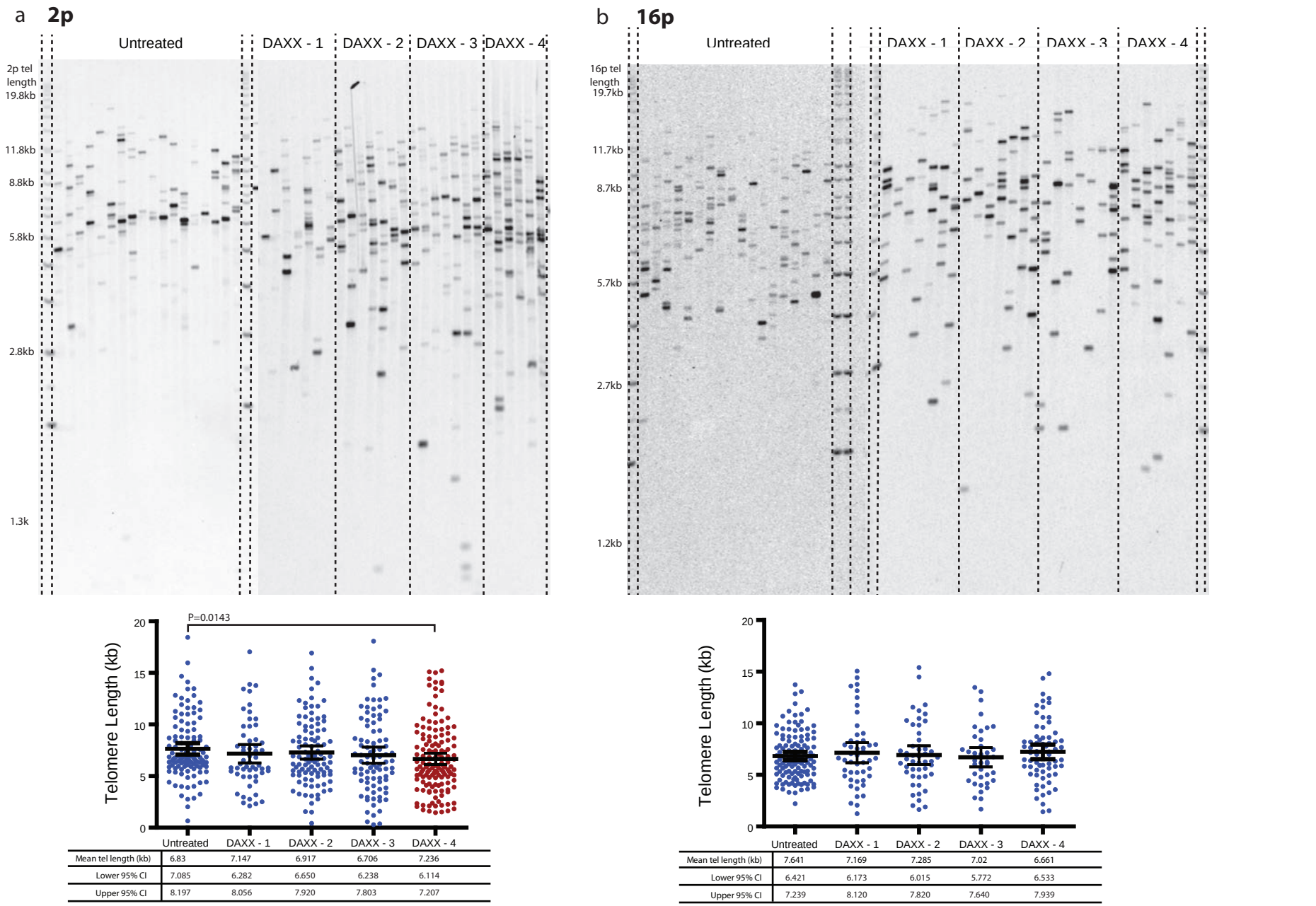

Figure 6.5. The effect of siRNA-mediated knockdown of DAXX on the telomere length distribution at 2p and 16p. kC1B cells were transfected with 25nm siRNA targeted against DAXX mRNA using DharmaFECT 1. DAXX-1, -2, -3 & -4 represent four biological replicates independently transfected. Each replicate was successively transfected three times at 96h intervals. 96 hours after the third transfection DNA was extracted. STELA was then performed at (a) 2p and (b) 16p using the 2p2 and 16prev1 primers respectively. Telomere length distributions were then quantified using Phoretix software (Nonlinear dynamics)

6.3.6 The rate of telomere shortening in DAXX-deficient kC1B cells

The telomere shortening phenotypes observed in DAXX deficient cells were seen after 8 days or 9-11 population doublings. As previously mentioned, the RNAi procedure involved three successive transfections at 96 hour intervals with DAXX-targeting siRNA. DNA extracted 96 hours after the third transfection was used to analyse the telomere lengths described above. DNA was also extracted 96 hours after the first transfection (3-4 PDs) and 96 hours after the second transfection (6-8 PDs). This DNA was used in STELA reactions to determine any telomere shortening phenotype at the 17p, 18q and XpYp telomeres in DAXX-deficient cells which had undergone fewer population doublings (PDs). Combining the telomere length profiles taken after each successive siRNA transfection for a given cell populations allows the pattern of telomere shortening over time to be observed.

Fig. 6.6 shows the 17p telomere length distributions of untreated and DAXX-deficient kC1B cells at 96h intervals. As expected the untreated cells show very little variation in 17p telomere length between time points (fig. 6.6a) however the DAXX-1 and -3 replicates showed a progressive telomere shortening (fig. 6.6b (I & iii)). These replicates had comparable mean 17p telomere length to the untreated cells after one DAXX-targeting siRNA transfection however after 10-11 PDs in low DAXX conditions 17p telomeres were significantly shorter (fig. 6.6b (i & iii)). The 17p telomere erosion rate in DAXX-1 cells after two siRNA transfections was 227bp/PD however this increased after the third siRNA transfection (271bp/PD). The erosion rate in the DAXX-3 cells was even greater: after two siRNA transfections it was 328bp/PD and increased to 488bp/PD after the third siRNA transection at which point the cells had undergone 10.31 PDs (fig. 6.6b (I & iii)). PD 9.57 DAXX-4 cells also displayed significantly shorter 17p telomeres compared to DAXX-4 cells

subjected to one siRNA transfection (PD 2.7) however this was after a slight increase in mean 17p telomere length in the PD 6.24 DAXX-4 cells (fig. 6.6b(iv)). 17p telomere length in DAXX-2 cells showed little variation between time points, although there was a slight increase in length after 6.32 PDs this was not significant (fig. 6.6b (ii)).

Unexpectedly, the mean 18q telomere length varied significantly between the DNA extraction time points: the mean 18q telomere length was significantly higher in untreated kC1B cells which had undergone 10.92 population doublings (PDs) than in cells that had only undergone 6.73 PDs (P=0.0138) (fig. 6.7a). This result was unexpected and may be due to inherent variation in the 18q assay mentioned in the previous chapter. In all four DAXX knockdown replicates 18q telomeres became progressively shorter as cells continued to divide (fig. 6.7b). This loss of 18q telomere length was most dramatic in the DAXX-1 cells: Cells which had been subject to two siRNA transfections (PD 6.71) showed a loss in mean 18q telomere length of 2.553kb compared to PD 2.99 cells subject to one siRNA transfection resulting in an erosion rate of 686bp/PD (fig. 6.7b (i). The rate of 18q telomere erosion then slowed to 232bp/PD after the third DAXX-targeting siRNA transfection resulting in an overall loss of 3.502kb in PD 10.78 cells compared to PD 2.9 cells (fig. 6.7b (i)).

At XpYp the rate of telomere erosion is more variable. Mean XpYp telomere length was very similar in the untreated kC1B cells between time points (fig. 6.8a). DAXX-1 and -2 XpYp telomeres became progressively shorter as the cells divided although this only resulted in statistically significant differences in mean XpYp telomere length between time points in DAXX-2 cells (fig. 6.8b (i & ii)). In the DAXX-3 and -4 replicate cells, mean XpYp telomeres were significantly shorter after 8 days of low DAXX levels (6.54 and 6.24 PDs respectively) however as the cells divided further mean XpYp telomere length increased (fig. 6.8b (iii & iv).

17p

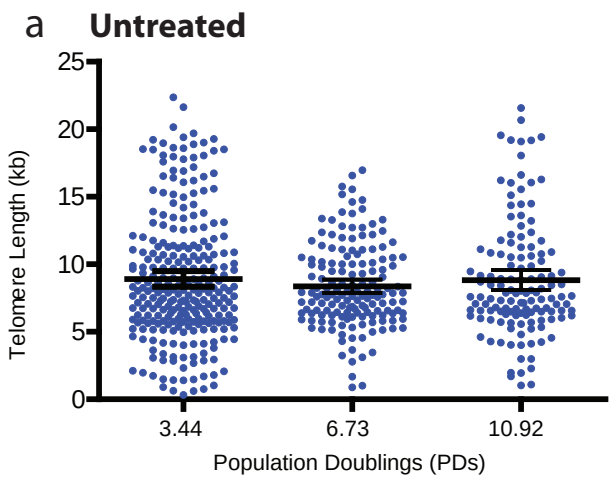

Mean tel length (kb)	8.916	8.367	8.831
Lower 95% CI	8.350	7.877	8.091
Upper 95% CI	9.481	8.856	9.571

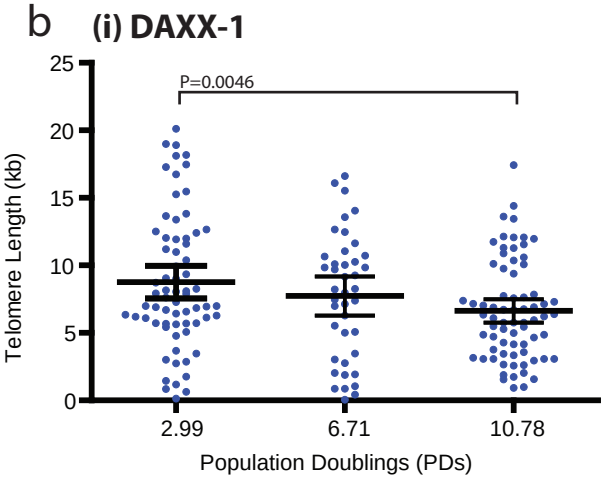

Mean tel length (kb)	8.754	7.731	6.628
Lower 95% CI	7.550	6.278	5.760
Upper 95% CI	9.959	9.184	7.495

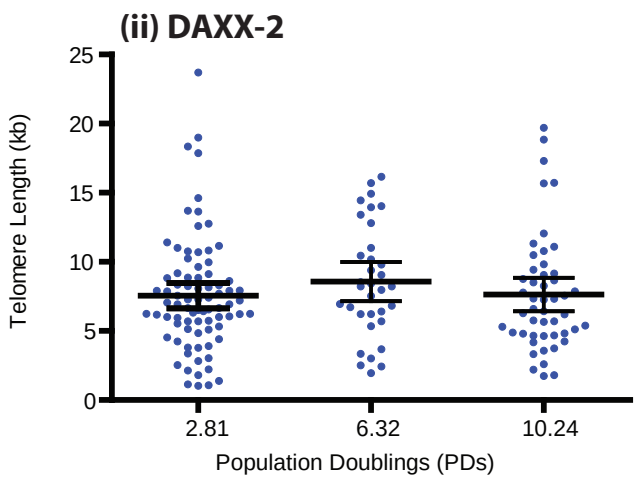

Mean tel length (kb)	7.551	8.574	7.633
Lower 95% CI	6.637	7.158	6.420
Upper 95% CI	8.466	9.990	8.845

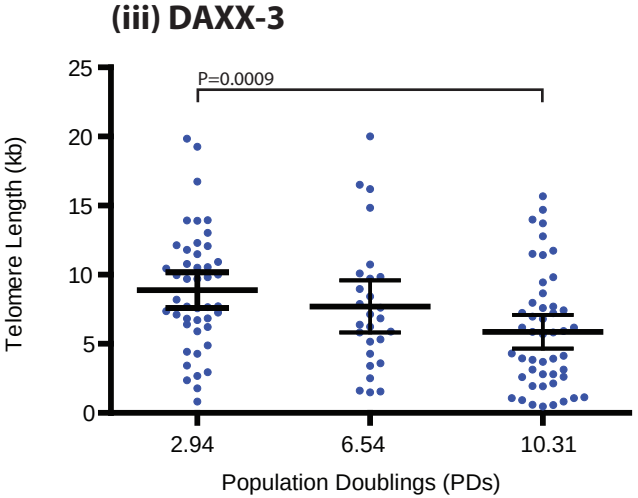

Mean tel length (kb)	8.888	7.708	5.867
Lower 95% CI	7.592	5.825	4.649
Upper 95% CI	10.18	9.591	7.085

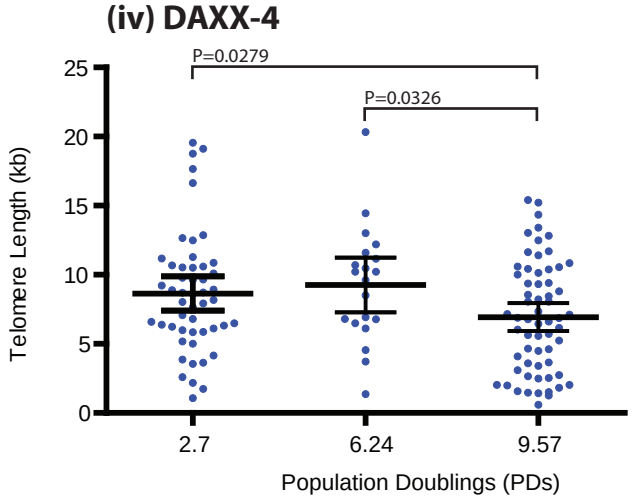

Mean tel length (kb)	8.641	9.259	6.933
Lower 95% CI	7.404	7.287	5.921
Upper 95% CI	9.878	11.23	7.945

Figure 6.6. Alterations in telomere length distributions at 17p in untreated and DAXX-deficient kC1B cells cultured for 8 days. Three successive siRNA transfections were perfored at 96h intervals. 96 hours after each siRNA transfection DNA was extracted from the DAXX- knockdown replicates and untreated cells. 17p STELA was performed and telomere length distributions were then quantified using Phoretix software (Nonlinear dynamics). The resulting telomere length distributions were plotted against population doubling. Any significant differences in mean telomere length between untreated kC1B cells at the different time points are stated as measured by t-test are stated.

18q

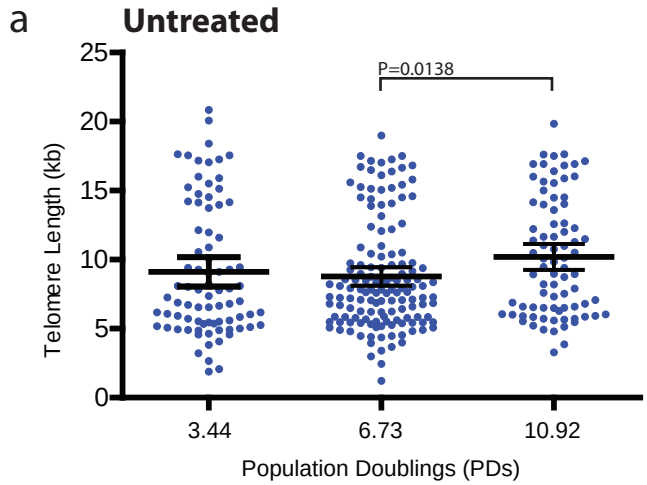

Mean tel length (kb)	9.107	8.780	10.19
Lower 95% CI	8.047	8.115	9.252
Upper 95% CI	10.17	9.444	11.14

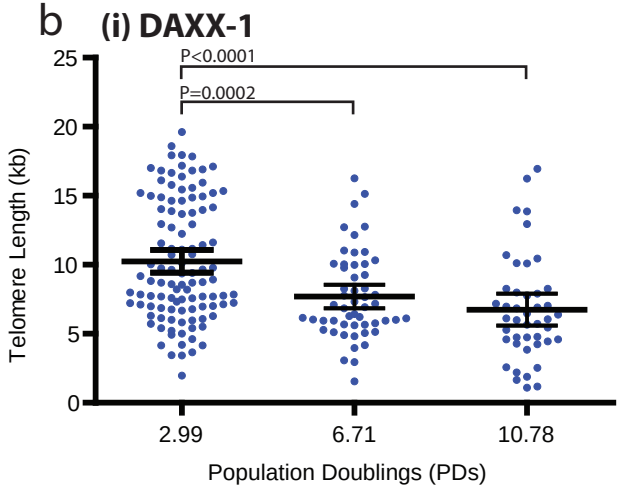

Mean tel length (kb)	10.25	7.697	6.748
Lower 95% CI	9.421	6.835	5.595
Upper 95% CI	11.08	8.558	7.902

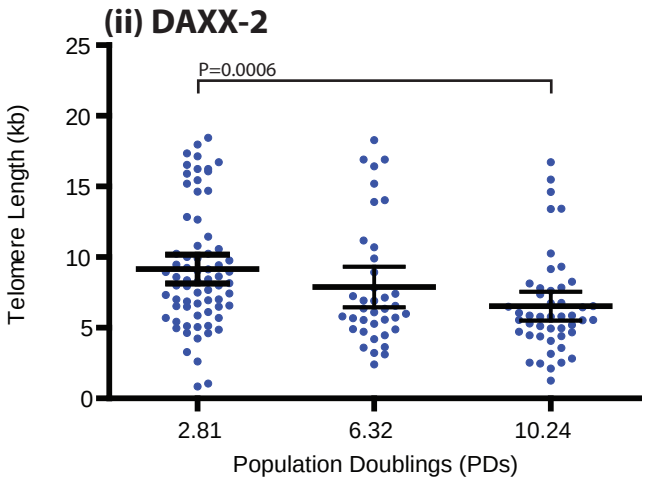

Mean tel length (kb)	9.164	7.892	6.529
Lower 95% CI	8.141	6.456	5.509
Upper 95% CI	10.19	9.328	7.549

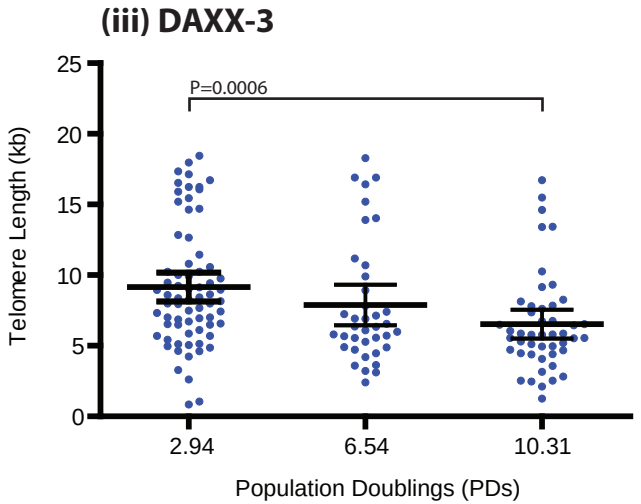

Mean tel length (kb)	9.798	8.711	7.803
Lower 95% CI	8.730	7.748	6.819
Upper 95% CI	10.87	9.674	8.786

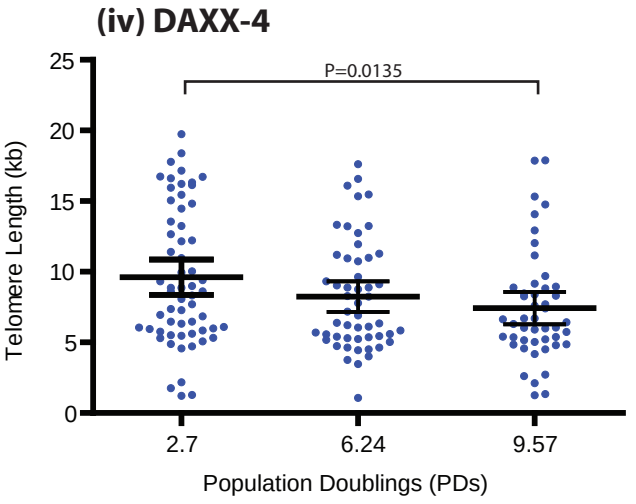

Mean tel length (kb)	9.613	8.246	7.434
Lower 95% CI	8.364	7.166	6.287
Upper 95% CI	10.86	9.325	8.581

Figure 6.7. Alterations in telomere length distributions at 18q in untreated and DAXX-deficient kC1B cells cultured for 8 days. Three successive siRNA transfections were perfored at 96h intervals. 96 hours after each siRNA transfection DNA was extracted from the DAXX- knockdown replicates and untreated cells. 18q STELA was performed and telomere length distributions were then quantified using Phoretix software (Nonlinear dynamics). The resulting telomere length distributions were plotted against population doubling. Any significant differences in mean telomere length between untreated kC1B cells at the different time points are stated as measured by t-test are stated.

XpYp

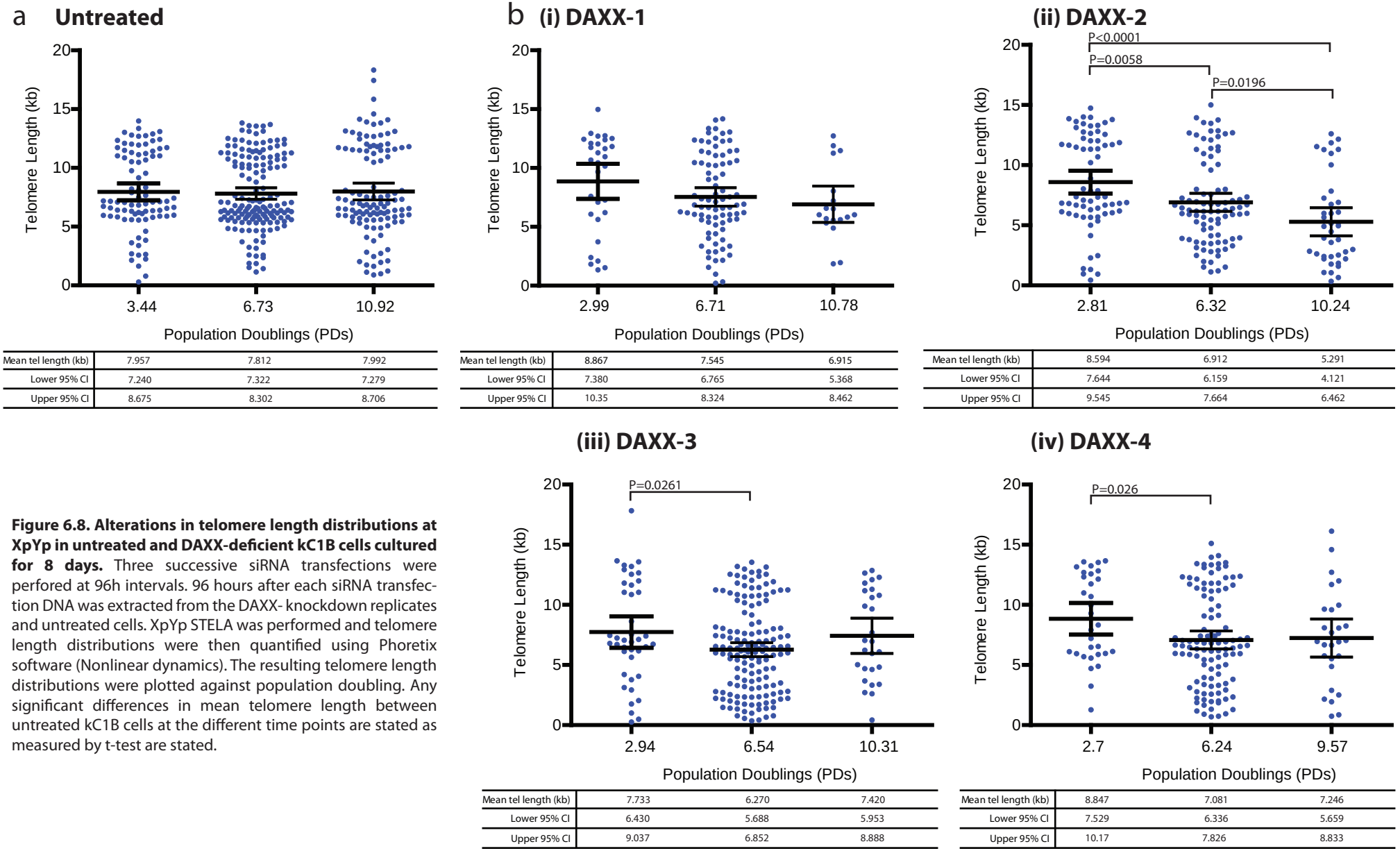

Mean tel length (kb)	7.957	7.812	7.992
Lower 95% CI	7.240	7.322	7.279
Upper 95% CI	8.675	8.302	8.706

Mean tel length (kb)	8.867	7.545	6.915
Lower 95% CI	7.380	6.765	5.368
Upper 95% CI	10.35	8.324	8.462

Mean tel length (kb)	8.594	6.912	5.291
Lower 95% CI	7.644	6.159	4.121
Upper 95% CI	9.545	7.664	6.462

Mean tel length (kb)	7.733	6.270	7.420
Lower 95% CI	6.430	5.688	5.953
Upper 95% CI	9.037	6.852	8.888

Mean tel length (kb)	8.847	7.081	7.246
Lower 95% CI	7.529	6.336	5.659
Upper 95% CI	10.17	7.826	8.833

Figure 6.8. Alterations in telomere length distributions at XpYp in untreated and DAXX-deficient kC1B cells cultured for 8 days. Three successive siRNA transfections were perfored at 96h intervals. 96 hours after each siRNA transfection DNA was extracted from the DAXX- knockdown replicates and untreated cells. XpYp STELA was performed and telomere length distributions were then quantified using Phoretix software (Nonlinear dynamics). The resulting telomere length distributions were plotted against population doubling. Any significant differences in mean telomere length between untreated kC1B cells at the different time points are stated as measured by t-test are stated.

6.3.7 Identifying mechanism responsible for telomere shortening in DAXX-deficient cells

The mechanism by which DAXX deficiency causes the dramatic telomere shortening phenotype in the kC1B cells is unknown. A mutation analysis method was developed in which very short telomeres generated in the DAXX-deficient cells where isolated and sequenced. By sequencing these short telomeres the distribution of telomere variant repeats could be determined which may shed light on the mechanism responsible for telomere shortening.

The proximal 1-3kb of human telomeres contains highly variable interspersion patterns of the canonical TTAGGG repeat sequence with telomere repeat variants (TVRs) (Baird et al. 2000; Baird et al. 1995; Coleman *et al.* 1999). Numerous TVRs exist and how these are distributed throughout a telomere varies between different chromosome ends and telomeric alleles of the same chromosome end (Baird et al. 1995).

Comparing the distribution patterns of TVRs between very short telomeres and unaffected telomeres could offer insight into the mutational mechanism responsible for the telomere length loss. For example recombination events occurring within the TVR tract, or deletion events, will display distinct changes in the TVR pattern. Additionally this comparison may also enable the identification of the progenitor telomeric allele from which the very short telomeres are generated.

In initial experiments, attempts were made to reamplify 17p STELA products directly from the original PCR reactions. PCR products were generated in these reamplification reactions however these PCR products did not correspond with the size of the telomeres on the STELA blot (appendix fig. 8). It is possible that the products observed may be generated from other additional background PCR products present in the STELA PCR reaction. Attempts were therefore made to purify STELA products prior to reamplification.

6.3.8 Purification of STELA products

Using electro-elution PCR products can be extracted from a gel by their capture on a dialysis membrane. This approach was used to isolate and purify very short telomeres at the XpYp telomere. This telomere was chosen because of the abundance of telomere adjacent primers closer to the telomeric repeats than the XpYpC primer used in the STELA reactions, which allowed more scope for nested PCR primer combinations (fig. 6.9b).

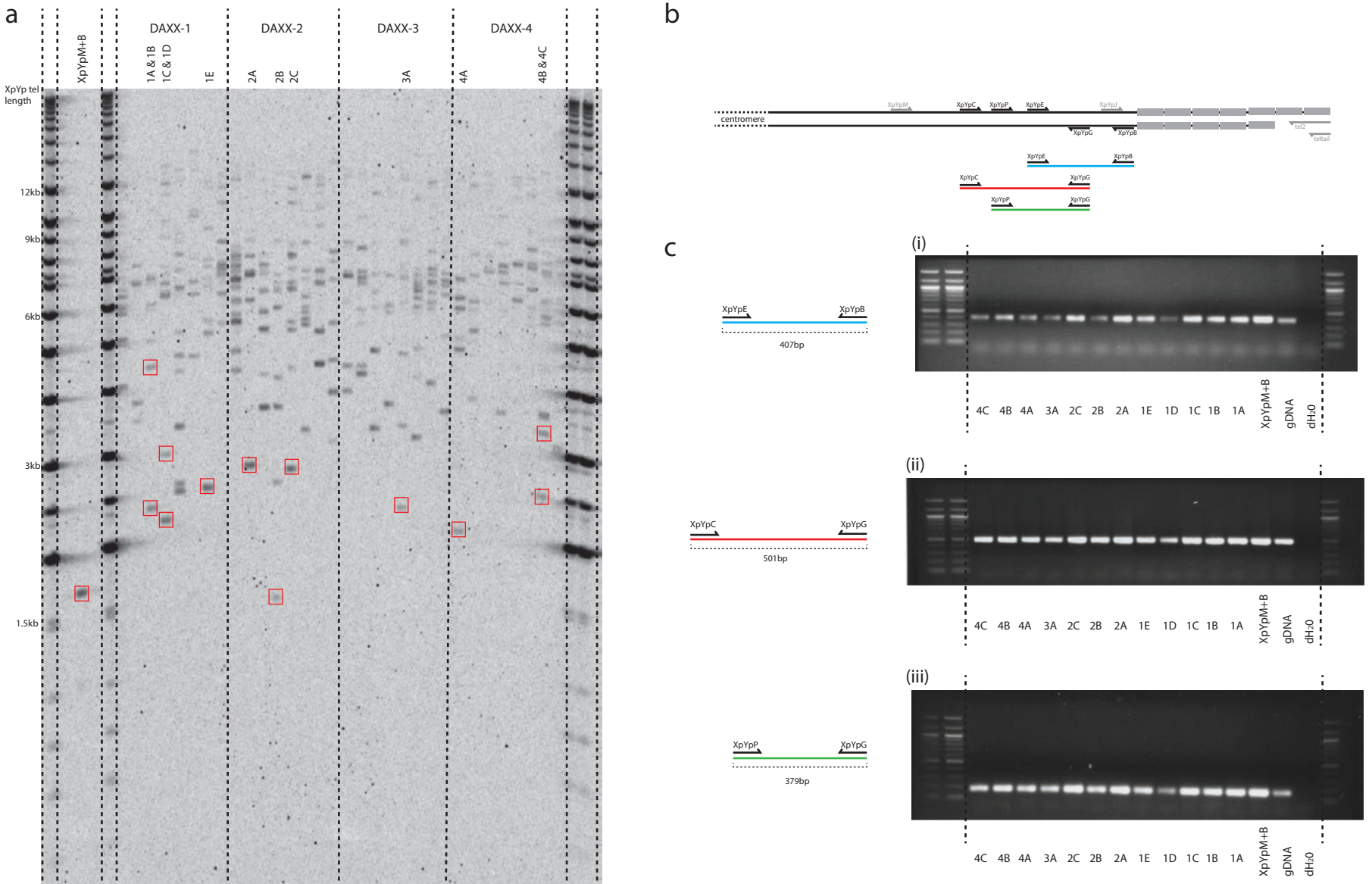

Figure 6.9. Isolation of STELA PCR products amplified from very short XpYp telomeres by electro-elution. (a) XpYp STELA was performed with XpYpC as the telomere adjacent primer (see (b)) using DAXX -1, -2, -3 & -4 DNA to determine PCR products amplified from very short XpYp telomeres (highlighted by red boxes) Also highlighted is XpYpM+B,a PCR product generated from XpYpM and XpYpB. These PCR products were isolated from the gel onto a dialysis membrane by electro-elution. (b) Representation of XpYp telomere. Positions of primers used for the initial STELA in (a) and subsequent analysis of electro-elution success are stated. (c) To determine whether PCR products had been successfully isolated 2µl of each eluted product was added to PCR reactions containing either XpYpE & XpYpB (i), XpYpC & XpYpG (ii) or XpYpP & XpYpG (iii). gDNA (positive control) was also added to PCR reactions containing each of the primer combinations as was dH20 (neagative control)

Initially a STELA-PCR was performed with some modifications: A larger reaction volume was used (20μl) and XpYpC was used as the telomere adjacent primer as opposed to XpYpE. 4μl of this reaction was resolved on a gel, blotted and visualised to determine not only the presence of very short telomeres but also their location on the gel relative to the DNA ladder (fig. 6.9a). This was necessary as when the remaining 16μl of the STELA reaction was resolved on another gel for electro-elution the STELA product that amplifies to an estimated 1-10 pg would not be visible and thus only the DNA ladder would be visible under a handheld UV lamp. Therefore the position on the gel where a well should be made (below the PCR product) could be judged by using the DNA ladder. Twelve telomeres of differing sizes were chosen to be isolated (fig. 6.9a) as well as a positive control PCR product: this was an amplicon generated by the XpYpB and XpYpM primers that could be visualised on the gel and was used to ensure that the electro-elution process worked. After attempting to isolate the PCR products from the gel the success of electro-elution was determined by a nested PCR in which 2μl of each isolated product was added to reactions containing XpYpE and XpYpB (fig. 6.9c (i)). PCR product of the correct size (407bp) was generated confirming that the electro-elution had been successful. When gDNA was used as the template for the nested PCR the same 407bp product was amplified and a dH20-template negative control generated no PCR product confirming that the product generated in the test samples was not a result of contamination and was in fact amplification of the isolated STELA products. Exactly the same results were obtained in other nested PCRs in which different XpYp primer combinations were used (fig. 6.9c (ii & iii)).

Initial attempts to re-amplify purified STELA products included using different primer combinations, changing $MgCl_2$ concentration, adding additional PCR cycles and also altering

the annealing temperature (fig. 6.10b&c). However these did not generate sufficient products of the correct size for sequence analysis. Therefore to generate enough reamplified PCR product each eluted STELA product was reamplified in multiple 50µl reactions. These reactions were combined and resolved (fig. 6.10d). Reamplification of only three STELA products produced enough PCR product that could be successfully sequenced. Two of these reamplified fragments derived from DAXX-deficient cells and one from untreated cells. Reamplified PCR product was gel excised and purified before being sequenced from the telomere-adjacent DNA using XpYpJ and from the telomere end using tel2 as the sequencing primer (fig. 6.11a). Sequencing from both ends of the telomere was performed as neither sequencing primer alone could sequence the entire telomere. The sequences generated from XpYpJ and tel2 were put into a single contig by using a specific telomere repeat variant pattern as a landmark. The 2B and U (untreated) PCR products were completely sequenced (fig. 6.11b). Because the 1A telomere was longer the XpYpJ- and tel2-derived sequences did not overlap and so this telomere was not fully sequenced. Unfortunately the XpYp telomere in these kC1B cells does not contain a complex TVR distribution interspersion pattern and thus was relatively uninformative for mutational analysis. No differences were seen between the TVR distributions of the individual telomeres (fig. 6.11b). This is consistent with the idea that the telomeric deletion mutation was not because of inter-chromosomal recombination events as no new TVRs appeared, but instead may involve a deletion within the TTAGGG repeat region and subsequent healing with telomerase.

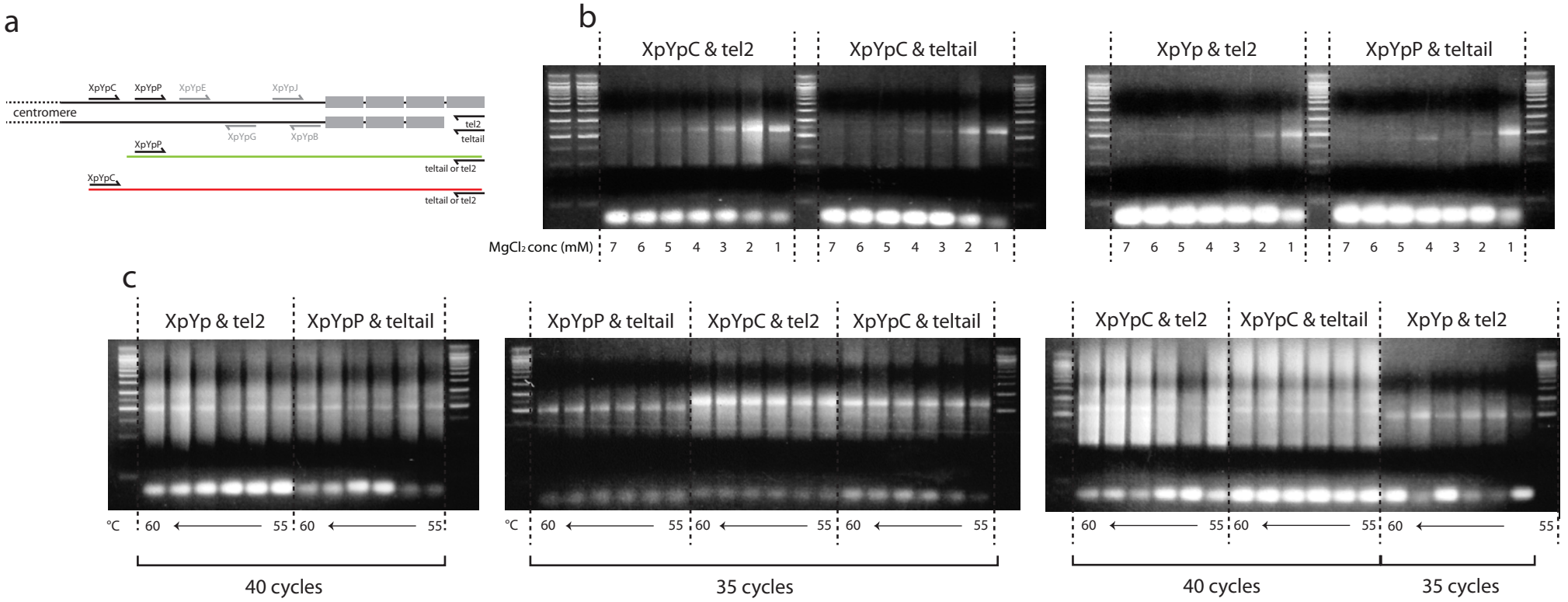

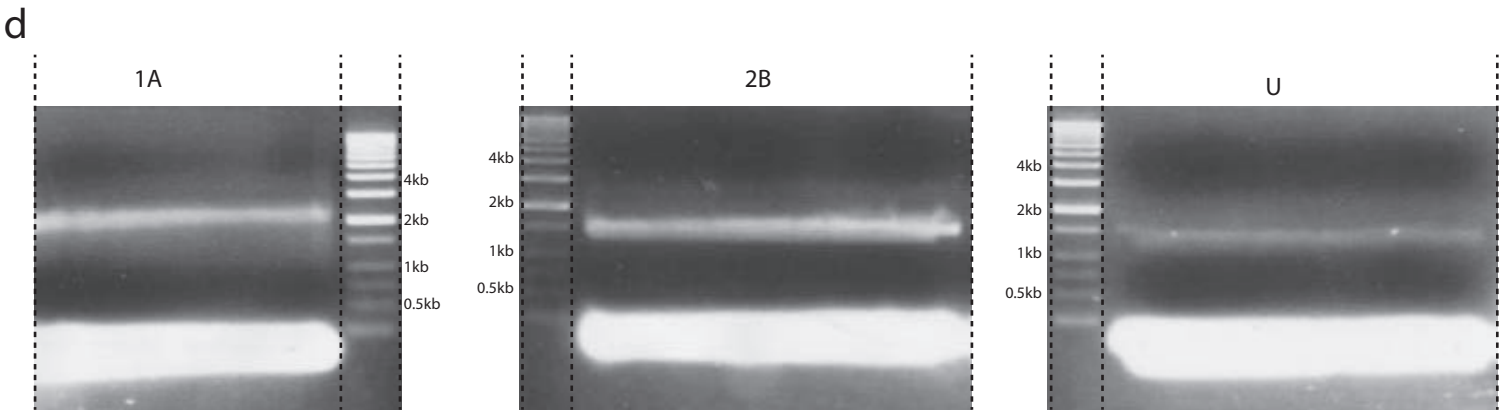

Figure 6.10. Optimisation of reamplification PCR for reamplifying death wishes. (a) Representation of the XpYp chromosome end. The primer combinations used for reamplification of eluted STELA products are highlighted. (b) Reamplifid STELA product was added to PCR reactions containing increasing MgCl2 concentrations (1-7mM) and one of four primer combinations: XpYpC & teltail, XpYpC & tel2, XpYpP & teltail or XpYpP & tel2. (c) Reamplifid STELA product was added to sets of six PCR reactions containing either XpYpC & teltail, XpYpC & tel2, XpYpP & teltail or XpYpP & tel2. These PCR reaction sets were then subject to PCR with an annealing temperature gradient ranging from 55-60°C for 35 cycles. This process was repeated with 40 PCR cycles (d) STELA PCR products 1A, 2B and U (untreated) were added to six 50µl reactions containing XpYpC & teltail primers with 2mM MgCl2. Reactions were subject to PCR for 35 cycles with an annealing teperature of 60°C. The six reactions were combined and resolved in large wells in a 1% TAE agarose gel and visualised.

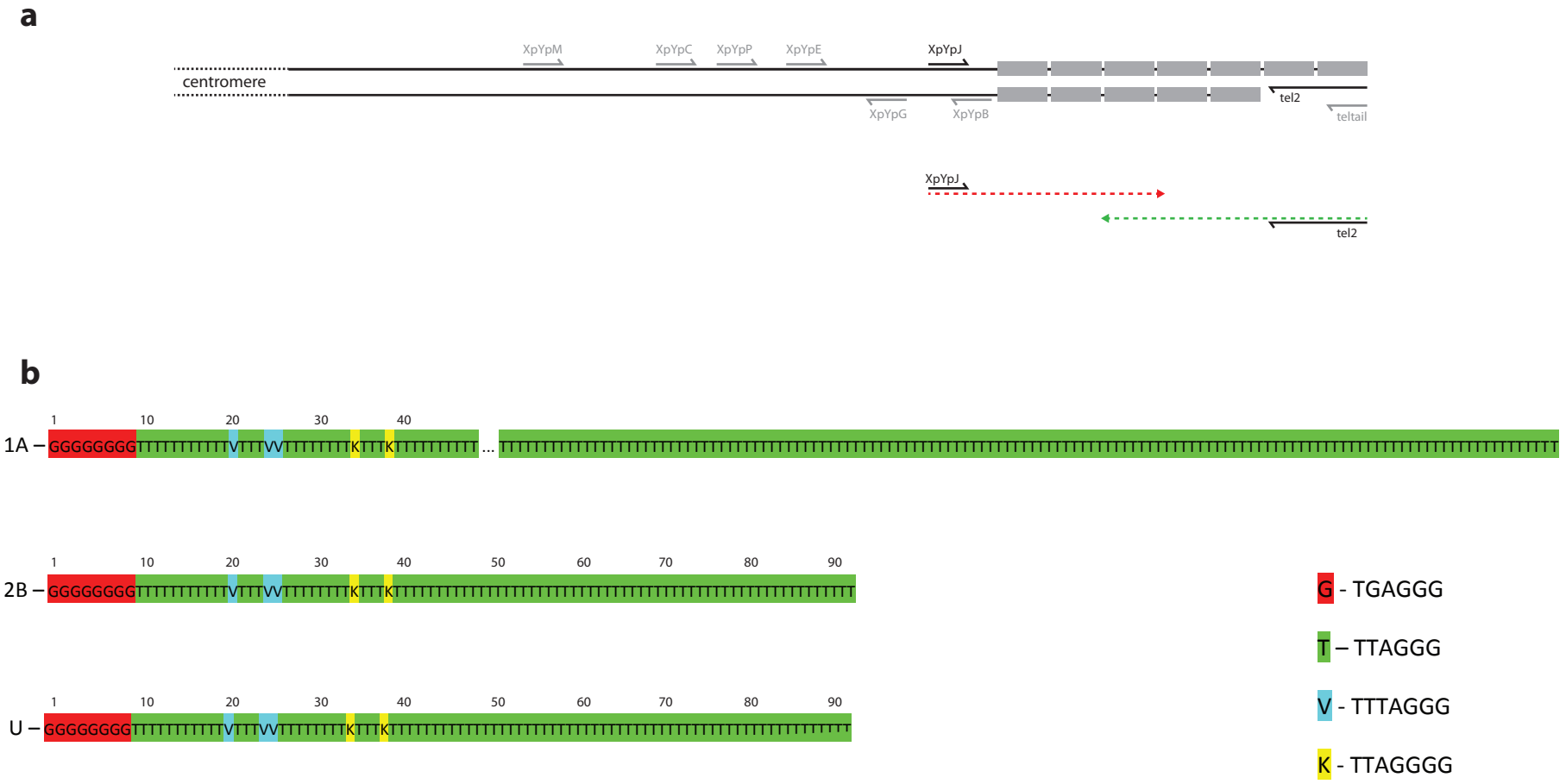

Figure 6.11. Telomere repeat variants (TVR) distributions of very short XpYp telomeres in untreated and DAXX deficient kC1B cells. (a) Representation of XpYp telomere, XpYpJ and tel2 highlighted were used to sequence the telomere. (b) Reamplified PCR product was gel excised and sequecned from the subtelomere using XpYpJ and from the distal end of the telomere using tel2. The distribution of telomere variant repeats observed after sequencing is summarised

6.3.9 DAXX deficiency causes a subtle increase in telomere-to-telomere fusion frequency

In addition to identifying aberrant telomere length phenotypes in the DAXX-deficient kC1B cells single molecule telomere fusion assays were performed to detect and characterise telomere-to-telomere fusions events. The PCR-based fusion assay detects fusions between the 17p and XpYp telomeres as well as the 16p telomere family (16p, 1p. 9p, 12p, 15q, XqYq, 2q14 (interstitial)) and the 21q telomere family (21q, 1q, 2q, 5q, 6q, 6p, 8p, 10q, 13q, 17q, 19p, 19q, 22q, 2q13 (interstitial)). The assay was performed using the same DNA as was used for the STELA analysis: either untreated kC1B DNA cells or DNA extracted from kC1B cells successively transfected three times with DAXX-targeting siRNAat 96 hour intervals. HEK293 DNA was also used as a positive control. 50ng DNA (≈8300 diploid genome equivalents) was added to fusion PCR reactions containing the fusion primers XpYpM, 21q1, 17p6 and 16p1 (fig. 6.12a). Amplification of any fusion events was then detected by hybridization using radioactively labelled probes specific to these chromosome ends.

No telomere fusion events of any kind were seen in the untreated kC1B cells: A total of 483,000 genome equivalents of untreated kC1B DNA was analysed in telomere fusion assays and no events that were consistent with telomere fusion could be detected (fig. 6.12b, c & d). This represents an estimated frequency as calculated using the modified Wald method (Agresti and Coull 1998) of 4.1×10^{-6} $\pm 9.9 \times 10^{-6}$. Fusion events were readily detected in a positive control DNA extracted from HEK293 cells that contain fusion events (Capper, Britt-Compton et al. 2007).

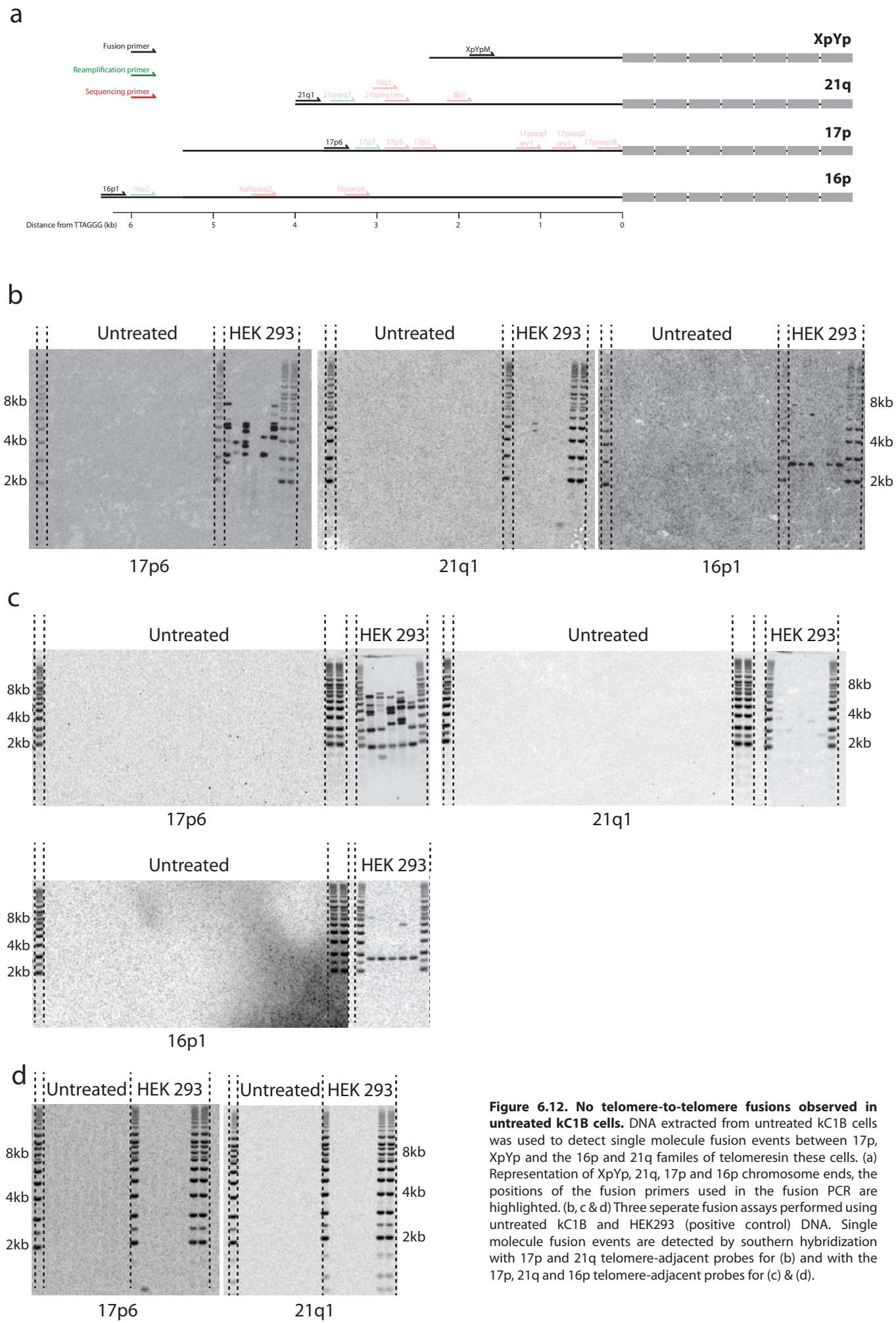

Figure 6.12. No telomere-to-telomere fusions observed in untreated kC1B cells. DNA extracted from untreated kC1B cells was used to detect single molecule fusion events between 17p, XpYp and the 16p and 21q familes of telomeresin these cells. (a) Representation of XpYp, 21q, 17p and 16p chromosome ends, the positions of the fusion primers used in the fusion PCR are highlighted. (b, c & d) Three seperate fusion assays performed using untreated kC1B and HEK293 (positive control) DNA. Single molecule fusion events are detected by southern hybridization with 17p and 21q telomere-adjacent probes for (b) and with the 17p, 21q and 16p telomere-adjacent probes for (c) & (d).

In contrast fusions between 17p and the 16p and 21q families were observed in three of the four DAXX-deficient kC1B knockdown replicate cell populations (fig. 6.13). For each knockdown a total of 375,000 diploid genome equivalents were analysed for fusion. From the DAXX-1 knockdown replicate DNA a total of four fusion events were detected (fig. 6.13a), a frequency of $1.2x10^{-5}$ $\pm 9.9x10^{-6}$ that was significantly different from untreated controls (p=0.02, Chi-squared). Fusion D1-1 was detected by the 16p and 21q probe (D1-1), two fusions (D1-2 & D1-4) were detected by the 17p and 21q probes and D1-3 was only detected by the 21q probe. The same fusion frequency was seen in the DAXX-3 knockdown replicate DNA (fig. 6.13c). Surprisingly one PCR reaction amplified two independent fusion events, one involving 17p and a 21q family member (D3-1) and another between members of the 16p and 21q families (D3-2). Two additional fusions involving a member of the 21q family were observed (D3-3 & D3-4). Three fusion events were detected from DAXX-2 DNA (fig. 6.13b), a frequency of $1.0x10^{-5}$ $\pm 9.1x10^{-6}$ that was significantly different from untreated controls (p=0.049, Chi-squared): D2-1, D2-2 and D2-3 all involve the 17p telomere however the telomere fusion partner is unknown for these fusions as the other telomere adjacent probes failed to detect these fusions. No fusions were detected in the DNA extracted from the DAXX-4 knockdown replicate kC1B cells.

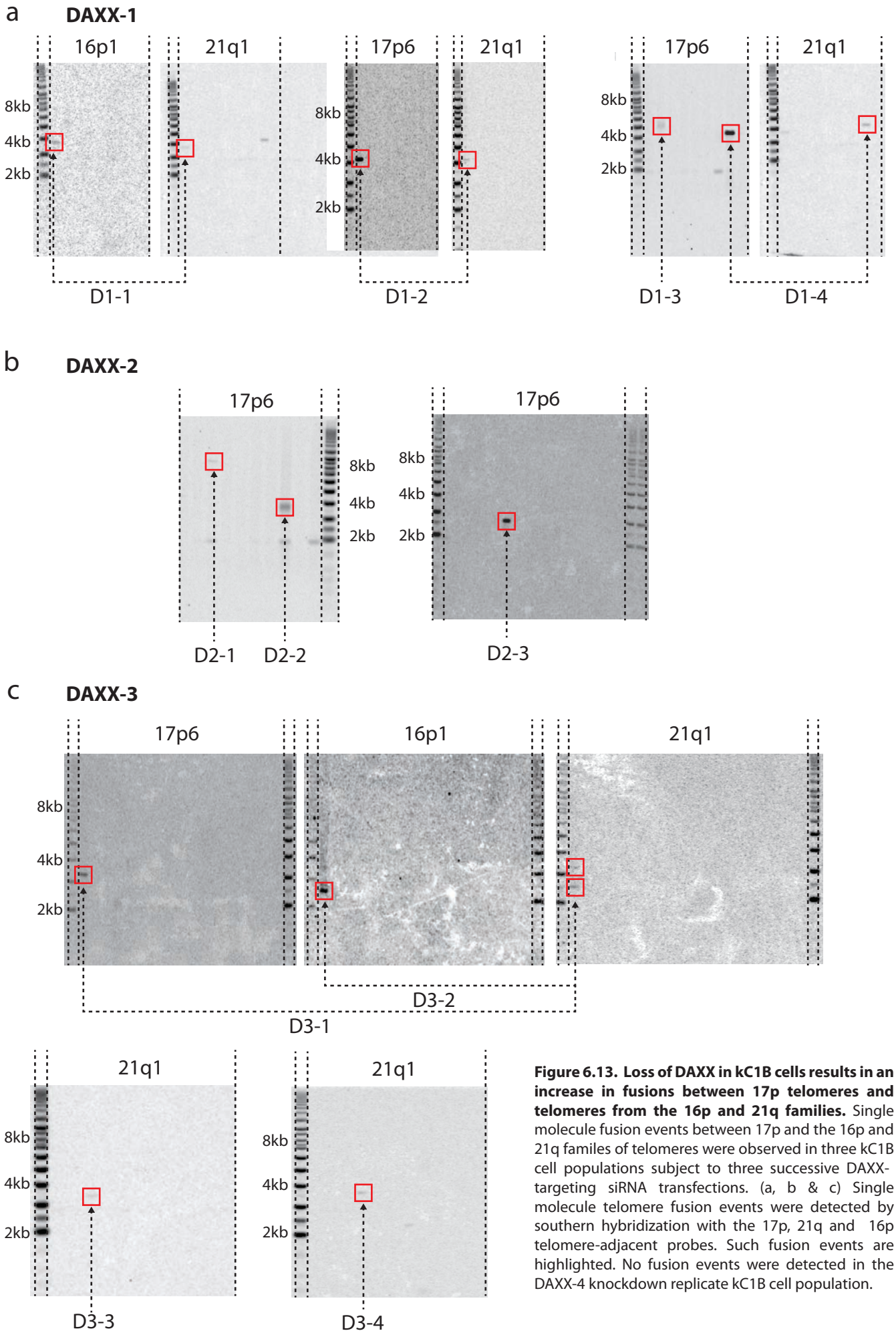

Figure 6.13. Loss of DAXX in kC1B cells results in an increase in fusions between 17p telomeres and telomeres from the 16p and 21q families. Single molecule fusion events between 17p and the 16p and 21q familes of telomeres were observed in three kC1B cell populations subject to three successive DAXX-targeting siRNA transfections. (a, b & c) Single molecule telomere fusion events were detected by southern hybridization with the 17p, 21q and 16p telomere-adjacent probes. Such fusion events are highlighted. No fusion events were detected in the DAXX-4 knockdown replicate kC1B cell population.

Of the eleven telomere fusion events identified in the DAXX-deficient cells only four could be successfully re-amplified in a nested PCR using the reamplification primers highlighted in fig. 6.14a. 17p-21q family fusions (D1-2 & D1-4) were reamplified using the 17p7 and 21qseq1 primers whereas fusions involving the 16p and 21q families (D1-1 & D3-2) were reamplified with 16p2 and 21qseq1 primers (fig. 6.14b). After gel excision and purification of the reamplified PCR product the fusion events were sequenced using sequencing primers highlighted in fig. 6.14a. By performing BLAST (Basic Local Alignment Search Tool) searches on the resulting sequences the identity of the 16p and 21q family members involved in the fusion events could be determined (fig. 6.14c). Such searches revealed that the D1-1 fusion was between the 12p and 12q telomeres suggesting formation of a ring chromosome. 12p was also one of the two fusion partners in the D3-2 fusion, the other partner being 1q from the 21q telomere family. The 17p chromosome end was a fusion partner in the other two fusion events observed: D1-4 involved a fusion event between 17p and 10q, the other fusion partner in the D1-2 fusion however was unknown as the BLAST search showed that the sequence of the reamplified fusion event was only completely homologous to an unidentified telomere.

Several common features were observed between fusion events: deletion of at least one of the fusion partners was seen in all the fusions sequenced. These deletions were extensive and extended up to 3.264kb into the subtelomeric regions (fig. 6.14c (i)). Another feature observed was microhomology at the fusion point in the D3-2, D1-4 and D1-events. The D1-1 fusion did not display microhomology however there was an insertion of a single nucleotide (A) at the fusion point whereas the other fusion events did not. Only one of the four sequenced fusion events contained telomere repeats immediately adjacent to the fusion

point: The D1-4 fusion contained 0.27kb TTAGGG repeats from the 17p chromosome end. Extensive deletion of the 10q subtelomeric region was also seen with this fusion.

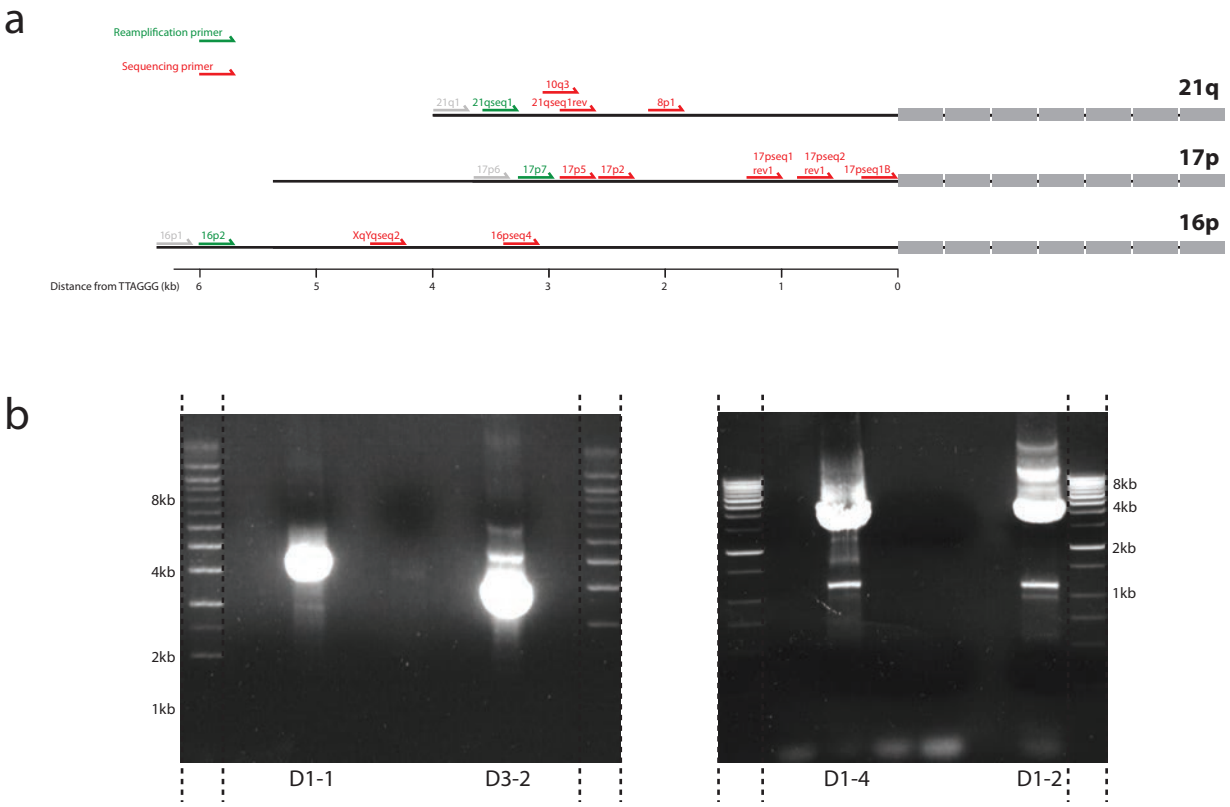

Figure 6.14. Reamplification and sequencing of fusions in DAXX-deificient cells. Fusion events observed in the single molecule fusion assay were reamplified, gel excised and sequenced. (a) Representation of the 21q, 17p & 16p chromosome ends, primers used for reamplification of fusion events are highlighted in green, sequencing of these reamplified PCR products was performed using the sequencing primers (red). (b) The D1, D2, D5 & D3 fusions seen in fig. 26 & 27 were reamplified using the appropriate reamplification primers and visualised. (c) These reamplified PCR products were then sequenced using the sequencing primers highlighted in (a), the fusion sequence is displayed on the top line with the fusion partners below. Sequence highlighted in red and underlined indicate duplicated sequences across the fusion point. * indicates homology shared between the fusion partners

6.3.10 EHMT2 depletion also causes a telomere shortening phenotype in the kC1B cells

In addition to ATRX, DAXX and EZH2, three successive siRNA mediated knockdowns of the HMTases DOT1L and EHMT2 was also performed in the kC1B cells and any aberrant telomere lengths were determined in the same manner as described earlier.

DOT1L depletion resulted in no aberrant telomere length phenotypes at 17p, 18q or XpYp (fig. 6.15a, b & c). However in one of the EHMT2 knockdown replicates EHMT2 depletion caused a telomere shortening phenotype at these chromosome ends: EHMT2-1 cells displayed a loss of 2.149kb in mean 17p telomere length compared to the untreated cells ($P<0.0001$) (fig. 6.16a). This telomere shortening phenotype in the EHMT2-1 cells was replicated at 18q where a loss of 2.238kb in mean 18q telomere length was recorded ($P=0.0005$) (fig. 6.16b), and also at XpYp where the mean telomere length was reduced by 1.387kb ($P=0.001$) (fig. 6.16c). The other two knockdown replicates did not display aberrant telomere length phenotypes at any of the chromosome ends tested. The fact that the telomere shortening phenotype was observed across different chromosome ends in the EHMT2-1 cells and that this phenotype was highly significant as determined by t-test analysis suggests that this result is not just a product of variability within the assay.

a

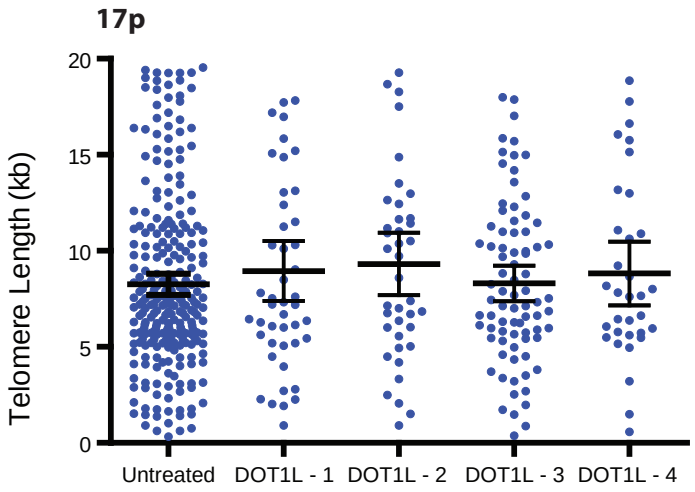

Mean tel length (kb)	8.259	8.946	9.314	8.307	8.82
Lower 95% CI	7.716	7.387	7.693	7.383	7.159
Upper 95% CI	8.803	10.50	10.93	9.231	10.48

b

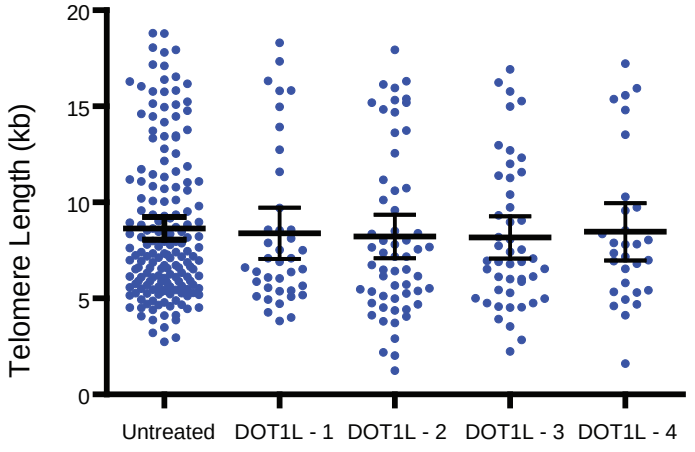

Mean tel length (kb)	8.646	8.398	8.219	8.175	8.473
Lower 95% CI	8.055	7.063	7.085	7.069	6.983
Upper 95% CI	9.237	9.732	9.354	9.282	9.962

c

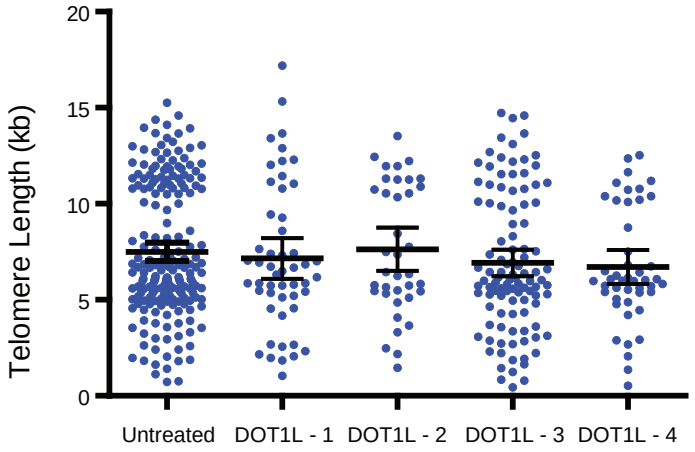

Mean tel length (kb)	7.5	7.151	7.626	6.919	6.714
Lower 95% CI	7.027	6.089	6.502	6.221	5.829
Upper 95% CI	7.973	8.214	8.751	7.616	7.599

Figure 6.15. The effect of siRNA-mediated knockdown of DOT1L on the telomere length distribution at 17p, 18q and XpYp. kC1B cells were transfected with 25nm siRNA targeted against DOT1L mRNA using DharmaFECT 1. DOT1L-1, -2, -3 & -4 represent four biological replicates independently transfected. Each replicate was successively transfected three times at 96h intervals. 96 hours after the third transfection DNA was extracted. STELA was then performed at 17p, 18q and XpYp using the 17pseqrev1, 18qrev4M and XpYpE primers respectively. Telomere length distributions were then quantified using Phoretix software (Nonlinear dynamics)

a

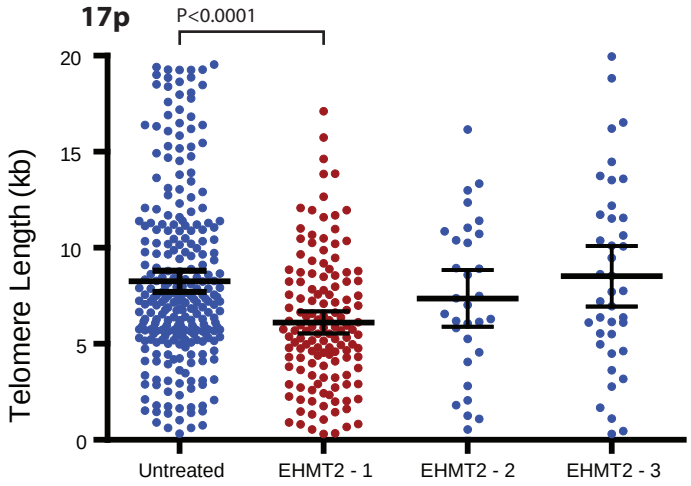

Mean tel length (kb)	8.259	6.11	7.366	8.517
Lower 95% CI	7.716	5.534	5.895	6.944
Upper 95% CI	8.803	6.687	8.837	10.09

b

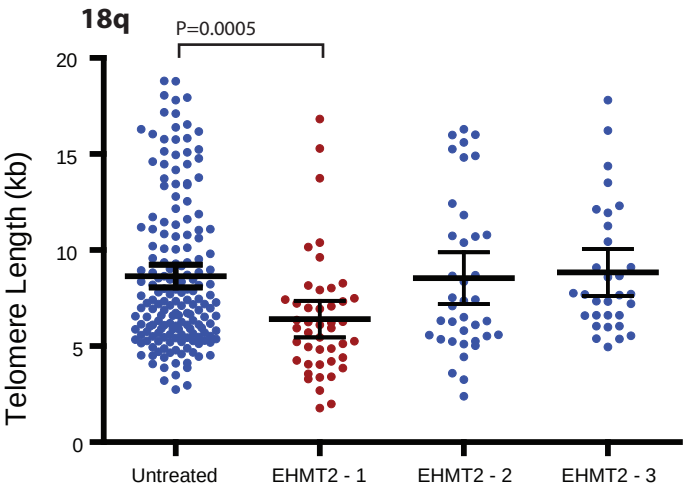

Mean tel length (kb)	8.646	6.408	8.54	8.836
Lower 95% CI	8.055	5.465	7.197	7.612
Upper 95% CI	9.237	7.350	9.884	10.06

c

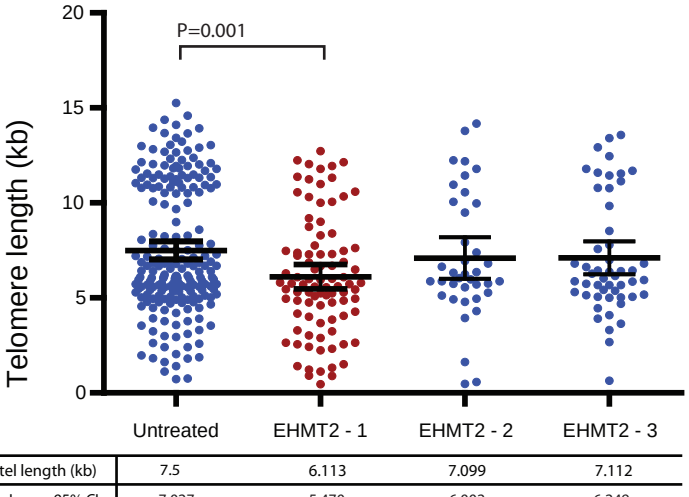

Mean tel length (kb)	7.5	6.113	7.099	7.112
Lower 95% CI	7.027	5.470	6.002	6.249
Upper 95% CI	7.973	6.756	8.195	7.974

Figure 6.16. The effect of siRNA-mediated knockdown of EHMT2 on the telomere length distribution at 17p, 18q and XpYp. kC1B cells were transfected with 25nm siRNA targeted against EHMT2mRNA using DharmaFECT 1. EHMT2-1, -2, -3 & -4 represent four biological replicates independently transfected. Each replicate was successively transfected three times at 96h intervals. 96 hours after the third transfection DNA was extracted. STELA was then performed at 17p, 18q and XpYp using the 17pseqrev1, 18qrev4M and XpYpE primers respectively. Telomere length distributions were then quantified using Phoretix software (Nonlinear dynamics)

6.4 Discussion

In this chapter an effect of the H3.3 chaperone DAXX on telomere length regulation has been identified in a keratinocyte holoclone population. Prolonged DAXX depletion over numerous cell divisions results in a telomere shortening at the 17p, 18q, XpYp and, to a lesser extent, 2p chromosome ends. DAXX loss also leads to an increased frequency in telomere-to telomere fusions between 17p and the 16p and 21q families of telomeres. Additionally EHMT2 was also shown to cause a telomere length shortening phenotype.

A role for EHMT2 in telomere length regulation has recently been suggested in a study in which associations between genetic variants in histone methylation and telomere length were analysed in human blood samples: The single nucleotide polymorphism (SNP) rs558702 G>A within the EHMT2 was one of six SNPs identified in the study to be associated with shorter telomere length (Kim et al. 2012). The RNAi screen performed in the previous chapter showed that siRNA-mediated knockdown of EHMT2 in HT1080 cl.2 cells resulted in generation of very short 17p telomeres. A similar telomere shortening phenotype was seen in the kC1B cells at 17p but also at 18q and XpYp. The significant loss in telomere length was only observed in one of the three knockdown replicate cell populations (EHMT2-1) and the extent of the knockdown of EHMT2 expression was not verified. Despite this it still seems likely that the telomere length shortening phenotype is due to EHMT2 loss and not just down to inherent variation within the assays as the losses in telomere length are striking and highly significant at all three chromosome ends.

The telomere length defects observed in DAXX-deficient kC1B cells in this chapter is somewhat consistent with the telomere shortening phenotype observed in HT1080 cl. 2 cells

targeted for DAXX knockdown. However whereas siRNA knockdown of DAXX in the HT1080 cl.2 cells resulted in a subtle telomere length defect only at 17p, the loss of telomere length in the kC1B cells was far greater and seen at more chromosome ends. A role for DAXX in telomere length regulation has also been previously reported in human pancreatic neuroendocrine tumours (PanNETs) (Heaphy et al. 2011) and in glioblastoma multiforme brain tumour samples (Schwartzentruber et al. 2012) where loss of DAXX expression was shown to be associated with telomere lengthening via the ALT pathway. Loss of DAXX in the kC1B cells had the opposing effect of dramatic telomere shortening suggesting that the mechanism by which DAXX contributes to telomere length maintenance in these kC1B cells is different to that in the mentioned tumour samples. The telomere length distributions were not consistent with ALT and no evidence of the ALT pathway was provided by the mutational analysis. The mechanism also seems unlikely to be telomerase-mediated. In normal somatic cells in which telomerase activity is either low or undetectable, telomere erosion occurs at a rate of 60-120bp/PD (Baird et al. 2003; Harley et al. 1990) which is a much lower erosion rate than what was observed in the DAXX-deficient kC1B cells. However the rate of erosion in the kC1B cells after telomerase knockdown is unknown and it would be an interesting to determine this in future experiments and compare it to the rate telomere loss observed in the DAXX-deficient kC1B cells.

An alternative mechanism which could be responsible for the dramatic telomere loss in the DAXX-deficient cells could be replication fork stalling. Telomeres are replicated by the conventional DNA replication machinery however it has been suggested that the repetitive telomeric sequence and the presence of secondary structures such as t-loops, G quadruplexes and heterochromatin may cause difficulties for the passage of the replication fork (Gilson and Geli 2007). Replication fork stalling has been observed at telomeres in yeast

and human fibroblasts (Ivessa *et al.* 2002; Verdun and Karlseder 2006) and results in a DNA damage response (DDR). The DDR results in the recruitment of DNA repair and DNA replication proteins which restart the stalled replication fork and complete replication at the chromosome end (Verdun and Karlseder 2006). Mutations in some of the factors required for the restart of replication leads to exposure of ssDNA that is susceptible to degradation and consequently telomere shortening (Nakamura *et al.* 2005; Pandita et al. 2006; Parenteau and Wellinger 1999). In addition to these factors other proteins have been implicated in telomere replication including RecQ helicase WRN. Loss of WRN also result in telomere shortening (Crabbe et al. 2007). WRN association at the telomere is dependent on the histone deacteylase activity of SIRT6 (Michishita et al. 2008). It is possible that the ability of DAXX to alter chromatin structure may also promote telomeric binding of proteins required for proper telomeric replication and avoiding telomere shortening. An argument against this idea is that DAXX has as yet only been shown to be involved in the replication-independent deposition of H3.3. However the telomere length losses in the DAXX-deficient kC1B cells did not appear to be mediated by ALT or inhibition of telomerase activity which suggests that they may have been due to defective telomere replication. Furthermore the increase in telomere-to-telomere fusions observed in the DAXX-deficient kC1B cells is also seen after loss of proteins implicated in telomere replication (Bai and Murnane 2003; Crabbe et al. 2007).

Another aspect of the telomere length maintenance role of DAXX in the kC1B cells which isn't consistent with previous reports is that it doesn't appear to be functioning with ATRX. ATRX is responsible for the recruitment of DAXX to the telomere in mouse ES cells as ATRX loss abolishes telomeric enrichment of DAXX (Lewis et al. 2010). Loss of DAXX in these cells results in reduced levels of ATRX suggesting DAXX may be required for ATRX protein stability

or expression. This interplay between the two complex partners in the maintenance of telomeric chromatin is not reflected in the data shown in this chapter as loss of ATRX in the kC1B cells did not result in a similar telomere shortening phenotype seen in DAXX deficient kC1B cells. If ATRX recruits DAXX to the telomere then ATRX deficiency should have reduced telomeric enrichment of DAXX causing a telomere length phenotype similar to what was seen in the DAXX-deficient kC1B cells. Similarly if DAXX indirectly regulates telomere length through its ability to promote ATRX expression or stabilise ATRX protein then similar telomere shortening should occur in both the ATRX- and DAXX-deficient kC1B cells. The inconsistency in telomere length defects between the DAXX- and ATRX-deficient kC1B cells does not appear to be due to unsuccessful knockdown of ATRX expression as RNA levels after knockdown were measured and showed that ATRX levels were reduced by over 80%. This raises the question of whether there may be alternative pathway through which DAXX exerts its influence over telomere length. No evidence has been found in support such an argument, but the observation that DAXX causes 17p telomere shortening in HT1080 cl. 2 cells and ATRX does not, is analogous to what was seen in the kC1B cells. An alternative explanation for the discrepancy could be that although the ATRX knockdown was successful, residual amounts of ATRX may have been sufficient for normal telomeric chromatin maintenance by the complex. RT-PCR was used to determine RNA levels of ATRX after transfection with ATRX-targeting siRNA. Although this method can determine the extent of the knockdown it would have been better to measure protein levels as the amount of ATRX in the cell is affected not only by RNA levels but also the rate at which the protein is degraded. Although performing a western would have given an indication of ATRX levels after knockdown it would not indicate whether any remaining ATRX left in the cell was functioning at the telomere. Therefore it would be interesting to examine telomeric enrichment of ATRX and also DAXX in kC1B cells targeted for ATRX knockdown to determine

whether residual ATRX is still present at the telomere and whether this or another protein recruits DAXX to the telomere.

The proximal 1-3kb of human telomeres contains distribution patterns of telomere repeat variants (TVRs) (Baird et al. 2000; Baird et al. 1995; Coleman et al. 1999) which vary between different chromosome ends, telomeric alleles of the same chromosome end and also in an intra-allelic manner. TVR distribution patterns have previously been used to determine telomere mutations occurring in ALT+ cells (Varley *et al.* 2002). In this study it was found that mutant telomeres consisted of progenitor sequence which was replaced at a discrete point by the sequence of another telomere repeat array. The aim of isolating and sequencing individual STELA products was to identify similar changes in TVR distributions. Although only three STELA products were successfully sequenced no such variation in TVR distribution was observed suggesting that the loss of telomere length was not ALT-mediated and may instead be due to telomeric deletions within the TTAGGG repeat region. This method would also have allowed the progenitor telomeric allele from which the short telomeres where generated to be identified. However due to the inability to reamplify and sequence XpYp telomeres >3kb in length comparisons being made between very short telomeres generated and normal length telomeres could not be made.

Despite the XpYp telomere in the kC1B cells being a poor candidate for the mutation analysis the rationale behind the method was reasonable and may have proved to be more informative in a telomere with a more complex TVR interspersion pattern. However the development of the method revealed certain experimental limitations that could not be overcome: The main problem faced was generating enough PCR product from the reamplification to allow for DNA sequence analysis. As described in the results section, many

strategies were taken to improve the PCR product yield however this optimisation was only partly successful for some of the PCR products meaning that out of the originally isolated STELA PCR products, only three were sequenced. Another limitation was the amount of telomere repeats that could be sequenced: XpYpJ, situated on the subtelomere-telomere boundary, enabled ~300p of telomeric DNA to be sequenced. At the distal end of the telomere tel2 was far more efficient than XpYpJ as a sequencing primer and sequenced a maximum of ~750bp. Therefore only telomeres of 1.05kb or less in size can be fully sequenced. There does however have to be a region containing a 'landmark' unique telomere variant/variants in the telomere sequenced by both primers to allow the two sequences to aligned into a single contig. Therefore 1.05kb is likely to be an overestimate in the maximum length of telomere that can be fully sequenced. This is a major drawback of this technique and because of the difficulty in sequencing repetitive DNA tracts one which will be very difficult to overcome. Nonetheless, development of the method to isolate, purify and sequence PCR products amplified from single telomeres is the first of its kind and could prove to be an informative tool when studying telomere dynamics in future.

Telomere shortening either through gradual erosion or by stochastic telomere deletion can lead to telomere dysfunction in which the telomere loses its end-capping function and becomes susceptible to fusion with other telomeres or double stranded breaks (Capper, Britt-Compton et al. 2007). Examples of telomere fusions resulting from loss of a chromatin remodeler have been reported in *Drosophila*: loss of the heterochromatin protein 1 (HP1) or it's interacting partners HOAP (HP1/ORC-associated protein) and HipHop (HP1-HOAP-interacting protein) results in increased levels of telomere-to-telomere fusions (Burgio et al. 2011; Cenci et al. 2003; Fanti et al. 1998; Gao et al. 2010) as does loss of Rpd3, the homolog of mammalian HDAC1 (Burgio et al. 2011). In WI-38 human fibroblasts siRNA knockdown of

the SIRT6 histone deacetylase leads to an increase in telomere fusions which contain no or very little telomere signal (Michishita et al. 2008). Similar fusions were observed in the DAXX-deficient cells in this chapter: sequencing the fusion events revealed extensive deletion of telomeric and subtelomeric regions in at least one of the fusion partners. Only one of the fusion events (D1-4) contained TTAGGG repeats however this only amounted to 270bp indicating that the 17p telomere involved in this fusion had also undergone dramatic telomere shortening. The large-scale deletion events present in the sequenced fusion events along with microhomology seen at the fusion point is consistent with Ku-independent alternative non-homologous end-joining process that results in the large deletion events and utilises small patches of homology to facilitate end-joining. This process has previously been implicated in the fusion of short dysfunctional telomeres (Capper et al. 2007; Tankimanova *et al.* 2012). The loss of subtelomeric sequence observed in the telomere fusion events show that the loss of DAXX in kC1B cells results in large-scale stochastic deletions at a chromosome end that extend into the subtelomeric region. These large-scale deletion events also increase the number of very short telomeres which contribute to the elevated rate of telomere erosion seen in the DAXX-deficient cells.

The structure of telomeric chromatin differs between pluripotent stem cells and differentiated cells. Whereas telomeric chromatin is more compact in differentiated cells with an accumulation of heterochromatin associated marks such as H3K9me3 and H4K20me3, in stem cells chromatin at telomeres is less heterochromatic (Marion et al. 2009). Stem cell telomeres are more susceptible to dysfunction after disruption to telomeric chromatin conformation. An example of this is seen upon disruption of the ATRX-DAXX-H3.3 deposition pathway which causes telomere dysfunction in mouse ESCs but not in differentiated mouse cells (Wong et al. 2009). The differences in the extent of telomere

length changes after DAXX knockdown seen between HT1080 cl.2 cells and the stem cell keratinocyte holoclone population is consistent with this idea, it would be interesting to analyse telomere length profiles in conditions of low DAXX in other stem cell populations including cancer stem cells to gain a broader view on the role of DAXX at the telomere.

In this chapter RNAi-mediated depletion of the H3.3 chaperone DAXX in a keratinocyte holoclone population (kC1B) was shown to result in a striking telomere shortening phenotype at 17p, 18q, XpYp and, to a lesser extent, 2p. This is the first direct demonstration of how depleting DAXX in human cells causes telomere length defects. Loss of DAXX in these cells also leads to an increase in telomere-to-telomere fusion events between 17p and the 16p and 21q family of telomeres. A mutation analysis method was developed to shed light on the telomere shortening mechanism in the DAXX-deficient cells. This approach showed no evidence of recombinational events at the severely truncated XpYp telomeres which is consistent with the idea that the telomeric deletion events may involve a deletion within the TTAGGG repeat region and subsequent healing with telomerase. In addition to the role of DAXX in telomere length regulation in these kC1B cells, loss of the histone methyltransferase EHMT2 was also shown to result in a telomere shortening phenotype at 17p, 18q and XpYp.

Chapter 7

General Discussion and Future Directions

7.1 Summary

Extensive inter-chromosomal variation in telomere length in both telomerase-positive and telomerase-negative cells has previously been reported by our lab (Britt-Compton et al., 2006). Upon ectopic expression of telomerase shorter telomeres are preferentially elongated (Britt-Compton et al., 2009). Furthermore, alleles from the same XpYp chromosome end have been shown to have differing telomere length distributions indicating that differences in telomere length between maternal and paternal alleles are maintained throughout development (Baird et al., 2003). These findings lead us to hypothesize whether telomeric chromatin structure confers this 'setting' of telomere length. The main aim of this project was to investigate whether the chromatin structure of a telomere is a determinant of its length. To address this issue two approaches were taken: firstly the chromatin structure of telomeres of different lengths was directly analysed by measuring the enrichment of histone modification known to be prominent at telomeres in other model organisms. This approach revealed differences in telomeric chromatin structure between telomeres of different lengths in telomerase-positive HT1080 fibrosarcoma cells. Shorter HT1080 telomeres had reduced H3 and TRF1 occupancy as well as lower levels of H4K20me3 and, to a lesser extent, H3K4me3 compared to longer telomeres. Such differences were not observed between telomeres of different lengths in telomerase-negative MRC5 fibroblasts however senescence-induced changes to telomeric chromatin structure were observed.

The second approach was to investigate any potential roles of chromatin remodeling proteins in telomere length maintenance. siRNA mediated knockdown of selected chromatin remodelers was performed in a clonal population of HT1080 cells followed by STELA analysis. Telomere length defects were observed after knockdown of histone methyltransferases (HMTases) EHMT2, DOT1L, MLL and EZH2, histone deacetylases (HDACs) HDAC1 and SIRT6, the SWI/SNF subunit BAF155 and the H3.3 histone chaperone DAXX. A similar siRNA mediated knockdown strategy in a keratinocyte holoclone population revealed a dramatic telomere shortening phenotype at a number of chromosome ends in EHMT2-depleted cells and DAXX-depleted cells. Prolonged depletion of DAXX also caused an increase in telomere-to-telomere fusions.

The importance of identifying telomere length regulators lies in the fact that the functionality of a telomere is directly related to its length. A number of factors influence telomere length in human cells including telomerase and other telomere-associated proteins, recombination-based mechanism and environmental factors such as smoking and obesity (Greider and Blackburn, 1985, Bryan et al., 1997, van Steensel and de Lange, 1997, Petersen et al., 1998, Smogorzewska et al., 2000, Valdes et al., 2005). In the past decade telomeric chromatin structure has also been shown to influence telomere length in mammalian cells however examples in human cells are scarce (Benetti et al., 2007b, Benetti et al., 2008, Garcia-Cao et al., 2004, Gonzalo et al., 2006). There is a clear need to shed more light on human telomeric chromatin structure and chromatin remodelers which specifically function at the telomere to maintain telomere length. This will allow a greater understanding into the role of telomeric chromatin in normal cellular functions, during ageing and during the initiation and progression of diseases such as cancer and premature

ageing syndromes. Elucidating the pathways regulating telomeric chromatin structure may provide targets for therapeutic intervention in disease driven by telomere dysfunction.

7.2 Implications of impaired telomeric chromatin maintenance in disease and ageing

The stabilisation of telomere length either by telomerase or by an ALT-mediated mechanism is a key determinant of cancer progression (Bodnar et al., 1998, Bryan et al., 1997). Conversely continued telomere attrition after each round of DNA replication limits the proliferative capacity of adult cells which leads to senescence and is associated with organismal ageing (Harley et al., 1990). Accelerated telomere shortening is found in many premature ageing syndromes such as Dyskeratosis Congenita (DC) and Werners Syndrome (WS). How the chromatin structure of telomeres is implicated in these roles is less well defined however the identification of a number of chromatin remodelling proteins as key mediators of telomeric chromatin structure and telomere length provides a link between telomeric chromatin maintenance and disease progression.

7.2.1 Reduced association of telomerase and other telomere binding proteins with telomeres

Alterations in telomeric chromatin structure could result in increased or decreased access to the telomere for telomere binding proteins required for maintaining telomere length and integrity. It is possible that a change to a more open telomeric chromatin structure may enhance the ability of telomerase to associate with telomeres providing a mechanism of telomere maintenance required for the progression of cancer

Evidence in support of this comes from nuclear reprogramming studies. Cancer has been described as a pathological reprogramming where from a normal tissue, tumour-initiating cells or cancer stem cells start a whole new cellular differentiation branch with its own hierarchy (Abollo-Jimenez et al., 2010). There are common features between reprogramming and tumourigenesis: in both processes the normal differentiation patterns are altered, both undergo global epigenetic changes that are necessary for the generation of a new gene expression program. Additionally both have to overcome the p53-mediated replicative barrier and have a mechanism of telomere length maintenance (Abollo-Jimenez et al., 2010, Marion et al., 2011). Studies in which mouse embryonic fibroblasts were reprogrammed to create induced pluripotent stem (iPS) cells have uncovered clear associations between telomeric chromatin structure and a telomerase-mediated reprogramming of telomere length. Chromosome ends in mouse embryonic fibroblasts (MEFs) are heterochromatic with an abundance of repressive marks such as H3K9me3 and H4K320me3, binding of heterochromatin protein 1 (HP1) and methylation of subtelomeric DNA (Benetti et al., 2007b, Garcia-Cao et al., 2004, Gonzalo et al., 2006). However reprogramming MEFs to iPS cells causes a change in the epigenetic status with reduced H3K9me3 and H4K20me3 and telomerase-mediated telomere elongation (Marion et al., 2009). Furthermore abrogation of the Suv4-20h H4K20-specific histone methytransferases in iPS cells accelerates telomere elongation and also leads to an increased growth rate and elongated telomeres in teratomas derived from iPS cells (Marion et al., 2011). These results suggest that a loss of heterochromatic features at a telomere increases the association of telomerase with telomeres resulting in telomere elongation during nuclear reprogramming, a process required for cancer progression.

Chromatin structure changes at the telomere may result in reduced access to telomere-associated proteins. This may lead to impaired telomere maintenance resulting in telomere attrition and subsequent loss of the end-capping function. Such an example has been suggested in the rare premature ageing syndrome Werners Syndrome (WS). WS is caused by mutations in the gene encoding the RecQ helicase WRN. Loss of WRN leads to dramatic telomere loss during DNA replication which results in extensive genomic instability and an increase in telomere-to-telomere fusions (Crabbe et al., 2007). The histone deacetylase SIRT6 is responsible for H3K9 deacetylation at telomeres and has been shown to be required for WRN association at telomeres (Michishita et al., 2008). Interestingly, in a mutational analysis of 129 WS patients 26 (20%) did not have mutations in the WRN gene (Chen et al., 2003). No evidence of physical interaction between SIRT6 and WRN has been found suggesting that SIRT6 does not function to recruit WRN to telomeres. Instead the compromised telomeric chromatin structure in the absence of SIRT6 may inhibit WRN binding at the telomere and therefore play a role in the progression of the disease.

7.2.2 Telomeric recombination in disease

Recombination events at chromosome ends have been implicated in a number of diseases including cancer, developmental delay and mental retardation (Bryan et al., 1997, Ravnan et al., 2006, Wu et al., 2010). Loss of heterochromatic features such as subtelomeric DNA methylation, and methylation of H3K9, H4K20 and H3K79 in both telomeric and subtelomeric regions resulted in increased telomeric recombination (Benetti et al., 2007b, Garcia-Cao et al., 2004, Gonzalo et al., 2006, Jones et al., 2008). Thus it seems likely that a more open telomeric and subtelomeric chromatin structure could facilitate disease progression.

Although ~85% of cancers express telomerase the remaining 15% maintain telomere length via the recombination-based alternative lengthening of telomeres pathway (ALT) (Bryan et al., 1997). Furthermore a subset of immortalized cell lines use ALT as their telomere length maintenance mechanism (Lovejoy et al., 2012). Decondensation of heterochromatin at telomeric and subtelomeric regions has been shown to cause ALT-mediated telomere elongation suggesting that a more open telomeric chromatin structure can promote a telomere length maintenance pathway required by some cancers.

A number of studies investigating the ATRX-DAXX-H3.3 deposition pathway in humans have supported this view. Telomeric deposition of the histone H3 variant H3.3 is essential for maintaining telomeric chromatin structure and preventing telomere dysfunction in mouse embryonic stem cells (Lewis et al., 2010, Wong et al., 2009, Wong et al., 2010) and it appears that disruption of this same pathway in humans promotes cancer progression. Mutations in the ATRX-DAXX-H3.3 pathway have been associated with aberrant telomere length phenotypes reminiscent of the ALT pathway in a number of cancers including human pancreatic neuroendocrine tumours (PanNETs) and in glioblastoma multiforme (GBM) tumours (de Wilde et al., 2012, Heaphy et al., 2011, Schwartzentruber et al., 2012). Additionally, loss of ATRX was observed in 90% of human cell lines immortalized via the ALT pathway (Lovejoy et al., 2012).

The repression of recombination events at chromosome ends by chromatin structure may not solely prevent telomere elongation seen in cancer. Telomere-associated chromosomal rearrangements are responsible for 2.6-5% of unexplained mental retardation syndromes (Ravnan et al., 2006, Wu et al., 2010). These chromosomal rearrangement included unbalanced translocations between two chromosome arms or two arms of the same

chromosome, deletion and insertion events within subtelomeric regions and also terminal deletions. Although a direct relationship between subtelomeric and telomeric chromatin structure and telomeric rearrangements in the context of these syndromes has yet to be determined the fact that loss of heterochromatic features is associated with increased recombination events at chromosome ends suggests that it may play a role.

7.2.3 Telomere length and Telomere Position Effect in disease

It has been suggested that telomere position effect (TPE) may have a role in human disease. Very recently evidence for such a role has been found in a study aiming to identify the mutational mechanism driving the progression of Facioscapulohumeral muscular dystrophy (FSHD1A). FSHD1A is the third most common muscular dystrophy after the dystrophinopathies and myotonic dystrophy and causes progressive atrophy of facial, scapular and upper arm muscles. The disease also has a delayed appearance, symptoms often do not appear until the second or third decade of life or later (Pandya et al., 2008). FSHD1A is genetically linked to a reduced number of tandemly repeated 3.3kb D4Z4 elements present near the 4q telomere. Unaffected individuals have up to 100 D4Z4 repeats whereas FSHD patients possess only 1-10 repeats (Stadler et al., 2013). These D4Z4 elements are thought to function by repressing the expression of the DUX4 gene located in the final D4Z4 repeat. This gene encodes the DUX4 homeobox protein that is thought to be a leading candidate for pathogenesis in FSHD (Dixit et al., 2007). In addition to D4Z4 elements, a number of observations pointed to additional contributing factors to DUX4 repression: Approximately 1% of the general population also contain D4Z4 deletions within the 4q telomere which is two orders of magnitude higher than the incidence of the disease (Scionti et al., 2012), also DUX4 is expressed in some unaffected individuals without D4Z4 deletions (Jones et al., 2012). Telomere position effect has been shown to be one of these factors. Not

only does TPE repress DUX4 expression but it also may provide an explanation to the late onset of the disease: Telomere length has previously been shown to influence TPE (Koering et al., 2002) and recent work found that clones generated with shorter telomeres had reduced TPE-mediated silencing of the DUX4 gene (Stadler et al., 2013). DUX4 expression was shown to be inversely proportional to telomere length suggesting that the progressive loss of telomere length with ageing may compromise the ability of TPE to silence DUX4, leading to its expression and pathogenesis in older individuals.

7.3 Roles for telomeric chromatin in senescence

The progressive loss of telomeric DNA with every cell division eventually leads to short dysfunctional telomeres which triggers a DNA damage response and subsequently growth arrest (d'Adda di Fagagna et al., 2003, Herbig et al., 2004). Alterations in telomeric chromatin structure result in the formation of dysfunctional telomeres (Wong et al., 2010, Deng et al., 2009, Michishita et al., 2008). Also, telomeric chromatin structure and telomere length appear mechanistically linked. These observations suggest that telomeric chromatin structure will play a role in the onset of senescence.

Telomeric chromatin structure has been established as an influencing factor on telomere length in mice however it has been suggested that the reverse is also true: that the length of a telomere may have an impact on its chromatin structure. Progressive telomere shortening in telomerase-deficient mouse embryonic fibroblasts (MEFs) is accompanied by loss of heterochromatin features such as H3K9me3, H4K20me3, heterochromatin protein 1 (HP1) binding and subtelomeric DNA methylation. Concomitant with this loss is an increase in H3 and H4 acetylation, markers of active chromatin regions (Benetti et al., 2007a). This suggests

a model for senescence where progressive telomere attrition leads to a gradual decondensation of telomeric chromatin which may facilitate association of DDR factors required for growth arrest in older cells.

Changes to telomeric chromatin structure in senescent human cells has also been recently observed. Loss of telomeric H3 occupancy in late passage (PD75) cells as well as changes in the cell cycle distribution of telomere-bound H4K20me3 and H4K16Ac compared to early passage cells (PD30) has been shown (O'Sullivan et al., 2010). DNA methylation and repressive H3K9me3 were recently shown to be reduced within subtelomere of 7q and 11q in senescent W1-38 fibroblasts compared to proliferating WI-38 fibroblasts (Thijssen et al., 2013). Concomitant with this loss was a senescence-induced increase in H3K27me3 and H3K36me3 however, unlike at mouse telomeres, no increase in euchromatin-associated marks were observed. The data in this project is somewhat consistent with these findings as heterochromatin associated marks were reduced in senescent MRC5 and IMR-90 fibroblasts however a decrease in the euchromatin associated H3K4me3 was also observed in senescent cells.

The mentioned studies indicate that changes to telomeric chromatin structure occur during the lifespan of a cell however the mechanistic consequences of these changes during the onset of senescence are less clearly defined. It is possible that the chromatin structure of a telomere may function upstream in telomere end protection by regulating access to the telomere for end-capping proteins. A model for this is proposed in fig. 7.1. Findings from this thesis and the previous studies are consistent with such a model: TRF1 binding at the telomere was shown to be reduced in senescent cells with altered telomeric chromatin structure in this thesis. Telomere-bound TRF2 is similarly reduced in senescent cells

(O'Sullivan et al., 2010). These proteins repress the DNA damage response at the telomere (Karlseder et al., 1999, Karlseder et al., 2004, Palm and de Lange, 2008) therefore their loss may promote recruitment of DDR factors and subsequently growth arrest. Furthermore H3K4 and H3K9 methylation as well as subtelomeric DNA methylation influence TERRA expression levels (Arnoult et al., 2012, Caslini et al., 2009, Nergadze et al., 2009, Yehezkel et al., 2008). TERRA has been shown to have a role in the protection of the single stranded chromosome end by promoting POT1 binding (Flynn et al., 2011). Loss of telomeric H3K4 and H3K9 methylation was observed at telomere in senescent cells in this thesis and loss of subtelomeric DNA methylation during senescence has previously been reported (Thijssen et al., 2013) therefore these structural changes to telomeric chromatin may cause mis-regulation of TERRA which in turn results in reduced POT1 association at the telomere. This model is speculative and more work is required to determine whether telomeric chromatin contributes towards growth arrest in this manner.

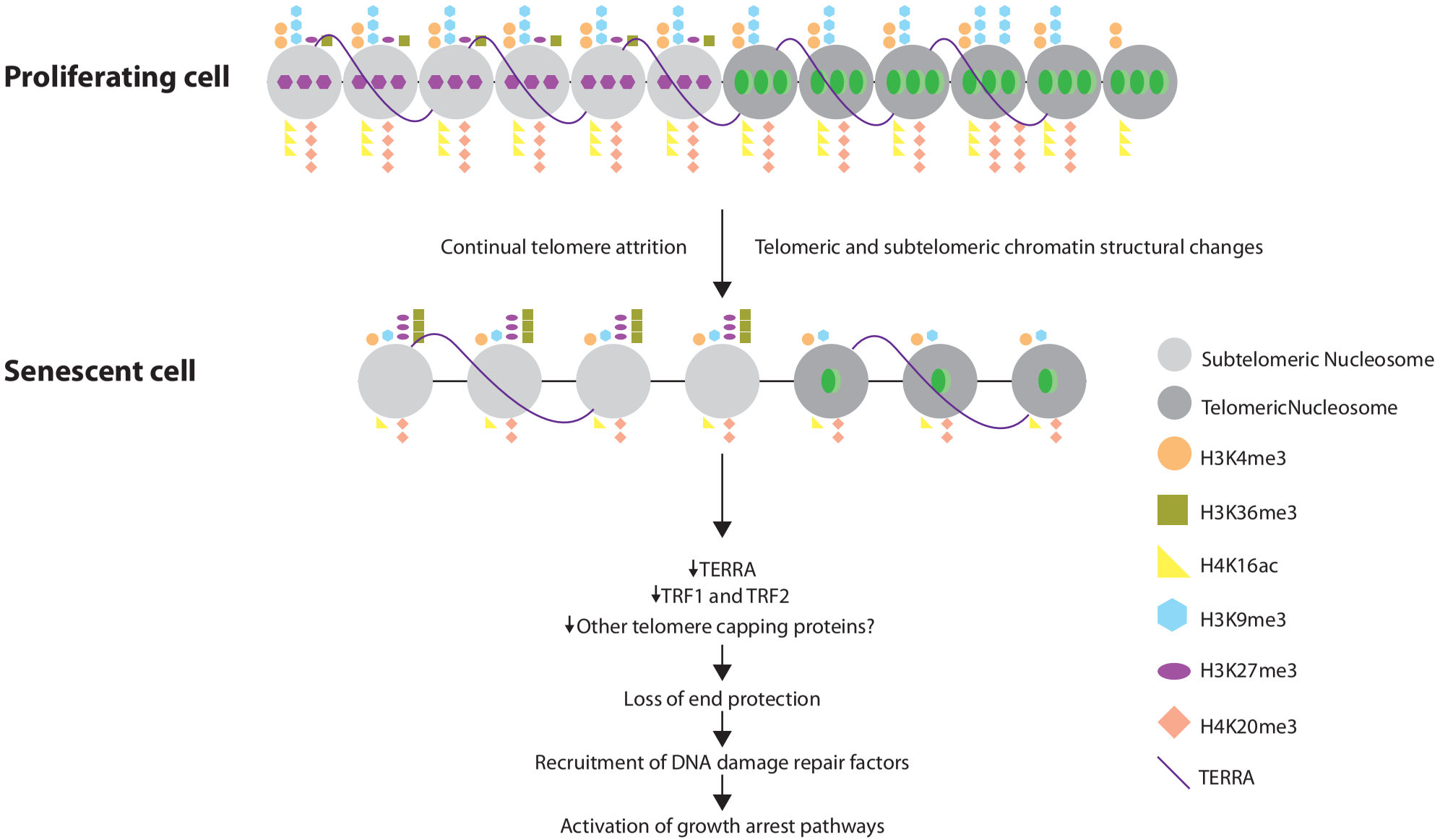

Fig. 7.1 Proposed model changes to telomeric chromatin structure influences replicative senescence. The chromatin structure at human chromosome ends undergoes structural changes as cells progress towards senescence in both telomeric and subtelomeric regions. Telomeric H3, TRF1 and TRF2 is reduced as is H3K4me3, H3K9me3 and H4K20me3. Subtelomeric DNA methylation, H3K9me3, H3K9me3, H4K16ac are reduced however H3K27me3 and H3K36me3 is increased. Additionally TERRA levels are also reduced. TRF1 and TRF2 repress the DNA damage response at the telomere. TERRA promotes POT1 binding and telomere capping. The model proposed suggests that the change in chromatin structure at the chromosome end in senescent cells impedes binding of shelterin and other proteins required for telomere capping resulting in telomere deprotection, recruitment of the DNA damage repair machinery and subsequent growth arrest

7.4 Technology development

During the course of this project a number of novel approaches were developed to gain insight into telomeric chromatin structure and its role in telomere length maintenance. Dot blots have been predominantly used for the post-ChIP analysis of the enrichment of telomere-bound protein however these assays lack telomere-specificity. TRF analysis has been used as the standard technique used for telomere length measurement for a number of years due to its relative ease and low cost to perform however it suffers from the same limitations as dot blot analysis. The increased sensitivity provided by STELA has allowed the detailed analysis of telomere loss during replicative senescence. Whereas TRF analysis estimated that telomere length at the point of replicative senescence was ~4kb, STELA showed that chromosome ends were virtually devoid of telomere repeats (Baird et al., 2003). Clearly STELA can allow the analysis of telomere length dynamics at a resolution that is beyond the limit of TRF analysis. It is possible that the telomere- and telomeric-allele specific qPCR assays developed during this project can provide a similarly high resolution for telomeric protein enrichment as STELA does for telomere length analysis and uncover subtle changes in telomeric chromatin structure that are undetectable by dot blot analysis.

Very recently a handful of studies of human telomeric chromatin structure have emerged that have employed a similar ChIP-qPCR approach as used in this project (Deng et al., 2012, Arnoult et al., 2012, Thijssen et al., 2013). QPCR assays were developed to the 7q and 11q chromosome ends in a study analysing the subtelomeric chromatin structure and TERRA transcription in senescing cells (Thijssen et al., 2013). However the regions amplified by the qPCR primers were at least 4kb away from the telomere repeat tract. Telomere-adjacent QPCR assays have also been designed however these assays amplify regions found at a number of chromosome ends (Deng et al., 2012). Although this provides a more quantitative

approach to measuring telomeric chromatin structure it still lacks telomere specificity. The assays presented in this thesis are the first examples of qPCR assays specific to individual chromosome ends which measure telomeric protein enrichment. The above studies analysed chromatin structure over a large subtelomeric region by using primers designed at various intervals across the subtelomere. Such an approach could be taken in this work to determine the extent at which a telomeric-specific chromatin mark is propagated along the subtelomeric region of the same chromosome end.

Another potential application for the primers designed for the qPCR assays is to use them for the development of telomere-specific qPCR measurement of telomere length. QPCR has previously developed as a method to measure telomere length (Cawthon, 2002, O'Callaghan and Fenech, 2011). The current method involves the use of primers that bind and amplify telomeric repeats. As telomere length increases the number of sites which the primers can anneal to increases. The amplification signal generated is then compared to signal from a single copy gene within the sample giving a measure of relative telomere length. QPCR has advantages over other telomere length measurement methods in that it is a high throughput technique meaning the telomere lengths of a large number of samples could be determined in a short space of time. Additionally small amounts of DNA are required. Very recently a qPCR-based analysis of telomere length for single cells has been described (Wang et al., 2013). One problem that may be difficult to overcome in developing telomere-specific qPCR length analyses is designing an assay of required efficiency. PCR efficiency greatly diminishes as PCR amplicon length increases. Furthermore in STELA a large amount of non-specific PCR product is amplified by the telomere-adjacent and teltail primers however these products are not detected by the telomere probe during hybrdization. Nonetheless, if such

problems are overcome this approach could be used for a fast, high throughput, telomere-specific analysis of telomere length.

The mutational analysis developed during this project could be another useful tool in telomere biology. Sequencing of single fusion events between telomeres has previously been designed by our lab (Capper et al., 2007). This allows the mutational profile of these events to be characterised which offers insight into the mechanistic basis of the telomere-to-telomere fusion. It is possible that the isolation and sequencing of very short telomeres performed in this project can have a similar use in identifying the mechanism by which telomere shortening occurs. The identification of changes in the distribution pattern of telomere variant repeats (TVRs) could indicate telomeric recombination events or telomere repeat loss and subsequent healing by telomerase. In this project the method didn't provide any insight into the mechanistic basis of telomere loss in DAXX depleted cells. This was due to the uninformative nature of the XpYp telomere analysed. Hence, this approach would only be useful when studying telomeres with a more variable distribution of TVRs.

7.5 Conclusions and future directions

To investigate whether the chromatin structure of a telomere was a determinant in its length two approaches were taken during this project: the first approach involved directly analysing the telomeric chromatin structure at telomeres of different lengths and the second approach was to identify chromatin remodelers which, when depleted resulted in aberrant telomere length profiles. It was initially thought that these two aspects of the project would not be mutually exclusive and that findings from one side of the project would influence the approach taken on the other side of the project. For example identification of

a particular chromatin remodeler in telomere length maintenance would have prompted the investigation of the telomeric enrichment of the histone modification it deposits. Unfortunately the project did not progress to a stage were such complementation was possible however this remains a possible approach to be taken in the future.

A number of chromatin remodelling proteins have been identified in this thesis as having a potential role in telomere length maintenance (summarised in fig. 7.2). Furthermore a handful of chromatin marks appear to correlate with telomere length. The mechanisms by which chromatin remodelling proteins exert their influence on telomere length are unknown. Changes in telomeric chromatin structure could influence telomerase access to the telomere. Alternatively the chromatin structure at a telomere may promote or repress recombination-based telomere elongation or deletion events. Another possibility is that their influence may be exerted through the restarting of stalled replication forks within telomeric DNA. The elucidation of these mechanisms is another future direction which could be taken with this work. This could include knockdown of a chromatin remodeler known to modulate telomere length and subsequent analysis of telomeric enrichment of proteins known to mediate the above processes. Functional interactions between chromatin remodelers and the marks they deposit at the telomere could also be examined. Additionally telomeric enrichment of histone modifications and the roles of chromatin remodelers could be studies in a variety of cell types to gain a broader view on telomeric chromatin structure.

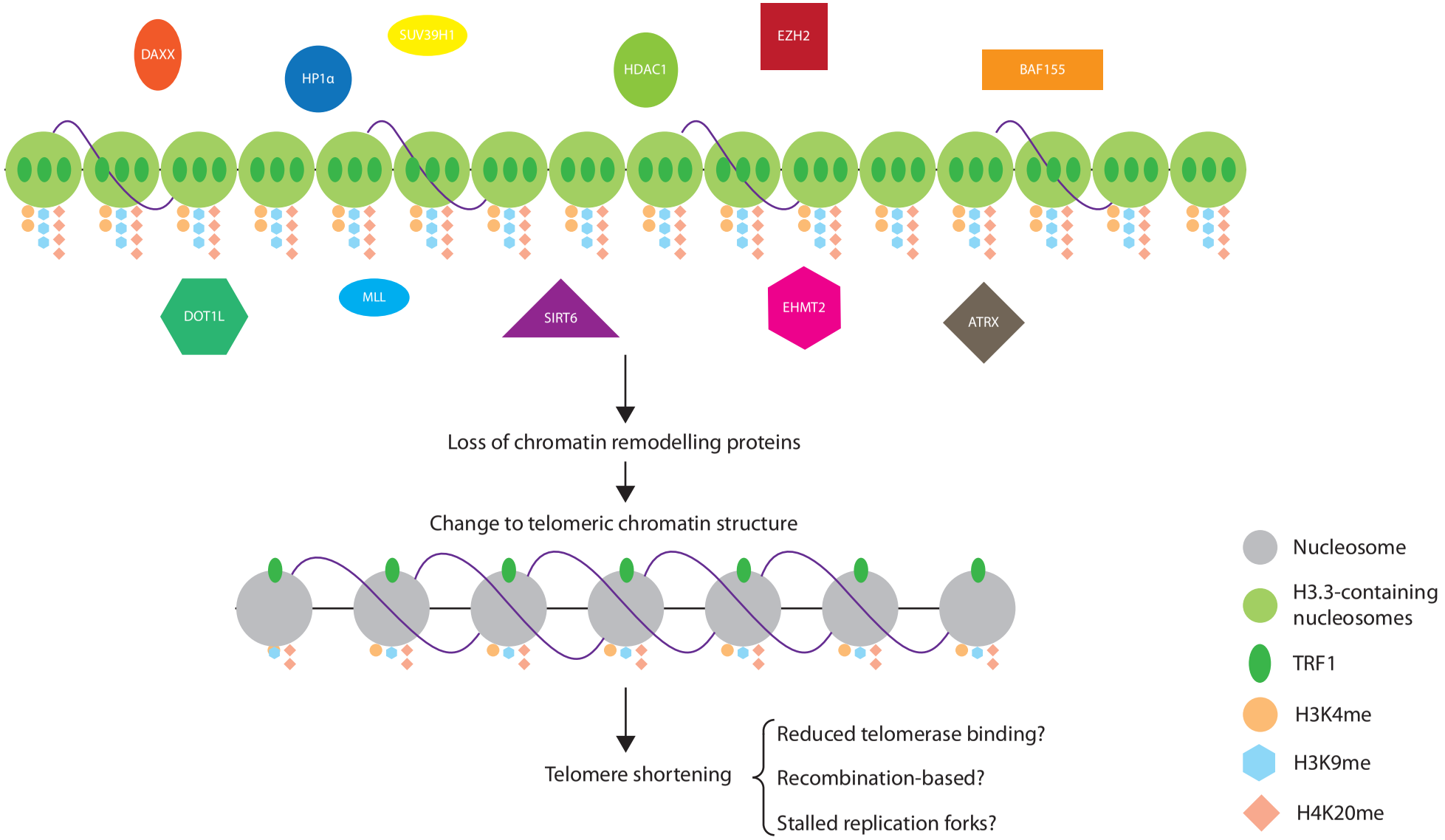

Fig. 7.2 Proposed model of how changes in chromatin structure at human telomeres influence telomere length In this thesis a potential role in telomere length regulation has been identified for a number of chromatin remodeling proteins including the HMTases DOT1L, MLL, EHMT2 and EZH2, the HDACs HDAC1 and SIRT6, the human SWI/SNF subunit BAF155 and the H3.3 chaperone DAXX. Additionally previous reports suggest a role for ATRX and histone H3.3 (Tankimanova, personal communication, Heaphy et al, 2011, Schwartzentruber et al, 2012). Telomerase-positive HT1080 cl.2 cells possessing longer telomeres have greater telomeric nucleosomal density and increased TRF1 H4K20me3 and, to a lesser extent H3K4me3 than shorter telomeres in HT1080 cl.4 cells. H3K9me3 and the presence of TERRA transcripts have also been shown to correlate with telomere length in HT1080 cells. This process is dependent on the HMTase Suv39h1 and heterochromatin protein 1α (HP1α) (Arnoult etal, 2012). Loss of remodeling proteins may result in a change in telomeric chromatin structure which may lead to loss of telomere length. The mechanism by which this could occur is unknown, it may be due to reduced access to the telomere for telomerase, recombination-based deletion events or by failing to restart stalled replication forks within telomeric DNA

Telomeres play a pivotal role in processes throughout the lifespan of a cell. The gradual erosion of telomeres after each cell division acts a molecular clock that limits the proliferative lifespan of a cell, thereby functioning as a tumour suppressor mechanism. They protect natural chromosome ends from being recognised as double stranded DNA breaks as well as silence the expression of telomere-proximal genes. All these processes function in the context of chromatin therefore gaining a deeper understanding into the regulatory network of telomeric chromatin maintenance is required. In recent years the chromatin structure at human telomeres has begun to be uncovered. As such there is great scope for research in this field and the methods developed during this project can contribute to answering some of the key questions yet to be addressed in telomeric chromatin dynamics.

Appendix

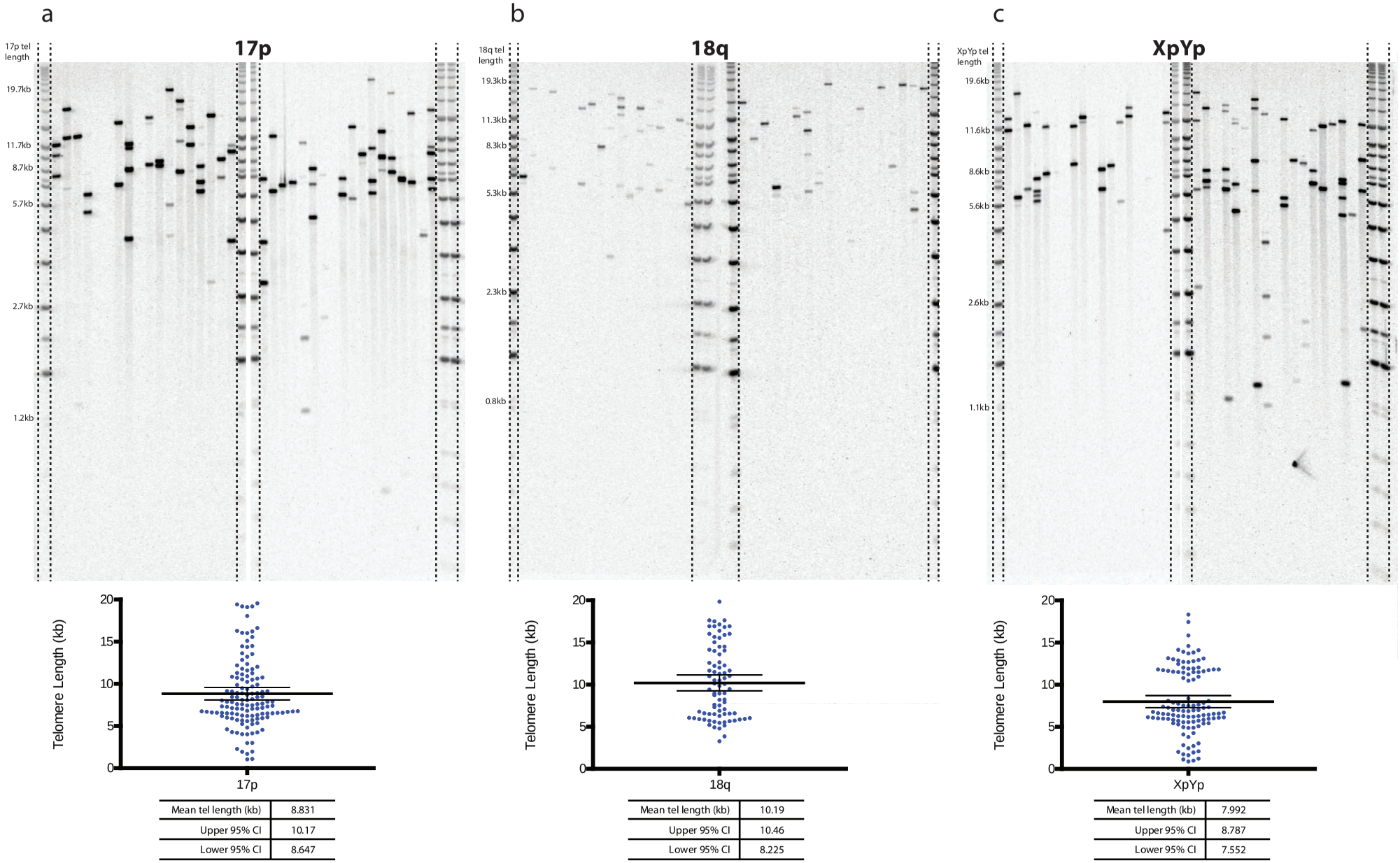

Appendix Figure 1. Telomere length profile of untreated keratinocyte clone C1B cells at 17p, 18q and XpYp. Untreated keratinocyte holoclone C1B cells were cultured in parallel to the cells subject to three successive siRNA transfections at 96 hour intervals. 96 hours after the third transfection DNA was extracted from all cells. STELA was performed at 17p (a), 18q (b) and XpYp (c) chromosome ends using the 17pseq1rev1, 18qrev4M and XpYpE primers respectively. Telomere length distributions were then quantified using Phoretix software (Nonlinear dynamics)

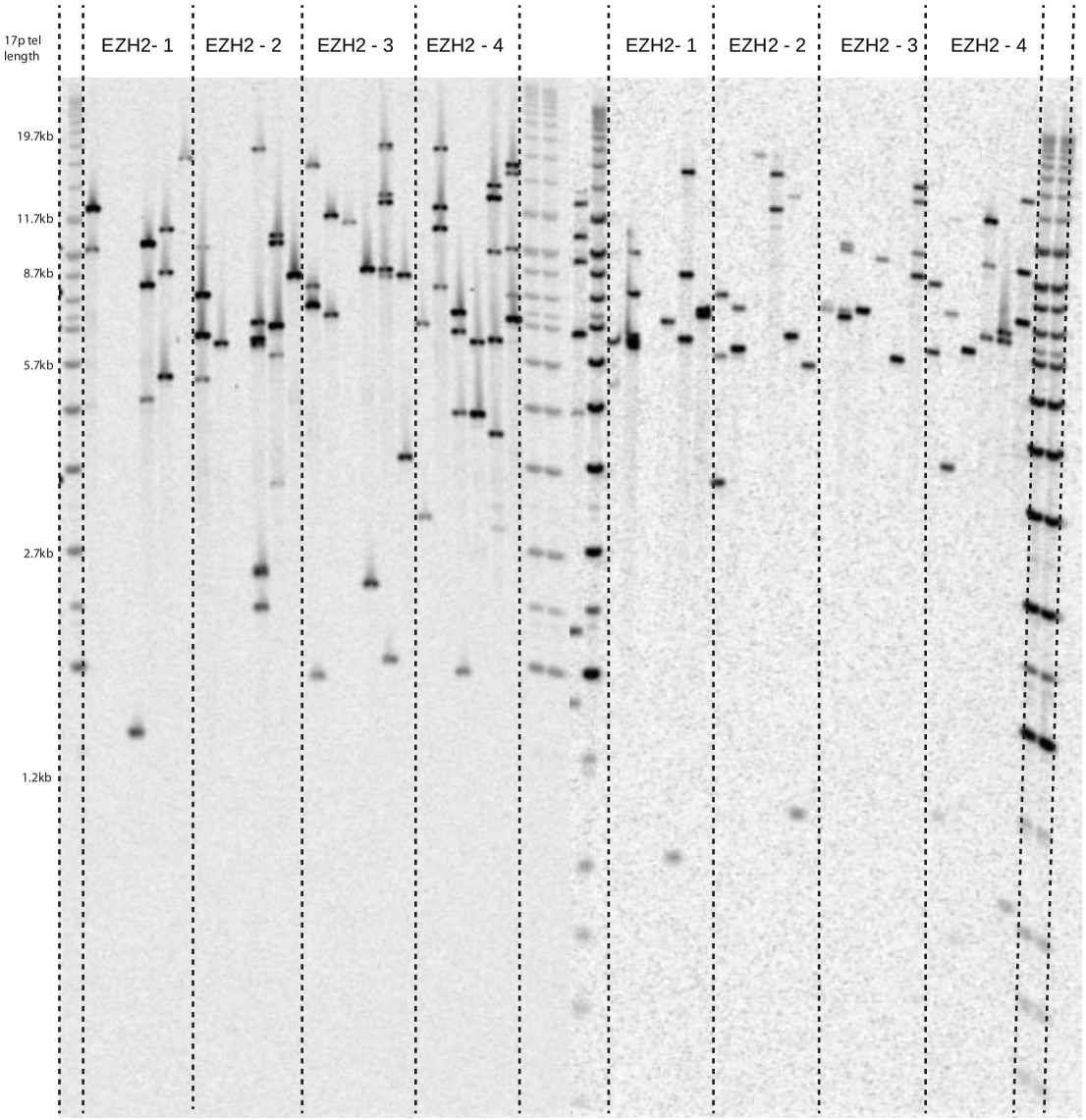

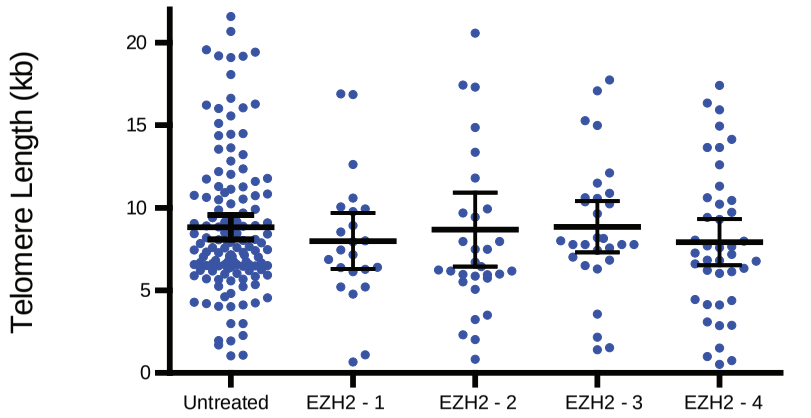

Mean tel length (kb)	8.831	7.987	8.677	8.852	7.915
Std. Error	0.3741	0.8187	1.096	0.7603	0.6899

Appendix Figure 2. The effect of siRNA-mediated knockdown of EZH2 on the telomere length distribution at 17p. kC1B cells were transfected with 25nm siRNA targeted against EZH2 mRNA using DharmaFECT 1. EZH2-1, -2, -3 & -4 represent four biological replicates independently transfected. Each replicate was successively transfected three times at 96h intervals. 96 hours after the third transfection DNA was extracted. STELA was then performed at 17p using the 17pseqrev1 primer. Telomere length distributions were then quantified using Phoretix software (Nonlinear dynamics)

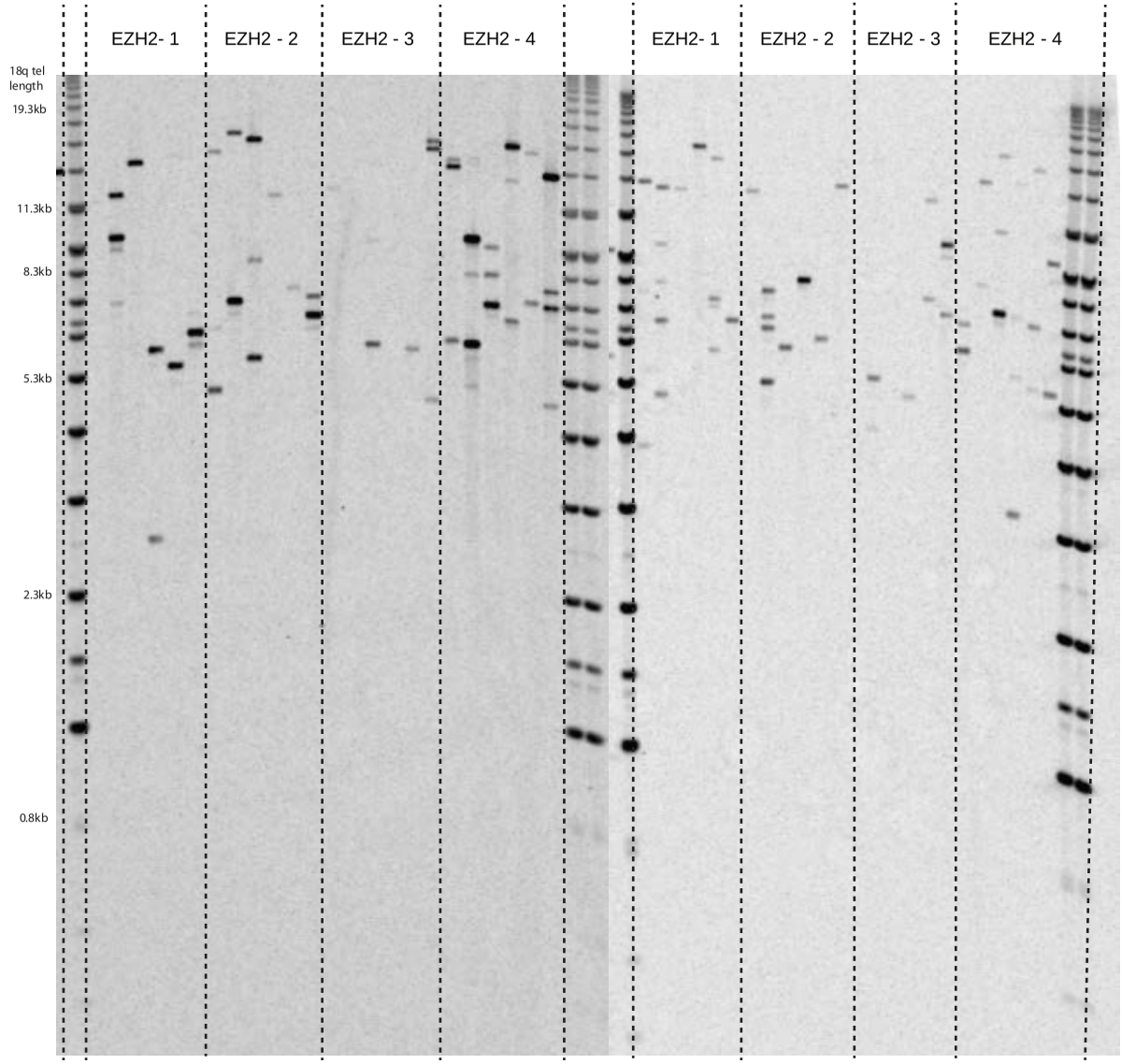

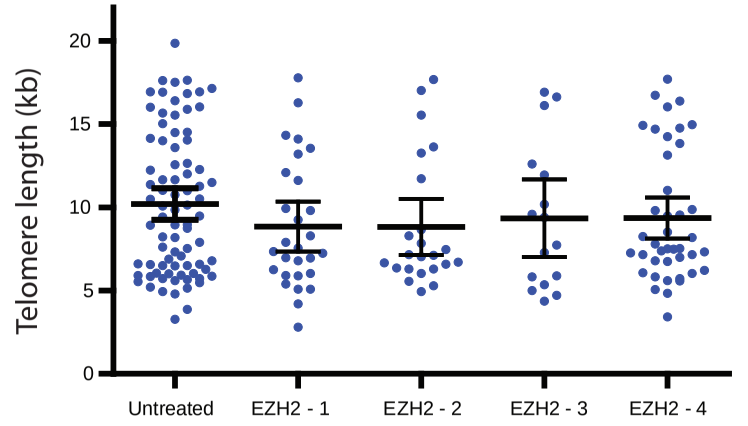

Mean tel length (kb)	10.19	8.843	8.83	9.346	9.356
Std. Error	0.4733	0.7308	0.8113	1.093	0.613

Appendix Figure 3. The effect of siRNA-mediated knockdown of EZH2 on the telomere length distribution at 18q. kC1B cells were transfected with 25nm siRNA targeted against EZH2 mRNA using DharmaFECT 1. EZH2-1, -2, -3 & -4 represent four biological replicates independently transfected. Each replicate was successively transfected three times at 96h intervals. 96 hours after the third transfection DNA was extracted. STELA was then performed at 18q using the 18qrev4M primer. Telomere length distributions were then quantified using Phoretix software (Nonlinear dynamics)

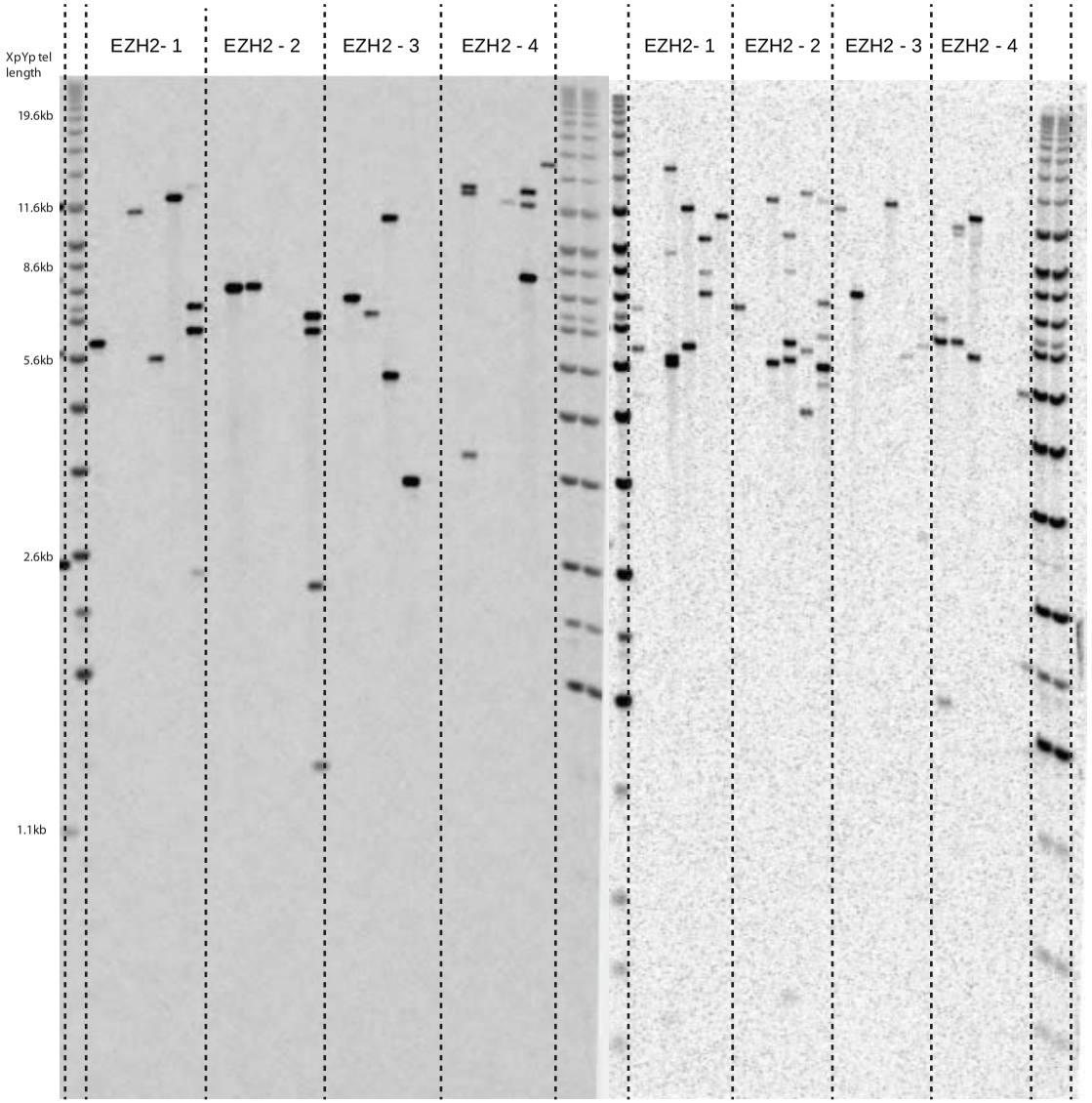

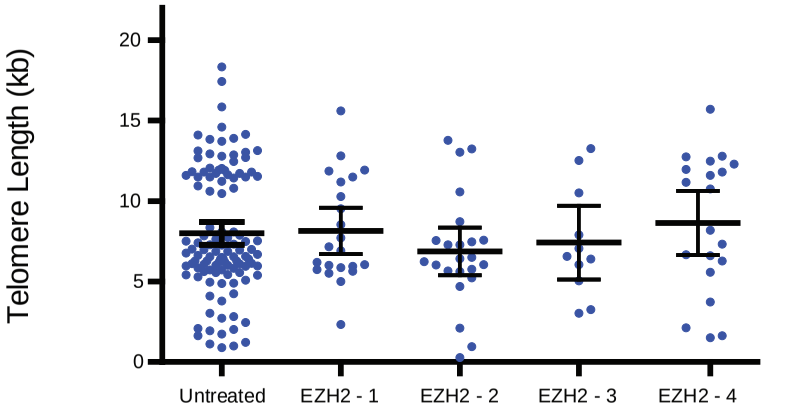

Mean tel length (kb)	7.992	8.149	6.87	7.419	8.645
Std. Error	0.3602	0.6913	0.7164	1.027	0.9517

Appendix Figure 4. The effect of siRNA-mediated knockdown of EZH2 on the telomere length distribution at XpYp. kC1B cells were transfected with 25nm siRNA targeted against EZH2 mRNA using DharmaFECT 1. EZH2-1, -2, -3 & -4 represent four biological replicates independently transfected. Each replicate was successively transfected three times at 96h intervals. 96 hours after the third transfection DNA was extracted. STELA was then performed at XpYp using the XpYpE. Telomere length distributions were then quantified using Phoretix software (Nonlinear dynamics)

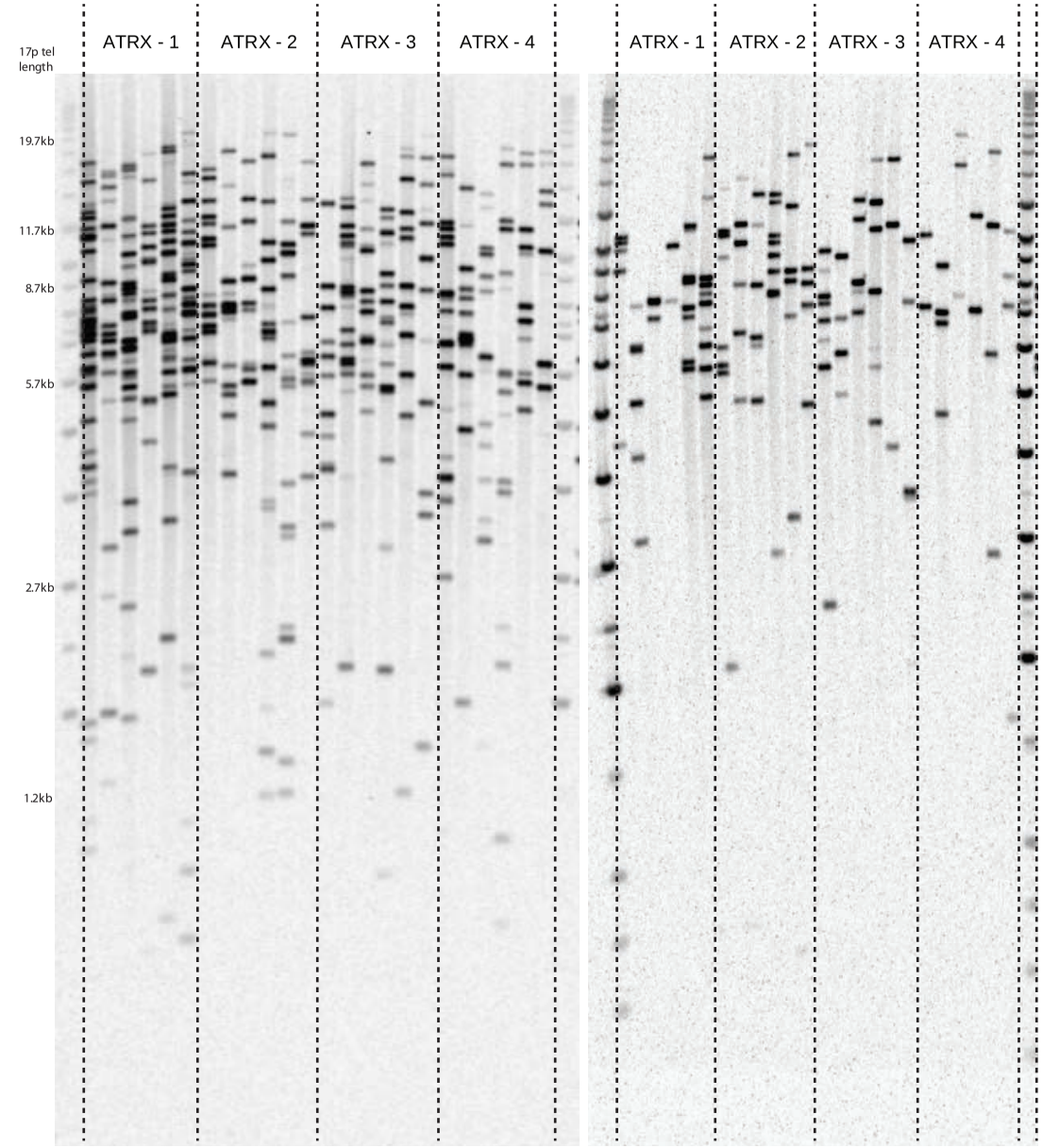

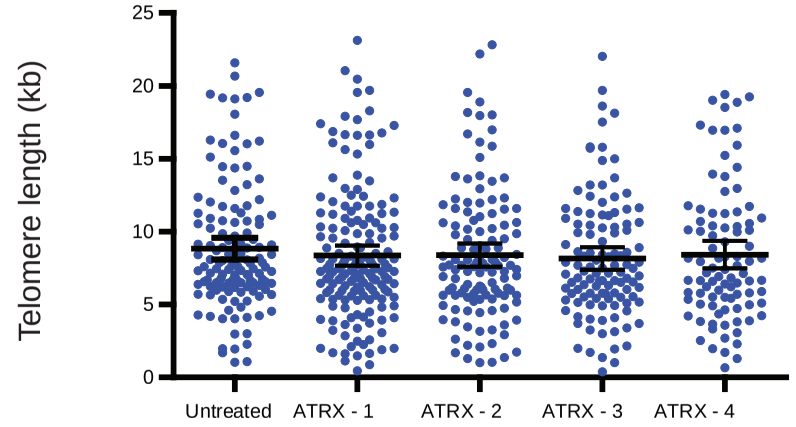

Mean tel length (kb)	8.831	8.358	8.397	8.159	8.426
Std. Error	0.3741	0.3463	0.4019	0.3837	0.4776

Appendix Figure 5. The effect of siRNA-mediated knockdown of ATRX on the telomere length distribution at 17p. kC1B cells were transfected with 25nm siRNA targeted against ATRX mRNA using DharmaFECT 1. ATRX-1, -2, -3 & -4 represent four biological replicates independently transfected. Each replicate was successively transfected three times at 96h intervals. 96 hours after the third transfection DNA was extracted. STELA was then performed at 17p using the 17pseqrev1 primer. Telomere length distributions were then quantified using Phoretix software (Nonlinear dynamics)

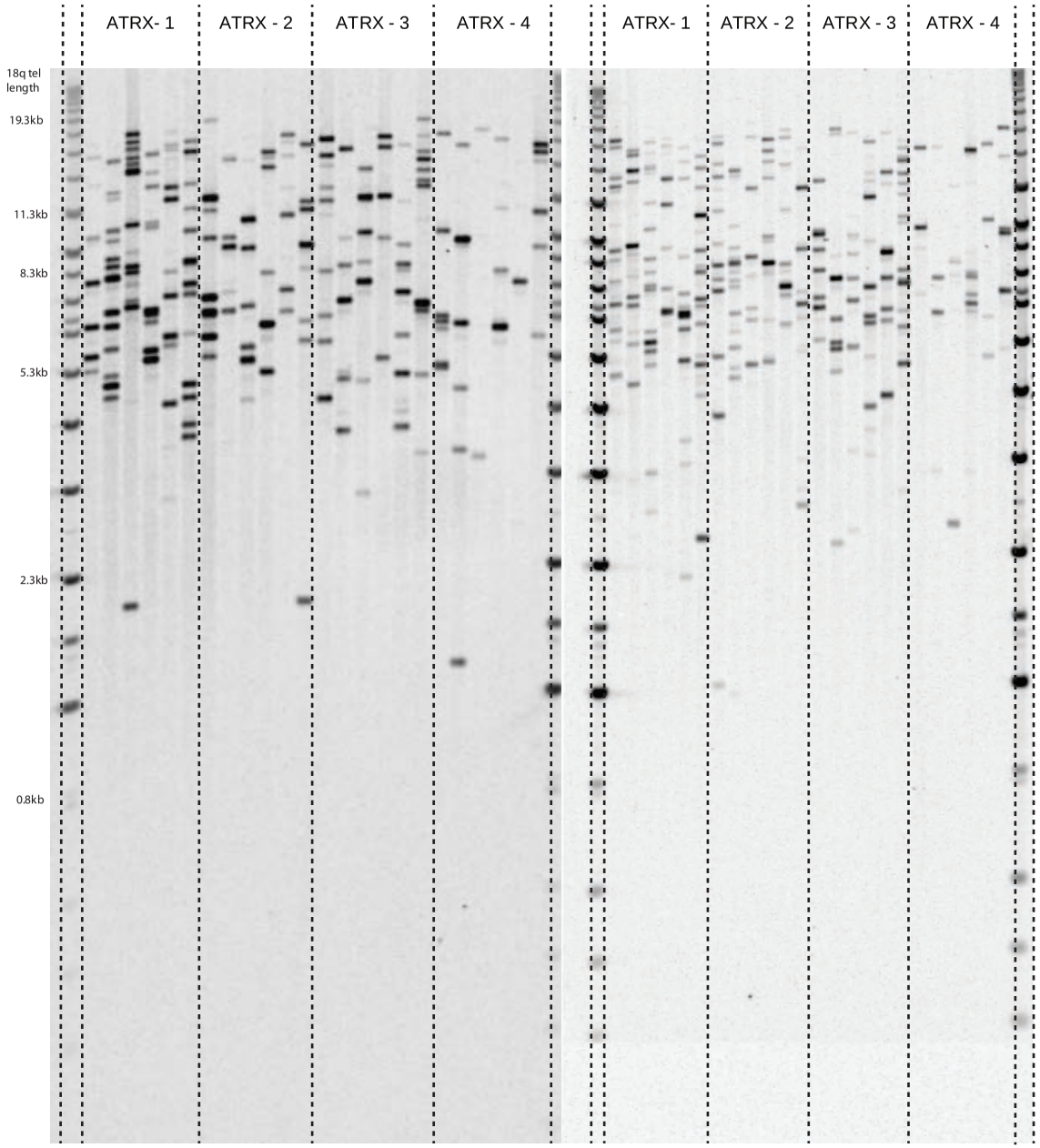

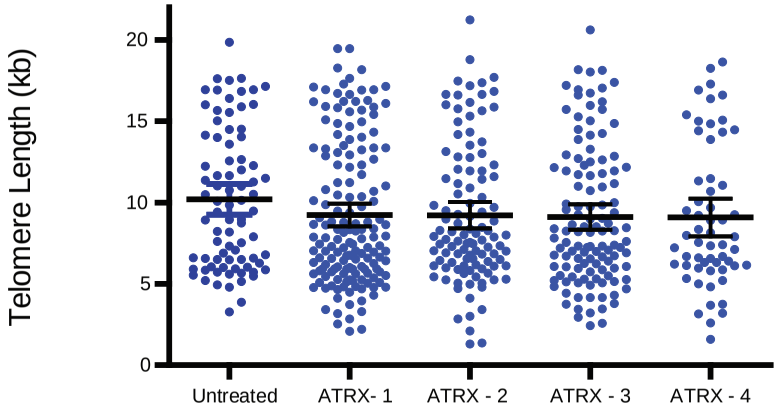

Mean tel length (kb)	10.19	9.233	9.222	9.113	9.081
Std. Error	0.4733	0.3515	0.408	0.3911	0.5782

Appendix Figure 6. The effect of siRNA-mediated knockdown of ATRX on the telomere length distribution at 18q. kC1B cells were transfected with 25nm siRNA targeted against ATRX mRNA using DharmaFECT 1. ATRX-1, -2, -3 & -4 represent four biological replicates independently transfected. Each replicate was successively transfected three times at 96h intervals. 96 hours after the third transfection DNA was extracted. STELA was then performed at 18q using the 18qrev4M primer. Telomere length distributions were then quantified using Phoretix software (Nonlinear dynamics)

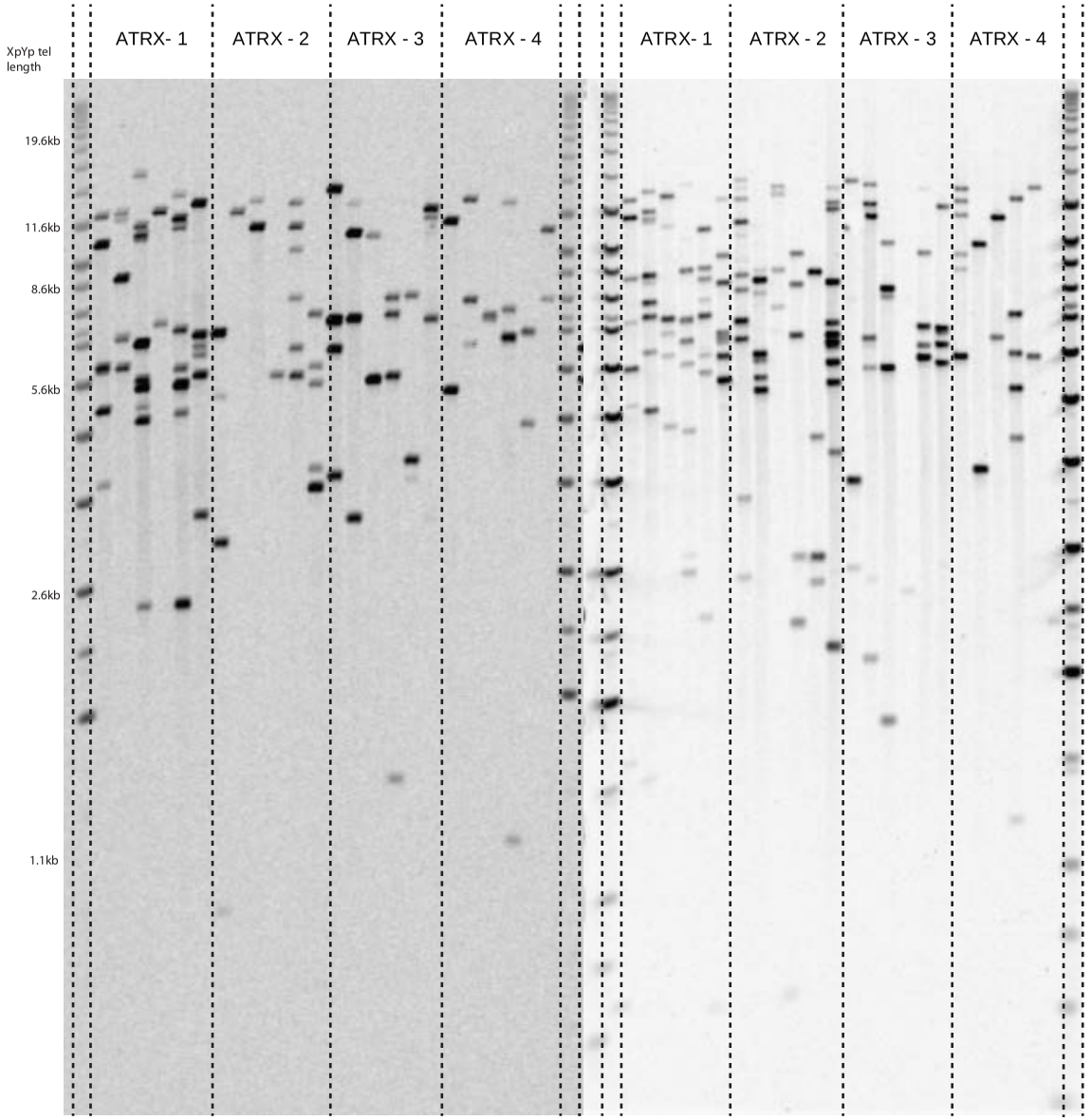

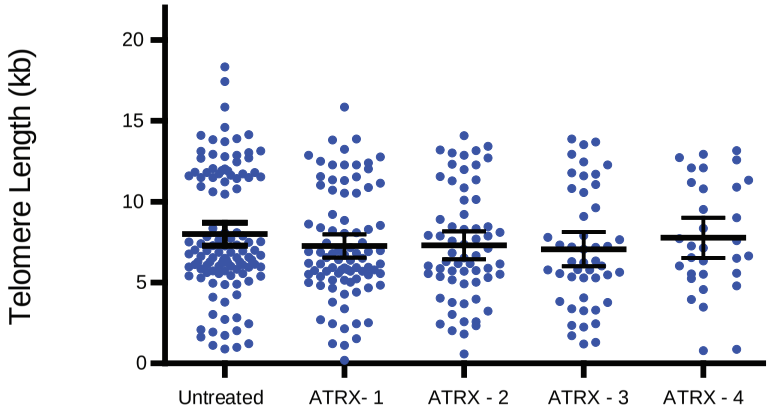

Mean tel length (kb)	7.992	7.268	7.304	7.066	7.773
Std. Error	0.3602	0.3622	0.434	0.5275	0.6097

Appendix Figure 7. The effect of siRNA-mediated knockdown of ATRX on the telomere length distribution at XpYp. kC1B cells were transfected with 25nm siRNA targeted against ATRX mRNA using DharmaFECT 1. ATRX-1, -2, -3 & -4 represent four biological replicates independently transfected. Each replicate was successively transfected three times at 96h intervals. 96 hours after the third transfection DNA was extracted. STELA was then performed at XpYp using the XpYpE primer. Telomere length distributions were then quantified using Phoretix software (Nonlinear dynamics)

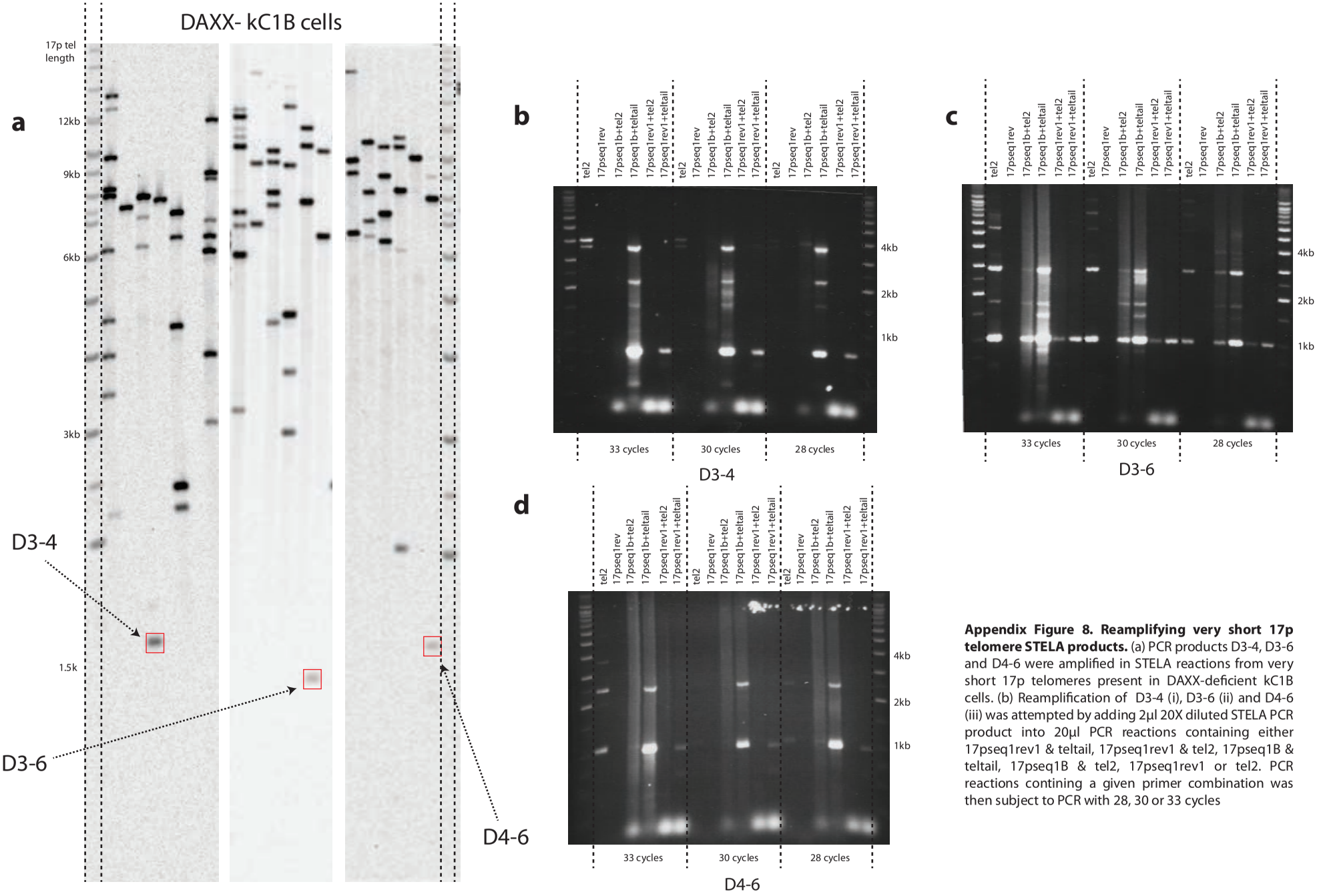

Appendix Figure 8. Reamplifying very short 17p telomere STELA products. (a) PCR products D3-4, D3-6 and D4-6 were amplified in STELA reactions from very short 17p telomeres present in DAXX-deficient kC1B cells. (b) Reamplification of D3-4 (i), D3-6 (ii) and D4-6 (iii) was attempted by adding 2µl 20X diluted STELA PCR product into 20µl PCR reactions containing either 17pseq1rev1 & teltail, 17pseq1rev1 & tel2, 17pseq1B & teltail, 17pseq1B & tel2, 17pseq1rev1 or tel2. PCR reactions contining a given primer combination was then subject to PCR with 28, 30 or 33 cycles

References

Abollo-Jimenez, F., Jimenez, R. and Cobaleda, C. (2010). Physiological cellular reprogramming and cancer. *Semin Cancer Biol* **20:**98-106.

Abreu, E., Aritonovska, E., Reichenbach, P., Cristofari, G., Culp, B., Terns, R. M., Lingner, J. *et al.* (2010). TIN2-tethered TPP1 recruits human telomerase to telomeres in vivo. *Mol Cell Biol* **30:**2971-2982.

Agrelo, R. and Wutz, A. (2010). X inactivation and disease. *Semin Cell Dev Biol* **21:**194-200.

Agresti, A. and Coull, B. (1998). Approximate Is Better than "Exact" for Interval Estimation of Binomial Proportions. *The American Statistician* **52:**119-126.

Ahmad, K. and Henikoff, S. (2002). The histone variant H3.3 marks active chromatin by replication-independent nucleosome assembly.*Mol Cell*. Vol. 9. United States, pp. 1191-1200.

Allfrey, V. G., Faulkner, R. and Mirsky, A. E. (1964). ACETYLATION AND METHYLATION OF HISTONES AND THEIR POSSIBLE ROLE IN THE REGULATION OF RNA SYNTHESIS. *Proc Natl Acad Sci U S A* **51:**786-794.

Allis, C. D., Bowen, J. K., Abraham, G. N., Glover, C. V. and Gorovsky, M. A. (1980). Proteolytic processing of histone H3 in chromatin: a physiologically regulated event in Tetrahymena micronuclei. *Cell* **20:**55-64.

Allshire, R. C. and Karpen, G. H. (2008). Epigenetic regulation of centromeric chromatin: old dogs, new tricks? *Nat Rev Genet* **9:**923-937.

Allshire, R. C., Nimmo, E. R., Ekwall, K., Javerzat, J. P. and Cranston, G. (1995). Mutations derepressing silent centromeric domains in fission yeast disrupt chromosome segregation. *Genes Dev* **9:**218-233.

Altaf, M., Utley, R. T., Lacoste, N., Tan, S., Briggs, S. D. and Cote, J. (2007). Interplay of chromatin modifiers on a short basic patch of histone H4 tail defines the boundary of telomeric heterochromatin. *Mol Cell* **28:**1002-1014.

Angelov, D., Molla, A., Perche, P. Y., Hans, F., Cote, J., Khochbin, S., Bouvet, P. *et al.* (2003). The histone variant macroH2A interferes with transcription factor binding and SWI/SNF nucleosome remodeling. *Mol Cell* **11:**1033-1041.

Aparicio, O. M., Billington, B. L. and Gottschling, D. E. (1991). Modifiers of position effect are shared between telomeric and silent mating-type loci in S. cerevisiae. *Cell* **66:**1279-1287.

Armanios, M. Y., Chen, J. J., Cogan, J. D., Alder, J. K., Ingersoll, R. G., Markin, C., Lawson, W. E. *et al.* (2007). Telomerase mutations in families with idiopathic pulmonary fibrosis. *N Engl J Med* **356:**1317-1326.

Arnoult, N., Van Beneden, A. and Decottignies, A. (2012). Telomere length regulates TERRA levels through increased trimethylation of telomeric H3K9 and HP1alpha.*Nat Struct Mol Biol*. Vol. 19. United States, pp. 948-956.

Askree, S. H., Yehuda, T., Smolikov, S., Gurevich, R., Hawk, J., Coker, C., Krauskopf, A. *et al.* (2004). A genome-wide screen for Saccharomyces cerevisiae deletion mutants that affect telomere length. *Proc Natl Acad Sci U S A* **101:**8658-8663.

Aubert, G. and Lansdorp, P. M. (2008). Telomeres and aging. *Physiol Rev* **88:**557-579.

Aviv, A., Hunt, S. C., Lin, J., Cao, X., Kimura, M. and Blackburn, E. (2011). Impartial comparative analysis of measurement of leukocyte telomere length/DNA content by Southern blots and qPCR. *Nucleic acids research* **39:**e134.

Azzalin, C. M., Reichenbach, P., Khoriauli, L., Giulotto, E. and Lingner, J. (2007). Telomeric repeat containing RNA and RNA surveillance factors at mammalian chromosome ends.*Science*. Vol. 318. United States, pp. 798-801.

Bae, N. S. and Baumann, P. (2007). A RAP1/TRF2 complex inhibits nonhomologous end-joining at human telomeric DNA ends. *Mol Cell* **26:**323-334.

Bai, Y. and Murnane, J. P. (2003). Telomere instability in a human tumor cell line expressing a dominant-negative WRN protein. *Hum Genet* **113:**337-347.

Baird, D. M. (2005). New developments in telomere length analysis.*Exp Gerontol*. Vol. 40. England, pp. 363-368.

Baird, D. M., Coleman, J., Rosser, Z. H. and Royle, N. J. (2000). High levels of sequence polymorphism and linkage disequilibrium at the telomere of 12q: implications for telomere biology and human evolution.*Am J Hum Genet*. Vol. 66. United States, pp. 235-250.

Baird, D. M., Jeffreys, A. J. and Royle, N. J. (1995). Mechanisms underlying telomere repeat turnover, revealed by hypervariable variant repeat distribution patterns in the human Xp/Yp telomere. *The EMBO journal* **14:**5433-5443.

Baird, D. M., Rowson, J., Wynford-Thomas, D. and Kipling, D. (2003). Extensive allelic variation and ultrashort telomeres in senescent human cells. *Nature Genetics* **33:**203-207.

Bannister, A. J. and Kouzarides, T. (2011). Regulation of chromatin by histone modifications. *Cell Res* **21:**381-395.

Bannister, A. J., Zegerman, P., Partridge, J. F., Miska, E. A., Thomas, J. O., Allshire, R. C. and Kouzarides, T. (2001). Selective recognition of methylated lysine 9 on histone H3 by the HP1 chromo domain. *Nature* **410:**120-124.

Barrandon, Y. and Green, H. (1987). Three clonal types of keratinocyte with different capacities for multiplication. *Proc Natl Acad Sci U S A* **84:**2302-2306.

Barski, A., Cuddapah, S., Cui, K., Roh, T. Y., Schones, D. E., Wang, Z., Wei, G. *et al.* (2007). High-resolution profiling of histone methylations in the human genome. *Cell* **129:**823-837.

Baumann, P. and Cech, T. R. (2001). Pot1, the putative telomere end-binding protein in fission yeast and humans. *Science* **292:**1171-1175.

Baur, J. A., Zou, Y., Shay, J. W. and Wright, W. E. (2001). Telomere position effect in human cells. *Science* **292:**2075-2077.

Becker-André, M. and Hahlbrock, K. (1989). Absolute mRNA quantification using the polymerase chain reaction (PCR). A novel approach by a PCR aided transcript titration assay (PATTY). *Nucleic Acids Res* **17:**9437-9446.

Belmont, A. S. and Bruce, K. (1994). Visualization of G1 chromosomes: a folded, twisted, supercoiled chromonema model of interphase chromatid structure. *J Cell Biol* **127:**287-302.

Belmont, A. S., Sedat, J. W. and Agard, D. A. (1987). A three-dimensional approach to mitotic chromosome structure: evidence for a complex hierarchical organization. *J Cell Biol* **105:**77-92.

Benetti, R., Garcia-Cao, M. and Blasco, M. A. (2007a). Telomere length regulates the epigenetic status of mammalian telomeres and subtelomeres. *Nature Genetics* **39:**243-250.

Benetti, R., Gonzalo, S., Jaco, I., Munoz, P., Gonzalez, S., Schoeftner, S., Murchison, E. *et al.* (2008). A mammalian microRNA cluster controls DNA methylation and telomere recombination via Rbl2-dependent regulation of DNA methyltransferases. *Nature structural & molecular biology* **15:**998.

Benetti, R., Gonzalo, S., Jaco, I., Schotta, G., Klatt, P., Jenuwein, T. and Blasco, M. A. (2007b). Suv4-20h deficiency results in telomere elongation and derepression of telomere recombination. *The Journal of cell biology* **178:**925-936.

Bernstein, B. E., Meissner, A. and Lander, E. S. (2007). The mammalian epigenome. *Cell* **128:**669-681.

Berthiau, A. S., Yankulov, K., Bah, A., Revardel, E., Luciano, P., Wellinger, R. J., Geli, V. *et al.* (2006). Subtelomeric proteins negatively regulate telomere elongation in budding yeast. *Embo J* **25:**846-856.

Blackburn, E. H. and Challoner, P. B. (1984). Identification of a telomeric DNA sequence in Trypanosoma brucei. *Cell* **36:**447-457.

Blackburn, E. H. and Gall, J. G. (1978). A tandemly repeated sequence at the termini of the extrachromosomal ribosomal RNA genes in Tetrahymena.*J Mol Biol*. Vol. 120. England, pp. 33-53.

Bochar, D. A., Wang, L., Beniya, H., Kinev, A., Xue, Y., Lane, W. S., Wang, W. *et al.* (2000). BRCA1 is associated with a human SWI/SNF-related complex: linking chromatin remodeling to breast cancer. *Cell* **102:**257-265.

Bodnar, A. G., Ouellette, M., Frolkis, M., Holt, S. E., Chiu, C. P., Morin, G. B., Harley, C. B. *et al.* (1998). Extension of life-span by introduction of telomerase into normal human cells. *Science* **279:**349-352.

Boulton, S. J. and Jackson, S. P. (1998). Components of the Ku-dependent non-homologous end-joining pathway are involved in telomeric length maintenance and telomeric silencing. *Embo J* **17:**1819-1828.

Bowen, N. J., Fujita, N., Kajita, M. and Wade, P. A. (2004). Mi-2/NuRD: multiple complexes for many purposes. *Biochim Biophys Acta* **1677:**52-57.

Boy de la Tour, E. and Laemmli, U. K. (1988). The metaphase scaffold is helically folded: sister chromatids have predominantly opposite helical handedness. *Cell* **55:**937-944.

Boyer, L. A., Langer, M. R., Crowley, K. A., Tan, S., Denu, J. M. and Peterson, C. L. (2002). Essential role for the SANT domain in the functioning of multiple chromatin remodeling enzymes. *Mol Cell* **10:**935-942.

Braig, M. and Schmitt, C. A. (2006). Oncogene-induced senescence: putting the brakes on tumor development. *Cancer Res* **66:**2881-2884.

Britt-Compton, B. and Baird, D. M. (2006). Intra-allelic mutation at human telomeres. *Biochemical Society transactions* **34:**581-582.

Britt-Compton, B., Capper, R., Rowson, J. and Baird, D. M. (2009). Short telomeres are preferentially elongated by telomerase in human cells. *FEBS Lett* **583:**3076-3080.

Britt-Compton, B., Rowson, J., Locke, M., Mackenzie, I., Kipling, D. and Baird, D. M. (2006). Structural stability and chromosome-specific telomere length is governed by cis-acting determinants in humans. *Human Molecular Genetics* **15:**725-733.

Broccoli, D., Smogorzewska, A., Chong, L. and de Lange, T. (1997). Human telomeres contain two distinct Myb-related proteins, TRF1 and TRF2. *Nat Genet* **17:**231-235.

Bryan, T. M., Englezou, A., Dalla-Pozza, L., Dunham, M. A. and Reddel, R. R. (1997). Evidence for an alternative mechanism for maintaining telomere length in human tumors and tumor-derived cell lines. *Nat Med* **3:**1271-1274.

Bryan, T. M., Englezou, A., Gupta, J., Bacchetti, S. and Reddel, R. R. (1995). Telomere elongation in immortal human cells without detectable telomerase activity. *Embo J* **14:**4240-4248.

Burgio, G., Cipressa, F., Ingrassia, A. M., Cenci, G. and Corona, D. F. (2011). The histone deacetylase Rpd3 regulates the heterochromatin structure of Drosophila telomeres.*J Cell Sci*. Vol. 124. England, pp. 2041-2048.

Burma, S., Chen, B. P., Murphy, M., Kurimasa, A. and Chen, D. J. (2001). ATM phosphorylates histone H2AX in response to DNA double-strand breaks. *J Biol Chem* **276:**42462-42467.

Byvoet, P., Shepherd, G. R., Hardin, J. M. and Noland, B. J. (1972). The distribution and turnover of labeled methyl groups in histone fractions of cultured mammalian cells. *Arch Biochem Biophys* **148:**558-567.

Cai, Y., Jin, J., Yao, T., Gottschalk, A. J., Swanson, S. K., Wu, S., Shi, Y. *et al.* (2007). YY1 functions with INO80 to activate transcription. *Nat Struct Mol Biol* **14:**872-874.

Cairns, B. R., Schlichter, A., Erdjument-Bromage, H., Tempst, P., Kornberg, R. D. and Winston, F. (1999). Two functionally distinct forms of the RSC nucleosome-remodeling complex, containing essential AT hook, BAH, and bromodomains. *Mol. Cell* **4:**715-723.

Campisi, J. and d'Adda di Fagagna, F. (2007). Cellular senescence: when bad things happen to good cells. *Nat Rev Mol Cell Biol* **8:**729-740.

Capper, R., Britt-Compton, B., Tankimanova, M., Rowson, J., Letsolo, B., Man, S., Haughton, M. *et al.* (2007). The nature of telomere fusion and a definition of the critical telomere length in human cells. *Genes & development* **21:**2495-2508.

Carrel, A. and Ebeling, A. H. (1921). AGE AND MULTIPLICATION OF FIBROBLASTS. *J Exp Med* **34:**599-623.

Caslini, C., Connelly, J. A., Serna, A., Broccoli, D. and Hess, J. L. (2009). MLL associates with telomeres and regulates telomeric repeat-containing RNA transcription. *Molecular and cellular biology* **29:**4519-4526.

Cawthon, R. M. (2002). Telomere measurement by quantitative PCR. *Nucleic Acids Res* **30:**e47.

Cawthon, R. M. (2009). Telomere length measurement by a novel monochrome multiplex quantitative PCR method. *Nucleic acids research* **37:**e21.

Celli, G. B. and de Lange, T. (2005). DNA processing is not required for ATM-mediated telomere damage response after TRF2 deletion. *Nat Cell Biol* **7:**712-718.

Cenci, G., Siriaco, G., Raffa, G. D., Kellum, R. and Gatti, M. (2003). The Drosophila HOAP protein is required for telomere capping.*Nat Cell Biol*. Vol. 5. England, pp. 82-84.

Cesare, A. J. and Griffith, J. D. (2004). Telomeric DNA in ALT cells is characterized by free telomeric circles and heterogeneous t-loops. *Mol Cell Biol* **24:**9948-9957.

Cesare, A. J., Quinney, N., Willcox, S., Subramanian, D. and Griffith, J. D. (2003). Telomere looping in P. sativum (common garden pea).*Plant J*. Vol. 36. England, pp. 271-279.

Cesare, A. J. and Reddel, R. R. (2010). Alternative lengthening of telomeres: models, mechanisms and implications. *Nat Rev Genet* **11:**319-330.

Chai, W., Shay, J. W. and Wright, W. E. (2005). Human telomeres maintain their overhang length at senescence.*Mol Cell Biol*. Vol. 25. United States, pp. 2158-2168.

Champagne, K. S. and Kutateladze, T. G. (2009). Structural insight into histone recognition by the ING PHD fingers. *Curr Drug Targets* **10:**432-441.

Chang, B., Chen, Y., Zhao, Y. and Bruick, R. K. (2007). JMJD6 is a histone arginine demethylase. *Science* **318:**444-447.

Chen, L., Lee, L., Kudlow, B. A., Dos Santos, H. G., Sletvold, O., Shafeghati, Y., Botha, E. G. *et al.* (2003). LMNA mutations in atypical Werner's syndrome. *Lancet* **362:**440-445.

Chen, L. Y., Liu, D. and Songyang, Z. (2007). Telomere maintenance through spatial control of telomeric proteins. *Mol Cell Biol* **27:**5898-5909.

Chen, Q., Ijpma, A. and Greider, C. W. (2001). Two survivor pathways that allow growth in the absence of telomerase are generated by distinct telomere recombination events. *Mol Cell Biol* **21:**1819-1827.

Chen, Y., Yang, Y., van Overbeek, M., Donigian, J. R., Baciu, P., de Lange, T. and Lei, M. (2008). A shared docking motif in TRF1 and TRF2 used for differential recruitment of telomeric proteins. *Science* **319:**1092-1096.

Cheung, I., Schertzer, M., Baross, A., Rose, A. M., Lansdorp, P. M. and Baird, D. M. (2004). Strain-specific telomere length revealed by single telomere length analysis in Caenorhabditis elegans. *Nucleic Acids Res* **32:**3383-3391.

Chiurillo, M. A., Cano, I., Da Silveira, J. F. and Ramirez, J. L. (1999). Organization of telomeric and sub-telomeric regions of chromosomes from the protozoan parasite Trypanosoma cruzi. *Mol Biochem Parasitol* **100:**173-183.

Chow, C. M., Georgiou, A., Szutorisz, H., Maia e Silva, A., Pombo, A., Barahona, I., Dargelos, E. *et al.* (2005). Variant histone H3.3 marks promoters of transcriptionally active genes during mammalian cell division. *EMBO Rep* **6:**354-360.

Cohen, S. B., Graham, M. E., Lovrecz, G. O., Bache, N., Robinson, P. J. and Reddel, R. R. (2007). Protein composition of catalytically active human telomerase from immortal cells. *Science* **315:**1850-1853.

Cohn, M. and Blackburn, E. H. (1995). Telomerase in yeast. *Science* **269:**396-400.

Coleman, J., Baird, D. M. and Royle, N. J. (1999). The plasticity of human telomeres demonstrated by a hypervariable telomere repeat array that is located on some copies of 16p and 16q.*Hum Mol Genet*. Vol. 8. England, pp. 1637-1646.

Colgin, L. M., Baran, K., Baumann, P., Cech, T. R. and Reddel, R. R. (2003). Human POT1 facilitates telomere elongation by telomerase. *Curr Biol* **13:**942-946.

Collins, N., Poot, R. A., Kukimoto, I., Garcia-Jimenez, C., Dellaire, G. and Varga-Weisz, P. D. (2002). An ACF1-ISWI chromatin-remodeling complex is required for DNA replication through heterochromatin. *Nat Genet* **32:**627-632.

Corona, D. F. and Tamkun, J. W. (2004). Multiple roles for ISWI in transcription, chromosome organization and DNA replication. *Biochim Biophys Acta* **1677:**113-119.

Costanzi, C. and Pehrson, J. R. (2001). MACROH2A2, a new member of the MARCOH2A core histone family. *J Biol Chem* **276:**21776-21784.

Counter, C. M., Avilion, A. A., LeFeuvre, C. E., Stewart, N. G., Greider, C. W., Harley, C. B. and Bacchetti, S. (1992). Telomere shortening associated with chromosome instability is arrested in immortal cells which express telomerase activity. *Embo j* **11:**1921-1929.

Crabbe, L., Jauch, A., Naeger, C. M., Holtgreve-Grez, H. and Karlseder, J. (2007). Telomere dysfunction as a cause of genomic instability in Werner syndrome. *Proc Natl Acad Sci U S A* **104:**2205-2210.

Craig, J. M. (2005). Heterochromatin--many flavours, common themes. *Bioessays* **27:**17-28.

Cuthbert, G. L., Daujat, S., Snowden, A. W., Erdjument-Bromage, H., Hagiwara, T., Yamada, M., Schneider, R. *et al.* (2004). Histone deimination antagonizes arginine methylation. *Cell* **118:**545-553.

d'Adda di Fagagna, F., Reaper, P. M., Clay-Farrace, L., Fiegler, H., Carr, P., Von Zglinicki, T., Saretzki, G. *et al.* (2003). A DNA damage checkpoint response in telomere-initiated senescence. *Nature* **426:**194-198.

Dalal, Y., Wang, H., Lindsay, S. and Henikoff, S. (2007). Tetrameric structure of centromeric nucleosomes in interphase Drosophila cells. *PLoS Biol* **5:**e218.

Daury, L., Chailleux, C., Bonvallet, J. and Trouche, D. (2006). Histone H3.3 deposition at E2F-regulated genes is linked to transcription. *EMBO Rep* **7:**66-71.

de Bruin, D., Zaman, Z., Liberatore, R. A. and Ptashne, M. (2001). Telomere looping permits gene activation by a downstream UAS in yeast.*Nature*. Vol. 409. England, pp. 109-113.

de Lange, T. (2005). Shelterin: the protein complex that shapes and safeguards human telomeres.*Genes Dev*. Vol. 19. United States, pp. 2100-2110.

de Lange, T., Shiue, L., Myers, R. M., Cox, D. R., Naylor, S. L., Killery, A. M. and Varmus, H. E. (1990). Structure and variability of human chromosome ends. *Mol Cell Biol* **10:**518-527.

De Rubertis, F., Kadosh, D., Henchoz, S., Pauli, D., Reuter, G., Struhl, K. and Spierer, P. (1996). The histone deacetylase RPD3 counteracts genomic silencing in Drosophila and yeast. *Nature* **384:**589-591.

de Wilde, R. F., Heaphy, C. M., Maitra, A., Meeker, A. K., Edil, B. H., Wolfgang, C. L., Ellison, T. A. *et al.* (2012). Loss of ATRX or DAXX expression and concomitant acquisition of the alternative lengthening of telomeres phenotype are late events in a small subset of MEN-1 syndrome pancreatic neuroendocrine tumors.*Mod Pathol*. Vol. 25. United States, pp. 1033-1039.

Decristofaro, M. F., Betz, B. L., Rorie, C. J., Reisman, D. N., Wang, W. and Weissman, B. E. (2001). Characterization of SWI/SNF protein expression in human breast cancer cell lines and other malignancies. *J Cell Physiol* **186:**136-145.

Dehe, P. M., Rog, O., Ferreira, M. G., Greenwood, J. and Cooper, J. P. (2012). Taz1 enforces cell-cycle regulation of telomere synthesis. *Mol Cell* **46:**797-808.

Delbarre, E., Jacobsen, B. M., Reiner, A. H., Sørensen, A. L., Küntziger, T. and Collas, P. (2010). Chromatin environment of histone variant H3.3 revealed by quantitative imaging and genome-scale chromatin and DNA immunoprecipitation. *Mol Biol Cell* **21:**1872-1884.

Denchi, E. L. and de Lange, T. (2007). Protection of telomeres through independent control of ATM and ATR by TRF2 and POT1. *Nature* **448:**1068-1071.

Deng, Z., Campbell, A. E. and Lieberman, P. M. (2010). TERRA, CpG methylation and telomere heterochromatin: lessons from ICF syndrome cells. *Cell Cycle* **9:**69-74.

Deng, Z., Dheekollu, J., Broccoli, D., Dutta, A. and Lieberman, P. M. (2007). The origin recognition complex localizes to telomere repeats and prevents telomere-circle formation. *Curr Biol* **17:**1989-1995.

Deng, Z., Norseen, J., Wiedmer, A., Riethman, H. and Lieberman, P. M. (2009). TERRA RNA binding to TRF2 facilitates heterochromatin formation and ORC recruitment at telomeres. *Mol Cell* **35:**403-413.

Deng, Z., Wang, Z., Stong, N., Plasschaert, R., Moczan, A., Chen, H. S., Hu, S. *et al.* (2012). A role for CTCF and cohesin in subtelomere chromatin organization, TERRA transcription, and telomere end protection.*EMBO J*. Vol. 31. England, pp. 4165-4178.

Deuring, R., Fanti, L., Armstrong, J. A., Sarte, M., Papoulas, O., Prestel, M., Daubresse, G. *et al.* (2000). The ISWI chromatin-remodeling protein is required for gene expression and the maintenance of higher order chromatin structure in vivo. *Mol Cell* **5:**355-365.

Dimitrova, N., Chen, Y. C., Spector, D. L. and de Lange, T. (2008). 53BP1 promotes non-homologous end joining of telomeres by increasing chromatin mobility. *Nature* **456:**524-528.

Dionne, I. and Wellinger, R. J. (1996). Cell cycle-regulated generation of single-stranded G-rich DNA in the absence of telomerase. *Proc Natl Acad Sci U S A* **93:**13902-13907.

Dixit, M., Ansseau, E., Tassin, A., Winokur, S., Shi, R., Qian, H., Sauvage, S. *et al.* (2007). DUX4, a candidate gene of facioscapulohumeral muscular dystrophy, encodes a transcriptional activator of PITX1. *Proc Natl Acad Sci U S A* **104:**18157-18162.

Dokal, I. (2006). Fanconi's anaemia and related bone marrow failure syndromes. *Br Med Bull* **77-78:**37-53.

Dokmanovic, M., Clarke, C. and Marks, P. A. (2007). Histone deacetylase inhibitors: overview and perspectives. *Mol Cancer Res* **5:**981-989.

Dorigo, B., Schalch, T., Bystricky, K. and Richmond, T. J. (2003). Chromatin fiber folding: requirement for the histone H4 N-terminal tail. *J Mol Biol* **327:**85-96.

Drané, P., Ouararhni, K., Depaux, A., Shuaib, M. and Hamiche, A. (2010). The death-associated protein DAXX is a novel histone chaperone involved in the replication-independent deposition of H3.3. *Genes Dev* **24:**1253-1265.

Duncan, E. M., Muratore-Schroeder, T. L., Cook, R. G., Garcia, B. A., Shabanowitz, J., Hunt, D. F. and Allis, C. D. (2008). Cathepsin L proteolytically processes histone H3 during mouse embryonic stem cell differentiation. *Cell* **135:**284-294.

Dunham, M. A., Neumann, A. A., Fasching, C. L. and Reddel, R. R. (2000). Telomere maintenance by recombination in human cells. *Nat Genet* **26:**447-450.

Egli, C., Thur, B., Liu, L. and Hofmann, M. A. (2001). Quantitative TaqMan RT-PCR for the detection and differentiation of European and North American strains of porcine reproductive and respiratory syndrome virus.*J Virol Methods*. Vol. 98. Netherlands, pp. 63-75.

Fairall, L., Chapman, L., Moss, H., de Lange, T. and Rhodes, D. (2001). Structure of the TRFH dimerization domain of the human telomeric proteins TRF1 and TRF2. *Mol Cell* **8:**351-361.

Fajkus, J., Kovarik, A., Kralovics, R. and Bezdek, M. (1995). Organization of telomeric and subtelomeric chromatin in the higher plant Nicotiana tabacum. *Mol Gen Genet* **247:**633-638.

Fan, Y., Nikitina, T., Zhao, J., Fleury, T. J., Bhattacharyya, R., Bouhassira, E. E., Stein, A. *et al.* (2005). Histone H1 depletion in mammals alters global chromatin structure but causes specific changes in gene regulation. *Cell* **123:**1199-1212.

Fanti, L., Giovinazzo, G., Berloco, M. and Pimpinelli, S. (1998). The heterochromatin protein 1 prevents telomere fusions in Drosophila.*Mol Cell*. Vol. 2. United States, pp. 527-538.

Feng, Q. and Zhang, Y. (2001). The MeCP1 complex represses transcription through preferential binding, remodeling, and deacetylating methylated nucleosomes. *Genes Dev* **15:**827-832.

Fernandez-Capetillo, O., Celeste, A. and Nussenzweig, A. (2003). Focusing on foci: H2AX and the recruitment of DNA-damage response factors. *Cell Cycle* **2:**426-427.

Fernandez-Capetillo, O., Chen, H. T., Celeste, A., Ward, I., Romanienko, P. J., Morales, J. C., Naka, K. *et al.* (2002). DNA damage-induced G2-M checkpoint activation by histone H2AX and 53BP1. *Nat Cell Biol* **4:**993-997.

Fernandez-Moreno, M., Tamayo, M., Soto-Hermida, A., Mosquera, A., Oreiro, N., Fernandez-Lopez, C., Fernandez, J. L. *et al.* (2011). mtDNA haplogroup J modulates telomere length and nitric oxide production.*BMC Musculoskelet Disord*. Vol. 12. England, p. 283.

Finch, J. T. and Klug, A. (1976). Solenoidal model for superstructure in chromatin. *Proc Natl Acad Sci U S A* **73:**1897-1901.

Fischle, W., Tseng, B. S., Dormann, H. L., Ueberheide, B. M., Garcia, B. A., Shabanowitz, J., Hunt, D. F. *et al.* (2005). Regulation of HP1-chromatin binding by histone H3 methylation and phosphorylation. *Nature* **438:**1116-1122.

Fisher, T. S., Taggart, A. K. and Zakian, V. A. (2004). Cell cycle-dependent regulation of yeast telomerase by Ku. *Nat Struct Mol Biol* **11:**1198-1205.

Flynn, R. L., Centore, R. C., O'Sullivan, R. J., Rai, R., Tse, A., Songyang, Z., Chang, S. *et al.* (2011). TERRA and hnRNPA1 orchestrate an RPA-to-POT1 switch on telomeric single-stranded DNA. *Nature* **471:**532-536.

Frietze, S., O'Geen, H., Blahnik, K. R., Jin, V. X. and Farnham, P. J. (2010). ZNF274 recruits the histone methyltransferase SETDB1 to the 3' ends of ZNF genes. *PLoS One* **5:**e15082.

Frydrychova, R. C., Mason, J. M. and Archer, T. K. (2008). HP1 Is Distributed Within Distinct Chromatin Domains at Drosophila Telomeres. *Genetics* **180:**121-131.

Fu, D. and Collins, K. (2007). Purification of human telomerase complexes identifies factors involved in telomerase biogenesis and telomere length regulation. *Mol Cell* **28:**773-785.

Fujimoto, K., Kyo, S., Takakura, M., Kanaya, T., Kitagawa, Y., Itoh, H., Takahashi, M. *et al.* (2000). Identification and characterization of negative regulatory elements of the human telomerase catalytic subunit (hTERT) gene promoter: possible role of MZF-2 in transcriptional repression of hTERT. *Nucleic Acids Res* **28:**2557-2562.

Fuks, F., Vire, E., Brenner, C., Deplus, R., Blanchon, L., Fraga, M., Didelot, C. *et al.* (2006). The Polycomb group protein EZH2 directly controls DNA methylation. *Nature* **439:**871-874.

Gangaraju, V. K. and Bartholomew, B. (2007). Mechanisms of ATP dependent chromatin remodeling. *Mutat Res* **618:**3-17.

Gao, G., Walser, J. C., Beaucher, M. L., Morciano, P., Wesolowska, N., Chen, J. and Rong, Y. S. (2010). HipHop interacts with HOAP and HP1 to protect Drosophila telomeres in a sequence-independent manner.*EMBO J*. Vol. 29. England, pp. 819-829.

Garcia, C. K., Wright, W. E. and Shay, J. W. (2007). Human diseases of telomerase dysfunction: insights into tissue aging. *Nucleic Acids Res* **35:**7406-7416.

Garcia-Cao, M., Gonzalo, S., Dean, D. and Blasco, M. A. (2002). A role for the Rb family of proteins in controlling telomere length. *Nature Genetics* **32:**415-419.

Garcia-Cao, M., O'Sullivan, R., Peters, A. H., Jenuwein, T. and Blasco, M. A. (2004). Epigenetic regulation of telomere length in mammalian cells by the Suv39h1 and Suv39h2 histone methyltransferases. *Nature Genetics* **36:**94-99.

Gehring, W. J., Klemenz, R., Weber, U. and Kloter, U. (1984). Functional analysis of the white gene of Drosophila by P-factor-mediated transformation. *Embo j* **3:**2077-2085.

Gilliland, G., Perrin, S., Blanchard, K. and Bunn, H. F. (1990). Analysis of cytokine mRNA and DNA: detection and quantitation by competitive polymerase chain reaction. *Proc Natl Acad Sci U S A* **87:**2725-2729.

Gillis, A. J., Stoop, H., Biermann, K., van Gurp, R. J., Swartzman, E., Cribbes, S., Ferlinz, A. *et al.* (2011). Expression and interdependencies of pluripotency factors LIN28, OCT3/4, NANOG and SOX2 in human testicular germ cells and tumours of the testis. *Int J Androl* **34:**e160-174.

Gilson, E. and Geli, V. (2007). How telomeres are replicated. *Nat Rev Mol Cell Biol* **8:**825-838.

Goldberg, A. D., Banaszynski, L. A., Noh, K. M., Lewis, P. W., Elsaesser, S. J., Stadler, S., Dewell, S. *et al.* (2010). Distinct factors control histone variant H3.3 localization at specific genomic regions. *Cell* **140:**678-691.

Goldmark, J. P., Fazzio, T. G., Estep, P. W., Church, G. M. and Tsukiyama, T. (2000). The Isw2 chromatin remodeling complex represses early meiotic genes upon recruitment by Ume6p. *Cell* **103:**423-433.

Gonzalo, S., Jaco, I., Fraga, M. F., Chen, T., Li, E., Esteller, M. and Blasco, M. A. (2006). DNA methyltransferases control telomere length and telomere recombination in mammalian cells. *Nature cell biology* **8:**416-424.

Gottschling, D. E., Aparicio, O. M., Billington, B. L. and Zakian, V. A. (1990). Position effect at S. cerevisiae telomeres: reversible repression of Pol II transcription. *Cell* **63:**751-762.

Gould, K. L. and Nurse, P. (1989). Tyrosine phosphorylation of the fission yeast cdc2+ protein kinase regulates entry into mitosis. *Nature* **342:**39-45.

Greer, E. L. and Shi, Y. (2012). Histone methylation: a dynamic mark in health, disease and inheritance. *Nat Rev Genet* **13:**343-357.

Greider, C. W. and Blackburn, E. H. (1985). Identification of a specific telomere terminal transferase activity in Tetrahymena extracts. *Cell* **43:**405-413.

Griffith, J. D., Comeau, L., Rosenfield, S., Stansel, R. M., Bianchi, A., Moss, H. and de Lange, T. (1999). Mammalian telomeres end in a large duplex loop.*Cell*. Vol. 97. United States, pp. 503-514.

Gross, T. J. and Hunninghake, G. W. (2001). Idiopathic pulmonary fibrosis. *N Engl J Med* **345:**517-525.

Grune, T., Brzeski, J., Eberharter, A., Clapier, C. R., Corona, D. F., Becker, P. B. and Muller, C. W. (2003). Crystal structure and functional analysis of a nucleosome recognition module of the remodeling factor ISWI. *Mol Cell* **12:**449-460.

Grunstein, M. (1998). Yeast heterochromatin: regulation of its assembly and inheritance by histones. *Cell* **93:**325-328.

Guccione, E., Bassi, C., Casadio, F., Martinato, F., Cesaroni, M., Schuchlautz, H., Luscher, B. *et al.* (2007). Methylation of histone H3R2 by PRMT6 and H3K4 by an MLL complex are mutually exclusive. *Nature* **449:**933-937.

Guschin, D., Geiman, T. M., Kikyo, N., Tremethick, D. J., Wolffe, A. P. and Wade, P. A. (2000). Multiple ISWI ATPase complexes from xenopus laevis. Functional conservation of an ACF/CHRAC homolog. *J Biol Chem* **275:**35248-35255.

Gut, M., Leutenegger, C. M., Huder, J. B., Pedersen, N. C. and Lutz, H. (1999). One-tube fluorogenic reverse transcription-polymerase chain reaction for the quantitation of feline coronaviruses.*J Virol Methods*. Vol. 77. Netherlands, pp. 37-46.

Hake, S. B., Garcia, B. A., Kauer, M., Baker, S. P., Shabanowitz, J., Hunt, D. F. and Allis, C. D. (2005). Serine 31 phosphorylation of histone variant H3.3 is specific to regions bordering centromeres in metaphase chromosomes. *Proc Natl Acad Sci U S A* **102:**6344-6349.

Hansen, J. C. (2002). Conformational dynamics of the chromatin fiber in solution: determinants, mechanisms, and functions. *Annu Rev Biophys Biomol Struct* **31:**361-392.

Hara, R. and Sancar, A. (2002). The SWI/SNF chromatin-remodeling factor stimulates repair by human excision nuclease in the mononucleosome core particle. *Mol Cell Biol* **22:**6779-6787.

Haring, M., Offermann, S., Danker, T., Horst, I., Peterhansel, C. and Stam, M. (2007). Chromatin immunoprecipitation: optimization, quantitative analysis and data normalization. *Plant Methods* **3:**11.

Harle-Bachor, C. and Boukamp, P. (1996). Telomerase activity in the regenerative basal layer of the epidermis inhuman skin and in immortal and carcinoma-derived skin keratinocytes. *Proceedings of the National Academy of Sciences of the United States of America* **93:**6476-6481.

Harley, C. B., Futcher, A. B. and Greider, C. W. (1990). Telomeres shorten during ageing of human fibroblasts. *Nature* **345:**458-460.

Hassa, P. O., Haenni, S. S., Elser, M. and Hottiger, M. O. (2006). Nuclear ADP-ribosylation reactions in mammalian cells: where are we today and where are we going? *Microbiol Mol Biol Rev* **70:**789-829.

Hayflick, L. (1965). THE LIMITED IN VITRO LIFETIME OF HUMAN DIPLOID CELL STRAINS. *Exp Cell Res* **37:**614-636.

Hayflick, L. and Moorhead, P. S. (1961). The serial cultivation of human diploid cell strains. *Exp Cell Res* **25:**585-621.

Hazelrigg, T., Levis, R. and Rubin, G. M. (1984). Transformation of white locus DNA in drosophila: dosage compensation, zeste interaction, and position effects. *Cell* **36:**469-481.

He, H., Multani, A. S., Cosme-Blanco, W., Tahara, H., Ma, J., Pathak, S., Deng, Y. *et al.* (2006). POT1b protects telomeres from end-to-end chromosomal fusions and aberrant homologous recombination. *Embo j* **25:**5180-5190.

Heacock, M., Spangler, E., Riha, K., Puizina, J. and Shippen, D. E. (2004). Molecular analysis of telomere fusions in Arabidopsis: multiple pathways for chromosome end-joining. *Embo j* **23:**2304-2313.

Heaphy, C. M., de Wilde, R. F., Jiao, Y., Klein, A. P., Edil, B. H., Shi, C., Bettegowda, C. *et al.* (2011). Altered telomeres in tumors with ATRX and DAXX mutations. *Science* **333:**425.

Heard, E. (2005). Delving into the diversity of facultative heterochromatin: the epigenetics of the inactive X chromosome.*Curr Opin Genet Dev*. Vol. 15. England, pp. 482-489.

Heintzman, N. D., Stuart, R. K., Hon, G., Fu, Y., Ching, C. W., Hawkins, R. D., Barrera, L. O. *et al.* (2007). Distinct and predictive chromatin signatures of transcriptional promoters and enhancers in the human genome. *Nat Genet* **39:**311-318.

Hemann, M. T. and Greider, C. W. (2000). Wild-derived inbred mouse strains have short telomeres. *Nucleic Acids Res* **28:**4474-4478.

Henson, J. D., Cao, Y., Huschtscha, L. I., Chang, A. C., Au, A. Y., Pickett, H. A. and Reddel, R. R. (2009). DNA C-circles are specific and quantifiable markers of alternative-lengthening-of-telomeres activity. *Nat Biotechnol* **27:**1181-1185.

Heo, K., Kim, H., Choi, S. H., Choi, J., Kim, K., Gu, J., Lieber, M. R. *et al.* (2008). FACT-mediated exchange of histone variant H2AX regulated by phosphorylation of H2AX and ADP-ribosylation of Spt16. *Mol Cell* **30:**86-97.

Herbig, U., Jobling, W. A., Chen, B. P., Chen, D. J. and Sedivy, J. M. (2004). Telomere shortening triggers senescence of human cells through a pathway involving ATM, p53, and p21(CIP1), but not p16(INK4a). *Mol Cell* **14:**501-513.

Hershko, A. and Ciechanover, A. (1998). The ubiquitin system. *Annu Rev Biochem* **67:**425-479.

Higuchi, R., Dollinger, G., Walsh, P. S. and Griffith, R. (1992). Simultaneous amplification and detection of specific DNA sequences. *Biotechnology (N Y)* **10:**413-417.

Hockemeyer, D., Palm, W., Else, T., Daniels, J.-P., Takai, K. K., Ye, J. Z. S., Keegan, C. E. *et al.* (2007). Telomere protection by mammalian Pot1 requires interaction with Tpp1. *Nat Struct Mol Biol* **14:**754-761.

Hockemeyer, D., Sfeir, A. J., Shay, J. W., Wright, W. E. and de Lange, T. (2005). POT1 protects telomeres from a transient DNA damage response and determines how human chromosomes end. *Embo j* **24:**2667-2678.

Hodawadekar, S. C. and Marmorstein, R. (2007). Chemistry of acetyl transfer by histone modifying enzymes: structure, mechanism and implications for effector design. *Oncogene* **26:**5528-5540.

Hong, L., Schroth, G. P., Matthews, H. R., Yau, P. and Bradbury, E. M. (1993). Studies of the DNA binding properties of histone H4 amino terminus. Thermal denaturation studies reveal that acetylation markedly reduces the binding constant of the H4 "tail" to DNA. *J Biol Chem* **268:**305-314.

Hoppe, G. J., Tanny, J. C., Rudner, A. D., Gerber, S. A., Danaie, S., Gygi, S. P. and Moazed, D. (2002). Steps in assembly of silent chromatin in yeast: Sir3-independent binding of a Sir2/Sir4 complex to silencers and role for Sir2-dependent deacetylation. *Mol Cell Biol* **22:**4167-4180.

Hsu, H. L., Gilley, D., Blackburn, E. H. and Chen, D. J. (1999). Ku is associated with the telomere in mammals. *Proc Natl Acad Sci U S A* **96:**12454-12458.

Humphrey, G. W., Wang, Y., Russanova, V. R., Hirai, T., Qin, J., Nakatani, Y. and Howard, B. H. (2001). Stable histone deacetylase complexes distinguished by the presence of SANT domain proteins CoREST/kiaa0071 and Mta-L1. *J Biol Chem* **276:**6817-6824.

Ivessa, A. S., Zhou, J. Q., Schulz, V. P., Monson, E. K. and Zakian, V. A. (2002). Saccharomyces Rrm3p, a 5' to 3' DNA helicase that promotes replication fork progression through telomeric and subtelomeric DNA. *Genes Dev* **16:**1383-1396.

Iyer, S., Chadha, A. D. and McEachern, M. J. (2005). A mutation in the STN1 gene triggers an alternative lengthening of telomere-like runaway recombinational telomere elongation and rapid deletion in yeast. *Mol Cell Biol* **25:**8064-8073.

Jacobs, S. A., Podell, E. R. and Cech, T. R. (2006). Crystal structure of the essential N-terminal domain of telomerase reverse transcriptase. *Nat Struct Mol Biol* **13:**218-225.

Jain, D., Hebden, A. K., Nakamura, T. M., Miller, K. M. and Cooper, J. P. (2010). HAATI survivors replace canonical telomeres with blocks of generic heterochromatin. *Nature* **467:**223-227.

Jenuwein, T. and Allis, C. D. (2001). Translating the histone code. *Science* **293:**1074-1080.

Jin, C., Zang, C., Wei, G., Cui, K., Peng, W., Zhao, K. and Felsenfeld, G. (2009). H3.3/H2A.Z double variant-containing nucleosomes mark 'nucleosome-free regions' of active promoters and other regulatory regions. *Nat Genet* **41:**941-945.

Jones, B., Su, H., Bhat, A., Lei, H., Bajko, J., Hevi, S., Baltus, G. A. *et al.* (2008). The histone H3K79 methyltransferase Dot1L is essential for mammalian development and heterochromatin structure. *PLoS genetics* **4:**e1000190.

Jones, R. S. and Gelbart, W. M. (1990). Genetic analysis of the enhancer of zeste locus and its role in gene regulation in Drosophila melanogaster. *Genetics* **126:**185-199.

Jones, T. I., Chen, J. C., Rahimov, F., Homma, S., Arashiro, P., Beermann, M. L., King, O. D. *et al.* (2012). Facioscapulohumeral muscular dystrophy family studies of DUX4 expression: evidence for disease modifiers and a quantitative model of pathogenesis. *Hum Mol Genet* **21:**4419-4430.

Kacem, S. and Feil, R. (2009). Chromatin mechanisms in genomic imprinting. *Mamm Genome* **20:**544-556.

Kanoh, J., Francesconi, S., Collura, A., Schramke, V., Ishikawa, F., Baldacci, G. and Geli, V. (2003). The fission yeast spSet1p is a histone H3-K4 methyltransferase that functions in telomere maintenance and DNA repair in an ATM kinase Rad3-dependent pathway.*J Mol Biol*. Vol. 326. England, pp. 1081-1094.

Karlseder, J., Broccoli, D., Dai, Y., Hardy, S. and de Lange, T. (1999). p53- and ATM-dependent apoptosis induced by telomeres lacking TRF2. *Science* **283:**1321-1325.

Karlseder, J., Hoke, K., Mirzoeva, O. K., Bakkenist, C., Kastan, M. B., Petrini, J. H. and de Lange, T. (2004). The telomeric protein TRF2 binds the ATM kinase and can inhibit the ATM-dependent DNA damage response. *PLoS Biol* **2:**E240.

Kato, T., Mizokami, M., Mukaide, M., Orito, E., Ohno, T., Nakano, T., Tanaka, Y. *et al.* (2000). Development of a TT virus DNA quantification system using real-time detection PCR. *J Clin Microbiol* **38:**94-98.

Kibe, T., Tomita, K., Matsuura, A., Izawa, D., Kodaira, T., Ushimaru, T., Uritani, M. *et al.* (2003). Fission yeast Rhp51 is required for the maintenance of telomere structure in the absence of the Ku heterodimer. *Nucleic Acids Research* **31:**5054-5063.

Kim, J., Daniel, J., Espejo, A., Lake, A., Krishna, M., Xia, L., Zhang, Y. *et al.* (2006). Tudor, MBT and chromo domains gauge the degree of lysine methylation. *EMBO Rep* **7:**397-403.

Kim, J., Guermah, M., McGinty, R. K., Lee, J. S., Tang, Z., Milne, T. A., Shilatifard, A. *et al.* (2009). RAD6-Mediated transcription-coupled H2B ubiquitylation directly stimulates H3K4 methylation in human cells. *Cell* **137:**459-471.

Kim, J. H., Park, S. M., Kang, M. R., Oh, S. Y., Lee, T. H., Muller, M. T. and Chung, I. K. (2005). Ubiquitin ligase MKRN1 modulates telomere length homeostasis through a proteolysis of hTERT. *Genes Dev* **19:**776-781.

Kim, N. W., Piatyszek, M. A., Prowse, K. R., Harley, C. B., West, M. D., Ho, P. L., Coviello, G. M. *et al.* (1994). Specific association of human telomerase activity with immortal cells and cancer. *Science* **266:**2011-2015.

Kim, S., Parks, C. G., Xu, Z., Carswell, G., DeRoo, L. A., Sandler, D. P. and Taylor, J. A. (2012). Association between genetic variants in DNA and histone methylation and telomere length. *PloS one* **7:**e40504.

Kim, S. H., Beausejour, C., Davalos, A. R., Kaminker, P., Heo, S. J. and Campisi, J. (2004). TIN2 mediates functions of TRF2 at human telomeres.*J Biol Chem*. Vol. 279. United States, pp. 43799-43804.

Kim, S. H., Kaminker, P. and Campisi, J. (1999). TIN2, a new regulator of telomere length in human cells. *Nat Genet* **23:**405-412.

Kipling, D. and Cooke, H. J. (1990). Hypervariable ultra-long telomeres in mice. *Nature* **347:**400-402.

Kirmizis, A., Santos-Rosa, H., Penkett, C. J., Singer, M. A., Vermeulen, M., Mann, M., Bahler, J. *et al.* (2007). Arginine methylation at histone H3R2 controls deposition of H3K4 trimethylation. *Nature* **449:**928-932.

Klose, R. J. and Zhang, Y. (2007). Regulation of histone methylation by demethylimination and demethylation. *Nat Rev Mol Cell Biol* **8:**307-318.

Koering, C. E., Pollice, A., Zibella, M. P., Bauwens, S., Puisieux, A., Brunori, M., Brun, C. *et al.* (2002). Human telomeric position effect is determined by chromosomal context and telomeric chromatin integrity. *EMBO Rep* **3:**1055-1061.

Kolquist, K. A., Ellisen, L. W., Counter, C. M., Meyerson, M., Tan, L. K., Weinberg, R. A., Haber, D. A. *et al.* (1998). Expression of TERT in early premalignant lesions and a subset of cells in normal tissues. *Nat Genet* **19:**182-186.

Kornberg, R. D. (1974). Chromatin structure: a repeating unit of histones and DNA. *Science* **184:**868-871.

Kotake, Y., Cao, R., Viatour, P., Sage, J., Zhang, Y. and Xiong, Y. (2007). pRB family proteins are required for H3K27 trimethylation and Polycomb repression complexes binding to and silencing p16INK4alpha tumor suppressor gene. *Genes Dev* **21:**49-54.

Kouzarides, T. (2007). Chromatin modifications and their function.*Cell*. Vol. 128. United States, pp. 693-705.

Kuroda, A., Rauch, T. A., Todorov, I., Ku, H. T., Al-Abdullah, I. H., Kandeel, F., Mullen, Y. *et al.* (2009). Insulin gene expression is regulated by DNA methylation. *PLoS One* **4:**e6953.

Kwon, J., Morshead, K. B., Guyon, J. R., Kingston, R. E. and Oettinger, M. A. (2000). Histone acetylation and hSWI/SNF remodeling act in concert to stimulate V(D)J cleavage of nucleosomal DNA. *Mol Cell* **6:**1037-1048.

Kyo, S., Takakura, M., Fujiwara, T. and Inoue, M. (2008). Understanding and exploiting hTERT promoter regulation for diagnosis and treatment of human cancers. *Cancer Sci* **99:**1528-1538.

Kyrion, G., Liu, K., Liu, C. and Lustig, A. J. (1993). RAP1 and telomere structure regulate telomere position effects in Saccharomyces cerevisiae. *Genes Dev* **7:**1146-1159.

Laible, G., Wolf, A., Dorn, R., Reuter, G., Nislow, C., Lebersorger, A., Popkin, D. *et al.* (1997). Mammalian homologues of the Polycomb-group gene Enhancer of zeste mediate gene silencing in Drosophila heterochromatin and at S. cerevisiae telomeres. *The EMBO journal* **16:**3219-3232.

Lane, D. P. (1984). Cell immortalization and transformation by the p53 gene. *Nature* **312:**596-597.

Lansdorp, P. M., Verwoerd, N. P., van de Rijke, F. M., Dragowska, V., Little, M. T., Dirks, R. W., Raap, A. K. *et al.* (1996). Heterogeneity in telomere length of human chromosomes. *Human Molecular Genetics* **5:**685-691.

Larrivee, M., LeBel, C. and Wellinger, R. J. (2004). The generation of proper constitutive G-tails on yeast telomeres is dependent on the MRX complex. *Genes Dev* **18:**1391-1396.

Lazzaro, M. A. and Picketts, D. J. (2001). Cloning and characterization of the murine Imitation Switch (ISWI) genes: differential expression patterns suggest distinct developmental roles for Snf2h and Snf2l. *J Neurochem* **77:**1145-1156.

Lee, J. S., Shukla, A., Schneider, J., Swanson, S. K., Washburn, M. P., Florens, L., Bhaumik, S. R. *et al.* (2007a). Histone crosstalk between H2B monoubiquitination and H3 methylation mediated by COMPASS. *Cell* **131:**1084-1096.

Lee, M. G., Villa, R., Trojer, P., Norman, J., Yan, K. P., Reinberg, D., Di Croce, L. *et al.* (2007b). Demethylation of H3K27 regulates polycomb recruitment and H2A ubiquitination.*Science*. Vol. 318. United States, pp. 447-450.

Lehnertz, B., Ueda, Y., Derijck, A. A. H. A., Braunschweig, U., Perez-Burgos, L., Kubicek, S., Chen, T. *et al.* (2003). Suv39h-Mediated Histone H3 Lysine 9 Methylation Directs DNA Methylation to Major Satellite Repeats at Pericentric Heterochromatin. *Current biology : CB* **13:**1192-1200.

Lei, M., Podell, E. R. and Cech, T. R. (2004). Structure of human POT1 bound to telomeric single-stranded DNA provides a model for chromosome end-protection. *Nat Struct Mol Biol* **11:**1223-1229.

Leteurtre, F., Li, X., Guardiola, P., Le Roux, G., Sergere, J. C., Richard, P., Carosella, E. D. *et al.* (1999). Accelerated telomere shortening and telomerase activation in Fanconi's anaemia. *Br J Haematol* **105:**883-893.

Letsolo, B. T., Rowson, J. and Baird, D. M. (2010). Fusion of short telomeres in human cells is characterized by extensive deletion and microhomology, and can result in complex rearrangements. *Nucleic Acids Res* **38:**1841-1852.

Levis, R., Hazelrigg, T. and Rubin, G. M. (1985). Effects of genomic position on the expression of transduced copies of the white gene of Drosophila. *Science* **229:**558-561.

Lewis, L. K., Westmoreland, J. W. and Resnick, M. A. (1999). Repair of endonuclease-induced double-strand breaks in Saccharomyces cerevisiae: essential role for genes associated with nonhomologous end-joining. *Genetics* **152:**1513-1529.

Lewis, P. W., Elsaesser, S. J., Noh, K. M., Stadler, S. C. and Allis, C. D. (2010). Daxx is an H3.3-specific histone chaperone and cooperates with ATRX in replication-independent chromatin assembly at telomeres. *Proceedings of the National Academy of Sciences of the United States of America* **107:**14075-14080.

Li, B., Carey, M. and Workman, J. L. (2007). The Role of Chromatin during Transcription. *Cell* **128:**707-719.

Li, B. and de Lange, T. (2003). Rap1 affects the length and heterogeneity of human telomeres. *Mol Biol Cell* **14:**5060-5068.

Li, B., Oestreich, S. and de Lange, T. (2000). Identification of human Rap1: implications for telomere evolution. *Cell* **101:**471-483.

Lin, A. W., Barradas, M., Stone, J. C., van Aelst, L., Serrano, M. and Lowe, S. W. (1998). Premature senescence involving p53 and p16 is activated in response to constitutive MEK/MAPK mitogenic signaling. *Genes Dev* **12:**3008-3019.

Lin, T. T., Letsolo, B. T., Jones, R. E., Rowson, J., Pratt, G., Hewamana, S., Fegan, C. *et al.* (2010). Telomere dysfunction and fusion during the progression of chronic lymphocytic leukemia: evidence for a telomere crisis. *Blood* **116:**1899-1907.

Lingner, J., Cech, T. R., Hughes, T. R. and Lundblad, V. (1997a). Three Ever Shorter Telomere (EST) genes are dispensable for in vitro yeast telomerase activity. *Proc Natl Acad Sci U S A* **94:**11190-11195.

Lingner, J., Hughes, T. R., Shevchenko, A., Mann, M., Lundblad, V. and Cech, T. R. (1997b). Reverse transcriptase motifs in the catalytic subunit of telomerase. *Science* **276:**561-567.

Lipps, H. J. and Rhodes, D. (2009). G-quadruplex structures: in vivo evidence and function. *Trends Cell Biol* **19:**414-422.

Liu, D., Safari, A., O'Connor, M. S., Chan, D. W., Laegeler, A., Qin, J. and Songyang, Z. (2004). PTOP interacts with POT1 and regulates its localization to telomeres. *Nat Cell Biol* **6:**673-680.

Liu, Y., Taverna, S. D., Muratore, T. L., Shabanowitz, J., Hunt, D. F. and Allis, C. D. (2007). RNAi-dependent H3K27 methylation is required for heterochromatin formation and DNA elimination in Tetrahymena. *Genes Dev* **21:**1530-1545.

Loayza, D. and De Lange, T. (2003). POT1 as a terminal transducer of TRF1 telomere length control. *Nature* **423:**1013-1018.

Loayza, D. and de Lange, T. (2003). POT1 as a terminal transducer of TRF1 telomere length control. *Nature* **423:**1013-1018.

Loayza, D., Parsons, H., Donigian, J., Hoke, K. and de Lange, T. (2004). DNA binding features of human POT1: a nonamer 5'-TAGGGTTAG-3' minimal binding site, sequence specificity, and internal binding to multimeric sites. *J Biol Chem* **279:**13241-13248.

Lopez-Serra, L., Ballestar, E., Ropero, S., Setien, F., Billard, L. M., Fraga, M. F., Lopez-Nieva, P. *et al.* (2008). Unmasking of epigenetically silenced candidate tumor suppressor genes by removal of methyl-CpG-binding domain proteins. *Oncogene* **27:**3556-3566.

Lovejoy, C. A., Li, W., Reisenweber, S., Thongthip, S., Bruno, J., de Lange, T., De, S. *et al.* (2012). Loss of ATRX, genome instability, and an altered DNA damage response are hallmarks of the alternative lengthening of telomeres pathway.*PLoS Genet*. Vol. 8. United States, p. e1002772.

Luk, E., Vu, N. D., Patteson, K., Mizuguchi, G., Wu, W. H., Ranjan, A., Backus, J. *et al.* (2007). Chz1, a nuclear chaperone for histone H2AZ. *Mol Cell* **25:**357-368.

Luke, B., Panza, A., Redon, S., Iglesias, N., Li, Z. and Lingner, J. (2008). The Rat1p 5' to 3' exonuclease degrades telomeric repeat-containing RNA and promotes telomere elongation in Saccharomyces cerevisiae. *Mol Cell* **32:**465-477.

Lundblad, V. and Blackburn, E. H. (1993). An alternative pathway for yeast telomere maintenance rescues est1- senescence. *Cell* **73:**347-360.

Makarov, V. L., Hirose, Y. and Langmore, J. P. (1997). Long G tails at both ends of human chromosomes suggest a C strand degradation mechanism for telomere shortening. *Cell* **88:**657-666.

Marcondes, A. M., Bair, S., Rabinovitch, P. S., Gooley, T., Deeg, H. J. and Risques, R. (2009). No telomere shortening in marrow stroma from patients with MDS. *Annals of hematology* **88:**623-628.

Marian, C. O., Cho, S. K., McEllin, B. M., Maher, E. A., Hatanpaa, K. J., Madden, C. J., Mickey, B. E. *et al.* (2010a). The telomerase antagonist, imetelstat, efficiently targets glioblastoma tumor-initiating cells leading to decreased proliferation and tumor growth. *Clin Cancer Res* **16:**154-163.

Marian, C. O., Wright, W. E. and Shay, J. W. (2010b). The effects of telomerase inhibition on prostate tumor-initiating cells. *Int J Cancer* **127:**321-331.

Marion, R. M., Schotta, G., Ortega, S. and Blasco, M. A. (2011). Suv4-20h abrogation enhances telomere elongation during reprogramming and confers a higher tumorigenic potential to iPS cells. *PloS one* **6:**e25680.

Marion, R. M., Strati, K., Li, H., Tejera, A., Schoeftner, S., Ortega, S., Serrano, M. *et al.* (2009). Telomeres acquire embryonic stem cell characteristics in induced pluripotent stem cells.*Cell Stem Cell*. Vol. 4. United States, pp. 141-154.

Marrone, A. and Mason, P. J. (2003). Dyskeratosis congenita. *Cell Mol Life Sci* **60:**507-517.

Marsden, M. P. and Laemmli, U. K. (1979). Metaphase chromosome structure: evidence for a radial loop model. *Cell* **17:**849-858.

Martens, J. A. and Winston, F. (2003). Recent advances in understanding chromatin remodeling by Swi/Snf complexes. *Curr Opin Genet Dev* **13:**136-142.

Martens, U. M., Zijlmans, J. M., Poon, S. S., Dragowska, W., Yui, J., Chavez, E. A., Ward, R. K. *et al.* (1998). Short telomeres on human chromosome 17p. *Nat Genet* **18:**76-80.

Martin, C. and Zhang, Y. (2005). The diverse functions of histone lysine methylation. *Nat Rev Mol Cell Biol* **6:**838-849.

Mattarucchi, E., Marsoni, M., Binelli, G., Passi, A., Lo Curto, F., Pasquali, F. and Porta, G. (2005). Different real time PCR approaches for the fine quantification of SNP's alleles in DNA pools: assays development, characterization and pre-validation. *J Biochem Mol Biol* **38:**555-562.

Maurer-Stroh, S., Dickens, N. J., Hughes-Davies, L., Kouzarides, T., Eisenhaber, F. and Ponting, C. P. (2003). The Tudor domain 'Royal Family': Tudor, plant Agenet, Chromo, PWWP and MBT domains. *Trends Biochem Sci* **28:**69-74.

McClintock, B. (1941). The Stability of Broken Ends of Chromosomes in Zea Mays. *Genetics* **26:**234-282.

McElligott, R. and Wellinger, R. J. (1997). The terminal DNA structure of mammalian chromosomes. *Embo j* **16:**3705-3714.

McGhee, J. D., Nickol, J. M., Felsenfeld, G. and Rau, D. C. (1983). Higher order structure of chromatin: orientation of nucleosomes within the 30 nm chromatin solenoid is independent of species and spacer length. *Cell* **33:**831-841.

Mefford, H. C. and Trask, B. J. (2002). The complex structure and dynamic evolution of human subtelomeres. *Nature reviews. Genetics* **3:**91-102.

Megee, P. C., Morgan, B. A. and Smith, M. M. (1995). Histone H4 and the maintenance of genome integrity. *Genes Dev* **9:**1716-1727.

Metcalfe, J. A., Parkhill, J., Campbell, L., Stacey, M., Biggs, P., Byrd, P. J. and Taylor, A. M. (1996). Accelerated telomere shortening in ataxia telangiectasia. *Nat Genet* **13:**350-353.

Meyne, J., Ratliff, R. L. and Moyzis, R. K. (1989). Conservation of the human telomere sequence (TTAGGG)n among vertebrates. *Proc Natl Acad Sci U S A* **86:**7049-7053.

Mhlanga, M. M. and Malmberg, L. (2001). Using molecular beacons to detect single-nucleotide polymorphisms with real-time PCR.*Methods*. Vol. 25. United States: 2001 Elsevier Science (USA). pp. 463-471.

Michaloglou, C., Vredeveld, L. C., Soengas, M. S., Denoyelle, C., Kuilman, T., van der Horst, C. M., Majoor, D. M. *et al.* (2005). BRAFE600-associated senescence-like cell cycle arrest of human naevi. *Nature* **436:**720-724.

Michishita, E., McCord, R. A., Berber, E., Kioi, M., Padilla-Nash, H., Damian, M., Cheung, P. *et al.* (2008). SIRT6 is a histone H3 lysine 9 deacetylase that modulates telomeric chromatin. *Nature* **452:**492-496.

Mitchell, J. R., Wood, E. and Collins, K. (1999). A telomerase component is defective in the human disease dyskeratosis congenita. *Nature* **402:**551-555.

Mito, Y., Henikoff, J. G. and Henikoff, S. (2005). Genome-scale profiling of histone H3.3 replacement patterns. *Nat Genet* **37:**1090-1097.

Mizuguchi, G., Shen, X., Landry, J., Wu, W. H., Sen, S. and Wu, C. (2004). ATP-driven exchange of histone H2AZ variant catalyzed by SWR1 chromatin remodeling complex. *Science* **303:**343-348.

Mizuguchi, G., Xiao, H., Wisniewski, J., Smith, M. M. and Wu, C. (2007). Nonhistone Scm3 and histones CenH3-H4 assemble the core of centromere-specific nucleosomes. *Cell* **129:**1153-1164.

Mohrmann, L. and Verrijzer, C. P. (2005). Composition and functional specificity of SWI2/SNF2 class chromatin remodeling complexes. *Biochim Biophys Acta* **1681:**59-73.

Morin, G. B. (1989). The human telomere terminal transferase enzyme is a ribonucleoprotein that synthesizes TTAGGG repeats. *Cell* **59:**521-529.

Morrison, A. J. and Shen, X. (2009). Chromatin remodelling beyond transcription: the INO80 and SWR1 complexes. *Nat Rev Mol Cell Biol* **10:**373-384.

Morshead, K. B., Ciccone, D. N., Taverna, S. D., Allis, C. D. and Oettinger, M. A. (2003). Antigen receptor loci poised for V(D)J rearrangement are broadly associated with BRG1 and flanked by peaks of histone H3 dimethylated at lysine 4. *Proc Natl Acad Sci U S A* **100:**11577-11582.

Moyzis, R. K., Buckingham, J. M., Cram, L. S., Dani, M., Deaven, L. L., Jones, M. D., Meyne, J. *et al.* (1988). A highly conserved repetitive DNA sequence, (TTAGGG)n, present at the telomeres of human chromosomes. *Proc Natl Acad Sci U S A* **85:**6622-6626.

Muller, H. J. (1938). The Remaking of Chromosomes. *Collect. Net* **13:**1181-1198.

Munoz-Jordan, J. L., Cross, G. A., de Lange, T. and Griffith, J. D. (2001). t-loops at trypanosome telomeres. *Embo j* **20:**579-588.

Munro, J., Barr, N. I., Ireland, H., Morrison, V. and Parkinson, E. K. (2004). Histone deacetylase inhibitors induce a senescence-like state in human cells by a p16-dependent mechanism that is independent of a mitotic clock. *Exp Cell Res* **295:**525-538.

Nabetani, A. and Ishikawa, F. (2009). Unusual telomeric DNAs in human telomerase-negative immortalized cells. *Mol Cell Biol* **29:**703-713.

Nakamura, M., Nabetani, A., Mizuno, T., Hanaoka, F. and Ishikawa, F. (2005). Alterations of DNA and chromatin structures at telomeres and genetic instability in mouse cells defective in DNA polymerase alpha. *Mol Cell Biol* **25:**11073-11088.

Nakayama, J., Rice, J. C., Strahl, B. D., Allis, C. D. and Grewal, S. I. (2001). Role of histone H3 lysine 9 methylation in epigenetic control of heterochromatin assembly. *Science* **292:**110-113.

Nandakumar, J., Bell, C. F., Weidenfeld, I., Zaug, A. J., Leinwand, L. A. and Cech, T. R. (2012). The TEL patch of telomere protein TPP1 mediates telomerase recruitment and processivity. *Nature* **492:**285-289.

Nathan, D., Ingvarsdottir, K., Sterner, D. E., Bylebyl, G. R., Dokmanovic, M., Dorsey, J. A., Whelan, K. A. *et al.* (2006). Histone sumoylation is a negative regulator in Saccharomyces cerevisiae and shows dynamic interplay with positive-acting histone modifications. *Genes Dev* **20:**966-976.

Neidle, S. and Parkinson, G. N. (2003). The structure of telomeric DNA. *Curr Opin Struct Biol* **13:**275-283.

Nemeth, A. and Langst, G. (2004). Chromatin higher order structure: opening up chromatin for transcription. *Brief Funct Genomic Proteomic* **2:**334-343.

Nergadze, S. G., Farnung, B. O., Wischnewski, H., Khoriauli, L., Vitelli, V., Chawla, R., Giulotto, E. *et al.* (2009). CpG-island promoters drive transcription of human telomeres. *Rna* **15:**2186-2194.

O'Callaghan, N. J. and Fenech, M. (2011). A quantitative PCR method for measuring absolute telomere length. *Biological procedures online* **13:**3.

O'Connor, M. S., Safari, A., Liu, D., Qin, J. and Songyang, Z. (2004). The human Rap1 protein complex and modulation of telomere length. *J Biol Chem* **279:**28585-28591.

O'Hagan, R. C., Chang, S., Maser, R. S., Mohan, R., Artandi, S. E., Chin, L. and DePinho, R. A. (2002). Telomere dysfunction provokes regional amplification and deletion in cancer genomes.*Cancer Cell*. Vol. 2. United States, pp. 149-155.

O'Sullivan, R. J., Kubicek, S., Schreiber, S. L. and Karlseder, J. (2010). Reduced histone biosynthesis and chromatin changes arising from a damage signal at telomeres.*Nat Struct Mol Biol*. Vol. 17. United States, pp. 1218-1225.

Oberdoerffer, P. and Sinclair, D. A. (2007). The role of nuclear architecture in genomic instability and ageing. *Nat Rev Mol Cell Biol* **8:**692-702.

Ogino, H., Nakabayashi, K., Suzuki, M., Takahashi, E., Fujii, M., Suzuki, T. and Ayusawa, D. (1998). Release of telomeric DNA from chromosomes in immortal human cells lacking telomerase activity. *Biochem Biophys Res Commun* **248:**223-227.

Ogryzko, V. V., Hirai, T. H., Russanova, V. R., Barbie, D. A. and Howard, B. H. (1996). Human fibroblast commitment to a senescence-like state in response to histone deacetylase inhibitors is cell cycle dependent. *Mol Cell Biol* **16:**5210-5218.

Oka, Y., Shiota, S., Nakai, S., Nishida, Y. and Okubo, S. (1980). Inverted terminal repeat sequence in the macronuclear DNA of Stylonychia pustulata. *Gene* **10:**301-306.

Olins, A. L. and Olins, D. E. (1974). Spheroid chromatin units (v bodies). *Science* **183:**330-332.

Olovnikov, A. M. (1971). [Principle of marginotomy in template synthesis of polynucleotides]. *Dokl Akad Nauk SSSR* **201:**1496-1499.

Olovnikov, A. M. (1973). A theory of marginotomy. The incomplete copying of template margin in enzymic synthesis of polynucleotides and biological significance of the phenomenon. *J Theor Biol* **41:**181-190.

Ooi, L., Belyaev, N. D., Miyake, K., Wood, I. C. and Buckley, N. J. (2006). BRG1 chromatin remodeling activity is required for efficient chromatin binding by repressor element 1-silencing transcription factor (REST) and facilitates REST-mediated repression. *J Biol Chem* **281:**38974-38980.

Opresko, P. L., von Kobbe, C., Laine, J. P., Harrigan, J., Hickson, I. D. and Bohr, V. A. (2002). Telomere-binding protein TRF2 binds to and stimulates the Werner and Bloom syndrome helicases. *J Biol Chem* **277:**41110-41119.

Osley, M. A., Tsukuda, T. and Nickoloff, J. A. (2007). ATP-dependent chromatin remodeling factors and DNA damage repair. *Mutat Res* **618**:65-80.

Ottaviani, A., Gilson, E. and Magdinier, F. (2008). Telomeric position effect: From the yeast paradigm to human pathologies? *Biochimie* **90:**93-107.

Pal, S., Vishwanath, S. N., Erdjument-Bromage, H., Tempst, P. and Sif, S. (2004). Human SWI/SNF-associated PRMT5 methylates histone H3 arginine 8 and negatively regulates expression of ST7 and NM23 tumor suppressor genes. *Mol Cell Biol* **24:**9630-9645.

Pal, S., Yun, R., Datta, A., Lacomis, L., Erdjument-Bromage, H., Kumar, J., Tempst, P. *et al.* (2003). mSin3A/histone deacetylase 2- and PRMT5-containing Brg1 complex is involved in transcriptional repression of the Myc target gene cad. *Mol Cell Biol* **23:**7475-7487.

Palacios, J. A., Herranz, D., De Bonis, M. L., Velasco, S., Serrano, M. and Blasco, M. A. (2010). SIRT1 contributes to telomere maintenance and augments global homologous recombination. *The Journal of cell biology* **191:**1299-1313.

Palm, W. and de Lange, T. (2008). How shelterin protects mammalian telomeres. *Annu Rev Genet* **42:**301-334.

Pandita, R. K., Sharma, G. G., Laszlo, A., Hopkins, K. M., Davey, S., Chakhparonian, M., Gupta, A. *et al.* (2006). Mammalian Rad9 plays a role in telomere stability, S- and G2-phase-specific cell survival, and homologous recombinational repair. *Mol Cell Biol* **26:**1850-1864.

Pandya, S., King, W. M. and Tawil, R. (2008). Facioscapulohumeral dystrophy. *Phys Ther* **88:**105-113.

Pardue, M. L. and DeBaryshe, P. G. (2003). Retrotransposons provide an evolutionarily robust non-telomerase mechanism to maintain telomeres. *Annu Rev Genet* **37:**485-511.

Pardue, M. L., Rashkova, S., Casacuberta, E., DeBaryshe, P. G., George, J. A. and Traverse, K. L. (2005). Two retrotransposons maintain telomeres in Drosophila. *Chromosome Res* **13:**443-453.

Parenteau, J. and Wellinger, R. J. (1999). Accumulation of single-stranded DNA and destabilization of telomeric repeats in yeast mutant strains carrying a deletion of RAD27. *Mol Cell Biol* **19:**4143-4152.

Parenteau, J. and Wellinger, R. J. (2002). Differential processing of leading- and lagging-strand ends at Saccharomyces cerevisiae telomeres revealed by the absence of Rad27p nuclease. *Genetics* **162:**1583-1594.

Patenge, N., Elkin, S. K. and Oettinger, M. A. (2004). ATP-dependent remodeling by SWI/SNF and ISWI proteins stimulates V(D)J cleavage of 5 S arrays. *J Biol Chem* **279:**35360-35367.

Pavesi, E., Avondo, F., Aspesi, A., Quarello, P., Rocci, A., Vimercati, C., Pigullo, S. *et al.* (2009). Analysis of telomeres in peripheral blood cells from patients with bone marrow failure. *Pediatr Blood Cancer* **53:**411-416.

Perrini, B., Piacentini, L., Fanti, L., Altieri, F., Chichiarelli, S., Berloco, M., Turano, C. *et al.* (2004). HP1 controls telomere capping, telomere elongation, and telomere silencing by two different mechanisms in Drosophila. *Mol Cell* **15:**467-476.

Peter, M., Couturier, J., Pacquement, H., Michon, J., Thomas, G., Magdelenat, H. and Delattre, O. (1997). A new member of the ETS family fused to EWS in Ewing tumors. *Oncogene* **14:**1159-1164.

Petersen, S., Saretzki, G. and von Zglinicki, T. (1998). Preferential accumulation of single-stranded regions in telomeres of human fibroblasts. *Exp Cell Res* **239:**152-160.

Phillips, D. M. (1963). The presence of acetyl groups of histones. *Biochem J* **87:**258-263.

Pich, U., Fuchs, J. and Schubert, I. (1996). How do Alliaceae stabilize their chromosome ends in the absence of TTTAGGG sequences? *Chromosome Res* **4:**207-213.

Pines, J. (1994). The cell cycle kinases. *Semin Cancer Biol* **5:**305-313.

Plath, K., Fang, J., Mlynarczyk-Evans, S. K., Cao, R., Worringer, K. A., Wang, H., de la Cruz, C. C. *et al.* (2003). Role of histone H3 lysine 27 methylation in X inactivation. *Science* **300:**131-135.

Plunkett, F. J., Soares, M. V., Annels, N., Hislop, A., Ivory, K., Lowdell, M., Salmon, M. *et al.* (2001). The flow cytometric analysis of telomere length in antigen-specific CD8+ T cells during acute Epstein-Barr virus infection. *Blood* **97:**700-707.

Pluta, A. F., Kaine, B. P. and Spear, B. B. (1982). The terminal organization of macronuclear DNA in Oxytricha fallax. *Nucleic Acids Res* **10:**8145-8154.

Pogo, B. G., Allfrey, V. G. and Mirsky, A. E. (1966). RNA synthesis and histone acetylation during the course of gene activation in lymphocytes. *Proc Natl Acad Sci U S A* **55:**805-812.

Pokholok, D. K., Harbison, C. T., Levine, S., Cole, M., Hannett, N. M., Lee, T. I., Bell, G. W. *et al.* (2005). Genome-wide map of nucleosome acetylation and methylation in yeast. *Cell* **122:**517-527.

Portela, A. and Esteller, M. (2010). Epigenetic modifications and human disease. *Nat Biotechnol* **28:**1057-1068.

Prowse, K. R., Avilion, A. A. and Greider, C. W. (1993). Identification of a nonprocessive telomerase activity from mouse cells. *Proc Natl Acad Sci U S A* **90:**1493-1497.

Raffa, G. D., Ciapponi, L., Cenci, G. and Gatti, M. (2011). Terminin: a protein complex that mediates epigenetic maintenance of Drosophila telomeres. *Nucleus* **2:**383-391.

Rank, G., Cerruti, L., Simpson, R. J., Moritz, R. L., Jane, S. M. and Zhao, Q. (2010). Identification of a PRMT5-dependent repressor complex linked to silencing of human fetal globin gene expression. *Blood* **116:**1585-1592.

Rattner, J. B. and Lin, C. C. (1985). Radial loops and helical coils coexist in metaphase chromosomes. *Cell* **42:**291-296.

Ravnan, J. B., Tepperberg, J. H., Papenhausen, P., Lamb, A. N., Hedrick, J., Eash, D., Ledbetter, D. H. *et al.* (2006). Subtelomere FISH analysis of 11 688 cases: an evaluation of the frequency and pattern of subtelomere rearrangements in individuals with developmental disabilities. *J Med Genet* **43:**478-489.

Ray-Gallet, D., Quivy, J. P., Scamps, C., Martini, E. M., Lipinski, M. and Almouzni, G. (2002). HIRA is critical for a nucleosome assembly pathway independent of DNA synthesis.*Mol Cell*. Vol. 9. United States, pp. 1091-1100.

Rea, S., Eisenhaber, F., O'Carroll, D., Strahl, B. D., Sun, Z. W., Schmid, M., Opravil, S. *et al.* (2000). Regulation of chromatin structure by site-specific histone H3 methyltransferases. *Nature* **406:**593-599.

Renauld, H., Aparicio, O. M., Zierath, P. D., Billington, B. L., Chhablani, S. K. and Gottschling, D. E. (1993). Silent domains are assembled continuously from the telomere and are defined by promoter distance and strength, and by SIR3 dosage. *Genes Dev* **7:**1133-1145.

Richards, E. J. and Ausubel, F. M. (1988). Isolation of a higher eukaryotic telomere from Arabidopsis thaliana.*Cell*. Vol. 53. United States, pp. 127-136.

Riethman, H., Ambrosini, A. and Paul, S. (2005). Human subtelomere structure and variation. *Chromosome Res* **13:**505-515.

Riethman, H. C., Xiang, Z., Paul, S., Morse, E., Hu, X. L., Flint, J., Chi, H. C. *et al.* (2001). Integration of telomere sequences with the draft human genome sequence. *Nature* **409:**948-951.

Riha, K., McKnight, T. D., Fajkus, J., Vyskot, B. and Shippen, D. E. (2000). Analysis of the G-overhang structures on plant telomeres: evidence for two distinct telomere architectures. *Plant J* **23:**633-641.

Riha, K. and Shippen, D. E. (2003). Ku is required for telomeric C-rich strand maintenance but not for end-to-end chromosome fusions in Arabidopsis. *Proc Natl Acad Sci U S A* **100:**611-615.

Rizzi, N., Denegri, M., Chiodi, I., Corioni, M., Valgardsdottir, R., Cobianchi, F., Riva, S. *et al.* (2004). Transcriptional activation of a constitutive heterochromatic domain of the human genome in response to heat shock. *Mol Biol Cell* **15:**543-551.

Robinson, P. J. and Rhodes, D. (2006). Structure of the '30 nm' chromatin fibre: a key role for the linker histone. *Curr Opin Struct Biol* **16:**336-343.

Roguev, A., Schaft, D., Shevchenko, A., Pijnappel, W. W., Wilm, M., Aasland, R. and Stewart, A. F. (2001). The Saccharomyces cerevisiae Set1 complex includes an Ash2 homologue and methylates histone 3 lysine 4. *EMBO J* **20:**7137-7148.

Rosenfeld, J. A., Wang, Z., Schones, D. E., Zhao, K., DeSalle, R. and Zhang, M. Q. (2009). Determination of enriched histone modifications in non-genic portions of the human genome.*BMC Genomics*. Vol. 10. England, p. 143.

Roth, S. Y., Denu, J. M. and Allis, C. D. (2001). Histone acetyltransferases. *Annu Rev Biochem* **70:**81-120.

Rouda, S. and Skordalakes, E. (2007). Structure of the RNA-binding domain of telomerase: implications for RNA recognition and binding. *Structure* **15:**1403-1412.

Roudier, F., Ahmed, I., Berard, C., Sarazin, A., Mary-Huard, T., Cortijo, S., Bouyer, D. *et al.* (2011). Integrative epigenomic mapping defines four main chromatin states in Arabidopsis. *Embo j* **30:**1928-1938.

Rufer, N., Dragowska, W., Thornbury, G., Roosnek, E. and Lansdorp, P. M. (1998). Telomere length dynamics in human lymphocyte subpopulations measured by flow cytometry. *Nat Biotechnol* **16:**743-747.

Ruggero, D., Grisendi, S., Piazza, F., Rego, E., Mari, F., Rao, P. H., Cordon-Cardo, C. *et al.* (2003). Dyskeratosis congenita and cancer in mice deficient in ribosomal RNA modification. *Science* **299:**259-262.

Sakabe, K., Wang, Z. and Hart, G. W. (2010). Beta-N-acetylglucosamine (O-GlcNAc) is part of the histone code. *Proc Natl Acad Sci U S A* **107:**19915-19920.

Salomoni, P. and Khelifi, A. F. (2006). Daxx: death or survival protein?*Trends Cell Biol*. Vol. 16. England, pp. 97-104.

Sambrook, J., Fritsch, E. F. and Maniatis, T. (1989). Molecular Cloning: a Laboratory Manual. New York: Cold Spring Harbor Laboratory Press.

Santenard, A., Ziegler-Birling, C., Koch, M., Tora, L., Bannister, A. J. and Torres-Padilla, M. E. (2010). Heterochromatin formation in the mouse embryo requires critical residues of the histone variant H3.3. *Nat Cell Biol* **12:**853-862.

Santos-Rosa, H., Kirmizis, A., Nelson, C., Bartke, T., Saksouk, N., Cote, J. and Kouzarides, T. (2009). Histone H3 tail clipping regulates gene expression. *Nat Struct Mol Biol* **16:**17-22.

Santos-Rosa, H., Schneider, R., Bannister, A. J., Sherriff, J., Bernstein, B. E., Emre, N. C., Schreiber, S. L. *et al.* (2002). Active genes are tri-methylated at K4 of histone H3. *Nature* **419:**407-411.

Sarthy, J., Bae, N. S., Scrafford, J. and Baumann, P. (2009). Human RAP1 inhibits non-homologous end joining at telomeres. *Embo j* **28:**3390-3399.

Savitsky, K., Sfez, S., Tagle, D. A., Ziv, Y., Sartiel, A., Collins, F. S., Shiloh, Y. *et al.* (1995). The complete sequence of the coding region of the ATM gene reveals similarity to cell cycle regulators in different species. *Hum Mol Genet* **4:**2025-2032.

Savitsky, M., Kravchuk, O., Melnikova, L. and Georgiev, P. (2002). Heterochromatin protein 1 is involved in control of telomere elongation in Drosophila melanogaster. *Mol Cell Biol* **22:**3204-3218.

Schoeftner, S. and Blasco, M. A. (2009). A 'higher order' of telomere regulation: telomere heterochromatin and telomeric RNAs. *The EMBO journal* **28:**2323-2336.

Schoeftner, S. and Blasco, M. A. (2010). Chromatin regulation and non-coding RNAs at mammalian telomeres.*Semin Cell Dev Biol*. Vol. 21. England: 2009 Elsevier Ltd, pp. 186-193.

Schwartz, B. E. and Ahmad, K. (2005). Transcriptional activation triggers deposition and removal of the histone variant H3.3. *Genes Dev* **19:**804-814.

Schwartzentruber, J., Korshunov, A., Liu, X. Y., Jones, D. T., Pfaff, E., Jacob, K., Sturm, D. *et al.* (2012). Driver mutations in histone H3.3 and chromatin remodelling genes in paediatric glioblastoma.*Nature*. Vol. 482. England, pp. 226-231.

Scionti, I., Greco, F., Ricci, G., Govi, M., Arashiro, P., Vercelli, L., Berardinelli, A. *et al.* (2012). Large-scale population analysis challenges the current criteria for the molecular diagnosis of fascioscapulohumeral muscular dystrophy. *Am J Hum Genet* **90:**628-635.

Sengupta, N. and Seto, E. (2004). Regulation of histone deacetylase activities. *J Cell Biochem* **93:**57-67.

Serrano, M., Lin, A. W., McCurrach, M. E., Beach, D. and Lowe, S. W. (1997). Oncogenic ras provokes premature cell senescence associated with accumulation of p53 and p16INK4a. *Cell* **88:**593-602.

Sfeir, A., Kabir, S., van Overbeek, M., Celli, G. B. and de Lange, T. (2010). Loss of Rap1 induces telomere recombination in the absence of NHEJ or a DNA damage signal. *Science* **327:**1657-1661.

Sfeir, A., Kosiyatrakul, S. T., Hockemeyer, D., MacRae, S. L., Karlseder, J., Schildkraut, C. L. and de Lange, T. (2009). Mammalian telomeres resemble fragile sites and require TRF1 for efficient replication. *Cell* **138:**90-103.

Shakirov, E. V. and Shippen, D. E. (2004). Length regulation and dynamics of individual telomere tracts in wild-type Arabidopsis. *Plant Cell* **16:**1959-1967.

Shampay, J., Szostak, J. W. and Blackburn, E. H. (1984). DNA sequences of telomeres maintained in yeast. *Nature* **310:**154-157.

Sharp, J. A., Franco, A. A., Osley, M. A. and Kaufman, P. D. (2002). Chromatin assembly factor I and Hir proteins contribute to building functional kinetochores in S. cerevisiae. *Genes Dev* **16:**85-100.

Shay, J. W. and Wright, W. E. (2005). Senescence and immortalization: role of telomeres and telomerase. *Carcinogenesis* **26:**867-874.

Shay, J. W. and Wright, W. E. (2011). Role of telomeres and telomerase in cancer. *Semin Cancer Biol* **21:**349-353.

Shi, X., Hong, T., Walter, K. L., Ewalt, M., Michishita, E., Hung, T., Carney, D. *et al.* (2006). ING2 PHD domain links histone H3 lysine 4 methylation to active gene repression. *Nature* **442:**96-99.

Shi, Y., Lan, F., Matson, C., Mulligan, P., Whetstine, J. R., Cole, P. A. and Casero, R. A. (2004). Histone demethylation mediated by the nuclear amine oxidase homolog LSD1. *Cell* **119:**941-953.

Shiio, Y. and Eisenman, R. N. (2003). Histone sumoylation is associated with transcriptional repression. *Proc Natl Acad Sci U S A* **100:**13225-13230.

Shiloh, Y. (2001). ATM and ATR: networking cellular responses to DNA damage. *Curr Opin Genet Dev* **11:**71-77.

Shippen-Lentz, D. and Blackburn, E. H. (1989). Telomere terminal transferase activity from Euplotes crassus adds large numbers of TTTTGGGG repeats onto telomeric primers. *Mol Cell Biol* **9:**2761-2764.

Shogren-Knaak, M., Ishii, H., Sun, J. M., Pazin, M. J., Davie, J. R. and Peterson, C. L. (2006). Histone H4-K16 acetylation controls chromatin structure and protein interactions. *Science* **311:**844-847.

Shore, D. (2001). Telomeric chromatin: replicating and wrapping up chromosome ends. *Curr Opin Genet Dev* **11:**189-198.

Sif, S., Saurin, A. J., Imbalzano, A. N. and Kingston, R. E. (2001). Purification and characterization of mSin3A-containing Brg1 and hBrm chromatin remodeling complexes. *Genes Dev* **15:**603-618.

Smith, S., Giriat, I., Schmitt, A. and de Lange, T. (1998). Tankyrase, a poly(ADP-ribose) polymerase at human telomeres. *Science* **282:**1484-1487.

Smogorzewska, A., van Steensel, B., Bianchi, A., Oelmann, S., Schaefer, M. R., Schnapp, G. and de Lange, T. (2000). Control of human telomere length by TRF1 and TRF2. *Mol Cell Biol* **20:**1659-1668.

Snowden, A. W., Gregory, P. D., Case, C. C. and Pabo, C. O. (2002). Gene-specific targeting of H3K9 methylation is sufficient for initiating repression in vivo. *Curr Biol* **12:**2159-2166.

Stadler, G., Rahimov, F., King, O. D., Chen, J. C., Robin, J. D., Wagner, K. R., Shay, J. W. *et al.* (2013). Telomere position effect regulates DUX4 in human facioscapulohumeral muscular dystrophy. *Nat Struct Mol Biol* **20:**671-678.

Stansel, R. M., de Lange, T. and Griffith, J. D. (2001). T-loop assembly in vitro involves binding of TRF2 near the 3' telomeric overhang. *EMBO J* **20:**5532-5540.

Stern, J. L., Zyner, K. G., Pickett, H. A., Cohen, S. B. and Bryan, T. M. (2012). Telomerase recruitment requires both TCAB1 and Cajal bodies independently. *Mol Cell Biol* **32:**2384-2395.

Stewart, S. A. and Weinberg, R. A. (2006). Telomeres: cancer to human aging. *Annu Rev Cell Dev Biol* **22:**531-557.

Straube, K., Blackwell, J. S., Jr. and Pemberton, L. F. (2010). Nap1 and Chz1 have separate Htz1 nuclear import and assembly functions. *Traffic* **11:**185-197.

Strohner, R., Nemeth, A., Jansa, P., Hofmann-Rohrer, U., Santoro, R., Langst, G. and Grummt, I. (2001). NoRC--a novel member of mammalian ISWI-containing chromatin remodeling machines. *Embo j* **20:**4892-4900.

Struhl, G. (1981). A gene product required for correct initiation of segmental determination in Drosophila. *Nature* **293:**36-41.

Sugiyama, T., Cam, H. P., Sugiyama, R., Noma, K., Zofall, M., Kobayashi, R. and Grewal, S. I. (2007). SHREC, an effector complex for heterochromatic transcriptional silencing. *Cell* **128:**491-504.

Suka, N., Luo, K. and Grunstein, M. (2002). Sir2p and Sas2p opposingly regulate acetylation of yeast histone H4 lysine16 and spreading of heterochromatin. *Nat Genet* **32:**378-383.

Sullivan, K. F., Hechenberger, M. and Masri, K. (1994). Human CENP-A contains a histone H3 related histone fold domain that is required for targeting to the centromere. *J Cell Biol* **127:**581-592.

Sun, J., Zhang, Q. and Schlick, T. (2005). Electrostatic mechanism of nucleosomal array folding revealed by computer simulation. *Proc Natl Acad Sci U S A* **102:**8180-8185.

Sykorova, E., Lim, K. Y., Kunicka, Z., Chase, M. W., Bennett, M. D., Fajkus, J. and Leitch, A. R. (2003). Telomere variability in the monocotyledonous plant order Asparagales. *Proc Biol Sci* **270:**1893-1904.

Syvänen, A. C., Bengtström, M., Tenhunen, J. and Söderlund, H. (1988). Quantification of polymerase chain reaction products by affinity-based hybrid collection. *Nucleic Acids Res* **16:**11327-11338.

Szenker, E., Ray-Gallet, D. and Almouzni, G. (2011). The double face of the histone variant H3.3.*Cell Res*. Vol. 21. England, pp. 421-434.

Szostak, J. W. and Blackburn, E. H. (1982). Cloning yeast telomeres on linear plasmid vectors. *Cell* **29:**245-255.

Tachibana, M., Sugimoto, K., Fukushima, T. and Shinkai, Y. (2001). Set domain-containing protein, G9a, is a novel lysine-preferring mammalian histone methyltransferase with hyperactivity and specific selectivity to lysines 9 and 27 of histone H3. *J Biol Chem* **276:**25309-25317.

Tachibana, M., Sugimoto, K., Nozaki, M., Ueda, J., Ohta, T., Ohki, M., Fukuda, M. *et al.* (2002). G9a histone methyltransferase plays a dominant role in euchromatic histone H3 lysine 9 methylation and is essential for early embryogenesis. *Genes Dev* **16:**1779-1791.

Tagami, H., Ray-Gallet, D., Almouzni, G. and Nakatani, Y. (2004). Histone H3.1 and H3.3 complexes mediate nucleosome assembly pathways dependent or independent of DNA synthesis. *Cell* **116:**51-61.

Takai, H., Smogorzewska, A. and de Lange, T. (2003). DNA damage foci at dysfunctional telomeres. *Curr Biol* **13:**1549-1556.

Takata, H., Kanoh, Y., Gunge, N., Shirahige, K. and Matsuura, A. (2004). Reciprocal association of the budding yeast ATM-related proteins Tel1 and Mec1 with telomeres in vivo. *Molecular Cell* **14:**515-522.

Takata, H., Tanaka, Y. and Matsuura, A. (2005). Late S phase-specific recruitment of Mre11 complex triggers hierarchical assembly of telomere replication proteins in Saccharomyces cerevisiae. *Molecular Cell* **17:**573-583.

Talbert, P. B. and Henikoff, S. (2010). Histone variants--ancient wrap artists of the epigenome. *Nat Rev Mol Cell Biol* **11:**264-275.

Tamkun, J. W., Deuring, R., Scott, M. P., Kissinger, M., Pattatucci, A. M., Kaufman, T. C. and Kennison, J. A. (1992). brahma: a regulator of Drosophila homeotic genes structurally related to the yeast transcriptional activator SNF2/SWI2. *Cell* **68:**561-572.

Tamura, T., Smith, M., Kanno, T., Dasenbrock, H., Nishiyama, A. and Ozato, K. (2009). Inducible deposition of the histone variant H3.3 in interferon-stimulated genes. *J Biol Chem* **284:**12217-12225.

Tankimanova, M., Capper, R., Letsolo, B. T., Rowson, J., Jones, R. E., Britt-Compton, B., Taylor, A. M. *et al.* (2012). Mre11 modulates the fidelity of fusion between short telomeres in human cells.*Nucleic Acids Res*. Vol. 40. England, pp. 2518-2526.

Tarsounas, M., Munoz, P., Claas, A., Smiraldo, P. G., Pittman, D. L., Blasco, M. A. and West, S. C. (2004). Telomere maintenance requires the RAD51D recombination/repair protein. *Cell* **117:**337-347.

Tennen, R. I., Bua, D. J., Wright, W. E. and Chua, K. F. (2011). SIRT6 is required for maintenance of telomere position effect in human cells.*Nat Commun*. Vol. 2. England, p. 433.

Thijssen, P. E., Tobi, E. W., Balog, J., Schouten, S. G., Kremer, D., El Bouazzaoui, F., Henneman, P. *et al.* (2013). Chromatin remodeling of human subtelomeres and TERRA promoters upon cellular senescence: Commonalities and differences between chromosomes. *Epigenetics* **8:**512-521.

Thoma, F., Koller, T. and Klug, A. (1979). Involvement of histone H1 in the organization of the nucleosome and of the salt-dependent superstructures of chromatin. *J Cell Biol* **83:**403-427.

Timinszky, G., Till, S., Hassa, P. O., Hothorn, M., Kustatscher, G., Nijmeijer, B., Colombelli, J. *et al.* (2009). A macrodomain-containing histone rearranges chromatin upon sensing PARP1 activation. *Nat Struct Mol Biol* **16:**923-929.

Timson, D. J., Singleton, M. R. and Wigley, D. B. (2000). DNA ligases in the repair and replication of DNA. *Mutat Res* **460:**301-318.

Tiwari, V. K., Cope, L., McGarvey, K. M., Ohm, J. E. and Baylin, S. B. (2008). A novel 6C assay uncovers Polycomb-mediated higher order chromatin conformations. *Genome Res* **18:**1171-1179.

Tjeertes, J. V., Miller, K. M. and Jackson, S. P. (2009). Screen for DNA-damage-responsive histone modifications identifies H3K9Ac and H3K56Ac in human cells. *Embo j* **28:**1878-1889.

Tokutake, Y., Matsumoto, T., Watanabe, T., Maeda, S., Tahara, H., Sakamoto, S., Niida, H. *et al.* (1998). Extra-chromosomal telomere repeat DNA in telomerase-negative immortalized cell lines. *Biochem Biophys Res Commun* **247:**765-772.

Tomaska, L., Willcox, S., Slezakova, J., Nosek, J. and Griffith, J. D. (2004). Taz1 binding to a fission yeast model telomere: formation of telomeric loops and higher order structures. *J Biol Chem* **279:**50764-50772.

Tong, J. K., Hassig, C. A., Schnitzler, G. R., Kingston, R. E. and Schreiber, S. L. (1998). Chromatin deacetylation by an ATP-dependent nucleosome remodelling complex. *Nature* **395:**917-921.

Tsai, W. W., Wang, Z., Yiu, T. T., Akdemir, K. C., Xia, W., Winter, S., Tsai, C. Y. *et al.* (2010). TRIM24 links a non-canonical histone signature to breast cancer. *Nature* **468:**927-932.

Tsakiri, K. D., Cronkhite, J. T., Kuan, P. J., Xing, C., Raghu, G., Weissler, J. C., Rosenblatt, R. L. *et al.* (2007). Adult-onset pulmonary fibrosis caused by mutations in telomerase. *Proc Natl Acad Sci U S A* **104:**7552-7557.

Tsukiyama, T., Palmer, J., Landel, C. C., Shiloach, J. and Wu, C. (1999). Characterization of the imitation switch subfamily of ATP-dependent chromatin-remodeling factors in Saccharomyces cerevisiae. *Genes Dev.* **13:**686-697.

Tsukiyama, T. and Wu, C. (1995). Puification and properties of an ATP-dependent nucleosome remodeling factor. *Cell* **83:**1011-1020.

Tsukuda, T., Fleming, A. B., Nickoloff, J. A. and Osley, M. A. (2005). Chromatin remodelling at a DNA double-strand break site in Saccharomyces cerevisiae. *Nature* **438:**379-383.

Ungar, L., Yosef, N., Sela, Y., Sharan, R., Ruppin, E. and Kupiec, M. (2009). A genome-wide screen for essential yeast genes that affect telomere length maintenance. *Nucleic acids research* **37:**3840-3849.

Vakoc, C. R., Mandat, S. A., Olenchock, B. A. and Blobel, G. A. (2005). Histone H3 lysine 9 methylation and HP1gamma are associated with transcription elongation through mammalian chromatin. *Mol Cell* **19:**381-391.

Valdes, A. M., Andrew, T., Gardner, J. P., Kimura, M., Oelsner, E., Cherkas, L. F., Aviv, A. *et al.* (2005). Obesity, cigarette smoking, and telomere length in women. *Lancet* **366:**662-664.

van Attikum, H., Fritsch, O., Hohn, B. and Gasser, S. M. (2004). Recruitment of the INO80 complex by H2A phosphorylation links ATP-dependent chromatin remodeling with DNA double-strand break repair. *Cell* **119:**777-788.

van der Vlag, J. and Otte, A. P. (1999). Transcriptional repression mediated by the human polycomb-group protein EED involves histone deacetylation. *Nat Genet* **23:**474-478.

van Steensel, B. (2011). Chromatin: constructing the big picture. *Embo j* **30:**1885-1895.

van Steensel, B. and de Lange, T. (1997). Control of telomere length by the human telomeric protein TRF1. *Nature* **385:**740-743.

Vaquero-Sedas, M. I., Gámez-Arjona, F. M. and Vega-Palas, M. A. (2011). Arabidopsis thaliana telomeres exhibit euchromatic features. *Nucleic Acids Res* **39:**2007-2017.

Vaquero-Sedas, M. I., Luo, C. and Vega-Palas, M. A. (2012). Analysis of the epigenetic status of telomeres by using ChIP-seq data.*Nucleic Acids Res*. Vol. 40. England, p. e163.

Vaquero-Sedas, M. I. and Vega-Palas, M. A. (2013). Differential association of Arabidopsis telomeres and centromeres with histone H3 variants. *Sci Rep* **3:**1202.

Varga-Weisz, P. D., Wilm, M., Bonte, E., Dumas, K., Mann, M. and Becker, P. B. (1997). Chromatin-remodelling factor CHRAC contains the ATPases ISWI and topoisomerase II. *Nature* **388:**598-602.

Varley, H., Pickett, H. A., Foxon, J. L., Reddel, R. R. and Royle, N. J. (2002). Molecular characterization of inter-telomere and intra-telomere mutations in human ALT cells. *Nat Genet* **30:**301-305.

Veldman, T., Etheridge, K. T. and Counter, C. M. (2004). Loss of hPot1 function leads to telomere instability and a cut-like phenotype. *Curr Biol* **14:**2264-2270.

Venteicher, A. S., Abreu, E. B., Meng, Z., McCann, K. E., Terns, R. M., Veenstra, T. D., Terns, M. P. *et al.* (2009). A human telomerase holoenzyme protein required for Cajal body localization and telomere synthesis. *Science* **323:**644-648.

Venteicher, A. S., Meng, Z., Mason, P. J., Veenstra, T. D. and Artandi, S. E. (2008). Identification of ATPases pontin and reptin as telomerase components essential for holoenzyme assembly. *Cell* **132:**945-957.

Verdun, R. E. and Karlseder, J. (2006). The DNA damage machinery and homologous recombination pathway act consecutively to protect human telomeres. *Cell* **127:**709-720.

Verreault, A., Kaufman, P. D., Kobayashi, R. and Stillman, B. (1996). Nucleosome assembly by a complex of CAF-1 and acetylated histones H3/H4.*Cell*. Vol. 87. United States, pp. 95-104.

Volpe, T. A., Kidner, C., Hall, I. M., Teng, G., Grewal, S. I. and Martienssen, R. A. (2002). Regulation of heterochromatic silencing and histone H3 lysine-9 methylation by RNAi. *Science* **297:**1833-1837.

Vrbsky, J., Akimcheva, S., Watson, J. M., Turner, T. L., Daxinger, L., Vyskot, B., Aufsatz, W. *et al.* (2010). siRNA-mediated methylation of Arabidopsis telomeres. *PLoS Genet* **6:**e1000986.

Vulliamy, T., Marrone, A., Goldman, F., Dearlove, A., Bessler, M., Mason, P. J. and Dokal, I. (2001). The RNA component of telomerase is mutated in autosomal dominant dyskeratosis congenita. *Nature* **413:**432-435.

Wade, P. A., Jones, P. L., Vermaak, D. and Wolffe, A. P. (1998). A multiple subunit Mi-2 histone deacetylase from Xenopus laevis cofractionates with an associated Snf2 superfamily ATPase. *Curr Biol* **8:**843-846.

Wang, F., Pan, X., Kalmbach, K., Seth-Smith, M. L., Ye, X., Antumes, D. M., Yin, Y. *et al.* (2013). Robust measurement of telomere length in single cells. *Proc Natl Acad Sci U S A* **110:**E1906-1912.

Wang, G. G., Allis, C. D. and Chi, P. (2007). Chromatin remodeling and cancer, Part II: ATP-dependent chromatin remodeling.*Trends Mol Med*. Vol. 13. England, pp. 373-380.

Wang, H., Wang, L., Erdjument-Bromage, H., Vidal, M., Tempst, P., Jones, R. S. and Zhang, Y. (2004a). Role of histone H2A ubiquitination in Polycomb silencing. *Nature* **431:**873-878.

Wang, P., Lin, C., Smith, E. R., Guo, H., Sanderson, B. W., Wu, M., Gogol, M. *et al.* (2009). Global analysis of H3K4 methylation defines MLL family member targets and points to a role for MLL1-mediated H3K4 methylation in the regulation of transcriptional initiation by RNA polymerase II. *Mol Cell Biol* **29:**6074-6085.

Wang, R. C., Smogorzewska, A. and de Lange, T. (2004b). Homologous recombination generates T-loop-sized deletions at human telomeres. *Cell* **119:**355-368.

Wang, S. S. and Zakian, V. A. (1990). Sequencing of Saccharomyces telomeres cloned using T4 DNA polymerase reveals two domains. *Mol Cell Biol* **10:**4415-4419.

Wang, Y., Wysocka, J., Sayegh, J., Lee, Y. H., Perlin, J. R., Leonelli, L., Sonbuchner, L. S. *et al.* (2004c). Human PAD4 regulates histone arginine methylation levels via demethylimination. *Science* **306:**279-283.

Ward, I. M. and Chen, J. (2001). Histone H2AX is phosphorylated in an ATR-dependent manner in response to replicational stress. *J Biol Chem* **276:**47759-47762.

Watson, J. D. (1972). Origin of concatemeric T7 DNA. *Nat New Biol* **239:**197-201.

Watson, J. M. and Shippen, D. E. (2007). Telomere rapid deletion regulates telomere length in Arabidopsis thaliana. *Mol Cell Biol* **27:**1706-1715.

Wellinger, R. J., Wolf, A. J. and Zakian, V. A. (1993). Saccharomyces telomeres acquire single-strand TG1–3 tails late in S phase. *Cell* **72:**51-60.

Whetstine, J. R., Nottke, A., Lan, F., Huarte, M., Smolikov, S., Chen, Z., Spooner, E. *et al.* (2006). Reversal of histone lysine trimethylation by the JMJD2 family of histone demethylases. *Cell* **125:**467-481.

Wicky, C., Villeneuve, A. M., Lauper, N., Codourey, L., Tobler, H. and Muller, F. (1996). Telomeric repeats (TTAGGC)n are sufficient for chromosome capping function in Caenorhabditis elegans. *Proc Natl Acad Sci U S A* **93:**8983-8988.

Widom, J. and Klug, A. (1985). Structure of the 300A chromatin filament: X-ray diffraction from oriented samples. *Cell* **43:**207-213.

Williams, C. J., Naito, T., Arco, P. G., Seavitt, J. R., Cashman, S. M., De Souza, B., Qi, X. *et al.* (2004). The chromatin remodeler Mi-2beta is required for CD4 expression and T cell development. *Immunity* **20:**719-733.

Williams, S. P., Athey, B. D., Muglia, L. J., Schappe, R. S., Gough, A. H. and Langmore, J. P. (1986). Chromatin fibers are left-handed double helices with diameter and mass per unit length that depend on linker length. *Biophys J* **49:**233-248.

Wirbelauer, C., Bell, O. and Schübeler, D. (2005). Variant histone H3.3 is deposited at sites of nucleosomal displacement throughout transcribed genes while active histone modifications show a promoter-proximal bias. *Genes Dev* **19:**1761-1766.

Wong, L. H., McGhie, J. D., Sim, M., Anderson, M. A., Ahn, S., Hannan, R. D., George, A. J. *et al.* (2010). ATRX interacts with H3.3 in maintaining telomere structural integrity in pluripotent embryonic stem cells. *Genome research* **20:**351-360.

Wong, L. H., Ren, H., Williams, E., McGhie, J., Ahn, S., Sim, M., Tam, A. *et al.* (2009). Histone H3.3 incorporation provides a unique and functionally essential telomeric chromatin in embryonic stem cells. *Genome Res* **19:**404-414.

Wong, L. S., Huzen, J., de Boer, R. A., van Gilst, W. H., van Veldhuisen, D. J. and van der Harst, P. (2011). Telomere length of circulating leukocyte subpopulations and buccal cells in patients with ischemic heart failure and their offspring. *PloS one* **6:**e23118.

Woodage, T., Basrai, M. A., Baxevanis, A. D., Hieter, P. and Collins, F. S. (1997). Characterization of the CHD family of proteins. *Proc Natl Acad Sci U S A* **94:**11472-11477.

Woodcock, C. L., Grigoryev, S. A., Horowitz, R. A. and Whitaker, N. (1993). A chromatin folding model that incorporates linker variability generates fibers resembling the native structures. *Proc Natl Acad Sci U S A* **90:**9021-9025.

Woodcock, C. L., Safer, J. P. and Stanchfield, J. E. (1976). Structural repeating units in chromatin. I. Evidence for their general occurrence. *Exp Cell Res* **97:**101-110.

Wu, Y., Ji, T., Wang, J., Xiao, J., Wang, H., Li, J., Gao, Z. *et al.* (2010). Submicroscopic subtelomeric aberrations in Chinese patients with unexplained developmental delay/mental retardation. *BMC Med Genet* **11:**72.

Wyatt, H. D., West, S. C. and Beattie, T. L. (2010). InTERTpreting telomerase structure and function. *Nucleic Acids Res* **38:**5609-5622.

Wysocka, J., Swigut, T., Xiao, H., Milne, T. A., Kwon, S. Y., Landry, J., Kauer, M. *et al.* (2006). A PHD finger of NURF couples histone H3 lysine 4 trimethylation with chromatin remodelling.*Nature*. Vol. 442. England, pp. 86-90.

Xiao, B., Jing, C., Wilson, J. R., Walker, P. A., Vasisht, N., Kelly, G., Howell, S. *et al.* (2003). Structure and catalytic mechanism of the human histone methyltransferase SET7/9. *Nature* **421:**652-656.

Xin, H., Liu, D., Wan, M., Safari, A., Kim, H., Sun, W., O'Connor, M. S. *et al.* (2007). TPP1 is a homologue of ciliate TEBP-beta and interacts with POT1 to recruit telomerase.*Nature*. Vol. 445. England, pp. 559-562.

Xue, Y., Wong, J., Moreno, G. T., Young, M. K., Cote, J. and Wang, W. (1998). NURD, a novel complex with both ATP-dependent chromatin-remodeling and histone deacetylase activities. *Mol Cell* **2:**851-861.

Yang, X., Khosravi-Far, R., Chang, H. Y. and Baltimore, D. (1997). Daxx, a novel Fas-binding protein that activates JNK and apoptosis. *Cell* **89:**1067-1076.

Yasui, D., Miyano, M., Cai, S., Varga-Weisz, P. and Kohwi-Shigematsu, T. (2002). SATB1 targets chromatin remodelling to regulate genes over long distances. *Nature* **419:**641-645.

Ye, J. Z., Donigian, J. R., van Overbeek, M., Loayza, D., Luo, Y., Krutchinsky, A. N., Chait, B. T. *et al.* (2004a). TIN2 binds TRF1 and TRF2 simultaneously and stabilizes the TRF2 complex on telomeres. *J Biol Chem* **279:**47264-47271.

Ye, J. Z. S., Hockemeyer, D., Krutchinsky, A. N., Loayza, D., Hooper, S. M., Chait, B. T. and de Lange, T. (2004b). POT1-interacting protein PIP1: a telomere length regulator that recruits POT1 to the TIN2/TRF1 complex. *Genes Dev* **18:**1649-1654.

Yeager, T. R., Neumann, A. A., Englezou, A., Huschtscha, L. I., Noble, J. R. and Reddel, R. R. (1999). Telomerase-negative immortalized human cells contain a novel type of promyelocytic leukemia (PML) body. *Cancer Res* **59:**4175-4179.

Yehezkel, S., Segev, Y., Viegas-Pequignot, E., Skorecki, K. and Selig, S. (2008). Hypomethylation of subtelomeric regions in ICF syndrome is associated with abnormally short telomeres and enhanced transcription from telomeric regions. *Hum Mol Genet* **17:**2776-2789.

Yu, E. Y., Steinberg-Neifach, O., Dandjinou, A. T., Kang, F., Morrison, A. J., Shen, X. and Lue, N. F. (2007). Regulation of telomere structure and functions by subunits of the INO80 chromatin remodeling complex. *Mol Cell Biol* **27:**5639-5649.

Yu, Y., Teng, Y., Liu, H., Reed, S. H. and Waters, R. (2005). UV irradiation stimulates histone acetylation and chromatin remodeling at a repressed yeast locus. *Proc Natl Acad Sci U S A* **102:**8650-8655.

Zahler, A. M. and Prescott, D. M. (1989). DNA primase and the replication of the telomeres in Oxytricha nova. *Nucleic Acids Res* **17:**6299-6317.

Zeng, L. and Zhou, M. M. (2002). Bromodomain: an acetyl-lysine binding domain. *FEBS Lett* **513:**124-128.

Zentner, G. E. and Henikoff, S. (2013). Regulation of nucleosome dynamics by histone modifications. *Nat Struct Mol Biol* **20:**259-266.

Zhang, H., Roberts, D. N. and Cairns, B. R. (2005). Genome-wide dynamics of Htz1, a histone H2A variant that poises repressed/basal promoters for activation through histone loss. *Cell* **123:**219-231.

Zhang, Y., LeRoy, G., Seelig, H. P., Lane, W. S. and Reinberg, D. (1998). The dermatomyositis-specific autoantigen Mi2 is a component of a complex containing histone deacetylase and nucleosome remodeling activities. *Cell* **95:**279-289.

Zhao, Y., Abreu, E., Kim, J., Stadler, G., Eskiocak, U., Terns, Michael P., Terns, Rebecca M. *et al.* (2011). Processive and Distributive Extension of Human Telomeres by Telomerase under Homeostatic and Nonequilibrium Conditions. *Molecular cell* **42:**297-307.

Zhao, Y., Sfeir, A. J., Zou, Y., Buseman, C. M., Chow, T. T., Shay, J. W. and Wright, W. E. (2009). Telomere Extension Occurs at Most Chromosome Ends and Is Uncoupled from Fill-In in Human Cancer Cells. *Cell* **138:**463-475.

Zhong, F. L., Batista, L. F., Freund, A., Pech, M. F., Venteicher, A. S. and Artandi, S. E. (2012). TPP1 OB-fold domain controls telomere maintenance by recruiting telomerase to chromosome ends. *Cell* **150:**481-494.

Zhu, J., Woods, D., McMahon, M. and Bishop, J. M. (1998). Senescence of human fibroblasts induced by oncogenic Raf. *Genes Dev* **12:**2997-3007.

Zhu, X. D., Kuster, B., Mann, M., Petrini, J. H. and de Lange, T. (2000). Cell-cycle-regulated association of RAD50/MRE11/NBS1 with TRF2 and human telomeres. *Nat Genet* **25:**347-352.

Zhu, X. D., Niedernhofer, L., Kuster, B., Mann, M., Hoeijmakers, J. H. and de Lange, T. (2003). ERCC1/XPF removes the 3' overhang from uncapped telomeres and represses formation of telomeric DNA-containing double minute chromosomes.*Mol Cell*. Vol. 12. United States, pp. 1489-1498.

Zoltewicz, J. S., Stewart, N. J., Leung, R. and Peterson, A. S. (2004). Atrophin 2 recruits histone deacetylase and is required for the function of multiple signaling centers during mouse embryogenesis.*Development*. Vol. 131. England, pp. 3-14.

Zucman, J., Delattre, O., Desmaze, C., Epstein, A. L., Stenman, G., Speleman, F., Fletchers, C. D. *et al.* (1993). EWS and ATF-1 gene fusion induced by t(12;22) translocation in malignant melanoma of soft parts. *Nat Genet* **4:**341-345.